Multi-class continuum traffic flow models: Analysis and simulation methods

Femke van Wageningen-Kessels

Delft University of Technology

This thesis is the result of a project funded by
ITS Edulab (a cooperation between Rijkswaterstaat Centre for Transport and
Navigation and Delft University of Technology) and
the Netherlands Research School for Transport, Infrastructure and Logistics TRAIL.

Cover illustration: Emma and Femke van Wageningen

Multi-class continuum traffic flow models: Analysis and simulation methods

Proefschrift

ter verkrijging van de graad van doctor
aan de Technische Universiteit Delft,
op gezag van de Rector Magnificus prof.ir. K.C.A.M. Luyben,
voorzitter van het College voor Promoties,
in het openbaar te verdedigen op woensdag 20 maart 2013 om 12.30 uur
door

Ferdinanda Lamberta Maria KESSELS

Master of Science in Applied Mathematics
geboren te Eersel.

Dit proefschrift is goedgekeurd door de promotoren:
Prof.dr.ir. S.P. Hoogendoorn
Prof.dr.ir. C. Vuik

Copromotor: Dr.ir. J.W.C. van Lint

Samenstelling promotiecommissie:

Rector Magnificus,	voorzitter
Prof.dr.ir. S.P. Hoogendoorn,	Technische Universiteit Delft, promotor
Prof.dr.ir. C. Vuik,	Technische Universiteit Delft, promotor
Dr.ir. J.W.C. van Lint,	Technische Universiteit Delft, copromotor
Prof.dr.ir. G.S. Stelling,	Technische Universiteit Delft
Prof.dr. L. Leclercq,	École Nationale des Travaux Publics de l'État
Prof.dr. R.E. Wilson,	University of Bristol
Prof.dr. R.L. Bertini,	Portland State University
Prof.dr.ir. B. van Arem,	Technische Universiteit Delft, reservelid

TRAIL Thesis Series no. T2013/7, the Netherlands Research School TRAIL

TRAIL
P.O. Box 5017
2600 GA Delft
The Netherlands
Phone: +31 (0) 15 27 86046
E-mail: info@rsTRAIL.nl

ISBN: 978-90-5584-163-9

Printed in the Netherlands

Contents

List of Figures

List of Tables

List of Symbols

a_u^{c}	congestion parameter of Fastlane, see (4.52a)	96
a_u^{f}	free flow parameter of Fastlane, see (4.52a)	95
b_u^{c}	congestion parameter of Fastlane, see (4.52b)	96
b_u^{f}	free flow parameter of Fastlane, see (4.52b)	95
i	vehicle group index (subscript), see (8.5)	164
j	grid cell index (subscript), see (8.1)	163
k	time step index (superscript), see (8.1), (8.5)	163, 164
L_u	gross vehicle length of class u, see Section 4.1.2	66, 86
M_γ	merge ratio parameter in upwind method, see Section 10.4.7	219
M_α	turn fraction parameter in upwind method, see Section 10.4.6	217
n	vehicle number, see Figure 6.1	120
Δn	vehicle group size, see (8.5)	164
q	flow: number of vehicles per unit time ($q = \rho v$), see Definition 2.1	49
q_{cap}	capacity flow (mixed-class): maximum number of vehicles per unit time, see Section 2.1.3	53
q_u	class specific flow: number of vehicles of class u per unit time ($q_u = \rho_u v_u$), see Definition 4.1	65
s	spacing: unit length per vehicle ($s = 1/\rho$), see Definition 2.4	50
s_{crit}	critical spacing (mixed-class), see Section 6.1	121
s_{crit}	critical spacing (multi-class), see Section 6.3	125
s_{jam}	jam spacing (mixed-class), see Section 6.1	121
s_{jam}	jam spacing (multi-class), see Section 6.3	125
s_u	class specific spacing: unit length per vehicle of class u ($s_u = 1/\rho_u$), see Definition 4.4	86
t	time coordinate, see Figure 6.1	49
Δt	time step size, see (8.1), (8.5)	163, 164
T_u	minimum time headway of class u (excluding gross vehicle length), see Section 4.1.2	67, 86
U	number of classes, see Section 2.4.2	65
v	vehicle velocity, see Definition 2.3	50
v_{crit}	critical velocity (multi-class), see Section 4.1.2	86
v_{crit}	critical velocity (mixed-class), see Section 2.1.3	53
v_{max}	maximum velocity (mixed-class)	52

v^*	vehicle velocity in Lagrangian formulation, see (6.3)	121
v_u	velocity of class u, see Definition 4.3	65
$v_{u,\max}$	maximum velocity of class u, see Section 4.1.2	86
w	congestion wave speed in mixed-class model, see Section 2.1.3	52
w	congestion parameter in multi-class model, see (4.9)	88
x	space coordinate, see Figure 6.1	49
Δx	grid cell size, see (8.1)	163
α_l	turn fraction: fraction of vehicles from incoming link that goes to outgoing link l, see Section 10.1.3	206
δ	demand (mixed-class), see (8.1)	163
δ	total demand (multi-class), see (9.1)	194
δ_u	class specific demand, see (9.3)	195
η_u	passenger car equivalent (pce) value of class u, see (4.11) for pce values in Fastlane	66, 89
γ_l	merge ratio: fraction of vehicles at outgoing link that comes from link l, see Section 10.1.4	208
ρ	density: number of vehicles per unit length, see Definition 2.2	50
ρ	effective density: number of pce vehicles per unit length, see (4.10), (4.51) for effective density in Fastlane	66, 89, 100
ρ_{crit}	critical density (mixed-class), see Section 2.1.3	53
ρ_{crit}	critical density (multi-class), see Section 4.1.2	86
ρ_{jam}	jam density (mixed-class, maximum number of vehicles per unit length), see Section 2.1.3	52
ρ_{jam}	jam density (multi-class, maximum number of pce vehicles per unit length), see Section 4.1.2	86
ρ_u	class specific density: number of vehicles of class u per unit length, see Definition 4.2	65
σ	supply (mixed-class), see (8.1)	163
σ	total supply (multi-class), see (9.1)	194
σ_u	class specific supply, see (9.3)	195
ω_u	space occupancy of class u, see (4.12)	89

Acknowledgements / Dankwoord

Het doen van wetenschappelijk onderzoek en het schrijven van een proefschrift is, in tegenstelling tot wat vaak wordt gedacht, geen eenzame taak. Daarom wil ik hier een aantal personen bedanken die ieder op hun eigen manier een bijdrage hebben geleverd aan mijn werk.

Ten eerste zijn dat mijn begeleiders. In april 2007 maakte ik kennis met Serge Hoogendoorn en Hans van Lint. Ze zochten een promovendus om binnen het ITS Edulab aan de verdere ontwikkeling van Fastlane te werken. Ik wist nauwelijks iets van verkeer, maar het leek mij een mooi project waar ik mijn passie voor toegepaste wiskunde in kwijt kon. Dat is terecht gebleken. In de jaren die volgden heeft Serge mij vaak gestimuleerd om paden op te gaan die niet voor de hand lagen, maar uiteindelijk zeer interessant bleken. Hans heeft mij vaak gevraagd om verduidelijking van mijn gedachtekronkels. Dat ben ik zeer gaan waarderen en ik denk dat het tot een goed leesbaar proefschrift heeft geleid. Kees Vuik heeft als begeleider voor de nodige wiskundige input gezorgd. Hij heeft me sinds mijn eerste bezoek aan de mastervoorlichting Applied Mathematics (in 2003) het vertrouwen gegeven dat mijn keuze voor toegepaste wiskunde een goede keuze is.

I enjoy doing research, but part of the joy of work and visiting conferences is due to good company. Yufei and Thomas, we have been working on Fastlane together. It is special to me that we will also defend our dissertations together during the FDW (Fastlane Defense Week). LaTeX has even proven to be powerful for preparing nice looking graphics: thanks Erik-Sander and Thomas for introducing me to Ti*k*z. Many more (former) colleagues and (former) room mates deserve thanks for their support and company, such as Victor, Nina, Adam, Giselle and Mario.

In het kader van de ‘mooie plaatjes’ wil ik ook Suzanne Mol bedanken voor haar professionele advies over de vormgeving van de stamboom.

I want to thank Guus Stelling, Ludovic Leclercq, Robert Bertini and Eddie Wilson for taking place in my committee and the valuable comments in the last phase of writing my thesis. Ludovic, also thanks for introducing me to variational theory. Furthermore, I want to thank you and your colleagues at LICIT for your hospitality during my stay in Lyon.

In de eerste jaren van mijn promotieonderzoek heb ik veel ‘wiskunde opgesnuifd’ bij het bedrijf waar ik ook ben afgestudeerd, VORtech Computing. Bas van ’t Hof,

bedankt voor je geduld en voor het mij leren geduld te hebben bij het uitschrijven van veel te lange vergelijkingen. En Mark Roest, bedankt dat je me aan Serge en Hans hebt geïntroduceerd en me op dit pad hebt gezet.

Ook mijn paranimfen verdienen dank. Anke, we hebben de afgelopen jaren heel veel samen meegemaakt. Ik vind het fijn dat je me ook in de laatste stap van mijn promotie wilt steunen. Giel, wie had ooit gedacht dat wij qua opleiding en werk naar elkaar toe zouden groeien? Ik doe iets met auto's, en jij doet onderzoek. Daarom vind ik het mooi dat ook jij mijn paranimf wilt zijn.

Dat brengt mij tot het bedanken van mijn overige familie en vrienden. Mam, ik vind het nog steeds super dat je elke dinsdag uren met het openbaar vervoer reist om tijd door te brengen met je kleindochters en mij de gelegenheid te geven te werken. Pap, Mia, Willy en Leen, bedankt voor jullie luisterend oor en de afleiding. Marieke, Mirjam en Roxanne, ook op afstand zijn jullie altijd betrokken.

Dit proefschrift, het onderzoek en het schrijven zijn belangrijk voor mij. Maar, het allermooiste dat mij, samen met Niels, de afgelopen jaren is overkomen, is de geboorte en het zien opgroeien van twee prachtige meiden. Niels, Emma en Julia, jullie maken mijn leven zo veel (waarde)voller!

Femke van Wageningen-Kessels, February 2013

Summary

Multi-class continuum traffic flow models: Analysis and simulation methods

Traffic flow modelling has developed rapidly over the last two decades. In many applications, the models are combined with measured data concerning the current traffic state and with fast computational methods. Because of this combination it has become possible to make accurate and useful short term predictions about the evolution of the traffic state. The predictions can be used to inform and advise road users, for example about alternative routes. Furthermore, the predictions can be used to control traffic in an efficient way in order to prevent or reduce delays. The predictions are in particular useful in the case of exceptional circumstances such as an accident, extreme weather conditions or festivities. In such cases historical data is less useful and routes that are optimal under normal circumstances are not optimal anymore.

The main contribution of this dissertation is the development and analysis of a new traffic flow model and accompanying numerical methods. This model, *Fastlane*, takes into account the differences between types of vehicles (for example passenger cars and trucks) and driving styles. Furthermore, the model is well suited to make useful short term predictions for the traffic state on a network of main roads. This is due to the development of efficient numerical methods.

This summary largely follows the outline of this dissertation: first the literature review is discussed, followed by the model development and analysis. We then make a short side step to discuss the Lagrangian coordinate system that has proven useful in the model analysis. Furthermore, the Lagrangian coordinate system is subsequently applied in numerical methods for homogeneous roads and networks of inhomogeneous roads. Finally, we present recommendations for both practice and science.

Model tree

The literature review in Chapter 2 is largely based on a newly developed genealogy of traffic flow models, see also Appendix A. This model tree shows how such models

have developed since their introduction in the 1930's. We distinguish four families: the fundamental relation, microscopic, mesoscopic and macroscopic models. The fundamental relation describes the (static) relation between the velocity of a vehicle and the distance to its leader. The other models describe how this relation develops over time and space, and how these dynamics are described, differs per family. Microscopic models describe and trace the movement of individual vehicles. Macroscopic models aggregate many vehicles and their 'average' behaviour (velocity, following distance, time headway) is described. The aggregation level in the mesoscopic family is between that of microscopic and macroscopic models.

Within each family many different branches are distinguished. Furthermore, connections can be made between the families. By analysis of the model tree we identify the following trends: 1) convergence to generic models that include all models in a certain branch, 2) extensions and adaptations of the prototype macroscopic model (the LWR model) to better reproduce relevant phenomena, 3) extensions of almost all types of models to model heterogeneity among vehicles and drivers, and 4) the development of hybrid models that combine the advantages of (for example) microscopic and macroscopic models. In the model development we combine these trends in a macroscopic model with heterogeneity. A small adaptation then gives a generic model. Subsequently, a new formulation of the model creates possibilities for the development of new hybrid models.

Model development and analysis

In Chapter 4 we develop the (macroscopic) Fastlane model based on the modeling principles that we introduce in Chapter 3. The model includes multiple classes which express the heterogeneity between vehicles and drivers. The model is formulated in a broad way, but it can, for example, distinguish between, on the one hand, passenger cars which are relatively short and have a high maximum velocity and short headways and, on the other hand, trucks which are long and have low maximum velocities and long headways. The heterogeneity is introduced in Fastlane mainly via pce (passenger car equivalent) values. The pce values express, per class, how much one vehicle of that class contributes to the traffic flow in comparison to one passenger car. For example, a large truck has a high impact on the traffic flow and thus a high pce value. A van has a somewhat smaller pce value, but it is larger than that of a passenger car. Fastlane is unique in that, in contrast to other multi-class kinematic wave models, the pce values depend on the actual traffic state. Therefore, the pce values are based on a simple microscopic model. This ensures that at high velocities and low densities, the pce values of trucks are relatively low and thus they contribute little to the total traffic flow. However, in (heavy) congestion (low velocities, high densities), trucks take up the same road space as multiple passenger cars. In this case the pce values of trucks are high and they contribute relatively a lot to the total flow. The heterogeneity ensures

that, even though the model is based on a simple kinematic wave model, it can describe and reproduce complex phenomena.

The Fastlane model is generalized in Chapter 5. We show that the generalized model includes all kinematic wave models known from the literature. The generalization enables us to compare the models in Chapter 7 with respect to the requirements that are formulated in Chapter 3. The requirements are related to for example, a consistent model formulation, the speed and direction of information (characteristic velocity, anisotropy) and intuitive relations between a change in the number of vehicles and a change in their velocity. We show that Fastlane and only one other model are the only models that satisfy all requirements. Furthermore, a step-by-step plan is introduced that can be applied to analyse any other (newly developed) multi-class kinematic wave model with respect to the requirements. For this model analysis, we need a new formulation of the generic model, which is introduced in Chapter 6.

Lagrangian coordinate system

Chapter 6 is the core chapter of this dissertation. The generalized model is reformulated in the Lagrangian coordinate system. Lagrangian coordinates travel with the vehicles of the fastest class. This new formulation makes it easier to analyse whether or not information goes faster than vehicles (anisotropy). This is because information travels with characteristic velocities which, in turn, are equal to the eigenvalues of a certain system of equations. However, the eigenvalues of that system in the traditional formulation are difficult to determine exactly, and if there are many classes it may even be impossible. The Lagrangian formulation offers the advantage that it is only necessary to determine the sign of the eigenvalues. In contrast to determining the value itself, it is possible to determine the sign of the eigenvalue. Finally, the Lagrangian coordinates are applied to develop more efficient numerical methods.

Numerical methods and road networks

In order to apply a traffic flow model like Fastlane in a simulation, the continuous equations need to be discretized and solved. In Chapter 8 we develop the accompanying numerical methods for kinematic wave models of one class. In Chapter 9 the methods are extended to models with multiple classes. Furthermore, in Chapter 8 we develop measures to qualify the accuracy of traffic flow models, using measures that are especially relevant for traffic flow.

The Lagrangian coordinate system offers advantages for the accuracy and speed of the simulation. In traditional numerical methods for traffic flow models, time and space are divided into discrete units (time steps and grid cells). The solution of the equations is then computed at each time step and in each grid cell. The disadvantage of this method

is that information can go both from a grid cell to its downstream neighboring grid cell (in free flow) or it can go to its upstream neighboring grid cell (in congestion). This results in relatively slow computation and inaccurate solutions. However, once we know that, in a certain model, information does not travel faster than vehicles, the Lagrangian coordinate system can be used to develop efficient numerical methods. Instead of dividing space into grid cells, vehicles are divided into groups. Because information does not travel faster than the vehicles or vehicle groups, information only travels from one group to its following group and never to its leading group. This results in fast and accurate computational methods.

In Chapter 10 we extend the methods from Chapter 8 and 9 to networks (so as to perform simulations on networks of roads). Therefore, we add discretisations of node models that describe inflow and outflow boundaries, on and off ramps and other inhomogeneities. These other inhomogeneities, such as a decrease or increase in the number of lanes, or a change in the speed limit, are expressed in temporary or local changes in the fundamental relation. The traditional numerical methods are in general more easy to extend with these node models, but also node models based on the Lagrangian coordinate system are possible and lead to satisfying results.

Recommendations

We conclude this summary with two types of recommendations: recommendations for applications of the results, including the Fastlane model, and recommendations for future research.

Applications

Fastlane is especially well suited for applications on networks of main roads with many different types of vehicles. For example, it can be applied for state estimation, and for prediction and control of road networks. Two colleagues discuss these applications in their dissertations: Yuan (2013) introduces methods for state estimation using Fastlane in Lagrangian coordinates, Schreiter (2013) introduces control methods that apply Fastlane for the road network in the port of Rotterdam. It is shown that Fastlane yields fast and accurate results which are superior to results achieved with the simulation tools that are currently applied in practice.

In cases where Fastlane does not satisfy the requirements for a certain application, the model tree (Chapter 2, Appendix A) or the step-by-step plan for the assessment of multi-class kinematic wave models (Chapter 7) can be applied to find another suitable model. The step-by-step plan especially provides an efficient method to distinguish qualitatively suitable models from unsuitable models. The advantage of the step-by-step plan is that it becomes unnecessary to perform (usually costly) calibration to all

models. The calibration to the qualitatively good models can then be performed by applying the accuracy measures that are proposed in Chapter 8.

Finally, the numerical methods for homogeneous roads and for networks of inhomogeneous roads (Chapter 8–10) can also be applied to other models than Fastlane.

Future research

We distinguish three main areas for future research: the model tree, the Fastlane model and the accuracy of numerical methods.

The model tree (Chapter 2, Appendix A) provides clues for the future development of traffic flow models. Firstly, generic models can be developed that include even more models than the current generic models. The generic models can in turn be applied to qualitatively assess the models that fit within the generic model. Secondly, hybrid models appear to be suitable to combine the advantages of the different types of models. This development can be continued for example by application of the Lagrangian formulation (Chapter 6) and by combining models with only one class with multi-class models.

The Fastlane model (Chapter 4) can be developed further. For example, the current method to determine pce values in free flow is not very realistic. This can be improved. Furthermore, the numerical methods can be improved further. The node models in Lagrangian coordinates deserve especial attention (Chapter 10).

The measures to determine the accuracy of numerical methods (Chapter 8) can be extended further. After small adaptations, they are also suitable to compare, for example, simulation results with measured traffic states. This innovation provides new and better methods for calibrating traffic flow models.

Samenvatting

Continuüm verkeersstroommodellen met meerdere klassen: Analyse en simulatiemethoden

Verkeersstroommodellen hebben zich de afgelopen twee decennia snel ontwikkeld. In veel toepassingen worden zulke modellen gecombineerd met meetgegevens over de huidige verkeerstoestand en met snelle rekenmethoden. Door deze combinatie is het mogelijk geworden om nauwkeurige en bruikbare korte-termijn voorspellingen te doen over hoe de verkeerstoestand zich zal ontwikkelen. De voorspellingen kunnen gebruikt worden om weggebruikers te informeren en adviseren, bijvoorbeeld over alternatieve routes. Bovendien kunnen de voorspellingen gebruikt worden om op een efficiënte manier het verkeer te regelen om zo vertragingen te voorkomen of verminderen. De voorspellingen zijn vooral nuttig bij bijzondere omstandigheden zoals een ongeluk, extreme weersomstandigheden of evenementen. In zulke gevallen zijn historische gegevens minder bruikbaar en routes die optimaal zijn onder normale omstandigheden, zijn opeens niet meer optimaal.

De belangrijkste bijdrage van dit proefschrift is de ontwikkeling en analyse van een nieuw verkeersstroommodel en bijbehorende numerieke methoden. Dit model, *Fastlane*, houdt rekening met verschillen tussen soorten voertuigen (bijvoorbeeld personenauto's en vrachtwagens) en rijstijlen. Bovendien is het geschikt om bruikbare korte-termijn voorspellingen te maken voor de verkeerstoestand op een netwerk van hoofdwegen. Dit komt door de ontwikkeling van efficiënte numerieke methoden,

Deze samenvatting volgt in grote lijnen de opbouw van dit proefschrift: ten eerste wordt het literatuuronderzoek besproken, daarna volgt de modelontwikkeling en -analyse. Dan maken we een korte uitstap naar het Lagrangiaanse coördinatensysteem dat bruikbaar is gebleken in de modelanalyse. Bovendien wordt het Lagrangiaanse coördinatensysteem vervolgens toegepast in de numerieke methoden voor homogene wegen en netwerken van inhomogene wegen. Als laatste volgen aanbevelingen voor zowel de praktijk als de wetenschap.

Stamboom

Het literatuuroverzicht in Hoofdstuk 2 is grotendeels gebaseerd op een nieuw ontwikkelde stamboom van verkeersstroommodellen, zie ook Appendix A. De stamboom laat zien hoe deze modellen zich hebben ontwikkeld sinds hun eerste introductie in de jaren '30 van de twintigste eeuw. We onderscheiden vier families van modellen: de fundamentele relatie, microscopische, mesoscopische en macroscopische modellen. De fundamentele relatie beschrijft het (statische) verband tussen snelheid van een voertuig en de afstand tot zijn voorligger. De andere modellen beschrijven hoe dit verband zich ontwikkelt over de tijd en ruimte. Hoe deze dynamica wordt beschreven, is per familie verschillend. Enerzijds beschrijven en volgen microscopische modellen de beweging van individuele voertuigen. Anderzijds aggregeren macroscopische modellen vele voertuigen en wordt hun 'gemiddelde' gedrag (snelheid, volgafstand, volgtijd) beschreven. Het aggregatieniveau in de mesoscopische familie zit tussen dat van de miscroscopische en macroscopische familie in.

Binnen iedere familie worden vele verschillende takken onderscheiden. Bovendien zijn er verbanden te leggen tussen de families. Door analyse van de stamboom identificeren we de volgende trends: 1) convergentie naar generieke modellen die alle modellen in een bepaalde tak omvatten, 2) uitbreidingen en aanpassingen van het oer-macroscopische model (het LWR kinematische golf-model) om beter relevante fenomenen te kunnen reproduceren, 3) uitbreidingen van bijna alle soorten modellen om heterogeniteit tussen voertuigen en bestuurders te modelleren, en 4) de vorming van hybride modellen die de voordelen van (bijvoorbeeld) microscopische en macroscopische modellen combineren. In de modelontwikkeling combineren we deze trends in een macroscopisch model met heterogeniteit. Een kleine aanpassing van het model levert een generiek model. Vervolgens levert een nieuwe formulering van het model mogelijkheden voor de ontwikkeling van nieuwe hybride modellen.

Modelontwikkeling en -analyse

In Hoofdstuk 4 ontwikkelen we het (macroscopisch) Fastlanemodel op basis van modelleerprincipes die we in Hoofdstuk 3 introduceren. Het model kent meerdere klassen waardoor de heterogeniteit tussen typen voertuigen en bestuurders tot uitdrukking komt. Het model is algemeen geformuleerd, maar kan bijvoorbeeld onderscheid maken tussen enerzijds personenauto's die relatief kort zijn, een hoge maximumsnelheid hebben en korte volgtijden en anderzijds vrachtwagens die lang zijn en een lage maximumsnelheid en lange volgtijden hebben. De heterogeniteit wordt in Fastlane met name geïntroduceerd via pce-waarden ('passenger car equivalent'-waarden). De pce-waarden drukken, per klasse, uit hoeveel één voertuig van die klasse bijdraagt aan de verkeersstroom ten opzichte van één personenauto. Een grote vrachtwagen heeft bijvoorbeeld een grote invloed op de verkeersstroom en dus een hoge pce-waarde. Een

bestelbus heeft een wat kleinere pce-waarde, maar de waarde is groter dan die van een personenauto. Het bijzondere aan Fastlane is dat, in tegenstelling tot andere kinematische golf-modellen met meerdere klassen, de pce-waarden afhankelijk zijn van de actuele verkeerstoestand. Daartoe worden de pce-waarden gebaseerd op een eenvoudig microscopisch model. Dit zorgt ervoor dat bij hoge snelheden en lage dichtheden, de pce-waarden van vrachtwagens relatief laag zijn en ze dus relatief weinig bijdragen aan de totale verkeersstroom. Echter, in (zware) congestie (lage snelheden, hoge dichtheden), nemen vrachtwagens dezelfde ruimte in als meerdere personenauto's. In dit geval zijn de pce-waarden van vrachtwagens dus hoog en dragen ze relatief veel bij aan de totale stroom. De heterogeniteit zorgt er vervolgens voor dat, ondanks dat het model gebaseerd is op een eenvoudig kinematische golf-model, het complexe fenomenen kan beschrijven en reproduceren.

Het Fastlane model wordt gegeneraliseerd in Hoofdstuk 5. We laten zien dat het gegeneraliseerde model alle kinematische golf-modellen met meerdere klassen omvat die bekend zijn uit de literatuur. De generalisatie stelt ons in staat om in Hoofdstuk 7 de modellen te vergelijken op basis van kwalitatieve vereisten die in Hoofdstuk 3 worden opgesteld. De vereisten hebben onder andere te maken met een consistente modelformulering, de snelheid en richting van informatie (karakteristieke snelheid, anisotropie) en intuïtieve verbanden tussen een verandering in het aantal voertuigen en een verandering in hun snelheid. We laten zien dat Fastlane en slechts één ander model, de enige modellen zijn die aan alle vereisten voldoen. Bovendien wordt een stappenplan geïntroduceerd dat toegepast kan worden om ieder ander (nieuw te ontwikkelen) kinematische golf-model met meerdere klassen te analyseren met betrekking tot de vereisten. Voor de modelanalyse die wordt gepresenteerd in Hoofdstuk 7 hebben we echter een nieuwe formulering van het generieke model nodig, die wordt geïntroduceerd in Hoofdstuk 6.

Lagrangiaans coördinatenssyteem

Hoofdstuk 6 vormt de kern van dit proefschrift. Het gegeneraliseerde model wordt geherformuleerd in het Lagrangiaanse coördinatensysteem. Lagrangiaanse coördinaten bewegen mee met de voertuigen van de snelste klasse. Deze nieuwe formulering maakt het eenvoudiger om te analyseren of informatie sneller gaat dan de voertuigen zelf (anisotropie). Dat is omdat informatie reist met de karakteristieke snelheden, die op hun beurt weer gelijk zijn aan de eigenwaarden van een bepaald systeem van vergelijkingen. De eigenwaarden van dat systeem in de traditionele formulering zijn echter moeilijk analytische te bepalen, en in gevallen met veel klassen kan dat zelfs onmogelijk zijn. De formulering in de Lagrangiaanse coordinaten biedt het voordeel dat het alleen nodig is om te bepalen wat het teken is van de eigenwaarden. In tegenstelling tot het bepalen van de waarde zelf, is het wel mogelijk om het teken van de eigenwaarde te bepalen. Tenslotte, worden Lagrangiaanse coordinaten toegepast om efficiënte numerieke methoden te ontwikkelen.

Numerieke methoden en netwerken van wegen

Om een verkeersstroommodel zoals Fastlane toe te passen in een simulatie, moeten de continue vergelijkingen gediscrediteerd en opgelost worden. In Hoofdstuk 8 ontwikkelen we de bijbehorende numerieke methoden voor kinematische golf-modellen met één klasse. In Hoofdstuk 9 worden de methoden uitgebreid naar modellen met meerdere klassen. Bovendien ontwikkelen we in Hoofdstuk 8 meetmethoden om de nauwkeurigheid van verkeerstroommodellen te kwantificeren, volgens grootheden die speciaal relevant zijn binnen verkeersstromingen.

Het Lagrangiaanse coördinatensysteem biedt voordelen voor de nauwkeurigheid en snelheid van de simulatie. In traditionele numerieke methoden voor verkeerstroommodellen worden tijd en ruimte in discrete eenheden (tijdstappen en roostercellen) verdeeld. De oplossing van de vergelijkingen kan dan iedere tijdstap en voor iedere roostercel benaderd worden. Het nadeel van deze methode is dat informatie zowel van een roostercel naar de stroomafwaartse roostercel kan gaan (in vrije afwikkeling), als van een roostercel naar de stroomopwaartse roostercel (in congestie). Dit levert relatief trage berekeningen en onnauwkeurige oplossingen op. Echter, zodra van een bepaald model bekend is dat informatie niet sneller reist dan de voertuigen, kan het Lagrangiaanse coördinatensysteem gebruikt worden om efficiënte numerieke methoden te ontwikkelen. In plaats van het verdelen van de ruimte in roostercellen, worden de voertuigen nu in groepen verdeeld. In iedere tijdstap wordt vervolgens de positie en de snelheid van iedere voertuiggroep benaderd. Omdat informatie niet sneller reist dan de voertuig(groep)en, reist informatie altijd van de ene groep naar de volgende groep, en nooit naar de vorige. Dit levert snelle en nauwkeurige rekenmethoden op.

In Hoofdstuk 10 presenteren we een uitbeiding van de numerieke methoden uit Hoofdstuk 8 en 9 naar netwerken, om simulaties uit te kunnen voeren op netwerken van wegen. Daarvoor voegen we discretisaties toe van knoopmodellen die instroom- en uitstroomranden, toe- en afritten en andere inhomogeniteiten beschrijven. Deze andere inhomogeniteiten zoals vermindering of vermeerdering van het aantal rijstroken of een verandering in de snelheidslimiet komen tot uiting in tijdelijke of plaatselijke veranderingen in de fundamentele relatie. De traditionele numerieke methoden zijn in het algemeen eenvoudiger uit te breiden met deze knoopmodellen, maar ook knoopmodellen gebaseerd op het Lagrangiaanse coördinatensysteem zijn mogelijk en leveren goede resultaten op.

Aanbevelingen

We sluiten deze samenvatting af met twee soorten aanbevelingen: aanbevelingen voor toepassingen van de resultaten, waaronder het Fastlane model, en aanbevelingen voor toekomstig onderzoek.

Toepassingen

Fastlane is in het bijzonder geschikt voor toepassing op netwerken van hoofdwegen met veel verschillende soorten voertuigen. Het kan bijvoorbeeld gebruikt worden voor toestandschatting, -voorspelling en -regeling voor wegennetwerken in havens. Twee collega's bespreken deze toepassingen in hun proefschriften: Yuan (2013) introduceert methoden voor toestandschatting met Fastlane in Lagrangiaanse coördinaten, Schreiter (2013) introduceert regelmethoden die gebruik maken van Fastlane voor het wegennetwerk in de Rotterdamse haven. Het is aangetoond dat Fastlane snelle en nauwkeurige resultaten oplevert die superieur zijn aan de resultaten die worden bereikt met simulatiegereedschappen die momenteel in de praktijk worden toegepast.

Indien Fastlane niet voldoet aan de eisen voor een bepaalde toepassing, kan de stamboom (Hoofdstuk 2, Appendix A) of het stappenplan voor de beoordeling van kinematische golf-modellen met meerdere klassen (Hoofdstuk 7) gebruikt worden om een ander geschikt model te vinden. Vooral het stappenplan levert een efficiënte methode om kwalitatief geschikte modellen te onderscheiden van ongeschikte modellen. Het voordeel van het stappenplan is dat de (meestal kostbare) kalibratie niet uitgevoerd hoeft te worden voor alle modellen. De kalibratie van de kwalitatief geschikte modellen kan vervolgens uitgevoerd worden door toepassing van de nauwkeurigheidsmaten die zijn voorgesteld in Hoofdstuk 8.

Als laatste kunnen de numerieke methoden voor homogene wegen en voor netwerken van inhomogene wegen (Hoofdstuk 8–10) ook toegepast worden op andere verkeersstroommodellen dan Fastlane.

Toekomstig onderzoek

We onderscheiden drie voorname gebieden voor verder onderzoek: de stamboom, het Fastlane model en de nauwkeurigheid van numerieke methoden.

De stamboom (Hoofdstuk 2, Appendix A) geeft een aantal aanknopingspunten voor de verdere ontwikkeling van verkeerstroommodellen. Ten eerste, kunnen er generieke modellen ontwikkeld worden die nog meer modellen omvatten dan de huidige generieke modellen. De generieke modellen kunnen vervolgens toegepast worden voor het kwalitatief beoordelen van de modellen die binnen het generieke model vallen. Ten tweede, blijken hybride modellen geschikt om de voordelen van verschillende typen modellen te combineren. Deze ontwikkeling kan voortgezet worden bijvoorbeeld door toepassing van de Lagrangiaanse formulering (Hoofdstuk 6) en door het combineren van modellen met slechts éń klasse met modellen met meerdere klassen.

Het Fastlane model (Hoofdstuk 4) kan verder ontwikkeld worden. De huidige manier waarop pce-waarden momenteel in vrije afwikkeling worden bepaald is bijvoorbeeld niet erg realistisch. Dat kan verbeterd worden. Bovendien kunnen de numerieke methoden verder verbeterd worden, met name de knoopmodellen in Lagrangiaanse coordinaten verdienen aandacht (Hoofdstuk 10).

De meetmethoden voor de nauwkeurigheid van numerieke methoden kunnen verder uitgebreid worden (Hoofdstuk 8). Na kleine aanpassingen, zijn ze bijvoorbeeld ook geschikt om simulatieresultaten te vergelijken met de gemeten verkeerstoestand. Deze innovatie levert nieuwe en betere methoden voor het kalibreren van verkeerstroom-modellen.

Chapter 1

Introduction

Traffic flow models are used to describe and predict traffic on roads. For example, they model the number of vehicles, their velocity, their acceleration and the distance and time between vehicles. By doing simulations based on these models, the performance of roads or traffic networks can be assessed. This includes answering questions about the presence and duration of congestion, travel times and travel time delays. This information can be used in many applications including providing information on congestion to road users, and in traffic control. In this dissertation we develop and analyze a traffic flow model and numerical methods that can be applied in a simulation tool.

The outline of this introductory chapter is as follows. We elaborate further on the context of this research in Section 1.1. In Section 1.2 we introduce our research objective and approach. In Section 1.3 we outline our main scientific contributions, whereas the main applications and practical contributions are discussed in Section 1.4. We conclude this chapter with an outline of the rest of this dissertation (Section 1.5).

1.1 Background and motivation

Figure 1.1 shows the traffic flow modelling cycle. It consist of five main items: observation, theory and model development, discretization and simulation. In this section we discuss the modelling cycle and position our research within this cycle.

The development of traffic flow models leans heavily on observations: the first step in Figure 1.1. Data is collected using, for example, loop detectors, cameras or GPS devices that many vehicles have on-board, such as the mobile phone of the driver. Alternatively, data is collected using lab experiments for example with a driving simulator. These observations are analyzed and phenomena that characterize traffic flow are recognized.

In the second step, observations are used to build a theoretical framework. The theoretical framework consists of (mainly qualitative) statements and (behavioural) assumptions. For example, it is assumed that drivers perceive short space headways as more

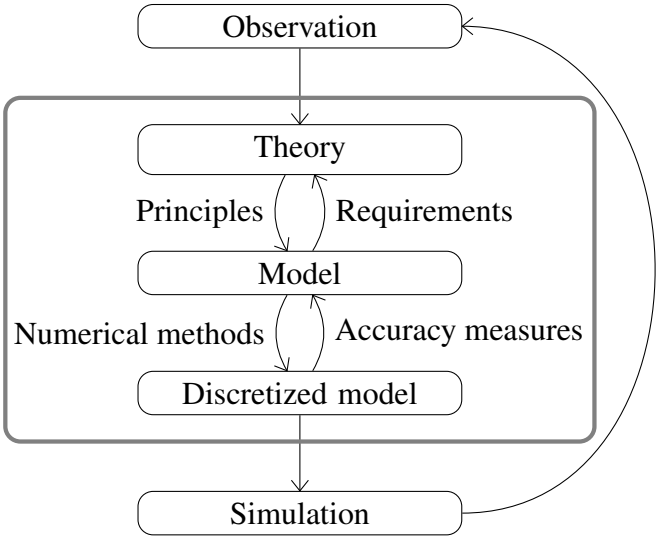

Figure 1.1 *Traffic flow modelling cycle. In this dissertation we focus on the center part (in the grey rectangle).*

dangerous at high velocities than at low velocities. This is assumed to be the reason why at low velocities shorter headways are maintained. Another assumption is that drivers only react to their leaders and not to their followers.

In the third step, the theoretical framework is used to build a traffic flow model. The model consists of a set of (usually continuous) equations. For example, the theory about short headways at low velocities and long headways at high velocities is quantified in a fundamental relation. The fundamental relation expresses the average vehicle velocity as a function of the average headway. Alternatively, a car-following model is developed that describes how a following vehicle reacts to its leader. In such models, the assumption that drivers only react to their leaders is applied.

The continuous models can not be used directly in a computer simulation and discretization is applied in the fourth step. In most simulation tools, time is divided into discrete time steps. Furthermore, depending on the model, also space or other continuous variables are discretized. Numerical methods are applied to approximate the new traffic state each time step. This results in a discrete traffic flow model.

Finally, the discrete traffic flow model is implemented in a computer program. Using the simulation tool, traffic state estimation and predictions can be made. Simulation results are compared to observations to calibrate the parameters and to validate the simulation tool.

Our work contributes to the entire traffic flow modelling cycle, while focussing on the central part in Figure 1.1: theory and model development and discretization.

1.2 Research objective and approach

In this section we discuss in more detail some of the elements in the traffic flow modelling cycle and identify the key areas to which this research contributes. We discuss which elements we have improved (i.e., our research objectives) and we describe how we improve those elements (i.e., our research approach).

1.2.1 Research objective

As mentioned before, we focus on the central part of the modelling cycle in Figure 1.1, including theory, modelling and discretization. The choice of phenomena that we want to model is mainly determined by our foreseen applications (traffic state estimation and prediction, traffic management, dynamic traffic assignment, see Section 1.4). The applications call for a deterministic traffic flow model that allows for efficient simulations (i.e., fast and accurate) but which also takes into account heterogeneity among vehicles and drivers. From here onward we build a framework and within the framework we develop a model and discretize it. Our main research objectives are related to these three steps in the modelling cycle:

1. Development of a theoretical framework for multi-class kinematic wave traffic flow modelling.
2. Development and analysis of a multi-class kinematic wave traffic flow model within the framework.
3. Development of numerical methods to solve the model equations efficiently (i.e., both fast and accurate).

The approach for each of the objectives is detailed below.

1.2.2 Research approach

In order to define the research needs more clearly, we start with a literature study on existing traffic flow models. We identify trends in the traffic flow modelling literature and determine which type of model is suitable for our purpose.

Based on the findings from the literature study and anticipated foreseen applications, we define a theoretical framework. The theoretical framework consists of a set of modelling principles and requirements. Most of the principles are common for all kinematic wave models or even for all macroscopic traffic flow models. However, we add a principle about the heterogeneity of vehicles and drivers. The principles are used as a foundation for the model. After the model has been formulated, we will test whether it satisfies the requirements. The requirements are related to the model formulation itself, the fundamental relation and the model dynamics.

Secondly, we develop a multi-class kinematic wave traffic flow model, that we call *Fastlane*. It is based on the above principles and we analyze it with respect to the requirements. Furthermore, we compare it to other, similar, models with respect to the requirements. The comparison is largely based on a thorough mathematical analysis of a novel generalized model. The analysis includes a reformulation of the model in the Lagrangian coordinate system. This system moves with the vehicles, as opposed to the traditional Eulerian coordinate system which is fixed in space. The reformulated model has the same mathematical properties as the original model, but it is easier to analyze.

Thirdly, we develop numerical methods to solve the model equations. The numerical methods are also based on the reformulated model in Lagrangian coordinates. We extend the methods for long homogeneous roads and mixed-class models to include road networks and multiple vehicle classes. The numerical methods based on the Lagrangian coordinate system are compared with more traditional numerical methods. Therefore we compare simulation results with the analytical solution of the model. For the comparison we develop two novel accuracy measures to measure the type of errors that are most important in the traffic flow context.

1.3 Scientific contribution

This dissertation includes the following main scientific contributions:

- A model tree showing the historical development of traffic flow models (see Section 1.3.1).
- A multi-class kinematic wave model (see Section 1.3.2) including:
  - A theoretical framework for multi-class kinematic wave modelling
  - A model based on sound principles and satisfying important requirements (Fastlane)
  - A generalized single-pipe multi-class kinematic wave model
  - A framework for the assessment of the generalized model and special cases thereof
- Application of the Lagrangian coordinate system to (multi-class) kinematic wave models (see Section 1.3.3)
- Efficient numerical methods for traffic flow models (see Section 1.3.4).
- Measures of accuracy both for numerical methods and traffic flow models (see Section 1.3.5).

We discuss the contributions in more detail below.

1.3.1 Model tree

We introduce a model tree showing the genealogy of traffic flow models. It provides an overview of the main traffic flow models and their relations since the first study on

the relation between traffic density and flow (Greenshields, 1934). It does not only give a description of the state-of-the-art, as most literature reviews do. But rather, by visualizing the information in the form of a genealogy it presents in a clear way:

- An historical overview of traffic flow models.
- The main families of traffic flow models.
- How certain models are derived from or inspired by other models.
- The convergence of certain branches of models to a generalized model.

Using the model tree we are able to identify research needs.

1.3.2 Multi-class kinematic wave modelling

We develop the Fastlane model. It is a novel type of multi-class kinematic wave model and is well suited for the anticipated applications. Just like many other multi-class models, it includes a passenger car equivalent (pce) value, expressing that certain types of vehicles (e.g., trucks) have a higher impact on traffic than others (e.g., passenger cars). Fastlane is distinguished from other models by the fact that it incorporates space occupancy in the pce-value, or in the pce function. It is the first multi-class model that bases its pce function (via the space occupancy function) on a set of behavioural assumptions. The behavioural assumptions are in line with assumptions in safe-distance car-following models. Moreover, the Fastlane model has a firm basis in a theoretical framework for multi-class kinematic wave traffic flow modelling, including a consistent set of principles. The framework furthermore includes a set of qualitative requirements, which are all satisfied by Fastlane.

We present a step-by-step plan for the qualitative assessment of multi-class kinematic wave models. Over the last decade, many multi-class kinematic wave models have been developed. We propose a generalized multi-class kinematic wave model, based on the Fastlane model that includes all these models as special cases. As far as we know, this is the only generalized model that includes all those models. Furthermore, we apply the generalized model to assess each model with respect to a consistent set of qualitative requirements. We develop a step-by-step plan to perform such an assessment. With the results of the assessment, it can be decided more easily which models need or deserve further development and which do not because they have qualitatively undesirable properties. We do not know of any previous rigorous effort to qualitatively assess such models. Individual models have been assessed before. This includes ‘basic’ models (Benzoni-Gavage & Colombo, 2003; Zhang et al., 2006) and more ‘advanced’ models (Ngoduy & Liu, 2007). In their assessments an eigenvalue analysis is performed. However, they apply the traditional Eulerian coordinate system. Therefore, the eigenvalue analysis is difficult, if possible at all, if there are many (more than 3 or 4) vehicle classes. We apply an alternative coordinate system which allows for an eigenvalue analysis even if there are arbitrary many vehicle classes.

1.3.3 Lagrangian coordinate system

The rigorous model assessment is possible due to the reformulation of the generalized model in Lagrangian coordinates. Multi-class kinematic wave models are traditionally formulated in the Eulerian coordinate system, which is fixed in space. We reformulate those models in the Lagrangian coordinate system, which moves with the vehicles. The new formulation has multiple advantages. Using this coordinate system, the assessment of the models with respect to certain criteria becomes easier. Furthermore, more efficient numerical methods can be based on this coordinate system.

1.3.4 Numerical methods

We model traffic flow using a nonlinear hyperbolic partial differential equation of the following form:

$$\frac{\partial u}{\partial t} + \frac{\partial f(u)}{\partial x} = 0 \tag{1.1}$$

with u a variable, $f(u)$ a convex function and t the time coordinate and x the space coordinate. We extend the model to include multiple classes, which implies that u becomes a vector of variables, and to include a source term on the right-hand side. The equation (1.1) is also know as the conservation equation (or conservation of mass, conservation of vehicles). In our application, the function f is a highly nonlinear function. One important difficulty is that its derivative changes sign. The Godunov method (Godunov, 1959) is often used to solve this type of equations. In traffic flow it is often referred to as the minimum supply demand method or the cell transmission model. However, this solution method is inaccurate because of the nonlinearity of f. We solve this problem by first reformulating the model in the Lagrangian coordinate system, which leads to a 'less nonlinear' function f^*: it is now nondecreasing and thus its derivative does not change sign. Secondly, we apply the Godunov method. We show that this numerical method, the upwind method, is more accurate than the traditional minimum supply demand method. Furthermore, we study alternative upwind methods which are expected to be even faster.

1.3.5 Accuracy measures

We develop two novel accuracy measures that are especially well suited to assess the accuracy of traffic flow models and simulations. They quantify phase and diffusion errors which are important in traffic flow context, unlike more commonly used measures of accuracy such as the root mean square error (RMSE). The phase error measures whether congestion in the simulation occurs at the same moment and at the same place as in the exact solution of the model equations or in real traffic. This is important in applications where one wants to know whether congestion will spill back to, for example,

an off ramp. Another important property of traffic flow (and traffic flow models) is that there are sharp discontinuities which do not smooth out over time. The diffusion error measures whether the discontinuities are preserved in the simulation. We only apply the measures to compare simulation results obtained using numerical methods with the analytical solution of the problem. That is, we quantify errors that are made in the step from model to discretization in the traffic flow modeling cycle (Figure 1.1). However, we foresee that these measures can be applied in other steps in the traffic flow modelling cycle as well. They can be applied to quantitatively compare traffic flow models and simulations or traffic state estimations with observations.

1.4 Application and practical contributions

The applications and practical contributions of this dissertation are partly related to the application of the Fastlane model. In this section we also discuss other applications and practical contributions.

1.4.1 Applications of Fastlane

Our traffic flow model is a deterministic model that includes multiple user classes. When compared to other multi-class models it is a relatively simple model, especially when formulated in the Lagrangian coordinate system. Because of its simplicity we are able to develop numerical methods which allow for efficient simulations. Because of these properties, the model is well suited for applications in which it is important that the model is deterministic and gives quick and accurate simulation results. Examples of such applications are:

- On-line traffic state estimation
- Real time traffic state prediction
- Traffic management
- Dynamic traffic assignment
- Training of traffic controllers
- Planning of evacuation strategies

All these applications serve the goal of improving transportation systems and especially motorway networks. However, vehicles and drivers on motorway networks can be highly heterogeneous. For example, passenger cars are usually shorter than trucks, have higher maximum velocities and acceleration. Furthermore, trucks have a large impact on traffic flow: only a small percentage of trucks can reduce the capacity of a road substantially (Elefteriadou et al., 1997; Kockelman, 1998). Therefore, in regions with many trucks, such as around logistics hubs, it is important to include the heterogeneity of vehicles and drivers in the traffic flow model.

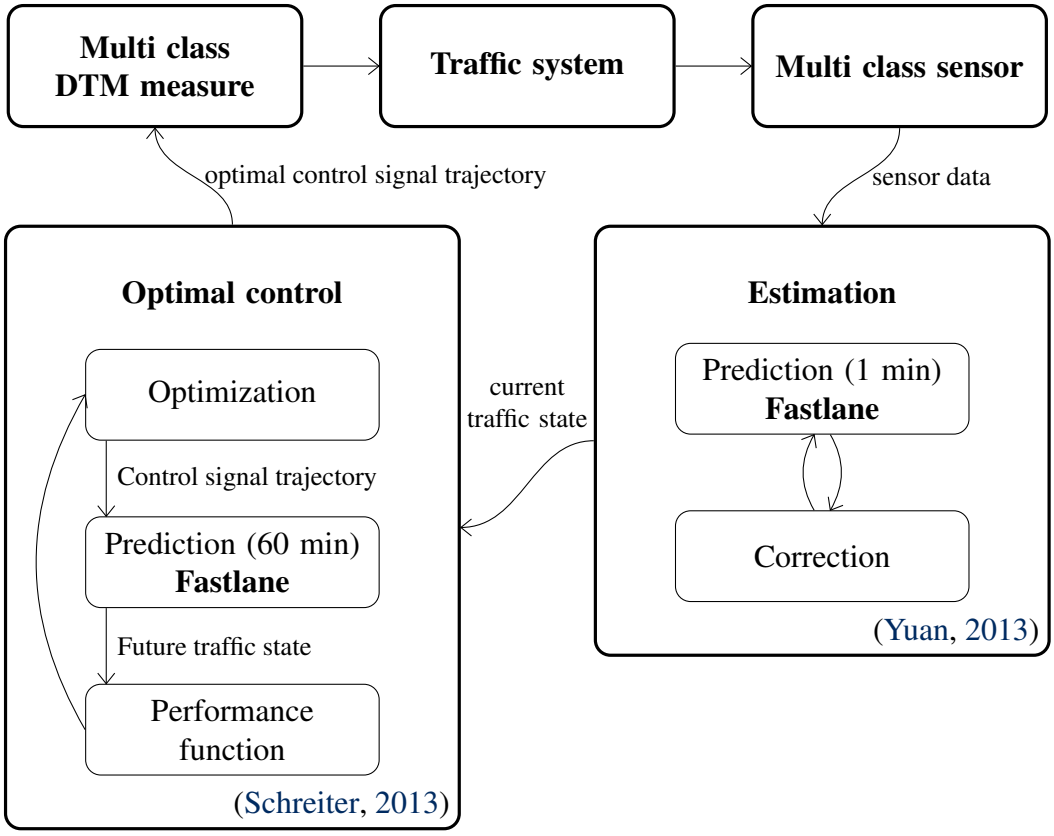

Figure 1.2 *Control loop for multi-class model predictive control using Fastlane.*

An example of the application of our Fastlane model is shown in Figure 1.2. It shows how sensors measure traffic characteristics such as class-specific flows and velocities. The data is then used to estimate the current traffic state. Based on this estimation a prediction of one hour ahead is made. This is done within an optimization loop: different traffic management scenarios are tested and their performance is assessed. The scenarios include different measures for different classes. For example, trucks may be instructed to use one route, while passenger cars are directed to another route. The optimal control scenario is then implemented in reality. The traffic system reacts to this and the loop starts again. Fastlane is especially well suited for this application because:

- Fastlane includes multiple vehicle/driver classes.
- Fastlane allows for efficient state estimation using Kalman filtering and the Lagrangian coordinate system (Yuan, 2013).
- Fastlane allows for quick and accurate predictions that can be used within an optimization loop (Schreiter, 2013).

1.4.2 Other applications and practical contributions

Other applications and practical contributions of this dissertation include:

- A step-by-step plan for the qualitative assessment of traffic flow models.

- Efficient numerical methods for traffic flow models.
- Accuracy measures for traffic flow models and simulation tools.

They are discussed in more detail below.

Our method for the qualitative assessment of traffic flow models helps in selecting an appropriate model. By first assessing a (new) model this way, it can be shown whether the model has qualitatively desirable properties. If it has, the model may be worth the effort of calibrating it to the problem at hand. If not, there is no need to try to calibrate and apply the model because it will not be able to reproduce observations accurately enough.

Once a traffic flow model has been evaluated as a qualitatively good model, the accuracy measures are useful in calibrating and validating the model. They can be applied to evaluate errors that are especially important in traffic flow, unlike most commonly used accuracy measures such as the RMSE.

Finally, we develop efficient numerical methods to be applied to Fastlane. However, they can also be applied to other multi-class or mixed-class macroscopic traffic flow models. They include methods to simulate traffic flow over nodes, which are essential elements if one wants to simulate traffic on a network.

1.5 Dissertation outline

The content of the main part of this dissertation is schematically outlined in Figure 1.3. The figure shows that the research focusses on two issues: multi-class traffic flow modelling and efficient simulation methods for networks with this type of models. In both parts we apply the Lagrangian formulation of a generic multi-class traffic flow model, which is introduced in the central chapter (Chapter 6).

In the first part of this dissertation we develop a macroscopic traffic flow model: Fastlane. The outline of this part is as follows. In Chapter 2 we review the existing literature on traffic flow models. The historical development of traffic flow models is condensed in a model tree, showing the genealogy of traffic flow models. We identify gaps and argue why we continue with the development of a multi-class kinematic wave model. In Chapter 3 we propose a theoretical framework for the development and analysis of multi-class kinematic wave models. The framework consists of a set of principles and a set of requirements. The principles are later used in the development of Fastlane. The requirements are later used to assess whether Fastlane and similar models have some important qualitative properties. The actual model development of Fastlane is described in Chapter 4. This chapter focusses on the model equations and their derivation and interpretation. In Chapter 5 we generalize the Fastlane model. This results in a generic single-pipe multi-class kinematic wave model in which all such models known from literature (Chapter 2) are contained. Finally, some results

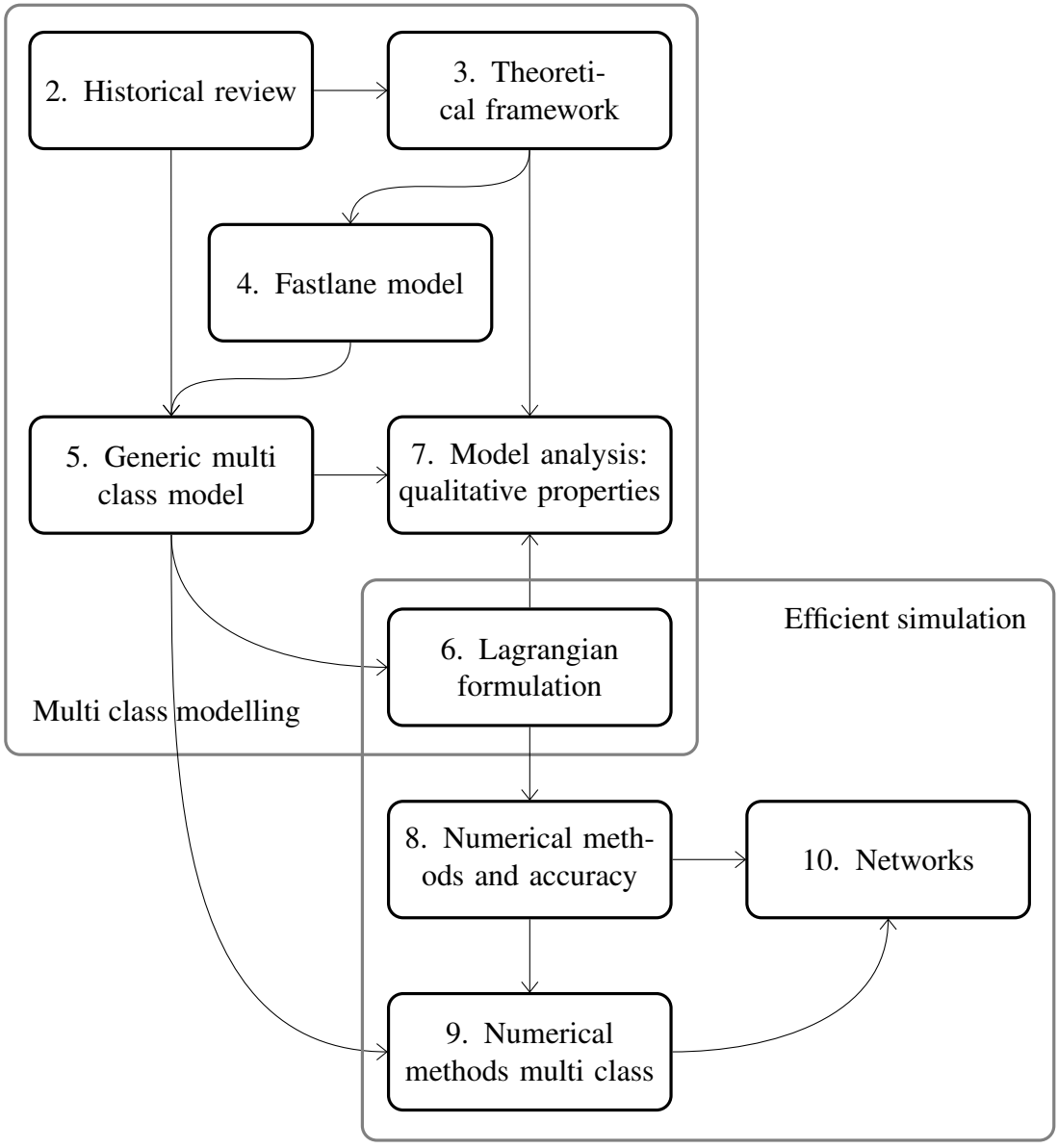

Figure 1.3 *Overview of the content of this dissertation.*

from Chapter 6 (outlined below) are used in Chapter 7 to assess the generalized kinematic wave model and all specific models known from theliterature. It is assessed whether the models satisfy the requirements proposed in Chapter 3.

In Chapter 6 we reformulate the generalized multi-class kinematic wave model in the Lagrangian coordinate system. The Lagrangian coordinate system moves with the vehicles. The reformulated model allows for an easier assessment of the requirements (Chapter 7). Furthermore, the Lagrangian formulation is used in the second part of this dissertation to develop more efficient simulation methods.

In Chapter 8 we develop numerical methods for mixed-class kinematic wave models. Furthermore, we develop accuracy measures and apply them in the assessment of the accuracy of numerical methods. In Chapter 9 we develop the numerical methods further for multi-class kinematic wave models. All numerical methods in Chapter 8 and 9 are developed for homogeneous roads without considering inflows or outflows. In Chapter 10 the numerical methods are developed further to include inflow and outflow boundaries and inhomogeneities including ramps. Finally, Chapter 11 concludes this dissertation by summarizing the main findings and applications and by suggesting future research directions.

Chapter 2

State-of-the-art traffic flow modelling

Traffic flow models have been developed and used since the beginning of the twentieth century. Traffic flow models are part of a long history of mathematical modelling of physical and other systems. Scientists and engineers use these models as simplified representations of real-world systems. They are applied to explain and predict weather or chemical reactions, behaviour of materials or humans, fluid or traffic flow, etc. In this chapter we present a review of traffic flow models. The discussion of the relations between traffic flow models and other models is postponed until the end of this chapter.

The review follows the historical lines of the development of traffic flow models since they were first studied in the 1930's. Previous reviews focus on the current state-of-the-art and review the models on their current value (Papageorgiou, 1998; Brackstone & McDonald, 1999; Zhang, 2001; Hoogendoorn & Bovy, 2001b; Helbing, 2001; Kerner, 2009; Treiber & Kesting, 2010; Treiber et al., 2010; Orosz et al., 2010; Wilson & Ward, 2011; Bellomo & Dogbe, 2011). We aim to take one step further back and give an historical overview of the highlights in traffic flow modelling. This approach shows better how traffic flow models have developed and how different types of models are related to each other. Furthermore, it forms the basis of our next step in traffic flow modelling, using a multi-class approach. To show the historical development of traffic flow models we introduce a model tree, see Figure 2.1. A more detailed version of the model tree is included as Appendix A. The rest of this chapter is devoted to discussing the model tree, the models in it and the relations between them.

All models in the tree have one common ancestor: the fundamental relation (or fundamental diagram). The other three families consist of micro-, meso- and macrosopic models. After the introduction of the fundamental relation in the 1930's, microscopic and macroscopic models were introduced simultaneously in the 1950's. Mesoscopic models are about a decade younger. The model tree shows that particularly over the last two decades, the fundamental relation and all three types of models have been developed further and many offshoots can be recognized. The fundamental diagram relates the headways (front-to-front following distance) to vehicle velocity. How headways and velocities change can be described by micro-, meso- or macroscopic models.

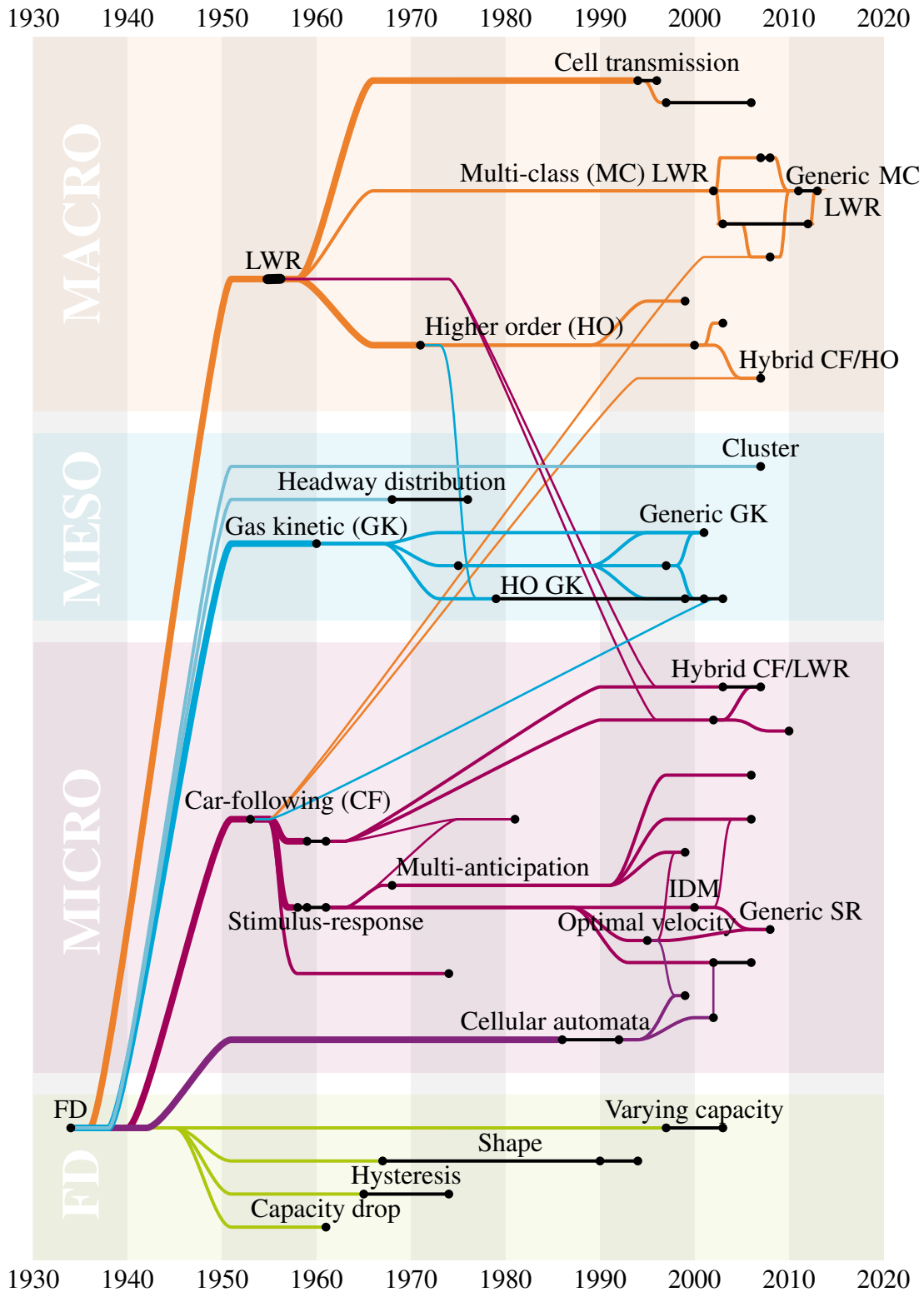

Figure 2.1 *Genealogical tree of traffic flow models. Grey lines indicate descent, black dots indicate publications, black lines indicate that the model has (or multiple very similar models have) been published multiple times. Most labels are omitted for readability. A larger and labeled version is included in Appendix A.*

On the one hand, microscopic models distinguish and trace the behaviour of each individual vehicle. On the other hand, macroscopic models aggregate vehicles and traffic is described as a continuum. Mesoscopic models are categorized in between micro- and macroscopic models as their aggregation level is between those of micro- and macroscopic models. Categorizing traffic flow models can be done according to other criteria such as whether the variables are continuous or discrete, the level of detail, stochastic or deterministic process representation and the scale of the application (large networks vs. links and intersections), type of model equations ((partial) differential equations, discrete model equations, static models) or the number of phases described by the model (Hoogendoorn & Bovy, 2001b; Treiber & Kesting, 2010; Treiber et al., 2010). Since the development of traffic flow models has followed largely the family lines of micro-, meso- and macrosopic models, we use this traditional categorization throughout the rest of this chapter.

In the model tree we omit models related to lateral behaviour such as lane changing and gap acceptance models. This would make the model tree, and especially the microscopic family much more extended without adding much to our aim of setting up a basis for the development of a novel multi-class kinematic wave model. For the same reasons, we only include models for homogeneous roads. The discussion on node models describing the behaviour at inhomogeneities such as on- and off ramps is postponed until Chapter 10. Moreover, we do extensively discuss the branch of multi-class kinematic wave models. By doing so, we can later (in Chapter 5) relate and compare our newly introduced model to other similar models. However, we do not include multi-class extensions of microscopic models. Again, this would have made the model tree much more extended without adding much insight since almost any microscopic model can be, and has been, formulated with multiple classes.

In this chapter we first discuss the fundamental relation in more detail, see Section 2.1. We then discuss models in each of the other three families: Section 2.2 presents microscopic models, Section 2.3 presents mesoscopic models and Section 2.4 presents macroscopic models. Section 2.5 discusses some relations between traffic flow models and other similar models, it reviews critical remarks on traffic flow models. Section 2.6 concludes this chapter with arguments as to why we have chosen to further develop the branch of multi-class kinematic wave traffic flow models.

2.1 Fundamental diagram

Most traffic flow models are based on the assumption that there is some relation between the distance between vehicles (headway or spacing) and their velocity, e.g., as in Figure 2.2(d). The relation between spacing and velocity was first studied by Greenshields (1934) and called the fundamental relation (or fundamental diagram) later. Taking one step further back in time, Knight (1924) was the first to discuss traffic equilibrium, in an example that has later become famous as Wardrop's principle. However,

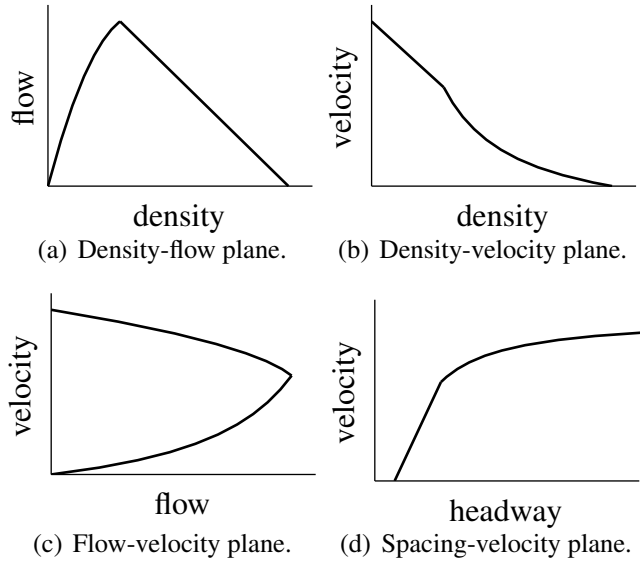

(a) Density-flow plane. (b) Density-velocity plane.

(c) Flow-velocity plane. (d) Spacing-velocity plane.

Figure 2.2 *Fundamental relations in different planes.*

Greenshields is often regarded as the founder of traffic flow theory as he was the first to observe and describe the movement of vehicles (Kühne, 2011). In fact, the article (Kühne, 2011) was presented on a conference devoted to the 75th anniversary of the introduction of the fundamental diagram by Greenshields (Kühne & Gartner, 2011).

In this section we consider the fundamental relation as (part of) a traffic flow model. Alternatively, the fundamental relation (or fundamental diagram) is often used to present observed traffic states. In Section 2.1.4 we discuss how these observations are used to adapt the fundamental relation which is applied in a model.

2.1.1 Definition of variables

Originally Greenshields studied the relation between the variables spacing and velocity. However, the fundamental relation can also be expressed in other variables such as density (average number of vehicles per unit length of road) and flow (average number of vehicles per time unit), see Figure 2.2. These variables were first defined rigorously by Edie (1965). Figure 2.3 illustrates the definitions. Edie defines flow as the flow in an area A with length $\mathrm{d}x$ and duration $\mathrm{d}t$ which is determined by the number of vehicles $N(A)$ that travel through the area and the distance y_n they travel through the area:

$$q_{\text{area}} = \frac{\sum_{n=1}^{N} y_n}{\mathrm{d}x\,\mathrm{d}t} \tag{2.1}$$

Similarly, Edie defines density as the density in an area using the time r_n vehicle n is present in the area:

$$\rho_{\text{area}} = \frac{\sum_{n=1}^{N} r_n}{\mathrm{d}x\,\mathrm{d}t} \tag{2.2}$$

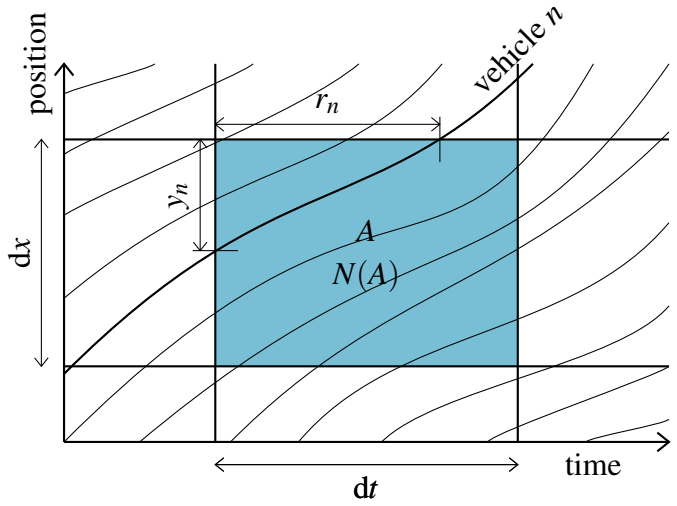

Figure 2.3 *Time-space region with some vehicle trajectories to illustrate Edie's definitions of flow and density. $N(A)$ is the number of vehicles that travel through the area A.*

Edie concludes with the intuitive definition of velocity in an area by dividing the total distance traveled by the total time spent:

$$v_{\text{area}} = \frac{q_{\text{area}}}{\rho_{\text{area}}} = \frac{\sum_{n=1}^{N} y_n}{\sum_{n=1}^{N} r_n} \tag{2.3}$$

These are workable definitions to extract flow, density and velocity from observations of a large area A with many vehicles N. Edie shows that they can even be applied to long road sections observed over a short period of time or, vice versa, short road sections observed over a long period of time. However, for other applications such as macroscopic traffic flow models, flows, densities and velocities at points in (x,t) are considered. Therefore, we have to assume that traffic is a continuum flow. In Section 2.5.1 we argue why this is a reasonable assumption. The assumption implies that N becomes continuous (instead of discrete). Furthermore, N is assumed to be continuously differentiable in x and t. Edie's definitions are then not applicable directly. However, by decreasing the area A such that it becomes a point, they reduce to definitions of flow, density and velocity at points.

The local and instantaneous flow, density and velocity are found using the procedure described by Leutzbach (1988). To find the local and instantaneous flow (the flow at a point in (x,t)) we decrease the length of the road section: $\mathrm{d}x \to 0$. This yields the local flow through a cross section x. Afterwards, we decrease the time $\mathrm{d}t \to 0$ and find:

Definition 2.1 ((local and instantaneous) flow)**.**

$$q(x,t) = \lim_{\mathrm{d}t\to 0} \lim_{\mathrm{d}x\to 0} \frac{\sum_{n=1}^{N} y_n}{\mathrm{d}x\,\mathrm{d}t} = \lim_{\mathrm{d}t\to 0} \underbrace{\frac{N(x,[t,t+\mathrm{d}t])}{\mathrm{d}t}}_{=q_{\text{local}}(x)} \tag{2.4}$$

To find the local and instantaneous density we decrease the time: $\mathrm{d}t \to 0$. This yields the instantaneous density through a cross section t. Afterwards, we decrease the length $\mathrm{d}x \to 0$ and find:

Definition 2.2 ((local and instantaneous) density)**.**

$$\rho(x,t) = \lim_{\mathrm{d}x\to 0}\lim_{\mathrm{d}t\to 0}\frac{\sum_{n=1}^{N} r_n}{\mathrm{d}x\,\mathrm{d}t} = \lim_{\mathrm{d}x\to 0}\underbrace{\frac{N([x,x+\mathrm{d}x],t)}{\mathrm{d}x}}_{=\rho_{\text{instantaneous}}(x)} \tag{2.5}$$

Finally, similar to Edie's definition of velocity (2.3), we define the local and instantaneous velocity:

Definition 2.3 ((local and instantaneous) vehicle velocity)**.**

$$v(x,t) = \frac{q(x,t)}{\rho(x,t)} \tag{2.6}$$

In addition, we define local and instantaneous spacing:

Definition 2.4 ((local and instantaneous) vehicle spacing)**.**

$$s(x,t) = \frac{1}{\rho(x,t)} \tag{2.7}$$

2.1.2 Shapes of the fundamental relation

In 1934, Greenshields proposed a fundamental relation that is linear in the spacing-velocity plane. However, his name has now been linked to the fundamental relation that he proposed one year later (Greenshields, 1935). This fundamental relation is linear in the density-velocity plane and thus parabolic in the density-flow plane, see Figures 2.4(a) and 2.5(a). Since then, many other shapes of fundamental relations have been proposed. The Daganzo (1994) fundamental relation is probably the most widespread. It is bi-linear (triangular) in the density-flow plane, see Figures 2.4(b) and 2.5(b). Figures 2.4(c) and 2.5(c) show the Smulders fundamental diagram (Smulders, 1990), which is a combination of the previous two: it is parabolic for low densities and linear for high densities (parabolic-linear). It satisfies, unlike Greenshields' fundamental relation, later findings that the relation between density and flow is (approximately) linear at large densities (Cassidy & Windover, 1995; Kerner & Rehborn, 1996; Treiber & Helbing, 2002). However, it does represent that also at low densities vehicles interact and their velocity decreases with an increase in density (Hoogendoorn, 1999, Chapter 8), unlike in Daganzo's fundamental relation. Finally, Figures 2.4(d) and 2.5(d) show the Drake fundamental relation (Drake et al., 1967). For a more detailed overview of different shapes of fundamental relations we refer to (Li, 2008).

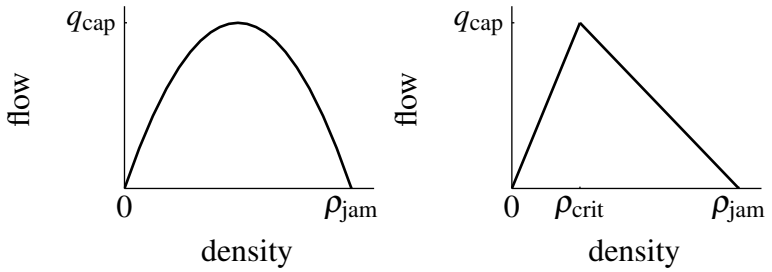

(a) Greenshields (parabolic). (b) Daganzo (bi-linear).

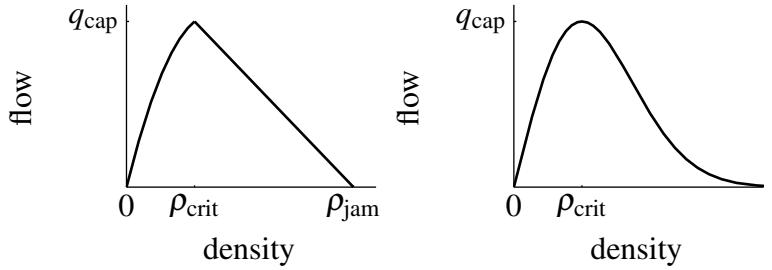

(c) Smulders (parabolic-linear). (d) Drake (bell shaped).

Figure 2.4 *Different shapes of density-flow fundamental relations.*

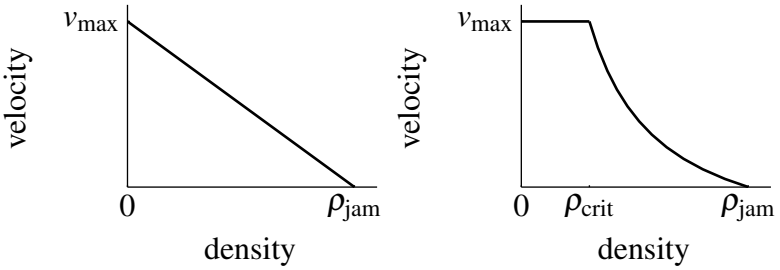

(a) Greenshields. (b) Daganzo.

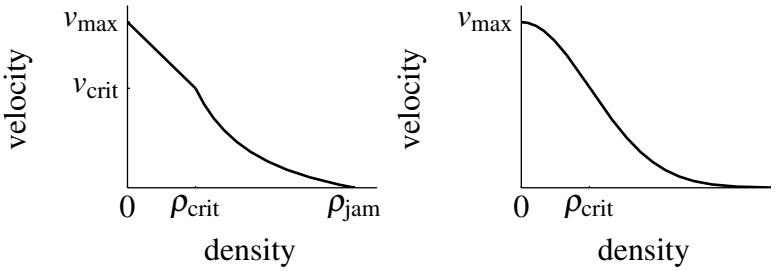

(c) Smulders. (d) Drake.

Figure 2.5 *Different shapes of density-velocity fundamental relations.*

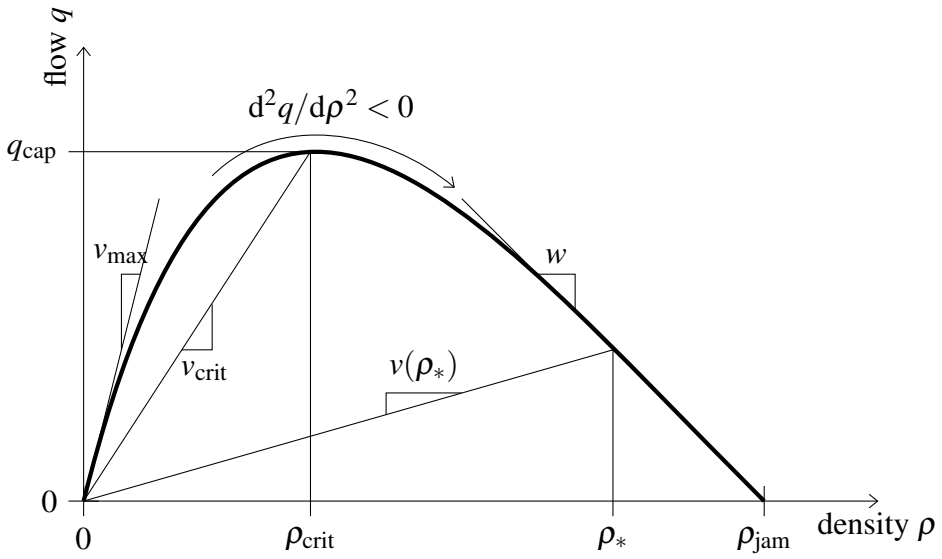

Figure 2.6 *A sound fundamental relation and its properties, according to Del Castillo (2012).*

2.1.3 Properties and requirements

Figure 2.6 illustrates some properties and requirements of fundamental relations. The properties of a sound fundamental relation are discussed by Del Castillo (2012):

1. Velocity ranges from zero to a maximum value $v_{\max}$.
2. Density ranges from zero to a maximum value ρ_{jam}.
3. Velocities at the extreme density values are $v(0) = v_{\max}$ and $v(\rho_{\mathrm{jam}}) = 0$.
4. Flows at the extreme density values are $q(0) = q(\rho_{\mathrm{jam}}) = 0$.
5. Maximum velocity and congestion wave speed are the slopes of the fundamental relation at the extreme density values: $v_{\max} = \mathrm{d}q/\mathrm{d}\rho\,(0)$ and $w = \mathrm{d}q/\mathrm{d}\rho\,(\rho_{\mathrm{jam}})$.
6. The fundamental relation is strictly concave: $\mathrm{d}^2q/\mathrm{d}\rho^2 < 0, \forall 0 < \rho < \rho_{\mathrm{jam}}$.

The first three properties can be regarded as requirements following from traffic flow fundamentals: they result from easily observable facts. First, velocities are bounded from above by (legal or technical) maximal vehicle velocity which is reached (in the limit) if there are no other vehicles. Second, vehicles take up space and there is a maximum number of vehicles that can be fitted on a certain road length. At this maximum density, vehicles can not move. Finally, both velocity and density can not be negative. The fourth and fifth property follow from the first three requirements combined with the definition of velocity (Definition 2.3). The fifth property furthermore includes the definition of congestion wave velocity w. Del Castillo (2012) argues that the sixth property is necessary to define a traffic flow model with a unique solution. However, there are no reasons to assume that real traffic can not behave in a way that would be described by a fundamental relation that is not strictly concave. In fact, Zhang (2001)

shows that a unique solution can be found even if the fundamental relation is convex and Herbin & Leclercq (2011) show that it is sufficient if the density-flow fundamental relation is Lipschitz-continuous. Furthermore, it is reasonable to assume that velocity does not increase with increasing density ($dv/d\rho \leq 0$). Del Castillo does not require that directly. However, it is a necessary, but not sufficient condition for his last property on the strict concavity of the fundamental relation.[1]

Another important property of fundamental relations is the existence of a maximum flow, or capacity: $q_{cap} = \max_{0<\rho<\rho_{jam}} q(\rho)$. Assuming the above requirements are satisfied, the capacity is related to a single density called critical density ρ_{crit} and a single velocity called critical velocity v_{crit}, with $q_{cap} = \rho_{crit} v_{crit}$. The critical density separates the fundamental relation into two parts: 1) a free flow branch with densities below critical, velocities above critical and increasing flow for increasing density and 2) a congestion branch with densities above critical, velocities below critical and a decreasing flow for increasing density.

The Greenshields fundamental relation is the only one of the fundamental relations introduced in Section 2.1.2 that satisfies all of Del Castillo's criteria. The other ones (the Daganzo, Smulders and Drake fundamental relation) are not strictly concave, though the first two are concave. Furthermore, in the Drake fundamental relation there is no jam density for which velocity and flow are zero.

2.1.4 Scatter in the fundamental relation

For many decades, it has been recognized that the points in observed density-flow plots usually are wide scattered, see Figure 2.7. (Zhang, 1999; Laval, 2011) argue that much of the scatter can be explained by non-equilibrium traffic conditions. Zhang defines traffic to be in equilibrium if over a sufficiently long time and road length velocity and density do not change: $\partial v/\partial t = 0$, $\partial \rho/\partial t = 0$, $\partial v/\partial x = 0$ and $\partial \rho/\partial x = 0$. Only points in the scatter plot that satisfy these criteria can be used to fit the fundamental relation. This is then called the equilibrium fundamental relation.

Furthermore, it has been argued that fundamental relations consisting of a continuous line, such as those discussed in the previous sections are not realistic. Edie (1961); Cassidy & Bertini (1999) explain part of the scatter with a capacity drop: just before the onset of congestion the outflow out of a bottleneck is higher than in congestion, see Figure 2.8(a). This phenomenon is still verified and studied nowadays (Coifman & Kim, 2011). The capacity drop has been explained by a low acceleration rate of vehicles leaving congestion (Treiterer & Myers, 1974). Slow acceleration can also be included in a fundamental diagram with hysteresis (Newell, 1965; Zhang, 1999), see Figure 2.8(b). From a different perspective, Kerner (2009) argues that observed scatter plots show too much scatter to derive a unique fundamental relation from, cf. (Kerner

[1] Application of the chain rule shows that if the $q(\rho)$ is concave then $dv/d\rho \leq 0$. That is: $d^2q/d\rho^2 = d^2(\rho v)/d\rho^2 = \rho dv/d\rho + v$ is negative only if $dv/d\rho \leq 0$, because $\rho \geq 0$ and $v \geq 0$.

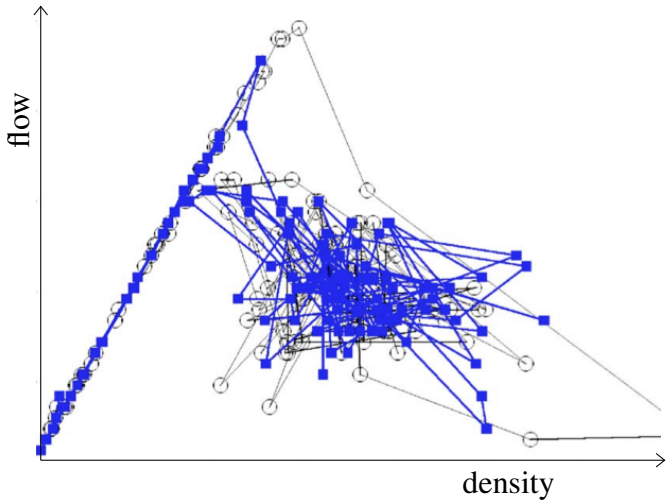

Figure 2.7 *Scatter in an observed density-flow plot (picture adapted from Treiber et al. (2006b)).*

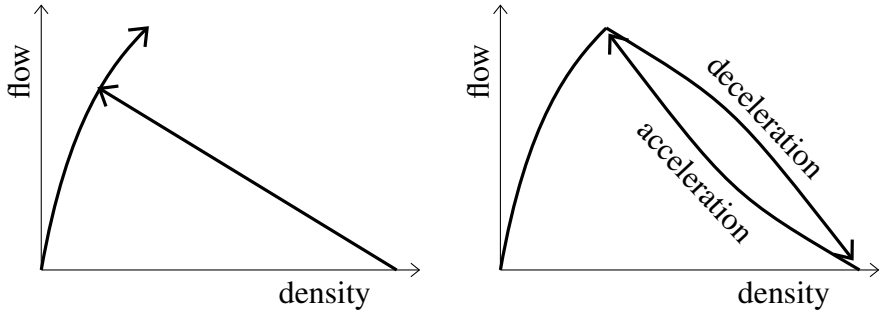

(a) Fundamental relation with capacity drop.

(b) Fundamental relation with hysteresis.

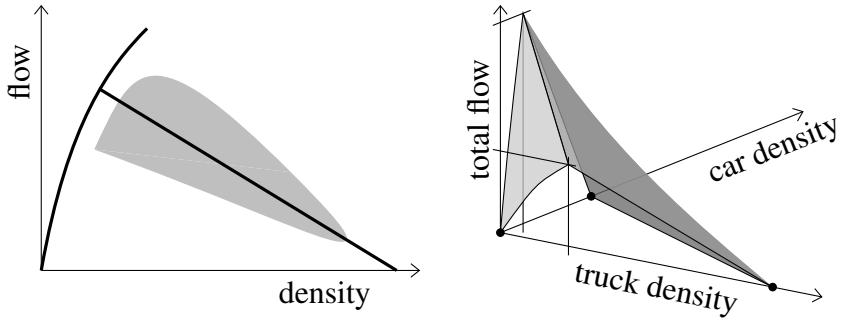

(c) Three-Phase fundamental 'relation': lines and grey area are admissible traffic states.

(d) Three-dimensional fundamental relation with multi-class approach.

Figure 2.8 *Fundamental 'relations' based on scatter in observations.*

& Rehborn, 1996; Kerner, 2004). He proposes to use a Three-Phase approach characterized by the existence of three phases, one of them featuring wide scatter in the density-flow plane. In his theory the fundamental relation is replaced by two lines and a two-dimensional region, see Figure 2.8(c).

Both fundamental relations with capacity drop (Figure 2.8(a)) and with hysteresis (Figure 2.8(b)) imply a non-unique fundamental relation: at a certain density (usually just above (outflow) capacity) the flow is not uniquely determined by the density but also depends on previous traffic states. Therefore, for a unique solution of the model, additional assumptions are needed on transitions between the branches of the fundamental relation (Zhang, 2001). Furthermore, the concavity requirement (see Section 2.1.3) is usually not satisfied by fundamental relations with capacity drop or hysteresis. The density-flow plane proposed by Kerner & Rehborn (1997); Kerner (2009) (Figure 2.8(c)) is even 'less unique'. Treiber et al. (2010) show that simulation results of simpler models with a unique fundamental diagram are similar to those of Three-Phase models, when parameters are chosen appropriately.

Finally, heterogeneity among vehicles and drivers has been used to explain scatter in observed density-flow plots. In this approach it is assumed that flow not only depends on density, but also on the traffic composition: a large fraction of trucks, which usually drive at low speeds and take much space, will result in a low flow. This leads to three-dimensional fundamental relations such as in Figure 2.8(d) (Chanut & Buisson, 2003). Its main advantage is that it is uniquely determined by the current densities and it does not depend on previous traffic states. Furthermore, the fundamental relation can satisfy all requirements proposed by Del Castillo (2012). We will come back to the fundamental relation with heterogeneity in Section 2.4.2.

Fundamental relations, whether equilibrium or non-equilibrium, unique or non-unique, are crucial in traffic flow models. One of the model assumption is that traffic is in a state on the fundamental relation, or that it tends towards it. Meso- and macroscopic models mostly include fundamental relations explicitly. Microscopic models usually have some underlying assumptions on a fundamental relation which can be revealed by careful analysis of the model or simulation. The other components of micro- meso- and macroscopic traffic flow models will be discussed in the next sections.

2.2 Microscopic models

The earliest family in the model tree incorporating dynamics are microscopic models. They are based on the assumption that drivers follow their leader and adjust their behaviour to that of the leading vehicle. Microscopic modelling has shown to be a fruitful line of thought, which is illustrated by the large part of the model tree taken up by this family. Microscopic models describe the longitudinal and lateral behaviour of individual vehicles. Only longitudinal behaviour is discussed here. In microscopic models vehicles are numbered to indicate their order: n is the vehicle under consideration,

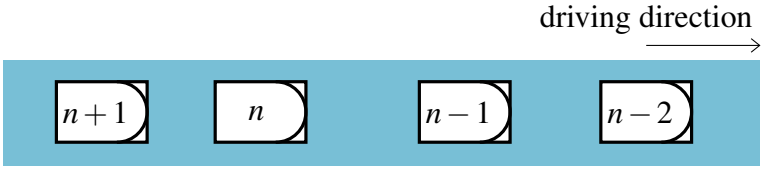

Figure 2.9 *Vehicle numbering in microscopic traffic flow models (and macroscopic models in Lagrangian formulation).*

$n-1$ its leader, $n+1$ its follower, etc., see Figure 2.9. The behaviour of each individual vehicle is modeled in terms of the position of the front of the vehicle x_n, velocity $v_n = \mathrm{d}x_n/\mathrm{d}t$, acceleration $a_n = \mathrm{d}v_n/\mathrm{d}t = \mathrm{d}x_n^2/\mathrm{d}t^2$ or a combination of the three.

Three types of car-following models will be discussed in Sections 2.2.1 (safe-distance models), 2.2.2 (stimulus-response models) and 2.2.3 (action point models). Section 2.2.4 discusses extensions of car-following models. Section 2.2.5 discusses the most recent branch of microscopic models, namely cellular-automata.

2.2.1 Safe-distance models

The earliest car-following models include a car-following rule based on safe following distance. Pipes (1953) proposes to express the position of the leader as a function of the position of its follower:

$$x_{n-1} = x_n + d + T v_n + l_{n-1}^{\mathrm{veh}} \tag{2.8}$$

with T the minimum time headway (excluding vehicle length), d the distance between two vehicles at standstill and l_{n-1}^{veh} length of the leading vehicle, see Figure 2.10. Tv_n is interpreted by Pipes as the "legal distance" between vehicle $n-1$ and n. By differentiating with respect to time, this model is reformulated as:

$$a_n = \frac{v_n - v_{n-1}}{T} \tag{2.9}$$

This formulation shows that a driver accelerates (decelerates) when the front gap becomes larger (smaller) and that this effect is stronger if the minimum time headway T is smaller.

Kometani & Sasaki (1961) derive a car-following model from basic Newtonian equations of motion. It is assumed that a driver acts such that he can avoid a collision even if the leader would act 'unpredictably'. Effectively, they replace the distance at standstill d in Pipes' model with a velocity-dependent term. Furthermore, their formulation includes a time delay τ. A positive τ represents that it takes some time between a change in the behaviour of a vehicle and the actual reaction of its follower to this change. It includes the reaction time of the driver, but can also depend on his perception and the time it takes between noticing that action is needed/desired and actual braking or accelerating.

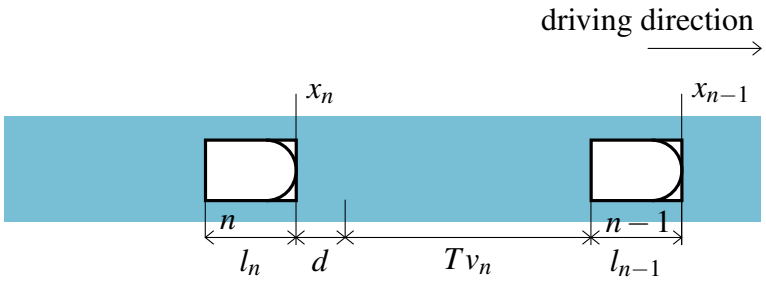

Figure 2.10 *Parameters of Pipes' safe-distance model.*

Gipps (1981) refines safe-distance car-following models by assuming that 'the driver travels as fast as safety and the limitations of the vehicle permit':

$$v_n(t+\tau) = \min \left\{ v_n(t) + 2.5 a_{\max} \tau \left(1 - \frac{v_n(t)}{v_{\max}}\right) \sqrt{0.25 - \frac{v_n(t)}{v_{\max}}}, \right.$$
$$\left. a_{\min}\tau + \sqrt{a_{\min}^2 \tau^2 - a_{\min}\left(2\big(x_{n-1}(t) - x_n(t) - s_{\text{jam}}\big) - v_n(t)\tau - \frac{v_{n-1}(t)^2}{b}\right)} \right\} \quad (2.10)$$

with $a_{\max}$ maximum acceleration, $a_{\min}$ maximum deceleration (minimum acceleration), $v_{\max}$ the desired (maximum) velocity and s_{jam} jam spacing. Jam spacing is the front-to-front (or equivalently rear-to-rear) distance between two vehicles at standstill. Therefore, if vehicle length is assumed to be equal for all vehicles ($l_n^{\text{veh}} = l^{\text{veh}}$) then $s_{\text{jam}} = d + l^{\text{veh}}$. Effectively, Gipps' approach introduces two regimes: one in which the vehicle itself limits its velocity (the top part in equation (2.10)), and one in which the safe distance to the leader limits the vehicles velocity (the bottom part in the equation).

The model tree shows one more development in safe-distance models. In the early years of car-following models, Newell (1961) proposed a simple safe-distance model with delay:

$$v_n = v_n\big(x_{n-1}(t-\tau) - x_n(t-\tau)\big) \quad (2.11)$$

with the function v_n at the right hand side a fundamental relation and τ the delay time. Later, he proposed another simple safe-distance model (Newell, 2002):

$$x_n(t+\tau_n) = x_{n-1}(t) - s_{\text{jam},n} \quad (2.12)$$

It is assumed that a vehicle follows the trajectory of its leader, translated by τ_n and $s_{\text{jam},n}$. We note that both reaction time τ_n and jam spacing $s_{\text{jam},n}$ may differ for each vehicle and driver. Daganzo (2006) shows the equivalence of such a simple car-following model with certain simple cellular-automata and kinematic wave models. Moreover, Leclercq et al. (2007) show that the model (2.12) is equivalent to a discretized macroscopic model if the fundamental relation $q(\rho)$ is triangular. To show this relation, the macroscopic LWR model is formulated in the Lagrangian (moving)

coordinate system. The Lagrangian formulation of macroscopic models will be discussed more extensively in Chapter 6 and further. The formulation is also applied to develop a hybrid model that couples the microscopic Newell car-following model with the macroscopic LWR model (Leclercq, 2007a). However, already in 2003, Bourrel & Lesort proposed another hybrid model combining Newell's earlier safe-distance model (2.11) with the LWR model. Laval & Leclercq (2010) propose a car-following model similar to that by Newell and extended it to include differences between 'timid' and 'aggressive' drivers.

2.2.2 Stimulus-response models

The second branch of car-following models consists of stimulus-response models. It is assumed that drivers accelerate (or decelerate) as a reaction to three stimuli:

1. own current velocity $v_n = \dfrac{\mathrm{d}x_n}{\mathrm{d}t}$
2. spacing with respect to leader $s_n = x_{n-1} - x_n$
3. relative velocity with respect to leader (receding rate) $\dot{s} = \dfrac{\mathrm{d}s_n}{\mathrm{d}t} = v_{n-1} - v_n$

It can be seen from the model tree that in the late 1950's and early 1960's there was a rapid development of these models (Chandler et al., 1958; Herman et al., 1959; Helly, 1961). The efforts consolidated in the now famous GHR-model, named after Gazis, Herman, & Rothery (1961):

$$a_n(t) = \gamma \frac{\big(v_{n-1}(t)\big)^{c_1}}{\big(s_n(t-\tau)\big)^{c_2}} \dot{s}_n(t-\tau) \tag{2.13}$$

$\gamma \frac{(v_{n-1}(t))^{c_1}}{(s_n(t-\tau))^{c_2}}$ is considered as the sensitivity of vehicle/driver n. γ is the sensitivity parameter and c_1 and c_2 are parameters that are used to fit the model to data. The receding rate $\dot{s}_n(t-\tau)$ is considered as the stimulus, the acceleration $a_n(t)$ as the response, hence the name 'stimulus-response' model.

Since those early developments a lot of work has been done in calibrating and validating this and other similar models. However, in 1999, Brackstone & McDonald concluded that stimulus-response models are being used less frequently, mainly because of contradictory findings on parameter values. Nevertheless, the model tree shows that in the last one or two decades many new models have been developed and it seems that stimulus-response models have become popular again. Wilson & Ward (2011) even argue that there are too many microsimulation models and that researchers should try to focus on a small subset that has good qualitative properties, which will be discussed at the end of this section. Some of the most popular more recent stimulus-response models are discussed below.

Bando et al. (1995) introduced the optimal velocity model (OVM) assuming that drivers accelerate (or decelerate) to their optimal velocity, which is a function of the headway:

$$a_n(t) = \gamma\big(v^*\big(s_n(t)\big) - v_n(t)\big) \tag{2.14}$$
$$v^*(s) = v_{\max}\big(\tanh(s-c_1)+c_2\big) \tag{2.15}$$

with γ the sensitivity parameter and c_1 and c_2 parameters of the optimal velocity function $v^*(s)$ such that $\tanh(s_{\text{jam}}-c_1)+c_2=0$. In this model, it is very clear how an equilibrium fundamental relation, in this case the optimal velocity function $v^*(s)$, is incorporated in a microscopic model. Bando et al. (1998) extended their model by introducing delay τ: in the right-hand side of (2.14) t is replaced by $t-\tau$. The model now takes into account that drivers do not react immediately to a stimulus, but it takes some time (delay) before they accelerate or decelerate.

The Intelligent Driver Model (IDM) by Treiber et al. (2000) was developed to better reproduce many different traffic states. The acceleration is described by:

$$a = a_{\max}\left(1-\left(\frac{v}{v_{\max}}\right)^{\delta}-\left(\frac{s^*(v,\dot{s})}{s}\right)^2\right) \tag{2.16}$$

with $a_{\max}$ the maximum acceleration, $v_{\max}$ the maximum velocity and δ the acceleration exponent. Similar to Gipps' model, the IDM includes two regimes in the desired space gap function (Treiber & Kesting, 2010):

$$s^*(v,\dot{s}) = s_{\text{jam}} + \max\left(0, Tv + \frac{v\dot{s}}{2\sqrt{a_{\max}a_{\min}}}\right) \tag{2.17}$$

with $a_{\min}$ the maximum deceleration (minimum acceleration), s_{jam} the jam spacing and T the minimum time headway.

The latest offshoots in the branch of stimulus-response models are based on Three-Phase-Theory. The acceleration delay model by Kerner & Klenov (2006) and a stochastic car-following model by the same authors (2002) take into account the three traffic regimes proposed in Three-Phase Traffic Theory (Kerner, 2009).

Already in the earliest days of stimulus-response models Chandler et al. (1958) introduced a general formulation:

$$a(t) = f\big(v(t), s(t-\tau), \dot{s}(t-\tau)\big) \tag{2.18}$$

It is interesting to note that, after reformulation, most safe-distance models also fit in this framework. Therefore, the distinction between safe-distance and stimulus-response models is not as clear as suggested by e.g., Brackstone & McDonald (1999); Hoogendoorn & Bovy (2001b). Instead, safe-distance models can be classified as car-following models in which the assumption that drivers keep a safe distance plays a large role. Therefore, the distinction rather lies in the assumptions then in the model equations themselves.

Currently, Wilson (2008); Wilson & Ward (2011) use the generic formulation (2.18) to qualitatively asses stimulus-response models. They perform stability analysis and put forward some constraints on the function f and its parameters. Assuming no time delay ($\tau = 0$) the requirements are:

- An equilibrium fundamental relation can be derived using the steady-state solution of f:
  $\forall s > 0$, $\exists v = V(s) > 0$ such that $f(v, s, 0) = 0$.
- Driving behaviour is 'rational', leading to some constraints on the derivatives:
  - If velocity increases, the vehicle accelerates less (or decelerates more):
    $\mathrm{d}f/\mathrm{d}v < 0$.
  - If headway increases, the vehicle accelerates more (or decelerates less):
    $\mathrm{d}f/\mathrm{d}s \geq 0$.
  - If relative velocity increases (that is: if approach rate decreases or receding rate increases), the vehicle accelerates more (or decelerates less):
    $\mathrm{d}f/\mathrm{d}\dot{s} \geq 0$.

However, Wilson & Ward (2011) do not draw any conclusions on which models are quantitatively good, and which are not. This is partly because such conclusions do not only depend on the model formulation but also on its parameters.

2.2.3 Action point models

The third, and last, branch of car-following models consists of action point models, first introduced by Wiedemann (1974), (Brackstone & McDonald, 1999). However, a decade earlier, Michaels (1965) discussed the underlying concept that drivers would only react if they perceive that they approach a vehicle. Therefore, the approach rate or the headway must reach some perception threshold before a driver reacts. The main advantage of action point models is that they incorporate, in contrast to other car-following models, that:

1. at large headways driving behaviour is not influenced by that of other vehicles,
2. at small headways driving behaviour is only influenced by that of other vehicles if changes in relative velocity and headway are large enough to be perceived.

If driving behaviour is influenced by that of others, any of the previously introduced safe-distance or stimulus-response models can be used to describe it. Therefore, action point models can be regarded as a generalization of stimulus-response models.

2.2.4 Multi-class and multi-anticipation car-following models

Most car-following models described and analyzed in literature assume homogeneous vehicle-driver units, that is: vehicles and drivers all behave identically. However, since each vehicle is modeled and simulated individually, it is relatively straightforward to

take into account heterogeneity. In that case model parameters such as desired (maximum) velocity, sensitivity and reaction time may vary over vehicles and drivers. In fact, most simulation tools based on car-following models are multi-class, that is: they do take into account heterogeneity. For example, originally the Intelligent Driver Model was formulated as a multi-class model with different parameters $a_{\max}$, $a_{\min}$, $v_{\max}$, s_{jam}, and T for each vehicle (Treiber et al., 2000).

Multi-anticipation is another way to extend car-following models. In this case more than one leading vehicle influences the behaviour of a driver. The concept was already used in the car-following model by Helly (1961) (Brackstone & McDonald, 1999). However, it has become widespread since Bexelius (1968) developed a multi-anticipation version of the GHR-model. More recently, multi-anticipation was incorporated in the optimal velocity model (Lenz et al., 1999) and the Intelligent Driver Model (Treiber et al., 2006a). Finally, multi-anticipation and multi-class have been combined to take into account that some drivers look further ahead than others (Ossen & Hoogendoorn, 2006).

2.2.5 Cellular-automata models

Cellular-automata models are usually categorized as microscopic models, even though they are a different, and much younger, branch in the model tree. This is because the movement of individual vehicles is modeled. The main difference with car-following models is that space, and sometimes time, is discretized. Moreover, the velocity is discretized. Therefore, they are in general computationally more efficient (Knospe et al., 2004). In cellular-automata models, the road is partitioned into cells of usually 7.5 meters long. In such a cell either a vehicle might be present or not. The model consists of a set of, either stochastic or deterministic, rules that determine when the vehicle will move to the next (downstream) cell. The first cellular-automata traffic flow models was introduced by Cremer & Ludwig (1986). The model by Nagel & Schreckenberg (1992) is regarded as the prototype cellular-automata model (Knospe et al., 2004). Each time step each vehicle is advanced a few (or zero) cells according to the following algorithm:

1. If maximum velocity has not been reached yet then accelerate: $\tilde{v} \rightarrow \min(\tilde{v}+1, \tilde{v}_{\max})$.
2. If headway is too small then decelerate: $\tilde{v} \rightarrow \min(\tilde{v}, \tilde{s}_{\text{jam}}-1)$
3. Decelerate at random: $\tilde{v} \rightarrow \max(\tilde{v}-1, 0)$ with probability π.
4. Move: $\tilde{x} \rightarrow \tilde{x}+\tilde{v}$.

Here $\tilde{v}$ denotes the normalized vehicle velocity in number of cells per time step, $\tilde{v}_{\max}$ the normalized maximum velocity and $\tilde{s}_{\text{jam}}$ the normalized jam spacing in number of cells. $\tilde{x}$ is the cell number and π the deceleration probability.

More recent developments combine cellular-automata models with the optimal velocity car-following model Helbing & Schreckenberg (1999) or Three-Phase-Theory

Kerner et al. (2002). Some of the most popular cellular-automata models have been compared by Knospe et al. (2004). They conclude that (certain) cellular-automata models are well able to describe traffic flow on urban roads and sometimes even on highways.

2.3 Mesoscopic models

Mesoscopic traffic flow models were developed to fill the gap between microscopic models that describe the behaviour of individual vehicles and macroscopic models that describe traffic as a continuum flow. Mesoscopic models describe vehicle behaviour in aggregate terms such as in probability distributions. However, behaviour rules are defined for individual vehicles. Within this family the branch of gas-kinetic models appears to be the most popular nowadays. Other branches include headway distribution models (Buckley, 1968; Branston, 1976) and cluster models (Mahnke & Kühne, 2007). In this section we discuss gas-kinetic models (Section 2.3.1) and macroscopic models derived from them (Section 2.3.2).

2.3.1 Gas-kinetic models

Gas-kinetic traffic flow models were developed in analogy to models describing the motion of large numbers of small particles (atoms or molecules) in a gas. When applied to traffic flow, these models describe the dynamics of velocity distribution functions of vehicles. Prigogine & Andrews (1960); Prigogine (1961) first introduced gas-kinetic models describing traffic flow by the following partial differential equation:

$$\frac{\partial \tilde{\rho}}{\partial t} + v\frac{\partial \tilde{\rho}}{\partial x} = \left(\frac{\partial \tilde{\rho}}{\partial t}\right)_{\text{acceleration}} + \left(\frac{\partial \tilde{\rho}}{\partial t}\right)_{\text{interaction}} \tag{2.19}$$

with $\tilde{\rho}$ the reduced phase-space density, which can be interpreted as follows. At time t, the expected number of vehicles between location x and $x + \mathrm{d}x$ that drive with a velocity between v and $v + \mathrm{d}v$ is the integral of the reduced phase-space density over this two-dimensional area:

$$\begin{aligned} &\text{expected \# of veh's in } [x, x+\mathrm{d}x) \text{ with velocity in } [v, v+\mathrm{d}v) \\ = &\int_x^{x+\mathrm{d}x} \int_v^{v+\mathrm{d}v} \tilde{\rho}(x,v,t)\,\mathrm{d}x\,\mathrm{d}v \;\approx\; \tilde{\rho}(x,v,t)\,\mathrm{d}x\,\mathrm{d}v \end{aligned} \tag{2.20}$$

where the approximation holds in the limit for an infinitesimal area with $\mathrm{d}x \to 0$ and $\mathrm{d}v \to 0$. The left-hand side of (2.19) consists of a time derivative and an advection term describing the propagation of the phase-space density with the vehicle velocity. At the right-hand side there is an acceleration term describing the acceleration towards

the equilibrium velocity:

$$\left(\frac{\partial\tilde{\rho}}{\partial t}\right)_{\text{acceleration}} = -\frac{\partial}{\partial v}\left(\tilde{\rho}\,\frac{\tilde{v}(v|x,t)-v}{t_{\text{acceleration}}}\right) \tag{2.21}$$

with $t_{\text{acceleration}}$ the acceleration time and $\tilde{v}$ is the desired velocity distribution. The other term at the right-hand side is an interaction term, or collision term, describing the interaction between nearby vehicles:

$$\left(\frac{\partial\tilde{\rho}}{\partial t}\right)_{\text{interaction}} = (1-\pi)\tilde{\rho}(x,v,t)\int(v_{\text{slow}}-v)\tilde{\rho}(x,v_{\text{slow}},t)\mathrm{d}v_{\text{slow}} \tag{2.22}$$

with v_{slow} the velocity of a slow vehicle, π the probability of immediate overtaking and hence $1-\pi$ the probability of slowing down.

Paveri-Fontana (1975) improved the above gas-kinetic model by relaxing the assumption that the behaviour of nearby vehicles is uncorrelated, which resulted in an adapted interaction term. Furthermore, the model includes an acceleration term with the desired velocity distribution $\tilde{v}$ independent of the local number of vehicles. In the mid 1990's a revival of gas-kinetic models occurred with the development of a multi-lane version of Paveri-Fontana's model, Helbing (1997b).Hoogendoorn & Bovy (2001a) propose a generic gas-kinetic traffic flow model including the previously mentioned models (Prigogine & Andrews, 1960; Paveri-Fontana, 1975; Helbing, 1997b) as special cases.

2.3.2 Continuum gas-kinetic models

Gas-kinetic models are usually not applied in simulations as such, but a continuum traffic flow model is derived and simulations are based on this continuum model. Continuum gas-kinetic models all include some equation describing the dynamics of the vehicle velocity and may therefore be categorized as higher-order (macroscopic) models, see Section 2.4.3. However, in the model tree we cluster them in the mesoscopic models family. Phillips (1979) derived a gas-kinetic higher-order model to better represent traffic flow at high densities. More recently, Treiber et al. (1999) incorporate a term reflecting the anticipation of drivers. Another example of a higher-order model derived from a gas-kinetic model is the master model by Helbing et al. (2001). It adds another partial differential equation to the original Payne model (see Section 2.4.3) describing the dynamics of the velocity variance. Hoogendoorn (1999) derives a multi-class multi-lane continuum traffic flow model from a gas-kinetic model. Finally, Tampère et al. (2003) propose a continuum gas-kinetic model that explicitly includes a simple car-following model with two regimes.

2.4 Macroscopic models

Macroscopic traffic flow models form the fourth, and last, family in the model tree. They describe traffic flow as if it were a continuum flow and are often compared to, or derived in analogy with, continuum models for compressible fluids. Individual vehicles are not modeled, however aggregated variables such as (average) density and (average) flow are used. In this section we discuss the two major branches of macroscopic models namely kinematic wave models (Section 2.4.1) and higher-order models (Section 2.4.3). Furthermore, in Section 2.4.2 we discuss in more detail multi-class kinematic wave models.

2.4.1 Kinematic wave models

Macrosopic traffic flow models were first introduced by Lighthill & Whitham (1955b) and, independently, Richards (1956). In their kinematic wave model the dynamics of traffic is described by a partial differential equation, which models the conservation of vehicles:

$$\frac{\partial \rho}{\partial t} + \frac{\partial}{\partial x}\big(q(\rho)\big) = 0 \tag{2.23a}$$

and a fundamental relation:

$$q = q(\rho) \tag{2.23b}$$

This model, often referred to as the LWR model, does not yield a unique solution. However, by using the entropy condition, i.e. assuming flow maximization, a unique solution is found (Ansorge, 1990; Lebacque, 1996). The entropy condition will be discussed in more detail in Section 3.2.1.

Because of its simplicity the LWR model has received both much attention and critique. The model tree shows that this resulted in many offshoots. The main drawback of the LWR model is that vehicles are assumed to attain the new equilibrium velocity immediately after a change in the traffic state, which implies infinite acceleration. This problem is addressed by higher-order models (see Section 2.4.3) but also by variants of the LWR wave model. Lebacque (2002); Leclercq (2007b) address it by introducing bounded-acceleration. Another drawback of the LWR model is that breakdown (the transition from the free flow regime to the congestion regime) always occurs at the same density and without a drop in the capacity. This is addressed by Daganzo et al. (1997); Laval & Daganzo (2006) by introducing lane changing in a discretized version of the LWR model (Daganzo, 1994). The stochastic kinematic wave model proposed by Hoogendoorn et al. (2009) uses breakdown probabilities to reflect that breakdown might occur at different densities.

2.4.2 Multi-class kinematic wave models

In the last decade many models that can be categorized in the branch of multi-class kinematic wave models have been developed. This follows the earlier development of other types of multi-class models (micro- and mesoscopic, higher-order macroscopic). Classes are distinguished based on driving behaviour and vehicle properties, such as (desired) velocity, vehicle length and driving style. Furthermore, classes may be distinguished based on route or destination. Similar, and usually even simpler, techniques can be applied in that case.

Daganzo (2002) proposes a multi-class multi-lane model based on the LWR model. It is assumed that there are two types of drivers: 'slugs' who drive slow and have little incentive to overtake and 'rabbits' who attempt to drive fast and overtake more often. Chanut (2005) extends his earlier single-pipe model (Chanut & Buisson, 2003) to include moving bottlenecks (e.g., trucks) which drive slowly on only one lane. Therefore, we also this model as a multi-lane model. Other multi-class kinematic wave models are single-pipe. This implies that there might be multiple lanes, however they are not distinguished in the model and overtakings or differences between the lanes are not taken into account explicitly.

The model tree shows that Wong & Wong (2002) were the first to introduce such a single-pipe multi-class kinematic wave model. They propose to use a class-specific version of the conservation equation for each of the U classes (2.24):

$$\frac{\partial \rho_u}{\partial t} + \frac{\partial q_u}{\partial x} = 0 \tag{2.24}$$

with ρ_u the class-specific density of class u, $q_u = \rho_u v_u$ the class-specific flow and v_u the class-specific velocity. The class-specific velocity depends on the total vehicle density. Effectively, the vertical axes of the density-flow and density-velocity fundamental relations are scaled differently for each class, see Figure 2.11(a). Wong & Wong show that their model is able to reproduce the capacity drop, hysteresis and platoon dispersion. Other authors have similarly found that multi-class models are able to reproduce phenomena related to scatter in the fundamental diagram better than mixed-class models (Treiber & Helbing, 1999; Daganzo, 2002; Ngoduy, 2011; Bellomo & Dogbe, 2011) and references therein. They do this by applying a different fundamental relation for each class, see Figure 2.11.

Benzoni-Gavage & Colombo (2003); Chanut & Buisson (2003) include the difference in length between the classes in the fundamental relation. Effectively, they scale both axes of the fundamental relation differently for each class. Chanut & Buisson show that this leads to a three-dimensional fundamental relation, see Figure 2.8(d).

A different approach to including heterogeneity in the LWR model is taken by Leclercq & Laval (2007). They first reformulate the model in the Lagrangian (moving) coordinate system, secondly the reformulated model is discretized. The discretization allows for a relatively simple introduction of vehicles of different classes. However, for an

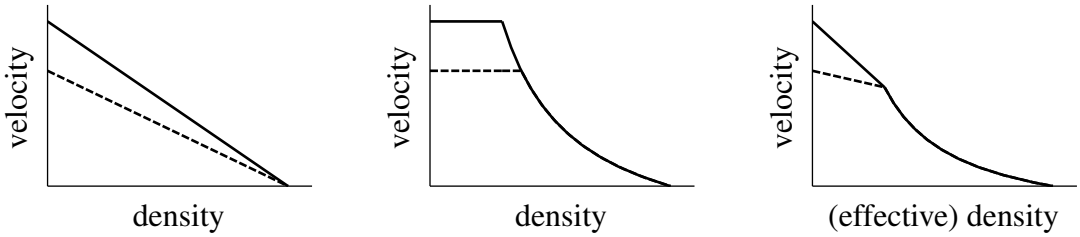

(a) Greenshields / Wong & Wong. (b) Daganzo / 3-regime. (c) Smulders / Fastlane.

Figure 2.11 *Different shapes of two-class fundamental relations. Solid lines indicate car velocity, broken lines truck velocity.*

accurate numerical solution of the model, the parameter choice is restricted severely (e.g., for each class the average vehicle length L_u needs to be an integer times the average length of a passenger car L_1).

Ngoduy & Liu (2007) use a similar approach as Benzoni-Gavage & Colombo (2003); Chanut & Buisson (2003) to the fundamental relation with state-dependent parameters

$$\rho_{\text{crit}}^{\text{scaled}} = \rho_{\text{crit}} \sum_u \frac{\alpha_u}{\eta_u}, \rho_{\text{jam}}^{\text{scaled}} = \rho_{\text{jam}} \sum_u \frac{\alpha_u}{\eta_u} \tag{2.25}$$

with α_u the road share that is assigned to class u:

$$\alpha_u = \frac{\rho_u}{\sum_{u=1}^{U} \rho_u} \tag{2.26}$$

Ngoduy & Liu refer to the Highway Capacity Manual (Transportation Research Board, 2000) to look up passenger car equivalent values η_u. The passenger car equivalent (pce) expresses how much a vehicle adds to the flow relatively to a passenger car. For example a light truck may count as 1.5 passenger cars, whereas a heavy truck may count as 3 passenger cars. The Highway Capacity Manual furthermore includes that on slopes trucks may have even higher pce-values and that the pce may also depend on the fraction of heavy vehicles. This model was later extended to include a discontinuous fundamental relation to reproduce the capacity drop (Ngoduy, 2010) and a stochastic term was included (Ngoduy, 2011) to reproduce hysteresis and scatter in the observed fundamental diagram.

The two-class model by Logghe & Immers (2008) includes a three-state fundamental relation, see Figure 2.11(b). It consists of a free flow, a congestion and a semi-congestion state. In semi-congestion one class (cars) behaves as if it is in a congestion regime (for increasing density, car flow decreases), while the other class (trucks) behaves as if it is in free flow (for increasing density, truck flow increases). The authors claim that this model correctly represents a user-equilibrium, that is: if one vehicle (or class) would change its behaviour, it would be off worse.

Fastlane is a recent offshoot in the branch of multi-class kinematic wave models (Van Lint et al., 2008; Van Wageningen-Kessels et al., under review). It takes a different

approach without rescaling the fundamental relation. Instead, an effective density is computed and this is used as a input for the fundamental relation. The fundamental relation now expresses the class-specific velocity as a function of the effective density, see Figure 2.11(c). The effective density is a weighted summation of the class-specific densities:

$$\rho = \sum_u \eta_u(\rho)\rho_u \tag{2.27}$$

with η_u the pce-value:

$$\eta_u(\rho) = \frac{L_u + T_u v_u(\rho)}{L_1 + T_1 v_1(\rho)} \tag{2.28}$$

with $L_u = s_{\text{jam},u} = 1/\rho_{\text{jam},u}$ the vehicle spacing at standstill if there would only be vehicles of class u. L_u includes the vehicle length l^{veh} and the distance between two vehicles at standstill d as they were introduced for Pipes' safe-distance model. T_u denotes the minimum time headway of class u. The Fastlane model will be derived, explained, analyzed and discussed in much more detail in the rest of this dissertation. Furthermore, and in (Van Wageningen-Kessels et al., 2011b) and in Chapter 5 we show that Fastlane is a generalization of previously introduced multi-class kinematic wave models.

The most recent multi-class kinematic wave model is the porous flow model by Nair et al. (2012). It considers heterogeneous traffic on a two-dimensional roadway. Small vehicles can drive through 'pores': openings between other vehicles. It is developed to model disordered traffic flow with different types of vehicles such as cars, scooters and bikes and without lanes. In Chapter 5 we show that the model can be reformulated in a form very similar to the models by Chanut & Buisson (2003); Benzoni-Gavage & Colombo (2003).

2.4.3 Higher-order models

Higher-order models form the other main branch of macroscopic traffic flow models. These models include an equation describing the acceleration ('velocity dynamics') towards the equilibrium velocity described by the fundamental relation. In 1971 Payne derived a macroscopic traffic flow model from a simple stimulus-response car-following model. It yielded a model consisting of the fundamental relation and two coupled partial differential equations, hence the name higher-order model. The partial differential equations are the conservation of vehicle equation (2.24) and an equation describing the velocity dynamics:

$$\frac{\partial v}{\partial t} + v\frac{\partial v}{\partial x} = \frac{v^*(\rho) - v}{t_{\text{relax}}} - \frac{c^2}{\rho}\frac{\partial \rho}{\partial x} \tag{2.29}$$

with $v^*(\rho)$ the equilibrium velocity described by the fundamental relation. The parameters in the model are interpreted differently by different authors. For example, Zhang (2001) interprets t_{relax} as the relaxation time and $c^2 = \mu/t_{\text{relax}}$ is the 'sound speed' with μ the anticipation coefficient.

Daganzo (1995b) has argued that higher-order models are flawed because they are not anisotropic, implying that vehicles do not only react to there leader but also on there follower, which results in vehicles driving backward. In general anisotropy implies that characteristic waves are not faster than vehicles, which is discussed extensively in Chapter 3 and 7. In the time Daganzo's article was written, existing higher-order models were indeed not anisotropic. Since then, many efforts have been undertaken to resolve the problems. Probably the most well-known of them is the model by Aw & Rascle (2000). They propose to use instead of Payne's velocity equation (2.29) the following velocity equation:

$$\frac{\partial}{\partial t}(v + p(\rho)) + v\frac{\partial}{\partial x}(v + p(\rho)) = 0 \tag{2.30}$$

with $p(\rho)$ a 'pressure' term. The (increasing) function $p(\rho)$ can have different forms, but $p(\rho) = \rho^c$ with some constant $c > 0$ is proposed as the prototype. In this model, when parameters have been chosen correctly, characteristic waves can not be faster than vehicles. This is also the case in Zhang (1999)'s model which is an adaptation of Payne's model which includes hysteresis. The model by Aw & Rascle was developed further by Greenberg et al. (2003) to include multiple lanes. A multi-class version of the model has been proposed in the same year (Bagnerini & Rascle, 2003). Furthermore, Lebacque et al. (2007) develop a generalized higher-order model that includes the models by Aw & Rascle (2000); Zhang (1999) as special cases.

Finally, Aw et al. (2002); Moutari & Rascle (2007) develop a hybrid model that couples the model by Aw & Rascle with a microscopic version of it. Similarly to Leclercq (2007a) they simplify the coupling by applying the Lagrangian formulation of the macroscopic model, based on a moving (Lagrangien) coordinate system. The Lagrangian formulation of macroscopic models is discussed in more detail in Chapter 6.

2.5 Discussion

In the previous sections many traffic flow models and their position in the model tree have been discussed. In the model tree several trends can be identified:

- Certain branches converge to a generalized model. The generalized model can be used to analyze qualitative properties of all models of that branch (Wilson, 2008; Hoogendoorn & Bovy, 2001a; Del Castillo, 2012; Van Wageningen-Kessels et al., 2011b).
- The LWR model is extended and adapted to better reproduce key phenomena

such as the capacity drop, hysteresis and scattered fundamental diagrams (Zhang, 1999; Lebacque, 2002; Wong & Wong, 2002).
- Multi-class versions of previously developed models are introduced (Hoogendoorn, 1999; Bagnerini & Rascle, 2003; Ossen & Hoogendoorn, 2006), and especially multi-class kinematic wave models (Wong & Wong, 2002; Benzoni-Gavage & Colombo, 2003; Chanut & Buisson, 2003; Zhang et al., 2006; Laval & Daganzo, 2006; Ngoduy & Liu, 2007; Logghe & Immers, 2008; Van Lint et al., 2008; Nair et al., 2012).
- Hybrid models combine microscopic and macroscopic models (Bourrel & Lesort, 2003; Leclercq, 2007a; Moutari & Rascle, 2007).

In the next chapters, we combine the trends in the development of a multi-class kinematic wave traffic flow model. It reproduces scattered fundamental diagrams. Furthermore, we generalize the model such that it allows for a qualitative analysis of the properties of this and similar models. Finally, we propose a reformulation (in Lagrangian coordinates) which simplifies hybridization of the model. In the rest of this chapter, we argue why we chose to further develop multi-class kinematic wave models and not any other type of traffic flow model. Therefore, we discuss the relations between traffic flow models and other types of mathematical models are discussed in Section 2.5.1. In Section 2.5.2 we discuss criteria for traffic flow models and we discuss to what extend the models satisfy these criteria.

2.5.1 Traffic flow, fluid flow and complex systems

Traffic flow models are often related to and derived in analogy with models for fluid flow. For example, the seminal paper on macroscopic traffic flow modelling (Lighthill & Whitham, 1955b), was published as 'On Kinematic Waves Part 2' together with Part 1 discussing flood movement in rivers (Lighthill & Whitham, 1955a). In turn, traffic flow models have recently inspired researchers to model pedestrian crowds and animal swarms in a similar way, cf. Bellomo & Brezzi (2008), other articles in that special issue of Mathematical Models and Methods in Applied Sciences on Traffic, Crowd, and Swarms and by Bellomo & Dogbe (2011). Furthermore, similarities between vehicular traffic, pedestrian and granular flow have been recognized and conferences on Traffic and Granular Flow are organized bi-annually, the most recent one being held in Moscow in 2011 (Traffic and Granular Flow, 2011). Finally, Helbing (2008) relates traffic flow to systems that might even seem more diverse such as those related to collective decision making, risk management, supply systems and management strategies. Similarities and differences between fluid flow modelling and traffic flow modelling are discussed in more detail below.

Despite the similarities between traffic and fluid flow, dissimilarities have been stressed as well. Papageorgiou (1998) argues that there is hardly any hope that traffic flow models will ever have the same descriptive accuracy as models in other domains such as Newtonian physics or thermodynamics. This is because 1) vehicles and humans

(drivers) all behave differently, and change there behaviour over time, unlike molecules of which the behaviour follows (usually simple and constant) physical laws, and 2) there are relatively few vehicles in the area of interest (at most a few hundred per kilometer), unlike in for example thermodynamics with around 10^{23} particles per cm^3. The second reason is also used by Darbha et al. (2008); Tyagi et al. (2008); Bellomo & Dogbe (2011) to argue that aggregating vehicles to develop a macroscopic traffic flow model is not justified. Furthermore, in fluid mechanics the Knudsen number is often used to choose between a continuum (macroscopic) or a particle (microscopic) approach. The Knudsen number is the ratio of the mean free path over a representative physical length scale. Only if it is much smaller than 1, can the fluid be approximated as a continuum. In vehicle flow the Knudsen number would be the following distance over a section length. Tyagi et al. (2008) argue that the Knudsen number is small enough (10^{-3}). However, in free flow (e.g., 100 meter following distance) on short sections (e.g., of 100 meter) the Knudsen number is much larger than 10^{-3} and the continuum approach is not justified. Still, Papageorgiou's first observation (drivers do not behave like molecules) shows that fluid flow and traffic flow are dissimilar in other aspects. Therefore, comparison of ratios such as the Knudsen number or the number of particles per region of interest can not be the only reason to justify (or falsify) a model approach. Therefore, below we discuss some other criteria that can be used when modelling traffic flow.

2.5.2 Criteria for and assessment of traffic flow models

In the previous sections we have already discussed some criteria for a limited class of models. Criteria for the fundamental relation (Del Castillo, 2012) are reviewed in Section 2.1, criteria for safe-distance and stimulus-response models (Wilson, 2008; Wilson & Ward, 2011) are reviewed in Section 2.2.2. Criteria for kinematic wave models and multi-class kinematic wave models are discussed in Chapter 3. Criteria for a broader range of traffic flow models include (Hoogendoorn & Bovy, 2001b; Helbing, 2001; Bellomo & Dogbe, 2011):

1. The model only has few parameters.
2. Parameters are (easily) observable and have realistic values.
3. Relevant phenomena are reproduced and predicted by the model.
4. The model allows fast numerical simulation.

The criteria are applicable to other types of models as well. However, in the following, the criteria are discussed in more detail for traffic flow models.

Number of parameters

Traffic flow models are often criticized for having many parameters, whose values are difficult to observe and estimate because of the dynamics of the system (Orosz et al.,

2010). Especially microscopic models are often said to have too many parameters (Brackstone & McDonald, 1999; Bellomo & Dogbe, 2011). Furthermore, in microscopic models stochasticity is often taken into account, which increases the number of parameters because not only the average value of the parameters has to be estimated but also their distribution. Moreover, microscopic models for multiple lane necessarily also include lane changing models, which increases the number of parameters further. Even without taking into account stochasticity and lane changing, most of the microscopic models have more parameters than the macroscopic models introduced in this chapter. An extreme example is the Deterministic Acceleration Time Delay Three-Phase Traffic Flow Model based on Three-Phase-Theory with, in its simplest form, 19 parameters (Kerner, 2009). The number of parameters in some microscopic and macroscopic, mixed-class and multi-class models is compared in Figure 2.12. Therefore, it is assumed that parameter values may vary over classes and over links, as in Table 2.1. By varying parameter values over classes heterogeneity of drivers and vehicles is taken into account. By varying parameter values over links it is taken into account that networks are usually not homogenous but consist of different type of roads (e.g., motorway and urban roads) with different characteristics (e.g., number of lanes, speed limit). Furthermore, we assume that the parameter values are independent. The analysis may become more realistic by taking into account that some parameters are not independent but, for example, a link with a high critical density, probably also has a high jam density and a class with a high free flow velocity $v_{\max}$ on a three-lane motorway, probably also has a high free flow velocity on a two-lane motorway.

Figure 2.12 shows that for mixed-class models on one link the number of parameters is 2 (simplified Newell model) to 6 (IDM, 1 class). However, if the number of classes increases, the number of parameters increases quickly. For macroscopic models the number of parameters increases from 4 (LWR) to 20 (Fastlane with 6 classes). For microscopic models it increases from 6 (IDM, mixed-class) to 31 (IDM, 6 classes). The figure furthermore shows the dependence on the number of links. If the number of links increases, the number of parameters increases as well. The rate of increase depends largely on the number of classes: if there are only few classes, the number of parameters remains relatively low. We conclude from Figure 2.12 that the number of parameters in a mixed-class microscopic model for one link may be comparable to that of a mixed-class macroscopic model for one link. The number of parameters in more realistic applications, however, depends largely on the number of links and the number of classes. Still, given the number of classes, the number of parameters in macroscopic models is, in general, lower than that in microscopic models.

Observable parameters with realistic values

Traffic flow models often include parameters that are not easily observable or even have no physical interpretation at all. For example, the constants c_1 and c_2 in the GHR model and the acceleration exponent δ in the IDM have no physical interpretation and are only used to fit the simulation results to data. Other parameters such as

Table 2.1 *Parameters of traffic flow models compared in Figure 2.12.*

Model and (if appropriate) fundamental relation	Type of parameter: Class-independent, Link-independent	Class-independent, Link-specific	Class-specific, Link-independent	Class-specific, Link-specific
Simplified Newell	τ	s_{jam}		
OVM		c_1 or c_2	γ_u	$v_{\max,u}$ $s_{\text{jam},u}$
IDM	δ		$a_{\max}, u$ $a_{\min,u}$	$v_{\max,u}$ T_u $s_{\text{jam},u}$
LWR, Smulders	w	ρ_{crit} ρ_{jam} $v_{\max}$		
Chanut & Buisson (2003)[1]	w	ρ_{crit} ρ_{jam}	L_u, $u \neq 1$	$v_{\max,u}$
Fastlane	w	ρ_{crit} ρ_{jam}	L_u, $u \neq 1$ T_u	$v_{\max,u}$
Payne, Daganzo	w t_{relax} c	ρ_{crit} ρ_{jam}		

[1] The original formulation includes other parameters, these parameters are based on the reformulation in Chapter 5.

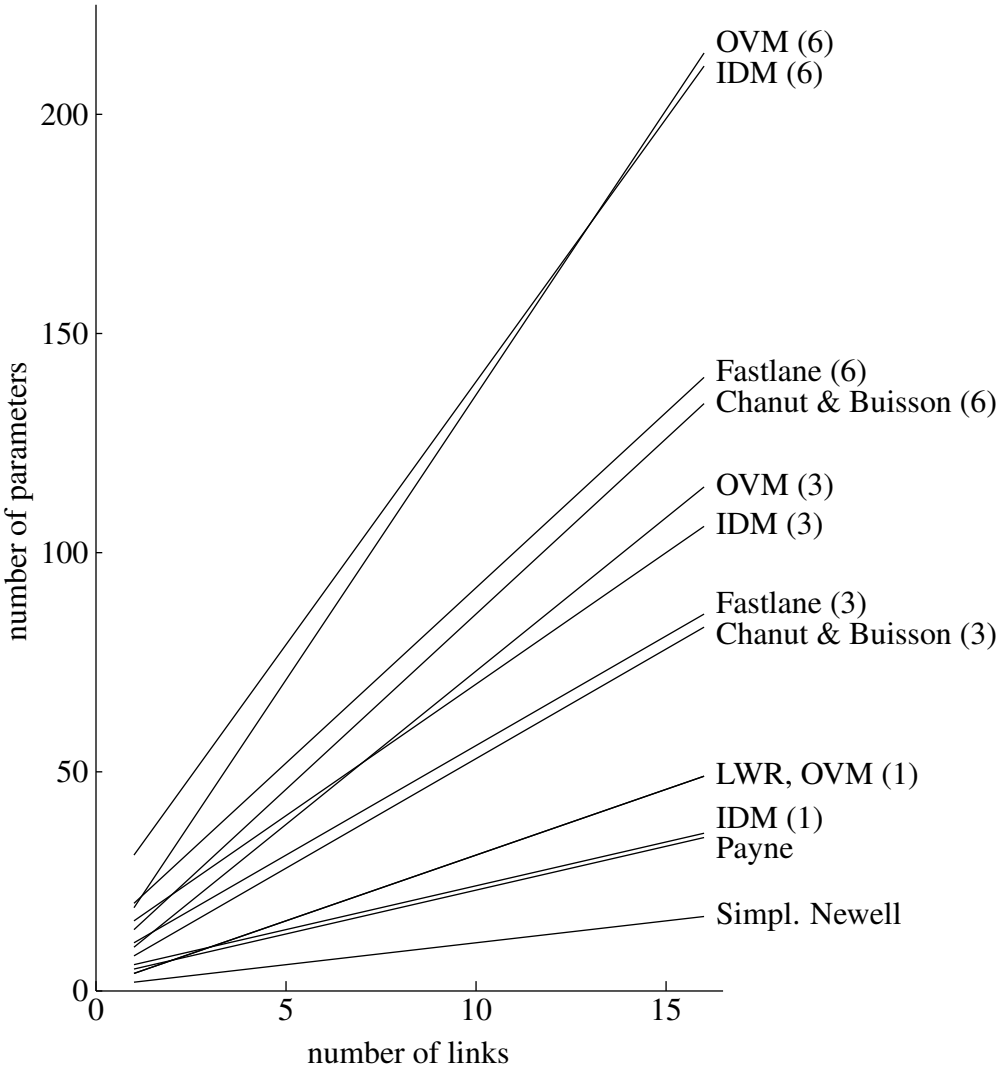

Figure 2.12 *The number of parameters for several micro- and macroscopic models as a function of the number of links in the network. The numbers between brackets indicate the number of classes. Both in the LWR and in the Payne model we use Daganzo's fundamental relation. The multi-class kinematic wave models by Chanut & Buisson and Fastlane include the Smulders fundamental relation.*

maximum and minimum acceleration $a_{\max}$ and $a_{\min}$ do have a physical interpretation but are not easily observable. To observe those parameters one would need detailed trajectory data including observations where this maximum (or minimum) acceleration is realized. Furthermore, microscopic traffic flow models often take into account stochasticity. This not only increases the number of parameters, but also makes them less easily observable.

Similar arguments hold for models including a fundamental diagram. The critical and jam density can only be observed if the data includes moments where traffic is in such as state. However, fundamental diagram estimation is becoming easier since the observation that the relation between density and flow is linear for large densities and its slope is constant over many observations (Cassidy & Windover, 1995; Kerner & Rehborn, 1996; Treiber & Helbing, 2002). Furthermore, traffic flow models are sometimes criticized for having unrealistic parameter values. For example, Brackstone & McDonald (1999) concluded that contradictory findings on parameter values c_1 and c_2 in the GHR model are the main reason why it is being used less frequently. Unrealistic parameter values also play a role in macroscopic models. The relaxation time t_{relax} in the Payne model is derived from the reaction time of a car-following model. However, its value has been estimated to be up to 30 seconds (Grewal & Payne, 1976).

Reproduction of phenomena

Many phenomena can be observed in traffic flow. Simple and easily observable ones include lower velocities at smaller headways, which is reflected in fundamental relations. Another example is spill-back of congestion: vehicles in a queue take up space and block parts of the road. Other phenomena include capacity drop and hysteresis. Recently, much attention goes to stop-and-go waves (Kerner & Rehborn, 1996). A stop-and-go wave is a heavily congested traffic state consisting of few vehicles that propagates upstream. Before and after the stop-and-go wave, traffic is much less congested or even in free flow. Some authors argue that all experimentally observed features, including stop-and-go waves should be reproduced by a traffic flow model (Helbing, 2001; Kerner, 2009; Bellomo & Dogbe, 2011). However, we believe that it largely depends on the model application whether such more complex phenomena need to be reproduced (Papageorgiou, 1998; Van Wageningen-Kessels et al., 2011a). Here, a comparison with fluid models is again appropriate. In some applications, such as the design of the propellor of a ship, it is very useful to know the details about turbulence, in others, such as climate predictions only large scale effects of turbulence need to be taken into account. Similarly, predicting the emergence and propagation of stop-and-go waves can be useful in some situations, for example, if one wants to warn drivers of unsafe situations such as stop-and-go waves. However, for relatively coarse predictions on large networks (the motorways of a metropolitan city) over long periods (one hour or more) it may not be necessary to predict individual stop-and-go waves.

Table 2.2 *The number of calculations of the traffic state for a micro and macro model with typical numerical settings.*

	Micro		Macro	
	congestion, 3 lanes	free flow, 1 lane	high resolution	low resolution
average density (veh/km)	300	10		
segment length (m)			100	200
time step size (s)	1	1	1	6
state calculations per km×min	18000	600	600	50

Fast numerical simulation

Microscopic models are in general computationally more demanding than macroscopic models, for two main reasons. First, the traffic state is calculated more often. In macroscopic models the road is usually divided into segments of a few hundred meters. The traffic state (density, velocity, flow) at each segment are calculated every time step of a few seconds. In microscopic models time steps are usually smaller and vehicles are not aggregated, instead the state (position, velocity, acceleration) of each vehicle is calculated. Furthermore, in microscopic models the number of calculations depends on the actual number of vehicles and therefore on the traffic state. Table 2.2 shows that in a microscopic model the state is computed up to several hundreds times as often as in a macrosopic model. Note that this does not necessarily mean that it is several hundreds times as slow: each state computation might take much less or more time than in a macroscopic model. Second, microscopic (and mesoscopic) models are often stochastic and simulation results vary each run. This is at least partly due to stochastic inflow at the inflow boundary. Therefore, many simulations are needed before conclusions can be drawn on the results. Furthermore, stochastic models are not tractable and therefore filtering and optimal control is much more difficult, if at all possible. Microscopic models do remain important because it depends largely on the application whether fast numerical simulation is necessary. However, we have already argued in the Introduction (Chapter 1) that new applications will continue to ask for faster simulations. Therefore, we will develop even more efficient computational methods for macroscopic models in Chapter 8.

2.6 Conclusions

In this chapter we proposed a model tree showing the genealogy of traffic flow models. Furthermore, we introduced criteria for such models and discussed how well certain types of models satisfy the criteria. The criteria can be in conflict with each other. In particular, accurately reproducing phenomena is in conflict with the other criteria because it requires more complex models with more, possibly not easily observable,

parameters. Furthermore, more complex models may also lead to more complex, and thus less efficient, numerical simulations. Wilson (2008) has argued that 'we can expect over the next few years to definitively resolve the conflict between the various traffic modelling schools', using novel, more detailed data. However, in each application the weights of the various criteria may be different. That is why the model tree shows divergence and many different branches have developed.

However, when analyzing the model tree we also observe convergence of certain branches of traffic flow models to a generalized model. The generalized models are applied to qualitatively assess models and to eliminate models with unwanted features. Having better knowledge on traffic flow may help to eliminate models with unwanted features, but it will not result in one model that is suitable in all applications. In fact, some applications call for models to be combined and coupled. This has led to the second trend in the model tree, namely the development of hybrid models combining micro- and macroscopic models. Furthermore, within the macroscopic family we observe that the LWR model has been adapted and extended to include more realistic features such as capacity drop and hysteresis. Moreover, multi-class versions of macroscopic models are under rapid development, also aiming at better reproducing certain characteristic features of traffic flow consisting of heterogeneous vehicles and drivers.

In the next chapters we develop and analyze a model that is aimed at online real time traffic flow prediction. However, the model may also be used in many other application that require fast numerical simulation but do not require accurately reproducing all phenomena such as stop-and-go waves and capacity drop. Therefore, we chose to combine some trends in the model tree. We further develop and analyze multi-class kinematic wave models. This type of models has few parameters compared to microscopic multi-class models. It does have more parameters than mixed class kinematic wave models but it can, in contrast to those models, reproduce scattered density-flow plots. Furthermore, numerical simulations can be done faster than microscopic simulations and we develop methods to make simulations even faster.

Chapter 3

Theoretical framework for multi-class kinematic wave traffic flow modelling

In this chapter we develop a framework within which we develop our traffic flow model: Fastlane. The framework consists of a set of principles and a set of requirements. The principles form the foundation on which we base the model in Chapter 4. The principles are partly common for all continuum traffic flow models, partly specific for multi-class kinematic wave models. The principles are used to build the model. The requirements are used afterwards to verify that the developed model has qualitatively desirable properties. The requirements relate to the model formulation, the fundamental relation and the model dynamics. The analysis of the model in Chapter 7 shows that our model, in contrast to some other models, indeed satisfies all requirements.

In this and the following chapters we restrict the theory and model development, analysis and numerical methods to infinitely long homogeneous roads. In Chapter 10 we extend all this to networks, including inflows, outflows and nodes at which roads merge or diverge or road properties change.

The outline of this chapter is as follows. Section 3.1 discusses the principles. In Section 3.2 the requirements are introduced.

3.1 Principles

The foundation of Fastlane is three groups of principles. The first group is common for all continuum traffic flow models. It consists of a conservation law and the continuum assumption. The second group consists of assumptions on the common behavior of vehicles and their interactions. They are applied in most kinematic wave models. The third group relates to behavioral differences between groups of vehicles and drivers. They form the basis of our multi-class modeling approach. The principles are as follows:

Continuum model principles:

1. Vehicles are conserved.
2. Traffic flow is a continuum flow.

Kinematic wave model principles:

3. Traffic flow is a single-pipe flow.
4. Traffic is always in equilibrium state.
5. Traffic flow is always in either of two regimes: free flow or congestion.

Multi-class model principle:

6. Traffic consists of homogeneous groups (classes) of vehicles and drivers.

Principles 3, 4 and 5 have been relaxed in some continuum models to better reproduce scattered density-flow plots. Fastlane reproduces scattered density-flow plots due to its multi-class approach (Principle 6). The principles are discussed in the following in more detail. We note that the principles are defined independently. Therefore, if one relaxes one or more of the principles, the others may still be used to build a traffic flow model.

3.1.1 Continuum model principles

Principle 1 is the single undisputed principle in traffic flow modelling. It states that vehicles are conserved. This means that vehicles can only enter the system through inflow at the boundaries and that they only leave the system through outflow at the boundaries. Vehicles are not created in the system itself, nor do they disappear. To the best of our knowledge, this principle is included in all traffic flow models.

Principle 2 assumes that vehicles can be aggregated and that the traffic state can be described by aggregate continuum variables such as density, flow and average velocity. All continuum models are based on this principle. Naturally, microscopic models are not based on this principle. In Section 2.5 we discussed the controversy around modelling traffic as a continuum flow. We concluded that, depending on the application, the advantages of continuum models outweigh the possibly less realistic representation of some traffic flow phenomena.

3.1.2 Kinematic wave model principles

Principle 3 assumes that traffic behaves similar to a flow in a single pipe. Traffic state variables such as density, flow and velocity are aggregated over all lanes and interactions between lanes are not taken into account explicitly. Therefore, overtakings are not taken into account explicitly. The single-pipe principle is relaxed in multi-lane models, which can be either mixed-class or multi-class.

Principle 4 assumes that traffic is always in an equilibrium state that is described by the fundamental relation. For example, in mixed-class continuum models, given the

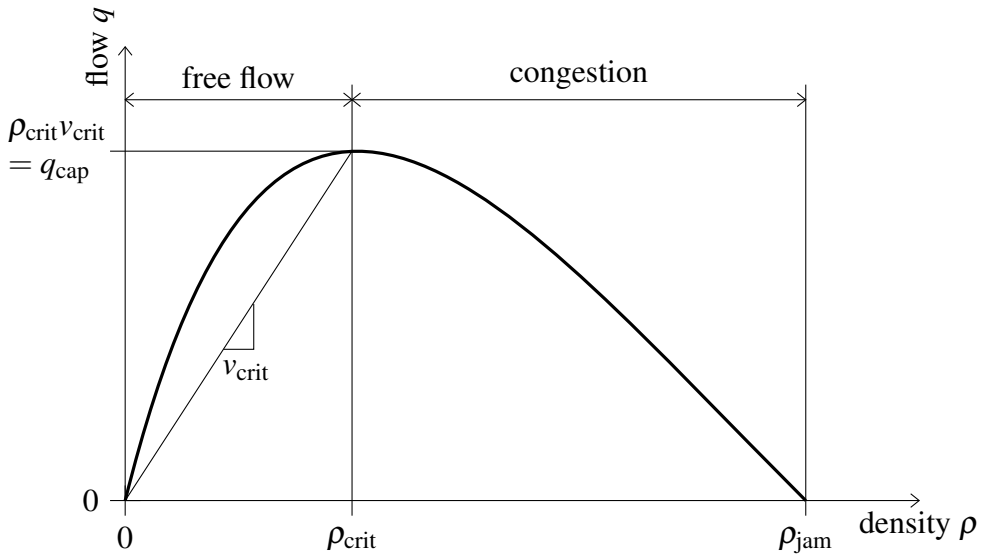

Figure 3.1 *Fundamental diagram with 2 regimes: free flow and congestion.*

current density, the flow and velocity do not depend on previous traffic states: it does not matter whether vehicles accelerate or decelerate. A consequence of this principle is that drivers adapt their velocity instantaneously to new traffic conditions such as a change in density. This implies that fundamental relations with hysteresis (see e.g., (Newell, 1965; Treiterer & Myers, 1974; Zhang, 1999), Figure 2.8(b)) can not be achieved. The principle is relaxed in the LWR model with bounded acceleration and in higher-order models.

Principle 5 assumes that there are two traffic flow regimes, see Figure 3.1. In free flow, if the density increases (a vehicle is added) the flow also increases. In congestion, if the density increases the flow decreases. In between those two regimes, maximum flow is reached. This point is often called capacity or capacity flow. The corresponding density and velocity are called critical density and critical velocity. Their values depend on the number of vehicles, but may also depend on traffic composition (e.g., percentage of heavy vehicles). Principle 5 is used in almost all continuum traffic flow models, however, it is relaxed in the three-regime multi-class model (Logghe & Immers, 2008). This model is discussed in more detail in Chapter 5.

3.1.3 Multi-class model principle

Principle 6 assumes that vehicle-driver units may differ and do not behave identically. They can be categorized into homogeneous classes: within one such class vehicles and drivers behave identically. As a consequence, each class may have a different fundamental relation. Mixed-class models such as the LWR model and many other

kinematic wave models and higher-order models assume that there is only one class and all vehicles and drivers behave identically. In multi-class models there may be two or more such classes.

The distinction between classes is made based on the physical properties of the vehicle and the driving style of the driver. This will result in classes that differ in, for example, maximum velocity, vehicle length and headway. In principle, vehicle properties and driving style may change over time and may depend on the traffic state. For example, a driver that becomes tired may increase his headway, and velocity may depend on weather conditions. Furthermore, vehicle classes can also be based on their origin, destination and route. This becomes especially interesting when networks need to be simulated. Throughout this dissertation classes are based on the physical properties of the vehicle and the driving style of the driver which are assumed to be static. However, the methods and analysis can be generalized to classes based on other criteria such as origin, destination or route. With some effort, vehicle properties and driving style can be made time-dependent.

3.2 Requirements

All traffic flow models should satisfy certain requirements. In Chapter 2 we discussed requirements on the fundamental relation introduced by Del Castillo (2012) and requirements on car-following models by Wilson (2008); Wilson & Ward (2011). Furthermore, we discussed the anisotropy criterium for continuum models (Daganzo, 1995b). For multi-class kinematic wave models, we formulate several qualitative requirements. Two requirements are related to the model formulation. The other requirements are related to the outcome of the model: the model must reproduce certain phenomena. These can be split into phenomena related to the shape of the fundamental relation and phenomena related to the dynamics of the model. We argue that any multi-class kinematic wave traffic flow model should satisfy the following qualitative requirements:

Model formulation requirements:

1. Given 'permissible' class-specific densities, (class-specific) velocities and flows are defined uniquely.
2. The model has a unique solution that maximizes flow.

Fundamental relation requirements:

3. In free flow the velocities of each class are allowed to differ.
4. In free flow the velocities of relatively fast classes are allowed to decrease with increasing density.
5. In congestion the velocity of each class is equal.
6. If the density reaches a certain threshold (which may depend on the traffic composition), vehicle velocity is zero.

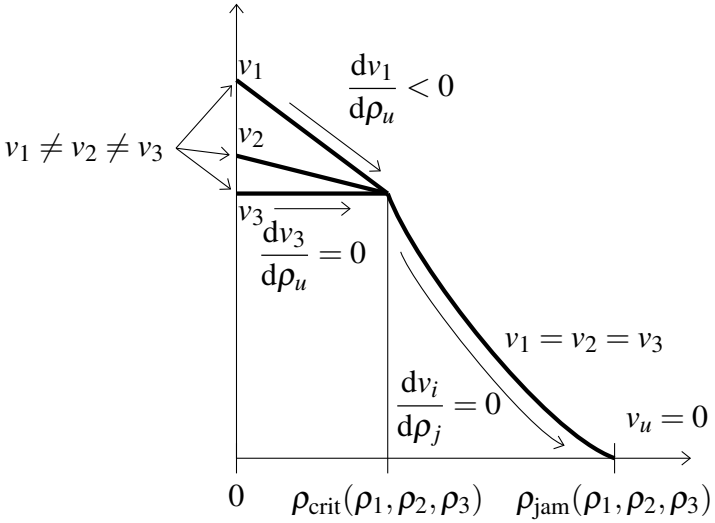

Figure 3.2 *Illustration of the fundamental relation requirements for a three-class model.*

7. If the density of only one class increases, while all other class-specific densities remain constant, vehicle velocities do not increase.

Model dynamics requirements:

8. Characteristics have finite velocity.
9. Characteristics do not have a larger velocity than vehicles.

The fundamental relation requirements are illustrated in Figure 3.2. All other requirements are discussed in more detail below.

3.2.1 Model formulation requirements

Requirement 1 states that there is one unique solution to the model equations, given 'permissible' class-specific densities. This implies that the model is formulated such that the state (velocity, flow) only depends on the density and composition and not on, for example, previous traffic states. 'Permissible' means that the given class-specific densities must be nonnegative and not above the threshold above which the velocity becomes zero (Requirement 6). It will become clear later (in Section 4.5) that Requirement 1 is not trivial.

Requirement 2 also states that the model has a unique solution. But rather, this requirement states that a well-posed initial value problem has a unique solution and that this solution maximizes flow. In relation to mixed-class models this solution is often referred to as the entropy solution. Ansorge (1990) introduced the entropy solution for traffic flow models in analogy to the entropy solution of gas flow models. Only after the discussion by Lebacque (1996), did traffic flow modellers become aware about it widely. Ansorge explains that the (mixed-class) kinematic wave traffic flow model has multiple weak solutions. For example, the solution where all vehicles in a queue remain at their position after a traffic light has turned green is a mathematically correct

(weak) solution of the model (2.23). Therefore, the ride impulse or flow maximization requirement is added to the model. This requirement selects out of all weak solutions the physically relevant one. In the traffic light example, that is the solution in which vehicles start driving as quickly and as fast as local conditions permit once the traffic light has turned green. Selecting the solution that maximizes flow, implies that vehicles drive as fast as possible given local traffic conditions.

Requirement 2 states that also in multi-class models the flow must be maximized locally and that vehicles drive as fast as possible given local traffic conditions. However, this does not necessarily yield a unique solution. Therefore, one has to consider which flow must be maximized. For example one may maximize the total flow in vehicles per second. Alternatively, the flow in passenger car equivalents per second may be maximized. The multi-class kinematic wave model is complete only if it defines a flow to be maximized.

3.2.2 Fundamental relation requirements

Requirements 3, 4 and 5 are important in multi-class models. Requirement 3 states that if density is below critical density, velocities of each class should be allowed to be different. It is not necessary that they are so for all possible parameter settings, but it must be possible to set the parameters such that the class-specific velocities are unequal. Requirement 4 states that the model must allow class-specific velocities to be decreasing in free flow. Again, it is not necessary that velocities are decreasing for all possible parameter settings, but it must be possible to set the parameters such that they are. Requirement 5 states that if density is above critical density (i.e. traffic is in congestion), velocities of all classes are equal.

We note that Requirements 3 and 5 are only relevant on multi-lane roads. On single-lane roads, without overtaking, velocities are naturally equal. Furthermore, Requirements 3, 4 and 5 are in line with observed decreasing car velocity even at low densities, unequal velocities of cars and trucks at low densities and equal velocities at high densities (Hoogendoorn, 1999, Chapter 8; Chanut, 2005). Requirement 5 is also in line with observed low velocity variance at high densities (Kerner & Rehborn, 1996; Helbing, 1997a).

Requirement 6 may seem trivial: if there are too many vehicles, they will come to a complete stop. However, not all fundamental relations applied in multi-class models satisfy this requirement (see Chapters 5 and 7). Del Castillo (2012) also formulates this as a requirement for the fundamental relation.

Requirement 7 states that if one vehicle is added to (removed from) the flow, the vehicle velocities of all classes do not increase (decrease). This is logical: if there are more vehicles, they do not drive faster, if there are fewer vehicles, they do not drive slower. In the mixed-class LWR model, this holds if the density-velocity fundamental relation

is nonincreasing. Del Castillo (2012) includes this requirement by stating that the density-flow fundamental relation should be concave (see Section 2.1.3).

3.2.3 Model dynamics requirements

Requirements 8 and 9 relate to the direction and speed of information propagation. Or, to put it differently, they relate to whether and how quickly vehicle-driver units react to other vehicle-driver units. Curves along which information propagates are often called characteristic curves, characteristic waves or simply characteristics. Along characteristics the traffic density is constant. In mixed-class kinematic wave models, the characteristic velocity is equal to the slope of the density-flow fundamental relation. A more rigorous (mathematical) definition of characteristics will be given in Chapter 7. Requirements 8 and 9 put limits on the value of the characteristic velocity.

Requirement 8 states that characteristics have finite velocity. It can be interpreted as follows: perturbations, such as a sudden braking operation of a driver, do not influence all drivers at once. Instead, it takes some time before other drivers will react, if they do so at all. For a model, this means that the characteristic velocity is bounded. This implies that there are no discontinuities in the fundamental relation, or there must be consistent rules on how to get from one branch to the other (Zhang, 2001).

Requirement 9 states that characteristic velocity (the velocity with which the characteristic travels downstream) is not larger than vehicle velocity (the velocity with which the vehicles travel downstream). This implies that the model is anisotropic. It can be interpreted as follows: perturbations, such as a sudden braking maneuver, only influence followers of the vehicle that brakes and do not influence vehicles in front of it. For a model, this means that the characteristic velocity is not higher than vehicle velocity.

The anisotropy requirement (Requirement 9) has received much research attention over the past two decades. Daganzo (1995b) initiated an ongoing debate on whether or not higher-order models are anisotropic and whether traffic flow models need to be (Aw & Rascle, 2000; Zhang, 2001, 2003; Helbing & Johansson, 2009; Zhang, 2009; Helbing, 2009). Traffic is supposed to be anisotropic because drivers usually do not react to their followers. Zhang (2003) argues that this does not imply that characteristics of the model should not be faster than the average vehicle velocity. This is because on roads where vehicles may overtake each other some vehicles may be faster than others. Those faster-than-average vehicles may also carry information with them. This would imply that the related characteristic is faster than the average vehicle velocity. This issue is addressed, at least partly, by splitting the vehicles into classes with different velocities. Still, in reality, the fastest vehicle may be faster than the average velocity of the fastest class.

3.3 Conclusions

Multi-class kinematic wave traffic flow models are based on principles that are common for all continuum traffic flow models. Some principles that were used in the LWR model have been relaxed previously. We relax the principle that all vechicle-driver units are identical and use a multi-class approach to reproduce scattered density-flow plots. Both the Fastlane model that is introduced in the next chapter (Chapter 4) and other multi-class models (see Chapter 5) are based on these principles.

Multi-class kinematic wave traffic flow models should satisfy qualitative requirements related to the model formulation, the applied fundamental relation and model dynamics. In Chapter 7, we show that Fastlane satisfies the requirements. Furthermore, we develop and apply a framework for the qualitative assessment of multi-class kinematic wave models.

Chapter 4

Model development: Fastlane

In this chapter we develop the Fastlane model. It consists of a system of equations, including the multi-class version of the conservation of vehicles equation and a fundamental relation. The principles in the previous chapter (Chapter 3) are used as the foundation of the model. Furthermore, we set some reasonable conditions on the values of the model parameters. In Chapter 7 we show that, if these conditions are satisfied, the model also satisfies the qualitative requirements introduced in Chapter 3.

The outline of this chapter is as follows. Section 4.1 introduces the variables and parameters of the model. Sections 4.2 and 4.3 introduce the model equations: the multi-class conservation of vehicles equation (Section 4.2) and the multi-class fundamental relation (Section 4.3). In Section 4.4 we set some 'reasonable' conditions for the model parameters. We interpret the conditions and show that they do not imply too strict limits on the parameter values. Finally, we note that the fundamental relation and effective density function as we introduce them in Section 4.3 are not well formulated: they do not uniquely define the velocities. Therefore, we reformulate them in Section 4.5, using the conditions from Section 4.4. At the end of this chapter (Section 4.6) we recapitulate the model.

4.1 Variables and parameters

Before introducing the model equations, we introduce its variables and parameters. For future reference a list of symbols, including variables and parameters is included on page 16.

4.1.1 Variables

Fastlane is based on the principle that traffic flow can be modelled as a continuum flow (Principle 2). Therefore, the variables describe traffic state in aggregated terms such

as density and flow. Due to the heterogeneity principle (Principle 6) the variables are class-specific. class-specific density, velocity and flow are defined similar to the definitions for mixed-class traffic flow (Definition 2.1–2.4, see Section 2.1.1). However, only vehicles of the class under consideration are taken into account. We define:

Definition 4.1 (class-specific flow)**.**

$$q_u(x,t) = \lim_{\mathrm{d}t \to 0} \frac{N_u(x,[t,t+\mathrm{d}t])}{\mathrm{d}t} \tag{4.1}$$

with $N_u(x,[t,t+\mathrm{d}t])$ the number of vehicles of class u that cross location x between or at times t and $t+\mathrm{d}t$. Since traffic flow is assumed to be a continuum flow, N_u is supposed to be continuous and furthermore it is supposed to be continuously differentiable.

Definition 4.2 (class-specific density)**.**

$$\rho_u(x,t) = \lim_{\mathrm{d}x \to 0} \frac{N_u([x,x+\mathrm{d}x],t)}{\mathrm{d}x} \tag{4.2}$$

with $N_u([x,x+\mathrm{d}x],t)$ the number of vehicles that are present on the location between or at x and $x+\mathrm{d}x$ at time t.

Definition 4.3 (class-specific vehicle velocity)**.**

$$v_u(x,t) = \frac{q_u(x,t)}{\rho_u(x,t)} \tag{4.3}$$

Later, we also need the class-specific spacing, which is defined analogously to the spacing in mixed-class models (Definition 2.4):

Definition 4.4 (class-specific spacing)**.**

$$s_u(x,t) = \frac{1}{\rho_u(x,t)} \tag{4.4}$$

4.1.2 Parameters

Furthermore, Fastlane includes several parameters. The class-specific maximum velocity $v_{u,\max}$, critical velocity v_{crit}, critical density ρ_{crit} and jam density ρ_{jam} are used in the fundamental relation. The class-specific gross vehicle length L_u and class-specific minimum time headway T_u are used in the space occupancy function. All these parameters are supposed to be nonnegative and furthermore critical density and all gross vehicle lengths should be positive ($\rho_{\mathrm{crit}} > 0$ and $L_u > 0$).

4.2 Conservation of vehicles

The multi-class conservation equation describes that vehicles of each class are conserved (Principle 1):

$$\frac{\partial \rho_u}{\partial t}(t,x) + \frac{\partial q_u}{\partial x}(t,x) = 0 \tag{4.5}$$

For readability we will omit (t,x) in the following. Since we model the road as a single pipe (Principle 3), we do not need to distinguish lanes.

Using Definition 4.3 the class-specific flow is:

$$q_u = \rho_u v_u \tag{4.6}$$

$v_u = v_u(\rho_1, \ldots, \rho_U)$ is some function of the traffic state defined by all class-specific densities. It is defined by the fundamental relation which will be introduced in the next section.

4.3 Fundamental relation

We apply the equilibrium principle (Principle 4). Consequently, we assume that traffic is always in a state described by the fundamental relation and the velocity only depends on the current traffic state. Below we define the fundamental relation. It expresses the velocity as a function of the effective density. The effective density is, in turn some 'total density' or 'accumulated density' based on all class-specific densities. To define the effective density we apply the concept of pce-value. The pce-value of class u expresses the impact on the flow of one vehicle of class u. In turn, the pce-value of class u is based on how much road space is occupied by one vehicle of class u in comparison to the space occupancy of one passenger car.

4.3.1 Shape of the fundamental relation

The shape of the fundamental relation is based on Principle 5 (two regimes: free flow and congestion) and 6 (homogeneous classes of vehicle-driver units). Therefore, we define a fundamental relation that may differ for each class. However, for a given traffic state, either all classes are in the free flow branch, or all of them are in the congestion branch. Furthermore, in free flow the velocities of each class may differ (Requirement 3), in congestion they are equal (Requirement 5). The Smulders fundamental relation (Smulders, 1990) allows for a multi-class generalization that satisfies these requirements. Furthermore, it is itself a generalization of other fundamental relations introduced in Section 2.1.2: the Daganzo fundamental relation and the Greenshields fundamental relation (see Section 2.1.2). We note that both the Daganzo and

Greenshields fundamental relations do not allow for multi-class generalizations with different velocities in free flow while still having only two regimes and being continuous. The mixed-class Smulders density-velocity fundamental relation is (see also Figure 2.5(c)):

$$v = v(\rho) = \begin{cases} v_{\max} - \dfrac{v_{\max} - v_{\text{crit}}}{\rho_{\text{crit}}}\rho & \text{(free flow, } 0 \leq \rho < \rho_{\text{crit}}\text{)} \quad (4.7a) \\ w\left(\dfrac{\rho_{\text{jam}}}{\rho} - 1\right) & \text{(congestion, } \rho_{\text{crit}} \leq \rho \leq \rho_{\text{jam}}\text{)} \quad (4.7b) \end{cases}$$

The multi-class Smulders fundamental relation is shown in Figure 4.1. The congestion branch is equal to that of the mixed-class fundamental relation. The only difference is the value of the maximum velocity, and consequently the slope in free flow. The multi-class fundamental relation is described by the following equations:

$$v_u = v_u(\rho) = \begin{cases} v_{u,\max} - \dfrac{v_{u,\max} - v_{\text{crit}}}{\rho_{\text{crit}}}\rho & \text{(free flow, } 0 \leq \rho < \rho_{\text{crit}}\text{)} \quad (4.8a) \\ w\left(\dfrac{\rho_{\text{jam}}}{\rho} - 1\right) & \text{(congestion, } \rho_{\text{crit}} \leq \rho \leq \rho_{\text{jam}}\text{)} \quad (4.8b) \end{cases}$$

with $v_{u,\max}$ maximum velocity of class u, v_{crit} critical velocity, which is reached at critical density ρ_{crit} and jam density is ρ_{jam}. Here w is class independent a parameter defined by:

$$w = \frac{\rho_{\text{crit}} v_{\text{crit}}}{\rho_{\text{jam}} - \rho_{\text{crit}}} \tag{4.9}$$

If all vehicles are of class 1, then effectively the model reduces to a mixed-class model and w is the characteristic wave speed in congestion.[1] However, as we will show in Chapter 7, if the composition changes, the characterstic velocity can change as well and is not necessarily equal to $-w$. Finally, we note that the fundamental relation (4.8) is continuous: at critical density both the velocity in the free flow branch and the velocity in the congestion branch are equal to the critical velocity v_{crit}.

4.3.2 Effective density

We propose a definition of the effective density. In Section 4.5, however, it turns out that this formulation does not lead to a unique effective density. Therefore, we reformulate the effective density in Section 4.5. However, the definition that we introduce here is easier to derive and interpret.

We define the effective density as a weighted summation of the class-specific densities:

$$\rho = \sum_u \eta_u \rho_u \tag{4.10}$$

[1] If $\rho = \rho_1$ then in congestion the characteristic velocity is $\mathrm{d}q/\mathrm{d}\rho = \mathrm{d}q_1/\mathrm{d}\rho_1 = \mathrm{d}(\rho_1 v_1)/\mathrm{d}\rho_1 = \rho_1 \mathrm{d}v_1/\mathrm{d}\rho_1 + v_1 = \rho_1(w\rho_{\text{jam}}/\rho^2)(\mathrm{d}\rho/\mathrm{d}\rho_1) + w(\rho_{\text{jam}}/\rho - 1) = w\rho_{\text{jam}}/\rho + w(\rho_{\text{jam}}/\rho - 1) = -w$.

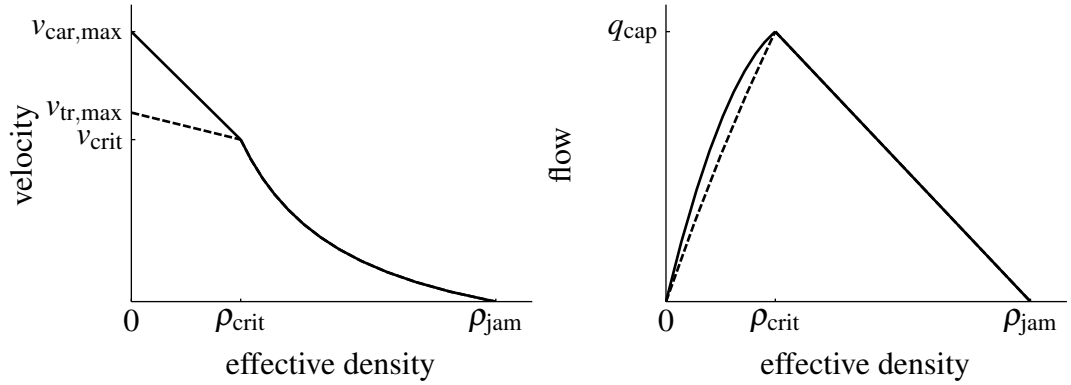

Figure 4.1 *Multi-class version of Smulders fundamental relation. The velocities and flows of two-classes (cars (solid line) and trucks (broken line)) are shown as a function of the effective density.*

where the pce-value η_u is the weight of class u. It depends on its relative space occupancy:

$$\eta_u = \frac{\omega_u}{\omega_1} \tag{4.11}$$

with the space occupancy:

$$\omega_u = L_u + T_u v_u \tag{4.12}$$

with the minimum time headway T_u and the gross vehicle length L_u. The gross vehicle length is the physical length of the vehicle plus the gap at complete stop and consequently, on a single lane road:

$$L_1 = \frac{1}{\rho_{jam}} \tag{4.13}$$

The space occupancy (4.12) is equivalent to the tail-to-tail spacing in Pipes' safe-distance car-following model (1953), see Section 2.2.1. Figure 2.10 and equation (2.8) show that the tail-to-tail spacing in Pipes' model is:

$$\begin{aligned}(x_{n-1} - l_{n-1}) - (x_n - l_n) &= (x_n + d + T v_n) - (x_n - l_n) = l_n + d + T v_n \\ &= L_u + T_u v_u \end{aligned} \tag{4.14}$$

The last equality holds if all classes u have the same minimum time headway: $T = T_u$ and if they furthermore have the same gross vehicle length: $l_n + d = L_u$ with l_u the net vehicle length from front to tail and d the distance between two vehicles at standstill.

Figure 4.2 shows how the space occupancy depends on the traffic state: in free flow and at high velocities, the space occupancy is mainly determined by the minimum time headway. Empirical studies show that the minimum values of observed time headways of trucks are almost equal to that of cars or at most two times larger (Tilch & Helbing, 2000; Hoogendoorn et al., 2006). Therefore, the headway is similar for both cars and

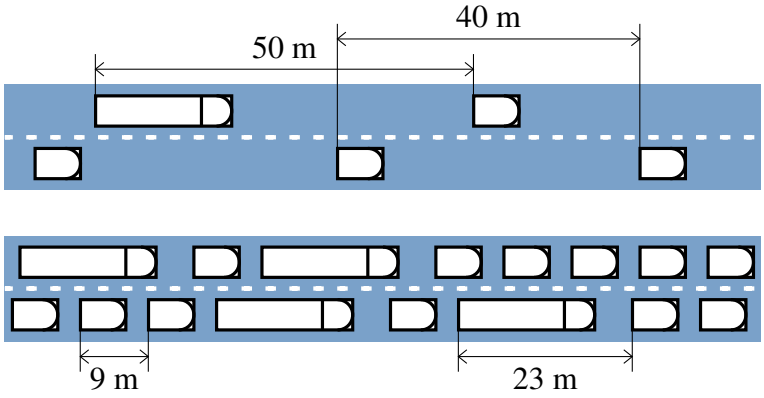

Figure 4.2 *Illustration of pce-values. Top: free flow, the space occupancy of a truck is close to the space occupancy of a car, therefore the pce-value of the truck is low. Bottom: congestion, the space occupancy of a truck and is much larger than the space occupancy of a car, therefore the pce-value of the truck is high.*

trucks and therefore the space occupancy and pce-value are similar as well. However, in congestion, the space occupancy is mainly determined by the vehicle length. For example, Elefteriadou et al. (1997) uses values of 5.2 meters for passenger cars, 12.2 meters for 'single unit vehicles', and up to 30.5 meters for long trucks. Therefore, trucks are longer than passenger cars, their space occupancy and thus also their pce-value is much larger than that of cars.

4.3.3 Flow maximization

We discuss the entropy requirement (Requirement 2) as the next element of the Fastlane model. The entropy requirement states that the solution of the model equations maximizes flow. We require the flow to be maximized to be the effective flow q:

$$q = \sum_u \eta_u q_u = \sum_u \eta_u \rho_u v_u \tag{4.15}$$

We will need the entropy requirement in Chapter 8 to develop a numerical method to approximate the unique solution that maximizes the effective flow (4.15).

4.4 Parameter conditions

Even by selecting the solution that maximizes the effective flow (4.15), a unique solution to the model equations can not be found. We note that (4.8), (4.10), (4.11) and (4.12) define the effective density implicitly, see also Figure 4.5: the effective density (4.10) is a function of the pce-values (4.11), which is in turn a function of the space occupancy (4.12), which is a function of the velocity (4.8), which is a function of the effective density (4.10), etc. In fact, it appears in Section 4.5 that (4.8), (4.10), (4.11)

and (4.12) do not define the effective density, nor the velocities uniquely. Therefore, we redefine the effective density uniquely in Section 4.5. However, for this redefinition, we need some conditions on the parameter values.

We propose some conditions on the parameters of the model developed in Section 4.2 and 4.3. We show that these conditions are 'reasonable': they do not include too strict conditions and (almost) all realistic parameter values satisfy the conditions. These conditions are used in the reformulation of the effective density in Section 4.5. Furthermore, In Chapter 7 we show that if these conditions hold, the model satisfies the qualitative requirements from Chapter 3.

4.4.1 Conditions on velocity parameters

In the following we show that the velocity parameters of the fundamental relation (4.8) must be chosen such that for all classes u:

$$v_{\text{crit}} \leq v_{u,\max} \leq v_{1,\max} \leq 2v_{\text{crit}} \tag{4.16}$$

Condition (4.16) puts some constraints on the shape of the fundamental relation (4.8) of each class, and on the connection between the fundamental relations of the classes. First of all, it states that at critical density, velocities are not higher than at zero density ($v_{\text{crit}} \leq v_{u,\max}$ for all classes u), which is reasonable to require because it implies non increasing velocity: at critical density, the velocity can not be higher than at zero density. Secondly, it states that class 1 is faster, or just as fast as all other classes ($v_{u,\max} \leq v_{1,\max}$ for all classes u). In fact, this condition is not necessary to satisfy the requirements. Even if the fastest class is not class 1 ($v_{u,\max} > v_{1,\max}$ for some classes u), the requirements may be satisfied. However, it does make the mathematical analysis in Chapter 7 easier, without loss of generality. Finally, condition (4.16) states that the difference between velocity at zero density and at critical density can not be 'too large' ($v_{1,\max} \leq 2v_{\text{crit}}$). This part of the condition is related to the maximum flow, or capacity and is discussed in more detail below.

We note that the critical density ρ_{crit} is defined as the density at which the free flow branch (4.8a) and the congestion branch (4.8b) of the fundamental relation intersect. Condition (4.16) implies that the maximum flow (capacity) is reached at critical density. We show that if the last part of Condition (4.16) is not satisfied, maximum flow may not be reached at critical density. This implies an unrealistic shape of the fundamental relation, as shown in Figure 4.3(b).

Theorem 4.1. *If the class-specific densities of all classes u are zero except for class 1 and furthermore $v_{1,max} > 2v_{crit}$, then the maximum flow is not reached at critical density.*

Proof. We consider the case with $\rho_u = 0$ for all u except for $u = 1$ and consequently

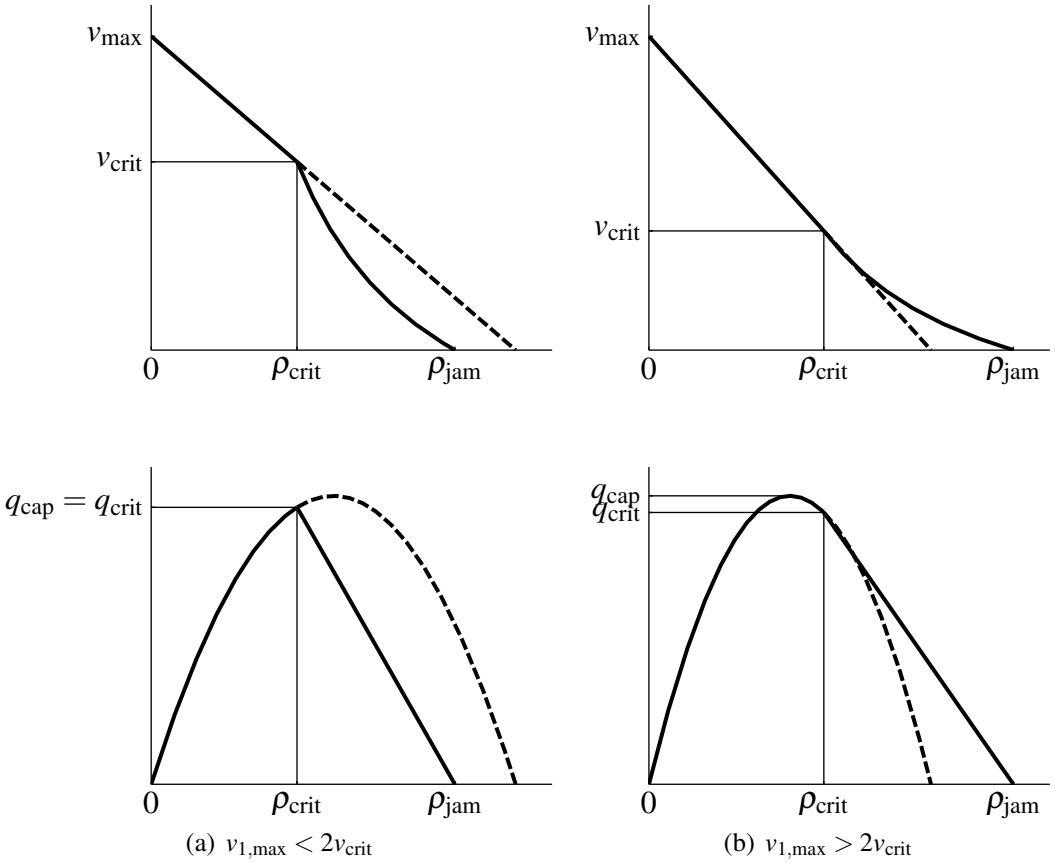

(a) $v_{1,max} < 2v_{crit}$ (b) $v_{1,max} > 2v_{crit}$

Figure 4.3 *Density-velocity (top) and density-flow (bottom) fundamental relations. If the maximum velocity is too large when compared to the critical velocity, the maximum flow is not equal to the flow at critical density.*

$\rho_1 = \rho$. This results in the following density-flow fundamental relation:

$$q = \rho_1 v_1 = \rho v_1 = \begin{cases} v_{1,max}\rho - \dfrac{v_{1,max} - v_{crit}}{\rho_{crit}}\rho^2 & \text{(free flow)} \quad (4.17a) \\ w\left(\rho_{jam} - \rho\right) & \text{(congestion)} \quad (4.17b) \end{cases}$$

This fundamental relation is shown in Figure 4.3. If the situation is as in Figure 4.3(b), the maximum flow is the flow at the top of the parabola. If, however, the situation is as in Figure 4.3(a), the maximum flow is the flow at critical density. The latter is the case if the top of the parabola is not part of the free flow branch. The density at the top of the parabola is:

$$\rho = v_{1,max}\frac{\rho_{crit}}{2(v_{1,max} - v_{crit})} \quad (4.18)$$

Consequently, the top of the parabola is not part of the free flow branch if $v_{1,max} \geq 2(v_{1,max} - v_{crit})$, which is equivalent to $v_{1,max} \leq 2v_{crit}$. We conclude that the maximum flow is not reached at critical density if $v_{1,max} > 2v_{crit}$. □

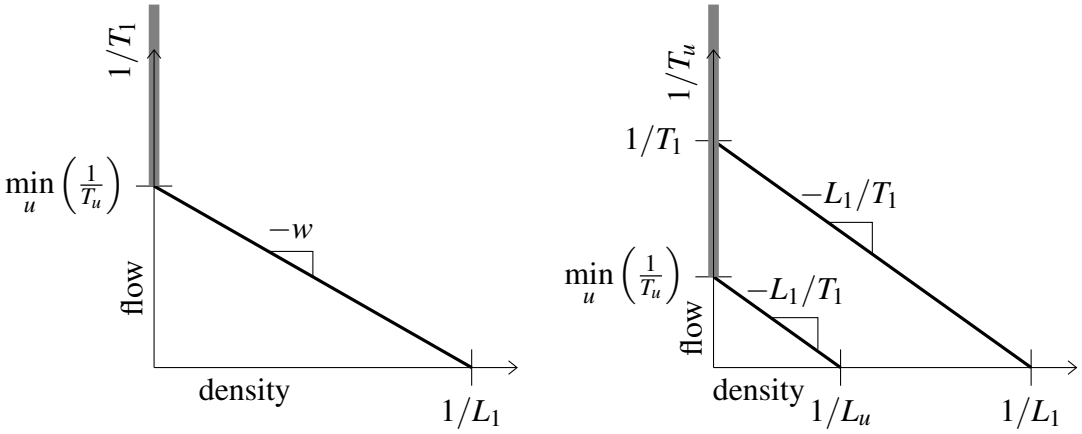

(a) First part: $w \leq \frac{L_1}{T_1}$, i.e. $\frac{1}{T_1} \geq \frac{w}{L_1}$

(b) Second part: $\frac{L_1}{T_1} \leq \frac{L_u}{T_u}$, i.e. $\frac{1}{T_u} \geq \frac{L_1}{T_1} L_u$.

Figure 4.4 *Schematic view of the condition on the space occupancy parameters, Condition (4.19). The grey areas illustrate the admissible values of* $1/T_1$ *and* $1/T_u$ *respectively.*

4.4.2 Conditions on parameters of space occupancy

In the following we show that the parameters of the space occupancy (4.12) must be chosen such that for all classes u:

$$w \leq \frac{L_1}{T_1} \leq \frac{L_u}{T_u} \tag{4.19}$$

Condition (4.19) puts constraints on the space occupancy function (4.12). It relates the characteristic velocity to the vehicle length and headway. The condition is illustrated in Figure 4.4(a).

The first inequality of Condition (4.19) implies that, in certain traffic states, space occupancy can not be larger than the spacing.

Theorem 4.2. *Consider any congested traffic state (i.e.* $\rho_{crit} \leq \rho \leq \rho_{jam}$*) with only vehicles of class 1 (i.e.* $\rho_u = 0$ *if* $u \neq 1$*). If the first inequality of (4.19) holds, then the space occupancy is not larger than the spacing:* $\omega_1 \leq s$.

Proof. There are only vehicles of class 1 and thus the spacing is $s = 1/\rho = 1/\rho_1$. We use the space occupancy function (4.12), the fundamental relation (4.8) and the definitions of jam density (4.13) and of spacing ($s = 1/\rho$) to find:

$$\omega_1 - s = L_1 + T_1 w \left(\frac{s}{L_1} - 1\right) - s \tag{4.20}$$

Rewriting gives:

$$\omega_1 - s = (L_1 - s) \frac{L_1 - T_1 w}{L_1} \tag{4.21}$$

The term between brackets is nonpositive. If the first inequality of (4.19) holds, then the fraction is nonnegative and thus the right-hand side is nonpositive. Consequently, space occupancy is not larger than the spacing: $\omega_1 \leq s$. □

Theorem 4.2 implies that, in the congested traffic state with only vehicles of class 1, no part of the road can be occupied by two vehicles at the same time. That is: their space occupancies do not overlap.

The second inequality of Condition (4.19) implies that in certain traffic states the pce-value is nondecreasing.

Theorem 4.3. *Consider any congested traffic state (i.e. $\rho_{crit} \leq \rho \leq \rho_{jam}$) with only vehicles of class 1 (i.e. $\rho_u = 0$ if $u \neq 1$). If the second inequality of (4.19) holds for a certain class u, then the pce-value of this class u is nondecreasing:* $\mathrm{d}\eta_u/\mathrm{d}\rho \geq 0$.

Proof. There are only vehicles of class 1 and thus the spacing is $s = 1/\rho = 1/\rho_1$. We first show that the velocity is decreasing in congestion:

$$\frac{\mathrm{d}v_1}{\mathrm{d}\rho} = -T_1 w \frac{\rho_{\mathrm{jam}}}{\rho^2} \leq 0 \tag{4.22}$$

We apply the pce function (4.11) and the space occupancy function (4.12) and use that $v_u = v_1$ and $\mathrm{d}v_u/\mathrm{d}\rho = \mathrm{d}v_1/\mathrm{d}\rho$ to compute the density derivative of the pce vale η_u:

$$\begin{aligned} \frac{\mathrm{d}\eta_u}{\mathrm{d}\rho} &= \frac{(L_1 + T_1 v_1) T_u \dfrac{\mathrm{d}v_u}{\mathrm{d}\rho} - (L_u + T_u v_u) T_1 \dfrac{\mathrm{d}v_1}{\mathrm{d}\rho}}{(\omega_1)^2} = \frac{L_1 T_u \dfrac{\mathrm{d}v_1}{\mathrm{d}\rho} - L_u T_1 \dfrac{\mathrm{d}v_1}{\mathrm{d}\rho}}{(\omega_1)^2} \\ &= \frac{T_1 T_u}{(\omega_1)^2} \left[\frac{L_1}{T_1} - \frac{L_u}{T_u} \right] \frac{\mathrm{d}v_1}{\mathrm{d}\rho} \end{aligned} \tag{4.23}$$

We have already shown that the velocity is decreasing (4.22). Therefore, if and only if the second inequality of (4.19) holds, the term between square brackets in (4.23) is nonpositive and the pce-value is nondecreasing. □

Theorem 4.3 implies that, if traffic is more congested, trucks (which are longer and have a larger minimum time headway than passenger cars) have a higher pce-value than in free flow. This reflects that at high densities they take relatively more space than in free flow, see Figure 4.2.

4.5 Reformulation of the effective density

The previous formulation of the effective density, consisting of equations (4.8), (4.10), (4.11) and (4.12) defined the effective density implicitly. We reformulate the effective density in an explicit way such that it is defined uniquely and only depends on the

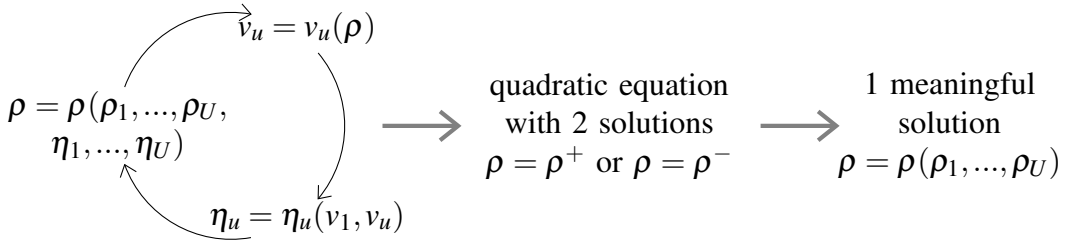

Figure 4.5 *Schematic view of the procedure in Section 4.5. We reformulate the implicit effective density (left) into a quadratic equation with two solutions (center, Section 4.5.1) and choose the correct one (right, Section 4.5.2). The reformulated function expresses the effective density as a function of only the class-specific densities.*

class-specific densities $\rho_1, ..., \rho_U$. During the reformulation we show that the previous formulation does not define the effective density uniquely, see Figure 4.5. To reformulate the effective density, we substitute the pce-function, the space occupancy and the fundamental relation into the effective density. We find a quadratic equation with two roots. We show that only one of the solutions is physically relevant. The approach is shown schematically in Figure 4.5.

4.5.1 Two effective density branches

To do this analysis for free flow and congestion, for the most part simultaneously, we write the effective density for both the free flow branch and the congestion branch in the same form. The derivation is done for free flow and congestion separately. For free flow, we substitute the free flow branch of the fundamental relation (4.8a) into the space occupancy (4.12):

$$\omega_u^{\mathrm{f}} = L_u + T_u v_u = L_u + T_u v_{u,\max} - T_u \frac{v_{u,\max} - v_{\mathrm{crit}}}{\rho_{\mathrm{crit}}} \rho = a_u^{\mathrm{f}} + b_u^{\mathrm{f}} \rho \tag{4.24}$$

with

$$a_u^{\mathrm{f}} := L_u + T_u v_{u,\max} \quad \text{and} \quad b_u^{\mathrm{f}} := -T_u \frac{v_{u,\max} - v_{\mathrm{crit}}}{\rho_{\mathrm{crit}}} \tag{4.25}$$

Substituting (4.24) and the pce-function (4.11) into the effective density function (4.10) gives:

$$\rho = \sum_u \frac{\omega_u^{\mathrm{f}}}{\omega_1^{\mathrm{f}}} \rho_u = \sum_u \frac{a_u^{\mathrm{f}} + b_u^{\mathrm{f}} \rho}{a_1^{\mathrm{f}} + b_1^{\mathrm{f}} \rho} \rho_u \tag{4.26}$$

Furthermore, we substitute the congestion branch of the fundamental relation (4.8b) into the space occupancy (4.12):

$$\omega_u^{\mathrm{c}} = L_u + T_u v_u = L_u - T_u w + T_u w \frac{\rho_{\mathrm{jam}}}{\rho} = b_u^{\mathrm{c}} + \frac{a_u^{\mathrm{c}}}{\rho} \tag{4.27}$$

with

$$a_u^{\mathrm{c}} := T_u w \rho_{\mathrm{jam}} \quad \text{and} \quad b_u^{\mathrm{c}} := L_u - T_u w \tag{4.28}$$

Substituting (4.24) and the pce-function (4.11) into the effective density function (4.10) gives:

$$\rho = \sum_u \frac{\omega_u^{\mathrm{c}}}{\omega_1^{\mathrm{c}}} \rho_u = \sum_u \frac{b_u^{\mathrm{c}} + a_u^{\mathrm{c}}/\rho}{b_1^{\mathrm{c}} + a_1^{\mathrm{c}}/\rho} \rho_u = \sum_u \frac{a_u^{\mathrm{c}} + b_u^{\mathrm{c}} \rho}{a_1^{\mathrm{c}} + b_1^{\mathrm{c}} \rho} \rho_u \tag{4.29}$$

In the last step we multiplied both numerator and denominator with ρ. Finally, we reformulate the effective density in a form that holds in both free flow and congestion:

$$\rho = \sum_u \left(\frac{a_u + b_u \rho}{a_1 + b_1 \rho} \rho_u \right) \tag{4.30}$$

with $a_u = a_u^{\mathrm{f}}$ and $b_u = b_u^{\mathrm{f}}$ in free flow (see (4.26)) and $a_u = a_u^{\mathrm{c}}$ and $b_u = b_u^{\mathrm{c}}$ in congestion (see (4.29)). This form (4.30) clearly shows how the effective density depends on itself.

We are going to rewrite (4.30) as a quadratic equation which has two roots. Multiplying both sides with $a_1 + b_1 \rho$ gives:

$$(a_1 + b_1 \rho)\, \rho = \sum_u \left[(a_u + b_u \rho) \rho_u \right] \tag{4.31}$$

Rearranging gives:

$$b_1 \rho^2 + \left(a_1 - \sum_u b_u \rho_u \right) \rho - \sum_u a_u \rho_u = 0 \tag{4.32}$$

If $b_1 = 0$ the quadratic equation (4.32) reduces to a linear equation with only one root:

$$\rho = \frac{\sum_u a_u \rho_u}{a_1 - \sum_u b_u \rho_u} \tag{4.33}$$

We note that, if Condition (4.16) holds, $b_1^{\mathrm{f}} = 0$ implies that $v_{1,\max} = v_{\mathrm{crit}} = v_{u,\max}$ for all user classes u. Therefore, the multi-class Smulders fundamental relation (4.8) reduces to Daganzo's fundamental relation and both in free flow and in congestion velocities are equal for all classes.

If $b_1 \neq 0$ the quadratic equation (4.32) has two roots. We find these roots, ρ^+ and ρ^-, by applying the quadratic formula:

$$\rho = \begin{cases} \rho^+ = \dfrac{a_1 - \sum_u b_u \rho_u + \sqrt{\left(a_1 - \sum_u b_u \rho_u\right)^2 + 4 b_1 \sum_u a_u \rho_u}}{-2 b_1} & \text{(4.34a)} \\ \rho^- = \dfrac{a_1 - \sum_u b_u \rho_u - \sqrt{\left(a_1 - \sum_u b_u \rho_u\right)^2 + 4 b_1 \sum_u a_u \rho_u}}{-2 b_1} & \text{(4.34b)} \end{cases}$$

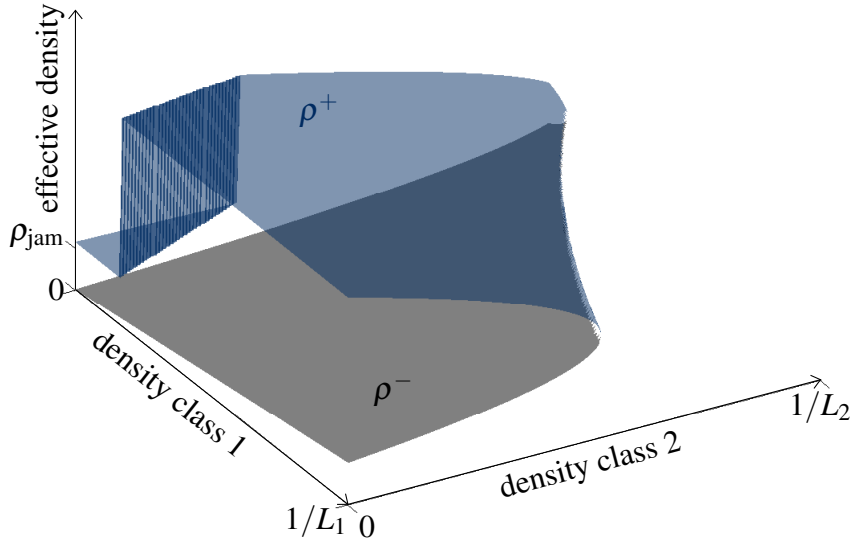

Figure 4.6 *The values of ρ^+ and ρ^- as functions of the class-specific densities of class 1 and 2. For low class-specific densities, ρ^+ and ρ^- are shown as distinct branches. If class-specific densities are high, the values of ρ^+ and ρ^- become complex and only the real parts are shown. We note that for different values of the parameters of the fundamental relation and the space occupancy, the shape of ρ^+ and ρ^- may change.*

The values of ρ^+ and ρ^- as functions of the class-specific densities are illustrated in Figure 4.6. This shows that the implicit set of equations (4.8), (4.10), (4.11) and (4.12) has two solutions: ρ^+ and ρ^-.

4.5.2 Choosing the correct effective density branch

The next step is to find out which of the two branches ρ^+ or ρ^- is correct. We do this by showing that ρ^- is equal to the effective density ρ if the parameters satisfy conditions (4.16) and (4.19). We also show that, if the conditions are satisfied, ρ^+ is unequal to the effective density ρ, in most traffic states. For this analysis we rewrite the parameter conditions (4.16) and (4.19) in terms of conditions on a_u and b_u. Furthermore, we define a new, state-dependent function.

The conditions on a_u and b_u are dependent on the regime (free flow or congestion).

Lemma 4.1. *If the parameters satisfy (4.16) then in free flow a_u and b_u satisfy:*

$$a_u^f \geq 0, \quad b_1^f \leq b_u^f \leq 0, \quad \textit{and} \quad a_u^f + 2b_u^f \rho \geq 0 \tag{4.35}$$

Proof. We use that all parameters are positive or nonnegative: $L_u > 0$, $T_u \geq 0$, $v_{u,\max} > 0$, $v_{\text{crit}} \geq 0$, $\rho_{\text{crit}} \geq 0$. From this we conclude that a_u^{f} is nonnegative: $a_u^{\text{f}} = L_u +$

$T_u v_{u,\max} > 0$. If (4.16) holds, then $v_{u,\max} \leq v_{1,\max}$ and thus $b_1^{\mathrm{f}} \leq b_u^{\mathrm{f}}$. Furthermore, if (4.16) holds, then $v_{u,\max} - v_{\mathrm{crit}} \geq 0$ and thus b_u^{f} is nonpositive: $b_u^{\mathrm{f}} = -T_u \frac{v_{u,\max} - v_{\mathrm{crit}}}{\rho_{\mathrm{crit}}} \leq 0$. Finally, we use that in free flow the effective density is not above critical ($\rho \leq \rho_{\mathrm{crit}}$) to find:

$$\begin{aligned} a_u^{\mathrm{f}} + 2b_u^{\mathrm{f}}\rho &\geq a_u^{\mathrm{f}} + 2b_u^{\mathrm{f}}\rho_{\mathrm{crit}} = L_u + T_u v_{u,\max} - 2T_u(v_{u,\max} - v_{\mathrm{crit}}) \\ &= L_u + T_u(2v_{\mathrm{crit}} - v_{u,\max}) > 0 \end{aligned} \tag{4.36}$$

The last inequality holds because $L_u > 0$ and because $2v_{\mathrm{crit}} \geq v_{u,\max}$ (see parameter condition (4.16)). □

Lemma 4.2. *If the parameters satisfy (4.19) then in congestion a_u and b_u satisfy:*

$$a_u^c \geq 0, \quad 0 \leq b_u^c \leq b_1^c \quad \textit{and} \quad a_u^c + b_u^c \rho \geq 0 \tag{4.37}$$

Proof. We use that all parameters are positive or nonnegative: $L_u > 0$, $T_u \geq 0$, $w > 0$, $\rho_{\mathrm{jam}} > 0$. From this we conclude that a_u^{c} is nonnegative: $a_u^{\mathrm{c}} = T_u w \rho_{\mathrm{jam}} \geq 0$. If (4.19) holds, then $L_u \geq T_u w$ and thus b_u^{c} is nonnegative: $b_u^{\mathrm{c}} = L_u - T_u w \geq 0$. Furthermore, if (4.19) holds, then $L_u - T_u w \leq L_1 - T_1 w$ and thus $b_u^{\mathrm{c}} \leq b_1^{\mathrm{c}}$. Finally, both a_u^{c} and b_u^{c} are nonnegative and thus: $a_u + b_u \rho \geq 0$. □

We define the function f which depends on the current traffic state:

$$f = f(\rho_1, \ldots, \rho_U) := a_1 - \sum_u b_u \rho_u \tag{4.38}$$

Furthermore, we define the determinant in (4.34):

$$d := \left(a_1 - \sum_u b_u \rho_u\right)^2 + 4 b_1 \sum_u a_u \rho_u \tag{4.39}$$

Lemma 4.3. *The determinant d (4.39) can be rewritten as:*

$$d = \left(\frac{\sum_u a_u \rho_u}{\rho} + b_1 \rho\right)^2 \tag{4.40}$$

Proof. We first rewrite f (4.38) using (4.30):

$$\begin{aligned} f &= a_1 - \sum_u b_u \rho_u - \frac{\sum_u a_u \rho_u}{\rho} + \frac{\sum_u a_u \rho_u}{\rho} = a_1 - \frac{1}{\rho}\sum_u (a_u + b_u \rho)\rho_u + \frac{\sum_u a_u \rho_u}{\rho} \\ &= a_1 - \frac{a_1 + b_1 \rho}{\rho} \underbrace{\sum_u \frac{a_u + b_u \rho}{a_1 + b_1 \rho} \rho_u}_{=\rho} + \frac{\sum_u a_u \rho_u}{\rho} = a_1 - (a_1 + b_1 \rho) + \frac{\sum_u a_u \rho_u}{\rho} \\ &= \frac{\sum_u a_u \rho_u}{\rho} - b_1 \rho \end{aligned} \tag{4.41}$$

We apply both forms of f (4.38), (4.41) to rewrite the determinant:

$$\begin{aligned} d &= \left(a_1 - \sum_u b_u \rho_u\right)^2 + 4b_1 \sum_u a_u \rho_u = f^2 + 4b_1 \sum_u a_u \rho_u \\ &= \left(\frac{\sum_u a_u \rho_u}{\rho} - b_1 \rho\right)^2 + 4b_1 \sum_u a_u \rho_u = \left(\frac{\sum_u a_u \rho_u}{\rho} + b_1 \rho\right)^2 \end{aligned} \tag{4.42}$$

□

We now show that the term between brackets in the determinant d (4.39) is nonnegative if the parameter conditions (4.16) and (4.19) are satisfied.

Lemma 4.4. *If the parameters satisfy (4.16) and (4.19) then*

$$\frac{\sum_u a_u \rho_u}{\rho} + b_1 \rho \geq 0 \tag{4.43}$$

Proof. In congestion both a_u and b_1 are nonnegative (see Lemma 4.2) and thus (4.43) is true. For the free flow regime we apply both forms of f (4.38), (4.41) to find:

$$\frac{\sum_u a_u \rho_u}{\rho} + b_1 \rho = f + 2b_1 \rho = a_1 - \sum_u b_u \rho_u + 2b_1 \rho > 0 \tag{4.44}$$

The inequality holds because from Lemma 4.1 we conclude that $a_1 + 2b_1\rho$ is positive and furthermore b_u is nonpositive. □

Lemma 4.4 implies that if (4.16) and (4.19) are satisfied, then the effective density takes a real value.

Theorem 4.4. *If the parameters satisfy (4.16) and (4.19) then the effective density given by ρ^- (4.34b) is the correct effective density.*

Proof. We apply both forms of f (4.38), (4.41) and Lemma 4.3 and 4.4 to find:

$$\begin{aligned} \rho^- &= \frac{a_1 - \sum_u b_u \rho_u - \sqrt{\left(a_1 - \sum_u b_u \rho_u\right)^2 + 4b_1 \sum_u a_u \rho_u}}{-2b_1} \\ &= \frac{a_1 - \sum_u b_u \rho_u - \left|\frac{\sum_u a_u \rho_u}{\rho} + b_1 \rho\right|}{-2b_1} = \frac{f - |f + 2b_1 \rho|}{-2b_1} = \frac{f - (f + 2b_1 \rho)}{-2b_1} \\ &= \rho \end{aligned} \tag{4.45}$$

We conclude that ρ^- gives the correct effective density ρ. □

Similarly, ρ^+ (4.34a) does in general not yield the correct effective density:

$$\rho^+ = \frac{f + |f + 2b_1 \rho|}{-2b_1} = \frac{f + (f + 2b_1 \rho)}{-2b_1} = -\left(\frac{f}{b_1} + \rho\right) \tag{4.46}$$

4.6 Summary of Fastlane model and conclusions

The Fastlane model follows naturally from the principles in Chapter 3. It is based on sound principles and is derived using assumptions from a simple car-following model. These assumptions are used to include interactions between different classes via the space occupancy and the passenger car equivalent value.

For later reference we summarize the Fastlane model equations. Fastlane consists of the multi-class conservation of vehicles equation:

$$\frac{\partial \rho_u}{\partial t}(t,x) + \frac{\partial q_u}{\partial x}(t,x) = 0 \tag{4.47}$$

with class-specific flow:

$$q_u = \rho_u v_u \tag{4.48}$$

The class-specific velocity is defined by the fundamental relation:

$$v_u = v_u(\rho) = \begin{cases} v_{u,\max} - \dfrac{v_{u,\max} - v_{\text{crit}}}{\rho_{\text{crit}}}\rho & \text{(free flow: } 0 \le \rho \le \rho_{\text{crit}}\text{)} \quad (4.49a) \\ w\left(\dfrac{\rho_{\text{jam}}}{\rho} - 1\right) & \text{(congestion: } \rho_{\text{crit}} \le \rho \le \rho_{\text{jam}}\text{)} \quad (4.49b) \end{cases}$$

with congestion parameter:

$$w = \frac{\rho_{\text{crit}} v_{\text{crit}}}{\rho_{\text{jam}} - \rho_{\text{crit}}} \tag{4.50}$$

and effective density:

$$\rho = \begin{cases} \dfrac{a_1 - \sum_u b_u \rho_u - \sqrt{(a_1 - \sum_u b_u \rho_u)^2 + 4 b_1 \sum_u a_u \rho_u}}{-2 b_1} & \text{if } b_1 \neq 0 \quad (4.51a) \\ \dfrac{\sum_u a_u \rho_u}{a_1 - \sum_u b_u \rho_u} & \text{if } b_1 = 0 \quad (4.51b) \end{cases}$$

with in free flow (if $0 \le \rho \le \rho_{\text{crit}}$):

$$a_u = L_u + T_u v_{u,\max} \quad \text{and} \quad b_u = -T_u \frac{v_{u,\max} - v_{\text{crit}}}{\rho_{\text{crit}}} \tag{4.52a}$$

and in congestion (if $\rho_{\text{crit}} \le \rho \le \rho_{\text{jam}}$):

$$a_u = T_u w \rho_{\text{jam}} \quad \text{and} \quad b_u = L_u - T_u w \tag{4.52b}$$

When solving the above model equations a unique solution is selected, namely the

solution that maximizes the effective flow:

$$q = \sum_u \eta_u q_u \tag{4.53}$$

Furthermore, we introduced the following conditions on the parameter values. Fundamental relation parameter conditions:

$$v_{\text{crit}} \leq v_{u,\max} \leq v_{1,\max} \leq 2v_{\text{crit}} \tag{4.54}$$

Space occupancy parameter conditions:

$$w \leq \frac{L_1}{T_1} \leq \frac{L_u}{T_u} \tag{4.55}$$

We have interpreted the conditions and we have shown that they are reasonable.

In the next chapter (Chapter 5) we generalize the model and show that the generalization also includes most other multi-class kinematic wave traffic flow models known from literature. The generalized model will be reformulated in Chapter 6. Only after this reformulation we are be able to show in Chapter 7 that Fastlane satisfies the requirements introduced in Chapter 3.

Chapter 5

Generalized formulation of multi-class models

We propose a generalized framework that contains all deterministic single-pipe multi-class kinematic wave models known from literature. We have identified eight models that have been developed in the last decade and are contained in this framework. In particular, we exclude models that explicitly consider multiple lanes Daganzo (2002); Chanut (2005) and models that include stochasticity (Ngoduy, 2010, 2011). The generalized model is largely the same as the Fastlane model. The models introduced by Wong & Wong (2002); Benzoni-Gavage & Colombo (2003); Chanut & Buisson (2003); Zhang et al. (2006); Ngoduy & Liu (2007); Logghe & Immers (2008); Nair et al. (2012) all fit into the generalized model, though some of them need to be reformulated first. Attempts to include all multi-class kinematic wave model in a generalized framework have been done before, most recently by Logghe & Immers (2008). However, the generalized model that we propose includes more models than previous generalized models. Moreover, our generalized model highlights the differences and similarities between the models. Furthermore, we can more easily analyze the models with respect to the qualitative requirements in Chapter 3. The analysis and comparison of models with Fastlane is presented in Chapter 7.

The focus of this chapter is on reformulating all models such that they are contained in our generalized framework. While introducing the models we also discuss the main modeling assumptions, usually related to the differences between the classes. Finally, we give an overview of the models to highlight their similarities and differences.

The outline of this chapter is as follows. In Section 5.1 we introduce the generalized model. In Section 5.2–5.5 we discuss and reformulate models known from literature to fit the generalized model. We start with the most complex models in Section 5.2 and end with the most simple ones in Section 5.5. Finally, in Section 5.6, we summarize and discuss the results.

5.1 Generalized multi-class kinematic wave model

We propose a generalized deterministic single-pipe multi-class kinematic wave model. It includes the multi-class conservation of vehicles equation and the definition of class-specific flow. We recall those equations from Chapter 4 (4.5) and (4.6):

$$\frac{\partial \rho_u}{\partial t} + \frac{\partial q_u}{\partial x} = 0 \tag{5.1a}$$

$$q_u = \rho_u v_u \tag{5.1b}$$

In the generalized model, the class-specific fundamental relation expresses the class-specific velocity v_u as a function of the effective density ρ:

$$v_u = v_u(\rho) \tag{5.1c}$$

We note that this implies that the class-specific velocity only depends on the effective density and that its parameters must be constant. Therefore, any fundamental relation parameters, such as maximum and critical velocity and critical and jam density, must be independent of the traffic state. Finally, the effective density is expressed as a function of all class-specific densities:

$$\rho = \rho(\rho_1, \ldots, \rho_U) \tag{5.1d}$$

Equations (5.1) form a generic deterministic multi-class single-pipe kinematic wave model. It can be generalized even further by combining (5.1c) and (5.1d) into:

$$v_u = v_u(\rho_1, \ldots, \rho_U) \tag{5.2}$$

This generalization is not needed for any of the models known from literature. However, it may be necessary if the fundamental relation of a future model can not only be expressed as a function of the effective density. For example, a relatively high truck density may have a different influence on cars than it has on other large vehicles.

We now discuss all models known from literature, and show how they are contained in the framework (5.1). In most cases this means that the model needs to be reformulated. We first discuss the most complex models which are based on making available road fractions to classes (Section 5.2). We continue with a short summary of the Fastlane model (Section 5.3). We then discuss the simpler models and show that they are specific forms of Fastlane. Some models include (constant) pce-values (Section 5.4), in others the effective density is an unweighted summation of the class-specific densities (Section 5.5). The results are summarized in Figure 5.1 and Table 5.2. The parameter values of the fundamental relations in Figure 5.1 are given in Table 5.1. The figure and tables are discussed in more detail later.

Table 5.1 *Parameter values of fundamental relations in Figure 5.1.*

General parameters				
maximum velocity class 1	$v_{1,\max}$	33.3 m/s	=	120 km/h
maximum velocity class 2 [1]	$v_{2,\max}$	25 m/s	=	90 km/h
critical velocity	v_{crit}	20.8 m/s	=	75 km/h
critical density	ρ_{crit}	0.033 veh/m	=	33 veh/km
jam density	ρ_{jam}	0.2 veh/m	=	200 veh/km
resulting congestion wave parameter	w	4.17 m/s	=	15 km/h
Logghe & Immers (2008)				
maximum velocity class 2	$v_{2,\max}$	20.8 m/s		v_{crit}
critical density class 1	$\rho_{1,\text{crit}}$	0.04 veh/m	=	40 veh/km
critical density class 2	$\rho_{2,\text{crit}}$	0.05 veh/m	=	50 veh/km
jam density class 1	$\rho_{1,\text{jam}}$	0.2 veh/m		ρ_{jam}
jam density class 2	$\rho_{2,\text{jam}}$	0.18 veh/m	=	180 veh/km
Ngoduy & Liu (2007)				
pce-value class 2	η_2	2		
Fastlane, Chanut & Buisson (2003); Benzoni-Gavage & Colombo (2003)				
gross vehicle length class 1	L_1	5 m		$1/\rho_{\text{jam}}$
gross vehicle length class 2	L_2	18 m		
Fastlane				
minimum time headway class 1	T_1	1 s		
minimum time headway class 2	T_2	1.5 s		
Nair et al. (2012)				
minimum bound pore size distribution	$b_{\min}$	0.01 m		
maximum bound pore size distribution	$b_{\max}$	3 m		
critical pore size class 1	$r_{1,\text{crit}}$	2.5 m		
critical pore size class 2	$r_{2,\text{crit}}$	0.8 m		
parameter fund. relation unrestricted	c^{ur}	0.8		
parameter fund. relation restricted	c^{rs}	2		
vehicle area class 1	a_1	8 m^2		
vehicle area class 2	a_2	1.6 m^2		
scaling parameter	d	1 m		

[1] Except for (Logghe & Immers, 2008)

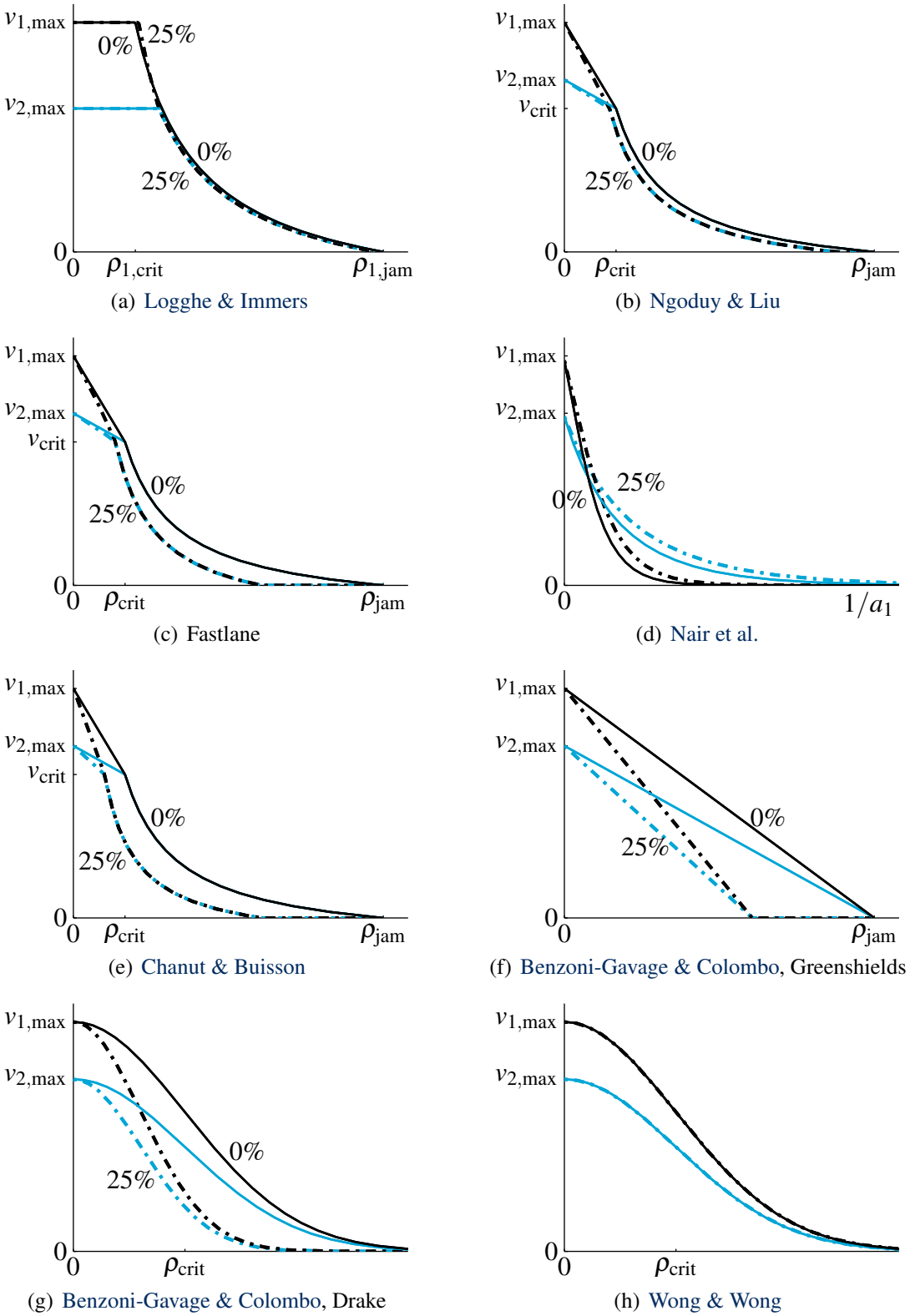

(a) Logghe & Immers

(b) Ngoduy & Liu

(c) Fastlane

(d) Nair et al.

(e) Chanut & Buisson

(f) Benzoni-Gavage & Colombo, Greenshields

(g) Benzoni-Gavage & Colombo, Drake

(h) Wong & Wong

Figure 5.1 *Fundamental relations of two-class models. The velocities of class 1 and 2 are expressed as function of the total densities (the number of vehicles per length unit). Each subfigure shows 4 fundamental relations. Black lines (starting at $v_{1,max}$) are velocities of class 1. Blue lines (starting at $v_{2,max}$) are velocities of class 2. Solid lines indicate the velocity if there are no vehicles of class 2, broken lines if 25% of the vehicles is of class 2.*

5.2 Models using road fractions

Both Logghe & Immers (2008) and Ngoduy & Liu (2007) use road fractions in their model formulation. For each class a certain fraction of the road is available. The fraction depends on the traffic composition and state. Depending on the fraction the fundamental relation is scaled. Using this scaled fundamental relation the class-specific velocities are determined. In the original formulation, the fundamental relation is not defined according to our generalized definition (5.1c). Furthermore, the model does not include an effective density (5.1d). However, both models can be reformulated, such that they are contained in the generalized formulation.

5.2.1 Model by Logghe & Immers

Logghe & Immers (2008) propose a two-class model including three regimes. In all these regimes the vehicles behave according to some user-equilibrium. The authors claim that due to the equilibrium approach slow vehicles influence fast vehicles, but not vice versa. In free flow both classes travel at their free flow velocity. It is assumed that there, is no interaction between drivers or vehicles, or at least they do not influence each others velocity. The main differences between classes can be seen in semi-congestion. In semi-congestion interaction between the vehicles does take place. However, only the vehicles of class 1 (e.g., passenger cars) react by slowing down. The velocity of vehicles of class 2 (e.g., trucks) is not influenced: they still travel at their free flow velocity. In congestion, vehicles of both classes are influenced by the presence of other vehicles and all vehicles slow down further.

In the original formulation, the velocity of each class v_u is determined by scaling the class-specific fundamental relation according to the road fraction α_u that is available for the class. The fundamental relation is a multi-class version of Daganzo's fundamental relation (see Section 2.1.2) with different parameters for each class, see Figure 5.1(a). The original formulation in density-flow form can be rewritten in density-velocity form:

$$v_u(\rho_1,\rho_2) = \begin{cases} v_{u,\max} & \text{(free flow)} \quad (5.3a) \\ w_u\left(\dfrac{\rho_{u,\text{jam}}}{\rho_u/\alpha_u} - 1\right) & \text{(congestion)} \quad (5.3b) \end{cases}$$

with parameter w_u:

$$w_u = \frac{\rho_{u,\text{crit}} v_{u,\max}}{\rho_{u,\text{jam}} - \rho_{u,\text{crit}}} \tag{5.4}$$

The class-specific free flow velocity, $v_{u,\max}$, the critical density $\rho_{u,\text{crit}}$ and the jam density $\rho_{u,\text{jam}}$ are constant parameters and therefore w_u (5.4) is constant as well.

We now reformulate the rest of the model, based on the original article (Logghe & Immers, 2008) and email communications with the first author. The reformulated model

includes the road fraction α_u and effective density ρ. It can be understood most easily by first considering semi-congestion.

Semi-congestion In semi-congestion the road fraction available for (the slower) class 2 is:

$$\alpha_2^{\mathrm{sc}} = \frac{\rho_2}{\rho_{2,\mathrm{crit}}} \tag{5.5}$$

The remaining capacity of the road is available for class 1. Therefore, its road fraction is:

$$\alpha_1^{\mathrm{sc}} = 1 - \frac{\rho_2}{\rho_{2,\mathrm{crit}}} = \frac{\rho_{2,\mathrm{crit}} - \rho_2}{\rho_{2,\mathrm{crit}}} \tag{5.6}$$

Class 2 is in free flow state and travels at its maximum velocity:

$$v_2 = v_2^{\mathrm{sc}} = v_{2,\max} \tag{5.7}$$

Class 1, however, is in the congestion state and its velocity is determined by the congestion branch of its scaled fundamental relation (5.3b). We reformulate its congestion branch as:

$$v_1^{\mathrm{sc}} = v_u^{\mathrm{c}}(\rho_1, \rho_2) = w_1 \left(\frac{\rho_{1,\mathrm{jam}}}{\rho} - 1 \right) \tag{5.8}$$

with effective density:

$$\rho = \frac{\rho_1}{\alpha_1} \tag{5.9}$$

and $\alpha_1 = \alpha_1^{\mathrm{sc}}$. Finally, we need to define when traffic is in semi-congestion. It is in semi-congestion if:

- the fraction of road for class 1 is too small for all vehicles of class 1 to maintain their free flow velocity ($\alpha_1^{\mathrm{sc}} \leq \rho_1/\rho_{1,\mathrm{crit}}$), and
- the velocity of class 1 is not smaller than the free flow velocity of class 2 ($v_1^{\mathrm{sc}} \geq v_{2,\max}$).

In all other cases traffic is either in free flow or congestion. We note that the introduction of the semi-congestion regime implies that generalization of the model to more than two classes is not straightforward.

Free flow. If $\alpha_1^{\mathrm{sc}} > \rho_1/\rho_{1,\mathrm{crit}}$ then there is enough road space for both classes to maintain their free flow velocity. The class-specific velocities are specified by the free flow branch of the fundamental relation (5.3a). Since the velocity does not depend on the effective density, it is not necessary to define the effective density.

Congestion. If $\alpha_1^{sc} \leq \rho_1/\rho_{1,crit}$ and $v_1^{sc} < v_{2,max}$ then traffic is in congestion. For both classes a certain road fraction is made available, such that their velocities are equal. Furthermore, the sum of their road fractions is one:

$$\alpha_1^c + \alpha_2^c = 1 \tag{5.10}$$

Substituting (5.10) into the congestion branch of the fundamental relation (5.3b) and setting the velocities of both classes equal gives:

$$w_1 \left(\frac{\rho_{1,jam}}{\rho_1/\alpha_1^c} - 1 \right) = w_2 \left(\frac{\rho_{2,jam}}{\rho_2/(1-\alpha_1^c)} - 1 \right) \tag{5.11}$$

The road fraction of class 1 is found by solving (5.11) for α_1^c:

$$\alpha_1^c = \frac{w_1 + w_2 \left(\frac{\rho_{2,jam}}{\rho_2} - 1 \right)}{w_1 \frac{\rho_{1,jam}}{\rho_1} + w_2 \frac{\rho_{2,jam}}{\rho_2}} \tag{5.12}$$

The velocity of both classes is determined by the congestion branch of the scaled fundamental relation (5.3b). Again, the fundamental relation can be rewritten as (5.8) with effective density (5.9) and road fraction $\alpha_1 = \alpha_1^c$ (5.12). The resulting fundamental relation for all states (free flow, semi-congestion and congestion) is shown in Figure 5.1(a). The model equations are repeated in Table 5.2 for later reference.

5.2.2 Model by Ngoduy & Liu

Ngoduy & Liu (2007) base their model on vehicle classes that are characterized by their maximum velocities in free flow and their pce-values. In congestion all vehicles travel at the same velocity. This model does not include semi-congestion. However, Ngoduy & Liu include the concept of road fractions in their model.

We first introduce the original formulation by Ngoduy & Liu (2007). Later we reformulate the model to be contained in the generalized model. Unlike Logghe & Immers (2008), Ngoduy & Liu simply assume that the road fraction α_u available for a class u is directly related to the fraction of vehicles of that class:

$$\alpha_u = \frac{\rho_u}{\rho^{tot}} \tag{5.13}$$

with $\rho^{tot} = \sum_u \rho_u$ the total density, which is in general not equal to the effective density, which will be defined later. For each class u they define a fundamental relation which is scaled according to the road fraction α_u available for a class u and its pce-value η_u. The fundamental relation is a multi-class version of the Smulders fundamental relation

(Smulders, 1990):

$$v_u = v_u(\tilde{\rho}) = \begin{cases} v_{u,\max} - \dfrac{v_{u,\max} - v_{\text{crit}}}{\tilde{\rho}_{\text{crit}}}\tilde{\rho} & \text{(free flow, } 0 \le \tilde{\rho} < \tilde{\rho}_{\text{crit}}) \quad (5.14a) \\ w\left(\dfrac{\tilde{\rho}_{\text{jam}}}{\tilde{\rho}} - 1\right) & \text{(congestion, } \tilde{\rho}_{\text{crit}} \le \tilde{\rho} \le \tilde{\rho}_{\text{jam}}) \quad (5.14b) \end{cases}$$

with parameter

$$w = \frac{\tilde{\rho}_{\text{crit}} v_{\text{crit}}}{\tilde{\rho}_{\text{jam}} - \tilde{\rho}_{\text{crit}}} \tag{5.15}$$

In the original formulation density is $\tilde{\rho}$ an unweighted summation of all class-specific densities:

$$\tilde{\rho} = \rho^{\text{tot}} = \sum_u \rho_u \tag{5.16}$$

The fundamental relation is scaled according to the road fraction α_u available for a class u and its pce-value η_u. This is done by scaling the parameters critical density ρ_{crit} and jam density ρ_{jam}:

$$\tilde{\rho}_{\text{crit}} = \rho_{\text{crit}} \sum_u \frac{\alpha_u}{\eta_u}, \quad \tilde{\rho}_{\text{jam}} = \rho_{\text{jam}} \sum_u \frac{\alpha_u}{\eta_u} \tag{5.17}$$

Ngoduy & Liu refer to the Highway Capacity Manual 2000 (Transportation Research Board, 2000) to look up pce-values η_u. The pce-values given there are constant or piecewise constant and may depend on vehicle type, vehicle length, slope of the road and fraction of heavy vehicles.

We reformulate the model such that the fundamental relation (5.14) expresses the class-specific velocities as a function of some effective density with constant parameters. The resulting fundamental relation is shown in Figure 5.1(b). Substitution of the scaled fundamental relation parameters (5.17) into the original fundamental relation (5.14) and rewriting the result gives the reformulated fundamental relation:

$$v_u = v_u(\rho) = \begin{cases} v_{u,\max} - \dfrac{v_{u,\max} - v_{\text{crit}}}{\rho_{\text{crit}}}\rho & \text{(free flow, } 0 \le \rho < \rho_{\text{crit}}) \quad (5.18a) \\ w\left(\dfrac{\rho_{\text{jam}}}{\rho} - 1\right) & \text{(congestion, } \rho_{\text{crit}} \le \rho \le \rho_{\text{jam}}) \quad (5.18b) \end{cases}$$

with

$$w = \frac{\tilde{\rho}_{\text{crit}} v_{\text{crit}}}{\tilde{\rho}_{\text{jam}} - \tilde{\rho}_{\text{crit}}} = \frac{\rho_{\text{crit}} v_{\text{crit}}}{\rho_{\text{jam}} - \rho_{\text{crit}}} \tag{5.19}$$

and effective density:

$$\rho = \bar{\eta}\rho^{\text{tot}} \tag{5.20}$$

with $\bar{\eta}$ the harmonic-weighted average of the class-specific pce-values:

$$\bar{\eta} = \frac{\sum_u \rho_u}{\sum_u \rho_u / \eta_u} = \frac{\rho^{\text{tot}}}{\sum_u \rho_u / \eta_u} \tag{5.21}$$

The model equations are repeated in Table 5.2 for later reference. Finally, we note that the stochastic extension of this model (Ngoduy, 2011) is not contained in the generalized formulation as it includes non-deterministic terms. Therefore, we do not include it further in our review and analysis.

5.3 Effective density using space occupancy (Fastlane)

Fastlane (see Chapter 4) distinguishes classes based on their maximum velocity, gross vehicle length and minimum time headway. Using these three differences between classes and a simple car-following model, Fastlane reflects that at low densities, heavy vehicles (e.g., trucks) have a relatively small influence and at high densities their influence is much larger. Furthermore, it is assumed that in congestion all vehicles travel at the same velocity.

In Fastlane the fundamental relation is specified by the same fundamental relation as the model by Ngoduy & Liu, namely the multi-class Smulders fundamental relation (5.18). The effective density is a weighted summation of all class-specific densities:

$$\rho = \sum_u \eta_u \rho_u \tag{5.22}$$

with pce-values:

$$\eta_u = \frac{L_u + T_u v_u}{L_1 + T_1 v_1} \tag{5.23}$$

We note that (5.22) and (5.23) can be reformulated such that the effective density is expressed similar toNgoduy & Liu's model (5.20) with $\bar{\eta}$ not the harmonic-weighted average but the arithmetic-weighted average pce-value:

$$\bar{\eta} = \frac{\sum_u \eta_u \rho_u}{\sum_u \rho_u} = \frac{\sum_u \eta_u \rho_u}{\rho^{\text{tot}}} \tag{5.24}$$

Recall that (5.14), (5.22) and (5.23) form an implicit set of equations. Therefore, this part of the model was reformulated in Section 4.5 as (4.49) and (4.51). The resulting fundamental relation is shown in Figure 5.1(c). The model equations are repeated in Table 5.2 for later reference. In all of the following models the effective density and pce-value is formulated as specific form of Fastlane's effective density (5.22) and pce-value (5.23). However, in some cases the fundamental relation takes a different shape (Greenshields or Drake instead of Smulders).

5.4 Effective density with constant pce-values

Chanut & Buisson (2003), Benzoni-Gavage & Colombo (2003) and Nair et al. (2012) propose multi-class models using effectively constant pce-values. However, Nair et al. reject the concept of pce-values for their application of disordered (non lane based) traffic flow. They base their model on the concept of pores. We show that the resulting model can be reformulated in the generalized framework with constant pce-values. Chanut & Buisson and Benzoni-Gavage & Colombo develop multi-class models based on a simpler set of assumptions, including different velocities for different classes. All three models in this section have fundamental relations with different shapes. Chanut & Buisson only include two-classes, while Benzoni-Gavage & Colombo and Nair et al. include an arbitrary number of classes.

5.4.1 Model by Nair et al.

Nair et al. developed a multi-class model to describe non lane-based traffic flow (Nair et al., 2011a,b, 2012). Such traffic situations often occur in developing countries. The model uses the concept of pores. Pores are the areas between vehicles and between vehicles and the roadside. Some (large) pores are accessible for almost any vehicle class, other (small) pores are only accessible for classes with small and highly manoeuvrable vehicles. A pore is said to be accessible by class u if its size r is larger than or equal to the critical pore size of the class $r_{u,\text{crit}}$ (in meters). In the following we only consider the most advanced model by Nair et al., which is proposed (Nair et al., 2012).

We now first introduce the original model formulation by Nair et al.. Later we reformulate the model to be contained in the generalized model. The class-specific (longitudinal) velocity is defined as a weighted average of restricted velocity (v_u^{rs}) and unrestricted velocity (v_u^{ur}):

$$v_u = \int_0^{r_{u,\text{crit}}} f(r)\mathrm{d}r\, v_u^{\text{rs}} + \int_{r_{u,\text{crit}}}^{\infty} f(r)\mathrm{d}r\, v_u^{\text{ur}} \tag{5.25}$$

The integrals denote the fraction of pores that are inaccessible $\left(\int_0^{r_{u,\text{crit}}} f(r)\mathrm{d}r\right)$ or accessible $\left(\int_{r_{u,\text{crit}}}^{\infty} f(r)\mathrm{d}r\right)$ for class u. Consequently the sum of the fractions is one:

$$\int_0^{r_{u,\text{crit}}} f(r)\mathrm{d}r + \int_{r_{u,\text{crit}}}^{\infty} f(r)\mathrm{d}r = 1 \tag{5.26}$$

The velocity of restricted and unrestricted vehicles is determined respectively by:

$$v_u^{\text{ur}} = v_{u,\max}\left(1 - \int_0^{r_{u,\text{crit}}} f(r)\mathrm{d}r\right)^{c^{\text{ur}}} \tag{5.27a}$$

$$\text{and} \quad v_u^{\text{rs}} = v_{u,\max}\left(1 - \int_0^{r_{u,\text{crit}}} f(r)\mathrm{d}r\right)^{c^{\text{rs}}} \tag{5.27b}$$

with c^{ur} and c^{rs} some parameters with $c^{\text{ur}} \leq c^{\text{rs}}$. Furthermore, pore spaces are assumed to be distributed negative exponentially with mean p. Consequently, the fraction of pores that is accessible to class u is:

$$\int_0^{r_{u,\text{crit}}} f(r)\mathrm{d}r = e^{-pr_{u,\text{crit}}} \tag{5.28}$$

Finally, the mean pore space $1/p$ depends on the traffic state and is defined by:

$$p = p(\rho_1, \ldots, k_U) = (b_{\max} - b_{\min}) \left(\sum_u a_u k_u \right) + b_{\min} \tag{5.29}$$

with $b_{\min}$ and $b_{\max}$ bounds on the mean of the distribution. a_u is a constant, denoting the area that vehicles of class u project on the roadway in m^2 (or m^2 per vehicle). k_u is the class-specific areal density in vehicle per m^2.

We reformulate the model. Therefore, we first redefine the fundamental relation by combining (5.25)–(5.28):

$$v_u = \left[g_u (1-g_u)^{c^{\text{rs}} - c^{\text{ur}}} + (1-g_u) \right] (1-g_u)^{c^{\text{ur}}} v_{u,\max} \tag{5.30}$$

with g the fraction of pores that is accessible to class u:

$$g_u = e^{-pr_{u,\text{crit}}} = \int_0^{r_{u,\text{crit}}} f(r)\mathrm{d}r \tag{5.31}$$

Furthermore, we redefine the mean pore space p. Nair et al. use the class-specific areal density k_u in the conservation equation (5.1a). Since the velocity is defined only in longitudinal direction, this implies a contradiction. Therefore, and to fit the model into the generalized formulation we reformulate the mean pore space p (5.29) with the following definitions:

$$\rho_u := d k_u \tag{5.32}$$

$$\text{and} \quad \rho := \sum_u \frac{a_u}{a_1} \rho_u = \sum_u \eta_u \rho_u \tag{5.33}$$

with d a scaling factor. Consequently, the pce-value η_u is constant. It is not based on the traffic state but only on the average vehicle areas a_u and a_1:

$$\eta_u = \frac{a_u}{a_1} \tag{5.34}$$

This yields the mean pore space $1/p$, which is now defined by:

$$p = p(\rho) = (b_{\max} - b_{\min}) \left(\frac{a_1}{d} \rho \right) + b_{\min} \tag{5.35}$$

It can be verified that (5.35) is equivalent to (5.29) by substitution of (5.32) and (5.33) into (5.35). The resulting fundamental relation is shown in Figure 5.1(d). The model

equations are repeated in Table 5.2 for later reference.

5.4.2 Model by Chanut & Buisson

Similar to the model by Ngoduy & Liu (2007), the original formulations of the models by Chanut & Buisson and Benzoni-Gavage & Colombo do not include an effective density but a total density (5.16). The fundamental relation is scaled according to the traffic state and expresses the class-specific velocity as a function of the total density.

The model by Chanut & Buisson (2003) only includes 2 classes. These classes have different lengths and different velocities in free flow. In the original formulation, they define the fundamental relation very similar to Ngoduy & Liu (2007). The shape and parameter w are defined by (5.14) and (5.15), respectively. However, they define the scaled parameters of the fundamental relation differently:

$$\tilde{\rho}_{\text{crit}}(\rho_1,\rho_2) = \beta\tilde{\rho}_{\text{jam}}(\rho_1,\rho_2), \quad \tilde{\rho}_{\text{jam}}(\rho_1,\rho_2) = \frac{\tilde{\rho}}{L_1\rho_1 + L_2\rho_2} \tag{5.36}$$

with $\beta \in [0.2, 0.5]$ some constant. $L_1 = \tilde{\rho}_{\text{jam}}(\rho_1, 0)$ and $L_2 = \tilde{\rho}_{\text{jam}}(0, \rho_2)$ are the gross vehicle lengths of class 1 and 2 respectively.

We reformulate the model such that the fundamental relation (5.14) expresses the class-specific velocities as a function of some effective density and with constant parameters. The resulting fundamental relation is shown in Figure 5.1(e). The reformulated model includes the fundamental relation (5.18) with parameter w as in (5.19). The other parameters of the reformulated fundamental relation are:

$$\rho_{\text{jam}} := \tilde{\rho}_{\text{jam}}(\rho_1, 0) \quad \text{and} \quad \rho_{\text{crit}} := \tilde{\rho}_{\text{crit}}(\rho_1, 0) = \beta\tilde{\rho}_{\text{jam}}(\rho_1, 0) \tag{5.37}$$

The effective density is defined by (5.22). The pce-value is a reduced version of Fastlane's pce function (5.23), with $T_u = 0$ for all user classes u. Consequently, the pce-values become:

$$\eta_u = L_u / L_1 \tag{5.38}$$

It can be verified that the above described reformulated model is indeed equivalent to the original model by Chanut & Buisson (2003) by substitution of the unscaled parameters (5.37) and the effective density (5.22) with pce-values (5.38) into the reformulated fundamental relation (5.18). By doing this, one will find the original fundamental relation (5.14) with scaled parameters (5.36) and total density (5.16). The resulting fundamental relation is shown in Figure 5.1(c). The model equations are repeated in Table 5.2 for later reference.

5.4.3 Model by Benzoni-Gavage & Colombo (2003)

Benzoni-Gavage & Colombo (2003) apply classes that differ with respect to vehicle length and with respect to maximum velocities. The authors claim that with this approach overtaking is, at least partly, taken into account. Due to the vehicle class-specific velocities, the first in first out (fifo) rule does not hold and one class (e.g., cars) may travel faster than other classes (e.g., trucks).

Benzoni-Gavage & Colombo define the effective density as a weighted summation of all class-specific densities. Therefore, reformulation of their model to be contained in the generalized model is not necessary and the effective density is defined by (5.22). pce-values are constant and depend on the gross vehicle length as in Chanut & Buisson's model (5.38).

Furthermore, Benzoni-Gavage & Colombo define the class-specific fundamental relation (5.1c) as a scaled version of the fundamental relation of class 1:

$$v_u = \beta_u v_1 \tag{5.39}$$

Finally, they propose two different shapes of the fundamental relation of class 1, see Figure 5.1(f) and 5.1(g). The first one is Greenshields' fundamental relation (Greenshields, 1935).

$$v_1(\rho) = v_{1,\max}\left(1 - \frac{\rho}{\rho_{\text{jam}}}\right) \tag{5.40}$$

We note that the fundamental relation (5.39) and (5.40) is a reduced version of Smulders' multi-class fundamental relation (5.18) with:

$$\rho_{\text{crit}} = \rho_{\text{jam}}, \quad v_{\text{crit}} = 0 \quad \text{and} \quad \beta_u = \frac{v_{u,\max}}{v_{1,\max}} \tag{5.41}$$

Alternatively, Benzoni-Gavage & Colombo propose to apply a multi-class version of Drake's fundamental relation (Drake et al., 1967):

$$v_1(\rho) = v_{1,\max} e^{-\frac{1}{2}\left(\frac{\rho}{\rho_{\text{crit}}}\right)^2} \tag{5.42}$$

The resulting fundamental relation is shown in Figure 5.1(c). The model equations are repeated in Table 5.2 for later reference.

5.5 Effective density with pce-value equal to one

The last two models (Wong & Wong, 2002; Zhang et al., 2006) that we discuss include an arbitrary number of classes. The classes only differ with respect to their velocity. Both Wong & Wong and Zhang et al. apply an effective density that is equal to the total

density (5.16). Again, this is a reduced version of Fastlane's effective density (5.22) and pce function (5.23). In this case the parameter values are $L_u = L_1$ and $T_u = 0$ for all classes u. Essentially, the effective density is equal to the effective density in Fastlane (5.22) but with pce-values one ($\eta_u = 1$). This implies that the velocities do not depend on the composition but only on the total number of vehicles. Zhang et al. analyze the model without specifying the shape of the fundamental relation. They only assume that the velocity of any class u is a factor times the velocity of class 1:

$$v_u = \frac{v_{u,\max}}{v_{1,\max}} v_1 \tag{5.43}$$

Both Zhang et al. and Wong & Wong scale the fundamental relation of class 1 to define the velocities of the other classes, such as Benzoni-Gavage & Colombo (5.39). Wong & Wong apply Drake's fundamental relation (5.42), see Figure 5.1(h). The model equations are repeated in Table 5.2 for later reference.

5.6 Conclusions

We have developed a generalized traffic flow model (5.1) that contains all deterministic single-pipe multi-class kinematic wave models known from literature. The models are based on different principles, such as making available fractions of road to classes, pce-values (constant or based on dynamic space occupancy) and analogy to porous flow. The principles and assumptions of the models are highlighted in Table 5.2. The table furthermore shows how this leads to different fundamental relations and effective density functions.

We have shown that all models may be cast in the same generalized model containing the following elements:

1. conservation of vehicles equation (5.1a)
2. definition of class-specific flow (5.1b)
3. class-specific fundamental relation (5.1c)
4. effective density function (5.1d)

The first two elements are equal for all models. Models can be distinguished based on the shape of the fundamental relation and the effective density function. The fundamental relation usually takes a traditional shape. However, the effective density function varies largely over the model. Finally, the models differ with respect to the number of classes. Most models do not put any restrictions on the number of classes. The model by Chanut & Buisson (2003) only includes 2 classes, but can be generalized relatively straightforward to include more classes. However, the model by Logghe & Immers (2008) also includes only 2 classes, but its generalization to more classes is not straightforward.

With the generalized model in hand, we can now more easily assess the models qualitatively. Most requirements from Chapter 3 can be assessed directly. However, some

requirements (such as the ones related to characteristic velocity) need another reformulation of the generalized model first. Therefore, in the next chapter (Chapter 6) we reformulate the generalized model in the Lagrangian coordinate system. In Chapter 7 we assess the generalized model and all specific models with respect to the qualitative requirements in Chapter 3.

Table 5.2 *Classification of multi-class models, according to the principles and assumptions on which they are based, maximum number of classes and according to the model equations (i.e. fundamental relation, effective density and pce function or value). (Regimes: ff: free flow, sc: semi-congestion, cn: congestion.)*

Principle / assumption	nr. of classes	Model	Class specific velocity $v_u(\rho)$	Effective density $\rho(\rho_1,\ldots,\rho_U)$
user equilibrium, 3 regimes	2	Logghe & Immers (2008)	Daganzo: $v_u = \begin{cases} v_{u,\max} & \text{ff, sc } u=2 \\ w_1\left(\frac{\rho_{1,\text{jam}}}{\rho}-1\right) & \text{sc } u=1\text{, cn} \end{cases}$	$\rho = \begin{cases} \text{undefined} & \text{ff } (\alpha_1^{\text{sc}} > \frac{\rho_1}{\rho_{1,\text{crit}}}) \\ \frac{\rho_1}{\alpha_1^{\text{sc}}},\quad \alpha_1^{\text{sc}} = 1-\frac{\rho_2}{\rho_{2,\text{crit}}} & \text{sc } (\alpha_1^{\text{sc}} \le \frac{\rho_1}{\rho_{1,\text{crit}}}) \text{ and } (v_1 \ge v_{2,\max}) \\ \frac{\rho_1}{\alpha_1^{\text{c}}},\quad \alpha_1^{\text{c}} = \frac{w_1+w_2\left(\frac{\rho_{2,\text{jam}}}{\rho_2}-1\right)}{w_1\frac{\rho_{1,\text{jam}}}{\rho_1}+w_2\frac{\rho_{2,\text{jam}}}{\rho_2}} & \text{cn } (v_1 < v_{2,\max}) \end{cases}$
road fractions	U	Ngoduy & Liu (2007)	Smulders: $v_u = \begin{cases} v_{u,\max} - \frac{v_{u,\max}-v_{\text{crit}}}{\rho_{\text{crit}}}\rho & \text{ff} \\ w\left(\frac{\rho_{\text{jam}}}{\rho}-1\right) & \text{cn} \end{cases}$	$\rho = \bar{\eta}\sum_u \rho_u,\quad \bar{\eta} = \frac{\sum_u \rho_u}{\sum_u(\rho_u/\eta_u)}$
space occupancy		Fastlane		$\rho = \begin{cases} \frac{(a_1-\sum_u b_u\rho_u)-\sqrt{(a_1-\sum_u b_u\rho_u)^2+4b_1\sum_u a_u\rho_u}}{-2b_1} & \text{if } b_1 \neq 0 \\ \frac{\sum_u a_u\rho_u}{a_1-\sum_u b_u\rho_u} & \text{if } b_1 = 0 \end{cases}$ $\begin{cases} a_u = L_u + T_u v_{u,\max},\quad b_u = -T_u\frac{v_{u,\max}-v_{\text{crit}}}{\rho_{\text{crit}}} & \text{ff} \\ a_u = T_u w \rho_{\text{jam}},\quad b_u = L_u - T_u w & \text{cn} \end{cases}$
flow through pores, vehicle area		Nair et al. (2012)	$v_u = \left[g_u(1-g_u)^{c^{\text{rs}}-c^{\text{ur}}} + (1-g_u)\right] \times (1-g_u)^{c^{\text{ur}}} v_{u,\max}$ $g_u = e^{-\gamma r_{u,\text{crit}}},\ \gamma = (b_{\max}-b_{\min})\frac{a_1}{d}\rho + b_{\min}$	$\rho = \sum_u \eta_u\rho_u,\quad \eta_u = \frac{\omega_u}{\omega_1} = \frac{L_u+T_u v_u}{L_1+T_1 v_1}$ $\omega_u = L_u + T_u v_u$ $T_u = 0,\ L_u = a_u,$ $\Rightarrow \omega_u = a_u \Rightarrow \eta_u = \frac{a_u}{a_1}$ $\Rightarrow \rho = \sum_u \frac{L_u+T_u v_u}{L_1+T_1 v_1}\rho_u$
vehicle length	2	Chanut & Buisson (2003)	Smulders	$T_u = 0$ $\Rightarrow \omega_u = L_u \Rightarrow \eta_u = \frac{L_u}{L_1}$ $\Rightarrow \rho = \sum_u \frac{L_u}{L_1}\rho_u$
	U	Benzoni-Gavage & Colombo (2003)	Greenshields: $v_u = v_{u,\max}\left(1-\frac{\rho}{\rho_{\text{jam}}}\right)$ i.e. Smulders with $\rho_{\text{crit}} = \rho_{\text{jam}},\ v_{\text{crit}} = 0$	
unequal velocities		Wong & Wong (2002)	Drake: $v_u = v_{u,\max} e^{-\frac{1}{2}\left(\frac{\rho}{\rho_{\text{crit}}}\right)^2}$	$T_u = 0,\ L_u = L_1$ $\Rightarrow \omega_u = L_1 \Rightarrow \eta_u = 1$ $\Rightarrow \rho = \sum_u \rho_u$
		Zhang et al. (2006)	$v_u = \frac{v_{u,\max}}{v_{1,\max}} v_1$, shape undefined	

Chapter 6

Lagrangian formulation

In Chapter 2 and 5 the mixed-class kinematic wave model and the generalized multi-class kinematic wave model were introduced, respectively. Traditionally, the models are formulated in the Eulerian coordinate system, which is fixed in space. Alternatively, they can be formulated in the Lagrangian coordinate system, which moves with the vehicles. In this chapter we discuss the state-of-the-art in the Lagrangian formulation of traffic flow models, we extend it to multi-class models and we discuss its advantages.

The outline of this chapter is as follows. In Section 6.1 we summarize the derivation of the Lagrangian formulation of the kinematic wave model as it was proposed by Leclercq et al. (2007). In Section 6.2 we propose a graphical, more intuitive derivation. In Section 6.3 we derive the Lagrangian formulation of the multi-class kinematic wave model. Again, this is followed by a graphical, more intuitive derivation in Section 6.4. Section 6.5 concludes this chapter with a discussion of the advantages of the Lagrangian formulation.

6.1 Lagrangian formulation of the kinematic wave model

We recall the Eulerian formulation of the kinematic wave model (2.23):

$$\frac{\partial \rho}{\partial t} + \frac{\partial}{\partial x}\big(q(\rho)\big) = 0 \tag{6.1a}$$

$$q = q(\rho) \tag{6.1b}$$

Location x and time t are the coordinates and the model describes how the variables (density ρ and flow q) change over location and time. The coordinate system is shown in Figure 6.1(a).

Leclercq et al. (2007) propose an alternative formulation using the cumulative count function (Newell, 1993a). Daganzo (2005a); Leclercq et al. (2007); Laval & Leclercq

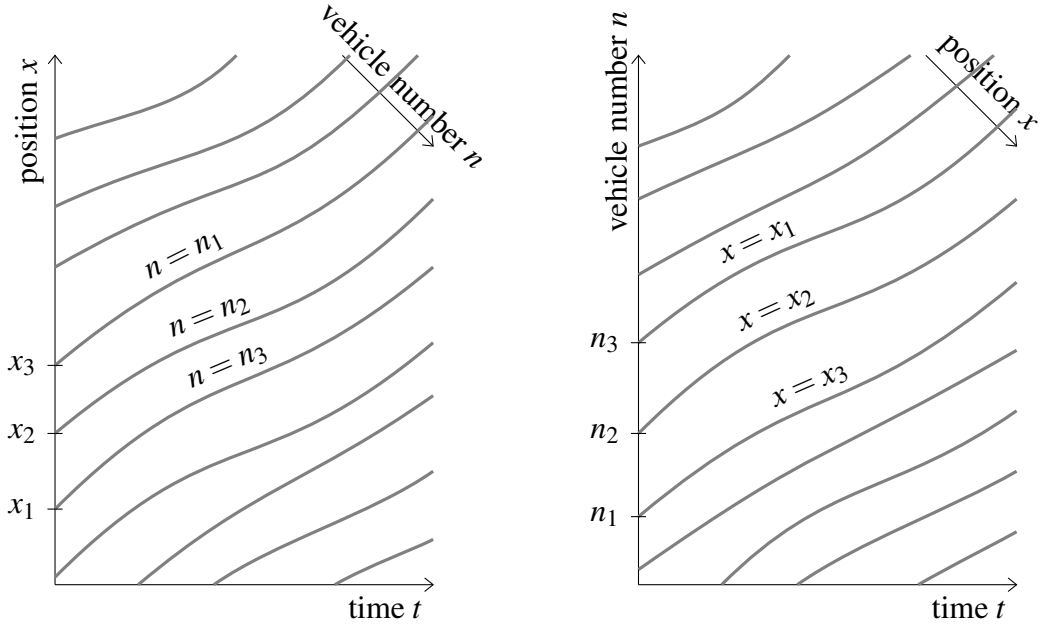

(a) Eulerian coordinate system with vehicle trajectories: vehicle number n increases over time for fixed position x.

(b) Lagrangian coordinate system: position x increases over time for fixed vehicle number n.

Figure 6.1 *Eulerian and Lagrangian coordinate system.*

(2013) show the close relation between the kinematic wave model, Hamilton-Jacobi partial differential equations and variational theory applied to traffic flow. The cumulative count function (Newell, 1993a) deals with the number of vehicles $n(x,t)$ that have passed location x until time t. The vehicles are numbered in the order they pass a certain location, thus $n(x,t)$ is the number of vehicles that have passed location x until time t. The cumulative count function and variational theory can be applied directly to solve the kinematic wave model, which will be discussed in more detail in Chapter 8. However, Leclercq et al. (2007) exploit the cumulative count function further and propose to transform the (Eulerian) coordinate system into a Lagrangian coordinate system, see Figure 6.1(b). Now the coordinate system moves with the vehicles. The same coordinate transformation is applied before to higher-order models (Greenberg, 2001; Aw et al., 2002). Recently, another alternative coordinate system has been introduced. Leclercq & Bécarie (2012); Laval & Leclercq (2013) propose a formulation of the kinematic wave model that calculates the time t at which vehicle n reaches location x.

The coordinate transformation from Eulerian to Lagrangian (t,n) formulation implies replacing spatial coordinate x by vehicle number n. Consequently, for a fixed vehicle number n, its location x changes over time t. Moreover, since we are dealing with a macroscopic (continuum) model, n is not integer but can take any (real) value. Time t remains a coordinate and the model now describes the change of the traffic state over vehicle number and time. Furthermore, instead of using density as a variable it is more

Table 6.1 *Comparison between Eulerian and Lagrangian formulation of the kinematic wave model.*

	Euler	Lagrange
coordinates	(x,t)	(n,t)
main variable	$\rho = -\partial n/\partial x$	$s = -\partial x/\partial n$
fundamental relation	$q(\rho)$	$v^*(s)$
conservation equation	$\frac{\partial \rho}{\partial t} + \frac{\partial q}{\partial x} = 0$	$\frac{\mathrm{D}s}{\mathrm{D}t} + \frac{\partial v^*}{\partial n} = 0$

convenient to replace it with spacing:

$$s = \frac{1}{\rho} \tag{6.2}$$

The other variable is velocity v^*.[1] The main differences between the two formulations of the kinematic wave model are highlighted in Table 6.1.

The kinematic wave model in Lagrangian formulation consists of a conservation equation and a fundamental relation. The fundamental relation expresses the vehicle velocity v^* as a function of the spacing s:

$$v = v^*(s) \tag{6.3}$$

Figure 2.2(d) shows such a Lagrangian fundamental relation. As an example we reformulate the mixed-class Smulders fundamental relation (4.7):

$$v = v(\rho) = \begin{cases} v_{\max} - \dfrac{v_{\max} - v_{\text{crit}}}{\rho_{\text{crit}}}\rho & \text{(free flow)} \quad (6.4a) \\ w\left(\dfrac{\rho_{\text{jam}}}{\rho} - 1\right) & \text{(congestion)} \quad (6.4b) \end{cases}$$

(6.4) is reformulated in its Lagrangian equivalent by applying the definition of spacing (6.2):

$$v = v^*(s) = \begin{cases} v_{\max} - \dfrac{v_{\max} - v_{\text{crit}}}{s} s_{\text{crit}} & \text{(free flow)} \quad (6.5a) \\ w\left(\dfrac{s}{s_{\text{jam}}} - 1\right) & \text{(congestion)} \quad (6.5b) \end{cases}$$

with critical spacing $s_{\text{crit}} = 1/\rho_{\text{crit}}$ and jam spacing $s_{\text{jam}} = 1/\rho_{\text{jam}}$.

Leclercq et al. (2007) derive the Lagrangian conservation equation from its Eulerian

[1] We use v^* to make a distinction between the velocity $v = v(\rho)$ as a function of the density in the Eulerian formulation and $v^* = v^*(s)$ as a function of the spacing in the Lagrangian formulation. For readability, whenever the distinction is clear from the context, we omit the *.

formulation (6.1). In Section 6.2 we propose an alternative, graphical derivation. However, we first discuss the mathematically more rigorous derivation by Leclercq et al. (2007). They use the definition of spacing (6.2) and express spacing as the partial derivative of the position x to vehicle number n:

$$s = -\frac{\partial x}{\partial n} \tag{6.6}$$

The minus sign results from the fact that vehicles are numbered opposite to the driving direction, see Figure 6.1(b).

Furthermore, the Lagrangian time derivative is applied:

$$\frac{\mathrm{D}}{\mathrm{D}t} = \frac{\partial}{\partial t} + v\frac{\partial}{\partial x} \tag{6.7}$$

$\mathrm{D}/\mathrm{D}t$ is the partial derivative with respect to time in Lagrangian coordinates, that is: the derivative with respect to time t with the other coordinate (vehicle number n) fixed. As n-coordinates move with vehicle velocity, $\mathrm{D}r/\mathrm{D}t$ is the rate of change of some variable r as it is observed by a driver moving with velocity $v(n,t) = v(x(n),t) = \partial x/\partial t$. This implies that $\mathrm{D}/\mathrm{D}t$ is a directional derivative in Eulerian coordinates: it is the derivative in the direction of the moving observer (the driver). Both coordinates t and x change in this direction. Conversely, $\partial/\partial t$ is a partial derivative in Eulerian coordinates and a directional derivative in Lagrangian coordinates.

The conservation equation in the Lagrangian coordinates can now be derived by substituting the definition of spacing (6.2) into the Eulerian conservation equation (6.1a), applying the quotient rule and rewriting the result:

$$\frac{\partial}{\partial t}(1/s) + \frac{\partial}{\partial x}(v/s) = 0 \quad \Rightarrow \quad \frac{\partial s}{\partial t} - s\frac{\partial v}{\partial x} + v\frac{\partial s}{\partial x} = 0 \tag{6.8}$$

Subsequently substituting the Lagrangian time derivative (6.7) yields:

$$\frac{\mathrm{D}s}{\mathrm{D}t} - s\frac{\partial v}{\partial x} = 0 \tag{6.9}$$

Finally, the definition of spacing (6.6) is substituted to find the Lagrangian conservation equation:

$$\frac{\mathrm{D}s}{\mathrm{D}t} + \frac{\partial v}{\partial n} = 0 \tag{6.10}$$

To avoid further confusion, in the following we write the Lagrangian time derivative (6.7) as $\partial/\partial t$, unless it is necessary to use $\mathrm{D}/\mathrm{D}t$ to distinguish between the Eulerian and the Lagrangian time derivative.

The conservation equation in Lagrangian formulation (6.10) can be understood qualitatively by considering two vehicles: a leader and a follower. If the follower has a higher velocity than the leader, the distance between the two vehicles decreases, i.e. if

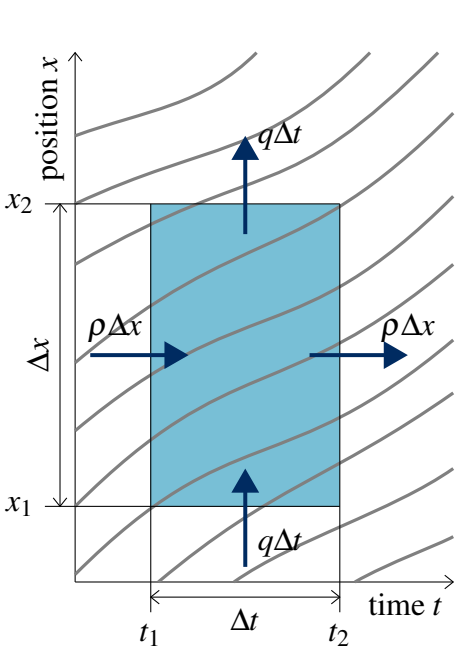

(a) A rectangular control volume that is fixed in space, applied to derive the Eulerian conservation equation.

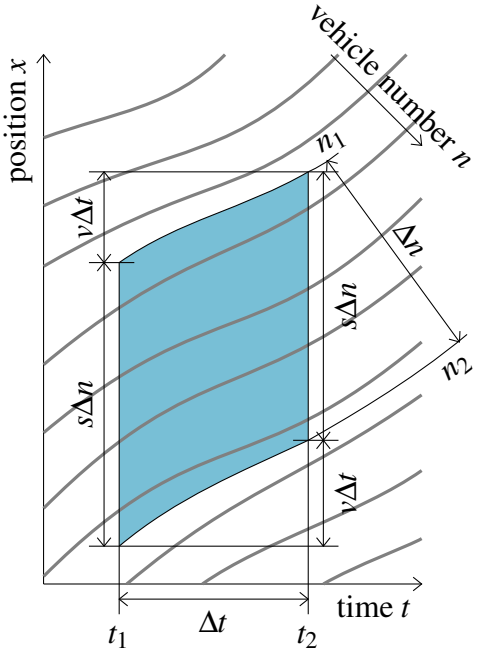

(b) A control volume that follows a platoon of Δn vehicles over a time Δt, applied to derive the Lagrangian conservation equation.

Figure 6.2 *Graphical derivation of Eulerian and Lagrangian conservation equation using vehicle trajectories and control volumes.*

$\partial v/\partial n > 0$ then $\mathrm{D}s/\mathrm{D}t < 0$. The reverse is also true: if the follower is slower than the leader the distance will increase.

6.2 Graphical derivation

The above derivation of the Lagrangian conservation equation (6.10) might be difficult to understand intuitively and has the disadvantage that it relies on the Eulerian formulation. We propose an alternative derivation that does not rely on the Eulerian formulation. Instead, it is similar to the (graphical) derivation of the Eulerian conservation equation. Furthermore, it uses similar concepts as Greens theorem and the divergence theorem (Stewart (1999) or any other textbook on partial differential equations). In the following, we first discuss the graphical derivation of the Eulerian conservation equation before turning to our graphical derivation of the Lagrangian conservation equation.

6.2.1 Graphical derivation of the Eulerian formulation

The Eulerian conservation equation can be derived using vehicle trajectories in a control volume as illustrated in Figure 6.2(a). The number of vehicles entering the control

volume (inflow) equals the number of vehicles leaving it (outflow). This can be written as:

$$\underbrace{\int_{x_1}^{x_2} \rho(t_1,x)\,\mathrm{d}x}_{\text{inflow from left}} + \underbrace{\int_{t_1}^{t_2} q(t,x_1)\,\mathrm{d}t}_{\text{inflow from below}} = \underbrace{\int_{x_1}^{x_2} \rho(t_2,x)\,\mathrm{d}x}_{\text{outflow to right}} + \underbrace{\int_{t_1}^{t_2} q(t,x_2)\,\mathrm{d}t}_{\text{outflow to above}} \tag{6.11}$$

We decrease the control volume to an infinitesimal volume: $x_2 = x_1 + \Delta x \to x_1$ and $t_2 = t_1 + \Delta t \to t_1$. Because the volume is small, we may assume density ρ and flow q are constant. Consequently, $\int_{x_1}^{x_2} \rho(t,x)\mathrm{d}x \to \rho(t,x)\Delta x$ and $\int_{t_1}^{t_2} q(t,x)\mathrm{d}t \to q(t,x)\Delta t$. Furthermore, rewriting (6.11) yields:

$$\frac{\rho(t_1+\Delta t,x)-\rho(t_1,x)}{\Delta t} + \frac{q(t,x_1+\Delta x)-q(t,x_1)}{\Delta x} = 0 \tag{6.12}$$

We now recall the definition of the partial derivatives of $f = f(y,z)$:

$$\frac{\partial}{\partial y} f(y,z) = \lim_{\Delta y \to 0} \frac{f(y+\Delta y,z)-f(y,z)}{\Delta y}, \quad \frac{\partial}{\partial z} f(y,z) = \lim_{\Delta z \to 0} \frac{f(y,z+\Delta z)-f(y,z)}{\Delta z} \tag{6.13}$$

We apply this definition (6.13) to the infinitesimal control volume and find the Eulerian conservation equation (6.1a).

6.2.2 Graphical derivation of the Lagrangian formulation

The Lagrangian conservation equation can be derived using a similar procedure. In this case, the control volume is not rectangular as in Figure 6.2(a) but it is a platoon of Δn vehicles that is followed over a time Δt, as in Figure 6.2(b). (However, the platoon is rectangular in the (t,n)-plane.) The road length taken by this platoon changes over time as it travels forward. On one hand, the original length at time t_1 is increased by the distance traveled by the first vehicle n_1. On the other hand, it is decreased by the distance traveled by the last vehicle $n_2 = n_1 + \Delta n$. (Note again the order of vehicles: vehicle n_2 is behind vehicle n_1.) This can be written as:

$$\underbrace{\int_{n_1}^{n_2} s(t_2,n)\mathrm{d}n}_{\text{final length}} = \underbrace{\int_{n_1}^{n_2} s(t_1,n)\mathrm{d}n}_{\text{initial length}} + \underbrace{\int_{t_1}^{t_2} v(t,n_1)\mathrm{d}t}_{\text{distance first veh}} - \underbrace{\int_{t_1}^{t_2} v(t,n_2)\mathrm{d}t}_{\text{distance last veh}}. \tag{6.14}$$

Again, by decreasing the control volume to an infinitesimal volume we may assume spacing s and velocity v are constant within this volume. Consequently, $\int_{n_1}^{n_2} s(t,n)\mathrm{d}n \to s(t,n)\Delta n$ and $\int_{t_1}^{t_2} v(t,n)\mathrm{d}t \to v(t,n)\Delta t$. Furthermore, rewriting (6.14) yields:

$$\frac{s(t_2,n)-s(t_1,n)}{\Delta t} + \frac{v(t,n_2)-v(t,n_1)}{\Delta n} = 0. \tag{6.15}$$

We take an infinitesimal volume, that is: we let $\Delta n \to 0$ and $\Delta t \to 0$ in (6.15). Furthermore, we use the definition of the partial derivative (6.13) to find the Lagrangian conservation equation (6.10).

The Lagrangian conservation equation that we derive in this graphical way, is exactly the same partial differential equation as was derived using the mathematically more rigorous approach in Section 6.1. However, we believe that the graphical derivation is easier to understand and interpret intuitively.

6.3 Multi-class kinematic wave model

We derive the Lagrangian formulation of the generic multi-class kinematic wave model (5.1) from its Eulerian formulation. The derivation in this section is mathematically rigorous and relies on the Eulerian formulation. In the next section (Section 6.4) we propose a graphical, more intuitive, derivation of the multi-class conservation equation. Let us first recall the Eulerian formulation of the model (5.1):

$$\frac{\partial \rho_u}{\partial t} + \frac{\partial q_u}{\partial x} = 0 \tag{6.16a}$$

$$q_u = \rho_u v_u = \rho_u v_u(\rho) \tag{6.16b}$$

$$\rho = \rho(\rho_1, \ldots, \rho_U) \tag{6.16c}$$

6.3.1 Reformulation of fundamental relation and effective density

The derivation of the Lagrangian formulation starts with the multi-class Lagrangian fundamental relation:

$$v_u = v_u^*(s) \tag{6.17}$$

As an example, the multi-class Smulders fundamental relation (4.49) can be reformulated as:

$$v_u = v_u^*(s) = \begin{cases} v_{u,\max} - \dfrac{v_{u,\max} - v_{\text{crit}}}{s} s_{\text{crit}} & \text{(free flow)} \quad (6.18a) \\ w\left(\dfrac{s}{s_{\text{jam}}} - 1\right) & \text{(congestion)} \quad (6.18b) \end{cases}$$

In the fundamental relation we apply the Lagrangian equivalent of the effective density, namely the effective spacing:

$$s = \frac{1}{\rho} \tag{6.19}$$

The effective spacing can be interpreted as the 'average' spacing of all vehicles. Analogously, the class-specific spacing is defined:

$$s_u = \frac{1}{\rho_u} \tag{6.20}$$

The class-specific spacing s_u can be interpreted as the distance between the fronts of two vehicles of class u. This implies that there may be vehicles of other classes in between.

We show how an effective density function can be reformulated into its Lagrangian equivalent. As an example, we take a weighted average of the class-specific densities with constant pce-values η_u (4.10):

$$\rho = \sum_u \eta_u \rho_u \tag{6.21}$$

The effective spacing in Lagrangian formulation is derived by applying the definition of class-specific and effective spacing (6.19):

$$s = \frac{1}{\sum_u \eta_u / s_u} \tag{6.22}$$

6.3.2 Reformulation of multi-class conservation equation

Before we reformulate the multi-class conservation equation into Lagrangian coordinates we need some definitions and preliminaries. We define class 1 as the reference class for the coordinate system. This implies that only vehicles of class 1 are numbered. Therefore, coordinate n refers to the number of vehicles of class 1 that have passed location x until time t. Furthermore, the coordinate system moves with the vehicles of class 1, i.e. with velocity v_1. Therefore, the Lagrangian time derivative in the multi-class model is defined by:

$$\frac{\mathrm{D}}{\mathrm{D}t} = \frac{\partial}{\partial t} + v_1 \frac{\partial}{\partial x} \tag{6.23}$$

Finally, the class-specific spacing of class 1 can be expressed as the partial derivative:

$$s_1 = -\frac{\partial x}{\partial n} \tag{6.24}$$

To find the Lagrangian multi-class conservation equation for the other classes, (6.20) is substituted into the Eulerian conservation equation (6.16a), the quotient rule is applied and the result is rewritten:

$$\frac{\partial}{\partial t}\left(\frac{1}{s_u}\right) + \frac{\partial}{\partial x}\left(\frac{v_u}{s_u}\right) = 0 \quad \Rightarrow \quad \frac{\partial s_u}{\partial t} - s_u \frac{\partial v_u}{\partial x} + v_u \frac{\partial s_u}{\partial x} = 0 \tag{6.25}$$

Subsequently, substituting the multi-class Lagrangian time derivative (6.23) yields:

$$\frac{\mathrm{D}s_u}{\mathrm{D}t} - s_u \frac{\partial v_u}{\partial x} + (v_u - v_1)\frac{\partial s_u}{\partial x} = 0 \tag{6.26}$$

Finally, (6.24) is substituted to find the Lagrangian multi-class conservation equation:

$$\frac{\mathrm{D}s_u}{\mathrm{D}t} + \frac{s_u}{s_1}\frac{\partial v_u}{\partial n} + \frac{v_1 - v_u}{s_1}\frac{\partial s_u}{\partial n} = 0 \tag{6.27}$$

We note that for class 1 the conservation equation (6.27) reduces to an equation very similar to the Lagrangian mixed-class conservation equation (6.10):

$$\frac{\mathrm{D}s_1}{\mathrm{D}t} + \frac{\partial v_1}{\partial n} = 0 \tag{6.28}$$

Yet an alternative formulation of the conservation equation in Lagrangian coordinates is proposed in (Yuan et al., 2011; Yuan, 2013):

$$\frac{\mathrm{D}s_u}{\mathrm{D}t} + \frac{\partial v_u}{\partial n_u} = 0 \tag{6.29}$$

with Lagrangian time derivative:

$$\frac{\mathrm{D}}{\mathrm{D}t} = \frac{\partial}{\partial t} + v_u \frac{\partial}{\partial x_u} \tag{6.30}$$

The main difference is that in this model a different coordinate system is introduced for each class. The coordinate systems are coupled via the fundamental relation and the effective density function. Yuan et al. (2011); Yuan (2013) argue that this formulation may lead to more efficient simulations if there are only few vehicles in the reference class.

Finally, the flow to be maximized needs to be defined. In Fastlane this is the effective flow:

$$q = \sum_u \eta_u q_u = \sum_u \eta_u \frac{v_u}{s_u} \tag{6.31}$$

6.4 Graphical derivation

The above derivation of the Lagrangian multi-class conservation equation (6.27) is mathematically rigorous and similar to the original derivation of the Lagrangian mixed-class conservation equation (see Section 6.1). However, the derivation is not very intuitive and relies on its Eulerian formulation. Therefore, we propose a graphical, more intuitive derivation of (6.27).

The graphical derivation of the Lagrangian multi-class conservation equation is a combination of the graphical derivation of both the Eulerian and Lagrangian mixed-class

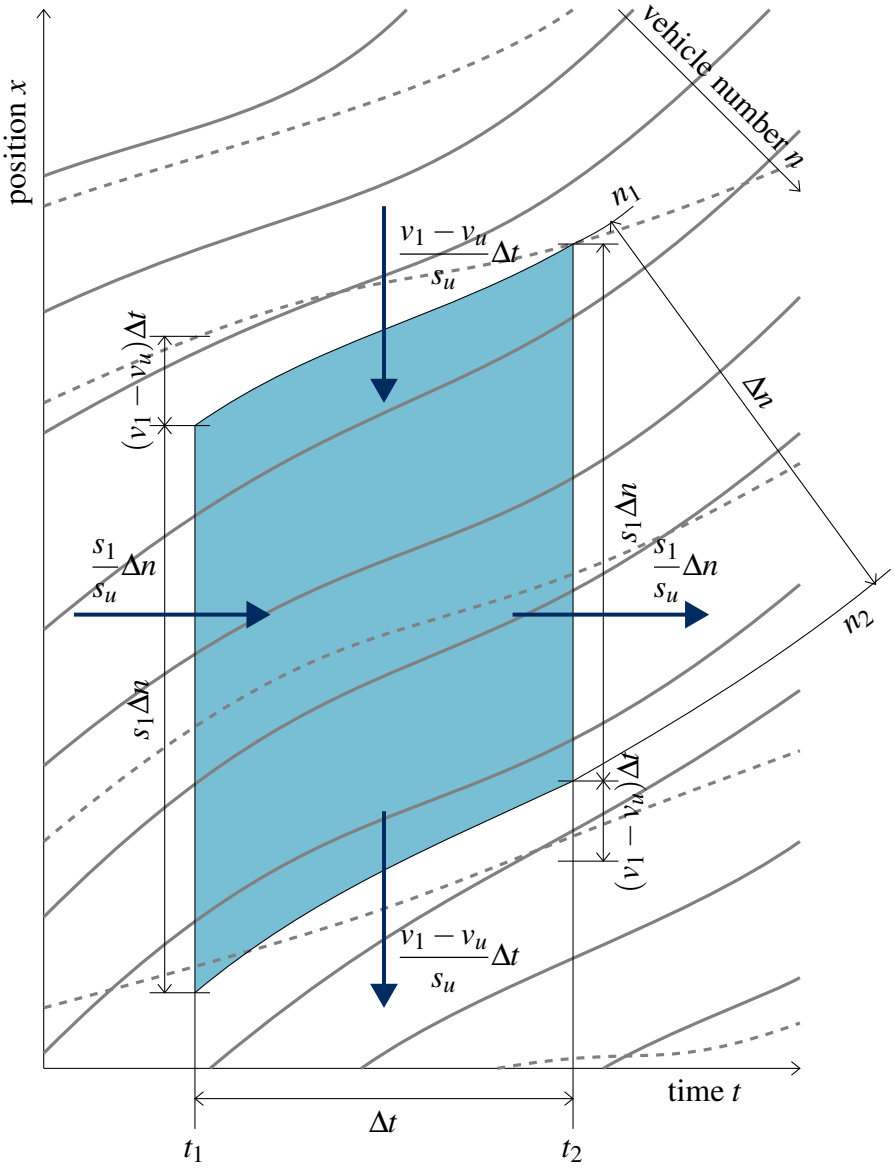

Figure 6.3 *Vehicle trajectories and control volume for the graphical derivation of the Lagrangian multi-class conservation equation. The solid lines represent trajectories of vehicles of class 1, the broken lines represent trajectories of vehicles of class u. The number of vehicles of class u that flows into the control volume equals the outflow of class u.*

conservation equations. The control volume consists of a platoon of Δn vehicles of class 1. The platoon is followed for a certain time Δt, see Figure 6.3. The conservation equation for class 1 (6.28) is derived similarly to the Lagrangian mixed-class conservation equation (see Section 6.2). The only difference is that spacing s is replaced by spacing of class 1 s_1 and velocity v is replace by velocity of class 1 v_1. For the conservation equations of all other classes, the platoon of vehicles of class 1 acts as a control volume. Similar to the graphical derivation of the Eulerian mixed-class conservation equation, vehicles of class u enter and leave the platoon.

Let us first assume that the vehicles of class u are not faster than those of class 1. Later, we relax this assumption. Vehicles of class u enter the control volume from the left and from above. Furthermore, vehicles of class u leave the control volume at the right and below. We assume that over each of those inflow and outflow boundaries of the control volume, the traffic state is constant. This assumption is reasonable if the control volume is small. Later, we will take an infinitesimal control volume and thus the assumption is justified. Each of the inflows in and outflows out of the control volume is discussed separately:

Inflow left Vehicles that enter the control volume from the left are originally (at t_1) in the platoon. The length of the platoon is the spacing of class 1 s_1 times the number of vehicles of class 1 in the platoon: $s_1(t_1)\Delta n$. The number of vehicles of class u that flows into the control volume at time t_1 is the platoon length divided by their spacing: $s_1(t_1)\Delta n/s_u(t_1)$.

Inflow above Vehicles that enter the control volume from above are overtaken by the first vehicle of class 1 in the platoon between t_1 and t_2. Those vehicles also pass the line at t_1 with length $(v_1(n_1) - v_u(n_1))\Delta t$. Since s_u is the spacing of class u, the number of vehicles that flows into the control volume from above is $(v_1(n_1) - v_u(n_1))\Delta t/s_u(n_1)$.

Outflow right Vehicles that leave the control volume at the right are in the platoon at t_2. Similar to the inflow from the left, the number of vehicles that flows out of the control volume at time t_2 is $s_1(t_2)\Delta n/s_u(t_2)$.

Outflow below Vehicles that leave the control volume below are overtaken by the last vehicle of class 1 in the platoon between t_1 and t_2. Similar to the inflow from above, the number of vehicles that flows out of the control volume below is $(v_1(n_2) - v_u(n_2))\Delta t/s_u(n_2)$.

The inflow into the control volume equals the outflow and thus:

$$\underbrace{\frac{s_1(t_1)}{s_u(t_1)}\Delta n}_{\text{inflow left}} + \underbrace{\frac{v_1(n_1) - v_u(n_1)}{s_u(n_1)}\Delta t}_{\text{inflow above}} = \underbrace{\frac{s_1(t_2)}{s_u(t_2)}\Delta n}_{\text{outflow right}} + \underbrace{\frac{v_1(n_2) - v_u(n_2))}{s_u(n_2)}\Delta t}_{\text{outflow below}} \tag{6.32}$$

Dividing both sides by $\Delta t \Delta n$ and rearranging gives:

$$\frac{\frac{s_1(t_1)}{s_u(t_1)} - \frac{s_1(t_2)}{s_u(t_2)}}{\Delta t} + \frac{\frac{v_1(n_1) - v_u(n_1)}{s_u(n_1)} - \frac{v_1(n_2) - v_u(n_2)}{s_u(n_2)}}{\Delta n} = 0 \tag{6.33}$$

Until now we assumed that the vehicles of class u are not faster than those of class 1. If, however, they are faster, the vehicles enter the platoon from the left and from below and leave it from the right and above. Applying the same procedure, the same result (6.33) is found. Finally, applying the definition of the derivative (6.13) to (6.33) gives the Lagrangian conservation equation.:

$$\frac{\mathrm{D}}{\mathrm{D}t}\left(\frac{s_1}{s_u}\right) + \frac{\partial}{\partial n}\left(\frac{v_1 - v_u}{s_u}\right) = 0 \tag{6.34}$$

We note that this Lagrangian conservation equation (6.34) takes a different form than the one we derived before (6.27). However, (6.34) can be rewritten as (6.27). Therefore, we first apply the quotient rule to (6.34) and find:

$$s_u \frac{\mathrm{D}s_1}{\mathrm{D}t} + s_u \frac{\partial v_1}{\partial n} - s_1 \frac{\mathrm{D}s_u}{\mathrm{D}t} - s_u \frac{\partial v_u}{\partial n} - (v_1 - v_u)\frac{\partial s_u}{\partial n} = 0 \tag{6.35}$$

By substituting the conservation equation for class 1 (6.28) we find that the first two terms drop out. Furthermore, dividing by $-s_1$ gives the conservation equation (6.27).

6.5 Discussion

We have introduced the Lagrangian formulation of both the mixed-class and the multi-class kinematic wave model. For both models the Lagrangian formulation was derived from the Eulerian formulation and graphically. Though the derivation from the Eulerian formulation is mathematically more rigorous, the graphical derivation is more intuitive and easier to understand.

The Lagrangian formulation of both models is valuable because this formulation yields considerable benefits over the Eulerian formulation, which are illustrated in the remainder of this dissertation. The advantages are related to:

1. efficiency of simulation (for traffic state prediction)
2. efficiency of traffic state estimation and traffic control
3. model analysis
4. coupling with microscopic models
5. adaptations and extensions of the model

The first three advantages have to do with the nonlinearity of the model. In the Eulerian formulation, the flow as a function of the density plays an important role. At low densities, the flow is an increasing function of the density, whereas, at high densities it

is a decreasing function. However, the role of the flow in the Eulerian formulation is taken over by the velocity in the Lagrangian formulation. The velocity is a nonincreasing function of the spacing. Therefore, the Lagrangian formulation is 'less nonlinear'. This advantage is used in applications such as traffic state estimation using Kalman filtering (Yuan et al., 2012). The same advantage of the Lagrangian formulation is exploited in efficient simulation methods (see Chapter 8 and 9) and in mathematical analysis of the multi-class model (see Chapter 7). The other two advantages are discussed below.

Leclercq (2007a) shows how the Lagrangian formulation simplifies the coupling between microscopic and macroscopic models. Microscopic and macroscopic models can be used in one simulation for example to have detailed results at locations or times when this is desired, while still benefitting from the low computational costs for the macroscopic model at other locations and times. Since both microscopic models and macroscopic models in Lagrangian formulation have vehicle number n and time t as coordinates, their coupling is simpler than when the Eulerian formulation of the macroscopic model was applied.

Certain extensions and adaptations of the kinematic wave model can be introduced in the Lagrangian formulation with less effort than in the Eulerian formulation. For example, the bounded acceleration model by Lebacque (2002) (see also Section 2.4.1) bounds the acceleration of vehicles by $\partial v/\partial t + v\partial v/\partial x \leq a_{\max}$ with $a_{\max}$ the maximum acceleration. The term $v\partial v/\partial x$ is needed to bound the acceleration of vehicles instead of bounding the rate of change in velocity at a location fixed in space. However, in the Lagrangian formulation the acceleration of vehicles is bounded by simply setting: $\mathrm{D}v/\mathrm{D}t \leq a_{\max}$ (Leclercq, 2009). Similarly, moving bottlenecks can be introduced in the kinematic wave model by applying the Lagrangian formulation (Leclercq et al., 2004).

In the next three chapters the Lagrangian formulation of the kinematic wave model plays an important role. In Chapter 7 it will be applied to analyze the generalized multi-class kinematic wave model. It turns out that especially for the analysis of the anisotropy requirement (Requirement 9, Chapter 3) the Lagrangian formulation of the model is very useful. In Chapter 8 and 9 numerical methods to solve the continuous model equations are introduced. It turns out that methods based on the Lagrangian formulation are more efficient, both in terms of accuracy and computing time. Finally, in Chapter 10 the Lagrangian formulation of the kinematic wave model for homogeneous roads will be extended to include inhomogeneities such as on and off ramps.

Chapter 7

Model analysis

In Chapter 3 we introduced the requirements for multi-class traffic flow models. All requirements are important qualitative properties of multi-class kinematic wave traffic flow models. Therefore, a multi-class kinematic wave model should satisfy the requirements. The requirements are related to the model formulation, the fundamental relation and the model dynamics. In Chapter 4 we introduced Fastlane and in Chapter 5 we summarized all multi-class kinematic wave models known from literature. In this chapter we assess whether the models satisfy the requirements. For part of this assessment, we apply the generalized formulation from Chapter 5 and its reformulation in Lagrangian coordinates introduced in Chapter 6.

We recall the requirements from Section 3.2:

Model formulation requirements:

1. Given 'permissible' class-specific densities, (class-specific) velocities and flows are defined uniquely.
2. The model has a unique solution that maximizes flow.

Fundamental relation requirements:

3. In free flow the velocities of each class are allowed to differ.
4. In free flow the velocities of relatively fast classes are allowed decrease with increasing density.
5. In congestion the velocity of each class is equal.
6. If the density reaches a certain threshold (which may depend on the traffic composition), vehicle velocity is zero.
7. If the density of only one class increases, while all other class-specific densities remain constant, vehicle velocities do not increase.

Model dynamics requirements:

8. Characteristics have finite velocity.
9. Characteristics do not have a larger velocity than vehicles.

We assess all multi-class models from Chapter 5 with respect to these requirements. The results are presented in Table 7.1 and discussed in more detail hereafter.

The outline of this chapter is as follows. We first discuss shortly the model formulation Requirements 1 and 2. With the results from Chapter 5 the models are relatively straightforward to assess with respect to the first four fundamental relation requirements (3–6). Therefore, in Section 7.1 we first do this part of the assessment. To assess the models with respect to the other requirements more effort is needed. Moreover, these requirements (7–9) turn out to be closely related. They are discussed in more detail in Section 7.2. In Section 7.3 we assess the generalized model with respect to Requirement 7–9. We do this using the model formulation in Lagrangian coordinates introduced in Chapter 6. This analysis results in a set of conditions on the fundamental relation and the effective density function. The conditions are applied in Section 7.4 to assess all models one by one with respect to Requirements 7–9. Finally, in Section 7.5 we summarize the results and discuss how the framework developed in this chapter may be applied to other (future) models.

7.1 Review of Requirements 1–6

We assess the multi-class models with respect to Requirements 1–6. We do not repeat the model equations here but refer to Table 5.2 for an overview of all multi-class models and Figure 5.1 for examples of their fundamental relations. Furthermore, we assume that parameters have 'feasible' values. Some parameters are positive: class-specific maximum velocity $v_{u,\max} > 0$, (class-specific) jam density $\rho_{\text{jam}} > 0$, $\rho_{u,\text{jam}} > 0$, and parameters $w = \rho_{\text{crit}} v_{\text{crit}} / (\rho_{\text{jam}} - \rho_{\text{crit}}) > 0$, $w_u = \rho_{u,\text{crit}} v_{u,\text{crit}} / (\rho_{u,\text{jam}} - \rho_{u,\text{crit}}) > 0$, class-specific vehicle length $L_u > 0$, constant pce-values $\eta_u > 0$. Some parameters are nonnegative: (class-specific) critical velocity $v_{u,\text{crit}} \geq 0$, $v_{\text{crit}} \geq 0$, (class-specific) critical density $\rho_{u,\text{crit}} \geq 0$, $\rho_{\text{crit}} \geq 0$, class-specific critical pore size $r_{u,\text{crit}} \geq 0$, (class-specific) minimum time headway $T_u \geq 0$. Finally, maximum velocities are not smaller than critical velocities ($v_{\max} \geq v_{\text{crit}}$, $v_{u,\max} \geq v_{u,\text{crit}}$, $v_{u,\max} \geq v_{\text{crit}}$) and jam densities are not smaller than critical densities ($\rho_{\text{jam}} \geq \rho_{\text{crit}}$, $\rho_{u,\text{jam}} \geq \rho_{u,\text{crit}}$).

7.1.1 Model formulation requirements

Requirement 1 states that velocities and flows must be defined uniquely when class-specific densities are given. The generalized multi-class model satisfies this requirement. Since all other models are contained in the generalized model, they also satisfy the requirement.

Requirement 2 states that there is a unique solution to the model equations that maximizes the flow. In multi-class models it is necessary to define which type of flow (total flow (in vehicles/s), effective flow (in pce/s), or even another type of flow) must be maximized. Both Zhang et al. (2006); Chanut & Buisson (2003) include the entropy condition in a discussion on solving a Riemann problem, without explicitly mentioning which type of flow is maximized. Logghe & Immers (2008) include the entropy

condition by stating that in their model vehicles maximize their velocity. In Fastlane we include that the effective flow $q = \sum_u \eta_u q_u$ must be maximized. Benzoni-Gavage & Colombo (2003) discuss the entropy condition in even much more detail. Other authors (Wong & Wong, 2002; Ngoduy & Liu, 2007; Nair et al., 2012) discuss flow maximization only in the context of numerical methods.

7.1.2 Fundamental relation Requirements 3–6

We refer to Figure 5.1 and Table 5.2 for the fundamental relations of all models. Requirement 3 states that the model must allow for unequal velocities in free flow. All models except the ones by Wong & Wong; Zhang et al. satisfy this requirement.

Requirement 4 states that the class-specific velocities must be allowed to be decreasing in free flow. The model by Logghe & Immers does not satisfy this requirement because velocities in free flow are constant. All other models do satisfy this requirement.

Requirement 5 states that in congestion velocities of all classes must be equal. The models with the Smulders fundamental relation (i.e. the models Ngoduy & Liu, Fastlane, and the model by Chanut & Buisson) satisfy this requirement. In the models by Nair et al.; Benzoni-Gavage & Colombo; Wong & Wong; Zhang et al. the class-specific velocities are unequal in all regimes. If both classes in the model by Logghe & Immers are in congestion, the class-specific velocities are equal. However, if only class 1 is in congestion (i.e. traffic is in semi-congestion) then the velocities are unequal.

Requirement 6 states that there must be a (jam) density for which the velocities are zero. It depends on the fundamental relations $v_u(\rho)$ whether a model satisfies this requirement. The Daganzo, Smulders and Greenshields fundamental relations satisfy the requirement. Therefore, the models by Logghe & Immers (2008); Ngoduy & Liu (2007); Chanut & Buisson (2003) and Fastlane satisfy the requirement. The model by Benzoni-Gavage & Colombo (2003) with Greenshields fundamental relation also satisfies it. However, the fundamental relation applied by Nair et al. (2012) and the Drake fundamental relation applied by Benzoni-Gavage & Colombo (2003); Wong & Wong (2002) do not reach zero velocities at high densities and thus do not satisfy the requirement. Zhang et al. (2006) do not specify a fundamental relation and the model can therefore not be assessed with respect to this requirement.

7.1.3 Velocities in the models by Logghe & Immers and Nair et al.

Finally, we make some observations of the velocities in the models by Logghe & Immers and Nair et al.

In the model by Logghe & Immers in some traffic states in semi-congestion the velocity of class 1 is higher if there are more vehicles of class 2, even if the total density (in number of vehicles per meter) remains the same. This can be observed in Figure 5.1(a)

because the velocity of class 1 with 25% vehicles of class 2 (broken line) is above the velocity of class 1 with 25% vehicles of class 2 (solid line) at total densities just above the critical density of class 1 ($\rho_{1,\mathrm{crit}}$). As an example we show more rigorously that this is the case with the parameters as in Table 5.1, i.e.: for class 1 maximum velocity $v_{1,\max} = 33.3$ m/s, critical density $\rho_{1,\mathrm{crit}} = 0.04$ veh/m, jam density $\rho_{1,\mathrm{jam}} = 0.2$ veh/m and for class 2 maximum velocity $v_{2,\max} = 20.8$ m/s and critical density $\rho_{2,\mathrm{crit}} = 0.05$ veh/m. We consider two slightly different traffic states, both semi-congestion. We analyze the velocities using the equations as presented in Table 5.2.

In the first case, the class-specific density of class 1 to be $\rho_1 = 0.03$ veh/m and one third of the total number of vehicles of class 2: $\rho_2 = 0.015$ veh/m. Therefore, the road fraction that is available to class 1 is: $\alpha_1^{\mathrm{sc}} = \frac{\rho_{2,\mathrm{crit}} - \rho_2}{\rho_{2,\mathrm{crit}}} = 0.7$. This leads to the effective density $\rho = \frac{\rho_1}{\alpha_1^{\mathrm{sc}}} = 0.043$ veh/m. We find the velocity of class 1:

$$v_1 = w_1 \left(\frac{\rho_{1,\mathrm{jam}}}{\rho} - 1 \right) = \frac{\rho_{1,\mathrm{crit}} v_{1,\max}}{\rho_{1,\mathrm{jam}} - \rho_{1,\mathrm{crit}}} \left(\frac{\rho_{1,\mathrm{jam}}}{\rho} - 1 \right) = 30.4 \text{ m/s} \tag{7.1}$$

We note that this is indeed semi-congestion because $\frac{\rho_1}{\rho_{1,\mathrm{crit}}} = 0.075 > \alpha_1^{\mathrm{sc}}$ and $v_1 > v_{2,\max}$.

In the second case we consider a different traffic state with the same total density, but with no vehicles of class 2. We show that this leads to a lower velocity for class 1. The total density in the above example was $0.03 + 0.015 = 0.045$ veh/m. In this case, we take $\rho_1 = 0.045$ veh/m and $\rho_2 = 0$. Consequently, $\alpha_1^{\mathrm{sc}} = 1$ and $\rho = \rho_1 = 0.045$ veh/m. We find the velocity of class 1:

$$v_1 = w_1 \left(\frac{\rho_{1,\mathrm{jam}}}{\rho} - 1 \right) = \frac{\rho_{1,\mathrm{crit}} v_{1,\max}}{\rho_{1,\mathrm{jam}} - \rho_{1,\mathrm{crit}}} \left(\frac{\rho_{1,\mathrm{jam}}}{\rho} - 1 \right) = 28.7 \text{ m/s} \tag{7.2}$$

We conclude that in the second case, with the same total density, but with less vehicles of class 2 the velocity of class 1 is lower ($v_1 = 28.7$ m/s) than in the first case ($v_1 = 30.4$ m/s). This is counterintuitive as it implies that if the percentage of trucks (class 2) is higher, the cars (class 1) travel faster.

In the model by Nair et al. something similar happens. As Figure 5.1(d) shows, if the percentage of vehicles of class 2 increases, the velocity of both classes increase. However, in this model, class 2 does usually not denote trucks but for example scooters. Since scooters are smaller than cars, pores remain large even at relatively high scooter densities. Therefore, also velocities are high at high scooter densities, which is reasonable in this context.

7.2 Review of requirements 7–9

In this section we formulate mathematically Requirement 7, 8 and 9 which are related to nonincreasing velocity, finite characteristic velocity and anisotropy, respectively.

This allows us to assess whether the generic and other multi-class models satisfy the requirements. We are only interested in the requirements for 'permissible' traffic states. With permissible we mean that the class-specific densities and class-specific velocities must all be nonnegative. If one or more of them is negative, this implies a traffic state that will not appear in reality and is thus not permissible. In the rest of this chapter, we only discuss permissible traffic states, however, for readability we do not always mention it.

For later reference we first summarize the Lagrangian formulation of the generalized multi-class kinematic wave model (6.17), (6.19), (6.20) and (6.27) from the previous chapter. The model consists of the following three equations:

$$\frac{\partial s_u}{\partial t} + \frac{s_u}{s_1}\frac{\partial v_u}{\partial n} + \frac{v_u - v_1}{s_1}\frac{\partial s_u}{\partial n} = 0 \tag{7.3a}$$

$$v_u = v_u^*(s) = v_u^*\left(\tfrac{1}{\rho}\right) = v_u(\rho) \tag{7.3b}$$

$$s = \tfrac{1}{\rho} = \frac{1}{\rho(\rho_1, \ldots, \rho_U)} = \frac{1}{\rho\left(\frac{1}{s_1}, \ldots, \frac{1}{s_U}\right)} \tag{7.3c}$$

Later, we need the conservation equation (7.3a) in matrix vector notation. Therefore, we reformulate it as:

$$\frac{\partial \vec{s}}{\partial t} + \mathbf{J}(\vec{s})\frac{\partial \vec{s}}{\partial n} = \vec{0} \tag{7.4}$$

with $\vec{s}$ the vector of class-specific spacings:

$$\vec{s} = \begin{pmatrix} s_1 \\ \vdots \\ s_U \end{pmatrix} \tag{7.5}$$

and Jacobian matrix:

$$\mathbf{J} = \begin{pmatrix} a_{1,1} & \cdots & a_{1,U} \\ \vdots & \ddots & \vdots \\ a_{U,1} & \cdots & a_{U,U} \end{pmatrix} \tag{7.6}$$

with the entries in the Jacobian matrix $\mathbf{J}$ defined by:

$$a_{i,j} = \begin{cases} \dfrac{s_i}{s_1}\dfrac{\partial v_i^*}{\partial s_i} + \dfrac{v_1 - v_i}{s_1} & \text{for } i = j \text{ (on the diagonal)} \quad (7.7a) \\ \dfrac{s_i}{s_1}\dfrac{\partial v_i^*}{\partial s_j} & \text{for } i \neq j \text{ (off the diagonal)} \quad (7.7b) \end{cases}$$

In (7.7) we find the elements $a_{i,j}$ of the Jacobian $\mathbf{J}(\vec{s})$ by applying:

$$\frac{\partial v_i^*}{\partial n} = \frac{\partial v_i^*}{\partial s_1}\frac{\partial s_1}{\partial n} + \ldots + \frac{\partial v_i^*}{\partial s_j}\frac{\partial s_j}{\partial n} + \ldots + \frac{\partial v_i^*}{\partial s_U}\frac{\partial s_U}{\partial n} \tag{7.8}$$

For readability we write v_u instead of v_u^* in the following whenever it is clear from the context that we mean the velocity as a function of the spacing s.

7.2.1 Requirements for mixed-class models

We first discuss the requirements in the context of mixed-class models. In the next subsection we extend the concepts to multi-class models.

Requirement 7 states that the velocity v is a nonincreasing funtion of the density ρ. In a mixed-class model this implies that the density-velocity fundamental relation $v(\rho)$ must be nonincreasing. The requirement can also be formulated in Lagrangian coordinates. In Chapter 6 the density-velocity fundamental relation was reformulated in Lagrangian coordinates. This results in the spacing-velocity fundamental relation $v^*(s)$, with v^* the velocity and $s = 1/\rho$ the spacing. If $v(\rho)$ is nonincreasing, its derivative is nonpositive: $\mathrm{d}v/\mathrm{d}\rho \leq 0$. The sign of the derivative of the spacing-velocity fundamental relation $v^*(s)$ is opposite to that of $v(\rho)$:

$$\frac{\mathrm{d}v^*}{\mathrm{d}s} = \frac{\mathrm{d}v}{\mathrm{d}\rho}\frac{\mathrm{d}\rho}{\mathrm{d}s} = \frac{\mathrm{d}v}{\mathrm{d}\rho}\frac{\mathrm{d}}{\mathrm{d}s}\left(\frac{1}{s}\right) = -\frac{1}{s^2}\frac{\mathrm{d}v}{\mathrm{d}\rho} \tag{7.9}$$

Consequently, the density-velocity fundamental relation is nonincreasing (and thus Requirement 7 is satisfied) if and only if the spacing-velocity fundamental relation is nondecreasing.

Requirements 8 and 9 state that the model must have finite characteristic velocities and that it is anisotropic. We recall from Chapter 3 that also anisotropy relates to the characteristic velocity. In a mixed-class model the characteristic velocity $c(\rho)$ equals to the slope of the density-flow fundamental relation:

$$c(\rho) = \frac{\mathrm{d}q}{\mathrm{d}\rho} \tag{7.10}$$

Or, equivalently, the characteristic velocity with respect to the Lagrangian coordinate system (t,n) is equal to the slope of the spacing-velocity fundamental relation:

$$c^*(s) = \frac{\mathrm{d}v^*}{\mathrm{d}s} \tag{7.11}$$

A mixed-class model has finite characteristic velocities if the derivative $\mathrm{d}q/\mathrm{d}\rho$ (or equivalently $\mathrm{d}v^*/\mathrm{d}s$) exists and is finite. This is the case if its fundamental relation is continuous and continuously differentiable. A model with finite (or real) characteristic velocities is sometimes referred to as hyperbolic. Because this term is not used

consistently in the traffic flow literature, we avoid it here.

Anisotropy means that characteristics are not faster than vehicles: information does not travel faster than vehicles. A mixed-class model is anisotropic if its characteristic velocity is not larger than its vehicle velocity. In Eulerian coordinates this implies $c \leq v$. In Lagrangian coordinates, the characteristic velocity c^* is the velocity of the characteristics with respect to the coordinates. Since the coordinates move with the velocity of the vehicles, the model is anisotropic if the characteristics do not 'overtake' the coordinates. That is, the model is anisotropic if the characteristic velocity is nonnegative: $c^* \geq 0$.

7.2.2 Requirements for multi-class models

We now extend Requirements 7–9 to multi-class models and define them mathematically. In a multi-class model, Requirement 7 implies that all class-specific velocities must be nonincreasing functions of all class-specific densities. That is: if one vehicle of a certain class is added (and the densities of all other classes remain the same) the velocities do not increase.

Definition 7.1 (Nonincreasing velocity)**.** *The multi-class traffic flow model with fundamental relation $v_i = v_i(\rho_1, \ldots, \rho_U)$ has nonincreasing velocities if and only if for all permissible traffic states and all classes i and j*

$$\frac{\partial v_i}{\partial \rho_j} \leq 0 \tag{7.12}$$

For the other two requirements (8 and 9) we need some more details on weak hyperbolicity, eigenvalues and characteristic velocities. In a multi-class model there are as many characteristics as classes. Their velocities are equal to the eigenvalues λ_u of the Jacobian (see LeVeque, Section 2.9 or any standard work on differential equations theory). Therefore, the model has finite characteristic velocities if all eigenvalues of the Jacobian are real and finite. This is equivalent to real and finite characteristic velocity c (or c^*) in mixed-class models. However, this does not imply that the derivative of the multi-class fundamental relation $\mathrm{d}q_u/\mathrm{d}\rho$ must be real and finite, because in general the eigenvalues of the Jacobian are not equal to the derivative of the fundamental relation. We first analyze whether the model has real characteristic velocities. A model is weakly hyperbolic if the eigenvalues of the Jacobian are real, but not necessarily finite.

Definition 7.2 (Weak hyperbolicity)**.** *The multi-class traffic flow model with conservation equation (7.4) is weakly hyperbolic if and only if for all permissible traffic states the eigenvalues of the Jacobian (7.6) are real.*

The second step is to analyze whether the characteristic velocities are furthermore finite.

Definition 7.3 (Finite characteristic velocity)**.** *The multi-class traffic flow model with conservation equation (7.4) has finite characteristic velocities if and only if for all permissible traffic states the eigenvalues of the Jacobian (7.6) are real and finite.*

In the Lagrangian formulation the Jacobian is defined by (7.6) and its eigenvalues are the characteristic velocities with respect to the Lagrangian coordinate system. The Lagrangian coordinate system travels with the same velocity as the vehicles of class 1. Therefore, the model is anisotropic if the vehicles of class 1 are the fastest vehicles and if furthermore the eigenvalues of the Jacobian are nonnegative: $\lambda_u \geq 0$.

Definition 7.4 (Anisotropy)**.** *If class 1 is the fastest class in all permissible traffic states, then the multi-class traffic flow model with conservation equation (7.4) is anisotropic if and only if for all permissible traffic states the eigenvalues of the Jacobian (7.6) are nonnegative.*

We note that a model can only have finite characteristic velocities (real and finite eigenvalues) if it is weakly hyperbolic (real eigenvalues). Furthermore, a model can only by anisotropic (nonnegative eigenvalues) if it is weakly hyperbolic. Finally, in the next section (Section 7.3) it will turn out that nonincreasing velocity is a sufficient (but not necessary) condition for weak hyperbolicity. The relations between weak hyperbolicity, nonincreasing velocity, finite characteristic velocities and anisotropy are shown in Figure 7.1. The details are discussed in Section 7.3.

The vehicle velocities and eigenvalues of the Jacobian and therefore also the characteristic velocities depend on the traffic state. Therefore, a model may satisfy the requirements for certain values of the class-specific densities and not for others. However, we require that a traffic flow model satisfies the requirements for all permissible traffic states.

7.3 Assessment of generalized model

In this section we prove that the generalized model, under certain conditions, satisfies Requirement 7, 8 and 9. We use Figure 7.1. We first consider the conditions for which the model has nonincreasing velocities v_u (Requirement 7), i.e. for which the model is in the upper circle of the diagram. Secondly, we consider the conditions for which the model is weakly hyperbolic. It turns out that all models that have nonincreasing velocities are weakly hyperbolic. This implies that all models that are in the upper circle of the diagram are weakly hyperbolic. Thirdly, we consider the conditions for which the model has finite characteristic velocities (Requirement 8). It turns out that a model satisfies this requirement if the velocity is nonincreasing and if furthermore the fundamental relation and the effective density function are bounded and continuous. This is shown in Figure 7.1 by the lower left circle. Fourthly, we consider the conditions for which the model is anisotropic (Requirement 9). It turns out that a model is anisotropic

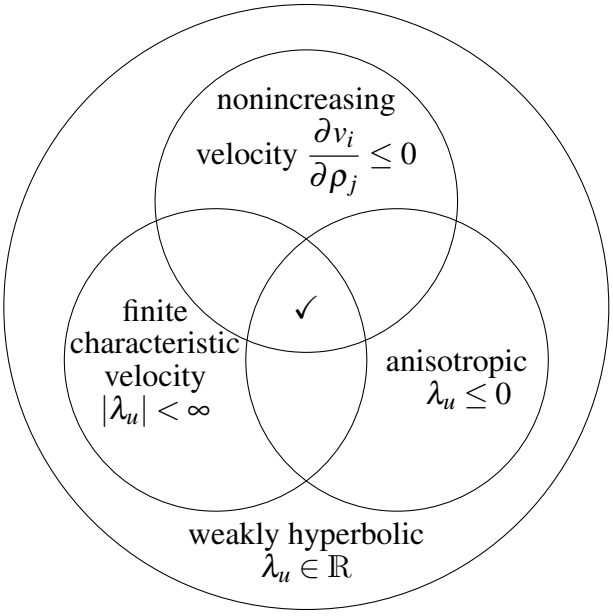

Figure 7.1 *Categorization of Requirements 7, 8 and 9 for multi-class traffic flow models. If all requirements are satisfied, the model is in the center area with the checkmark (✓).*

if two conditions holds. First, the velocities v_u are nonincreasing. Secondly, there is a class that is not slower than any other class in any permissible traffic state. This is shown in Figure 7.1 by the lower right circle. We note that weak hyperbolicity (real eigenvalues) is not a requirement itself. However, it is a necessary (but not sufficient) condition for all Requirements 7, 8 and 9.

In this section we show that Requirement 7, 8 and 9 are satisfied if the following conditions hold:

Condition 7.1 (Nonincreasing effective density-velocity fundamental relation)**.** *The class-specific velocity v_i expressed as a function of the effective density ρ is nonincreasing. That is, for all classes i:*

$$\frac{\partial v_i}{\partial \rho} \leq 0 \tag{7.13}$$

Condition 7.2 (Nondecreasing effective density)**.** *The effective density ρ is a nondecreasing function of the class-specific densities:*

$$\frac{\mathrm{d}\rho}{\mathrm{d}\rho_j} \geq 0 \tag{7.14}$$

Condition 7.3 (Continuous fundamental relation)**.** *The fundamental relation is either continuously differentiable or it is bounded and continuous. Furthermore, the effective density function is either continuously differentiable or it is bounded and continuous.*

As we will see later, the condition that the fundamental relation or the effective density function is bounded and continuous is a sufficient, but not necessary, condition. We

will show that if it is bounded and continuous, it can be approximated by a continuously differentiable fundamental relation or effective density function.

Condition 7.4 (Fastest class)**.** *There is one class j that is not slower than any other class i in all traffic states. That is for some class j, for all classes i:*

$$v_j \geq v_i \tag{7.15}$$

In the remainder of this section we will discuss the relation between Requirement 7–9, Definition 7.1–7.4 and Condition 7.1–7.4. We show that the generic multi-class model satisfies the nonincreasing velocity requirement (Requirement 7, see Definition 7.1) if both Condition 7.1 and 7.2 hold. Furthermore, if Conditions 7.1 and 7.2 hold, the model is weakly hyperbolic (see Definition 7.2). Weak hyperbolicity is a necessary condition for both the finite characteristic velocity requirement (Requirement 8, see Definition 7.3) and the anisotropy requirement (Requirement 9, see Definition 7.4). For Requirement 8 to be satisfied, also Condition 7.3 hold must hold. For Requirement 9 to be satisfied, also Condition 7.4 hold must hold.

7.3.1 Nonincreasing velocities

We show the generalized model has non increasing velocities in Condition 7.1 and 7.2 are satisfied. It may be possible to directly assess whether the class-specific velocity is a nonincreasing function of the class-specific densities, i.e. whether (7.12) holds for all classes i and j. However, the velocity can be written as a function of the effective density and the effective density as a function of all class-specific densities. Therefore, we formulate the following theorem.

Theorem 7.1. *The generalized multi-class model has nonincreasing velocities, i.e. it satisfies (7.12), if both Condition 7.1 and Condition 7.2 are satisfied.*

Proof. The left-hand side of (7.12) can be rewritten as:

$$\frac{\partial v_i}{\partial \rho_j} = \frac{\partial v_i}{\partial \rho} \frac{\mathrm{d}\rho}{\mathrm{d}\rho_j} \tag{7.16}$$

If Condition 7.1 and 7.2 are satisfied, then the right-hand side is nonpositive and thus (7.12) holds. □

7.3.2 Preliminaries for characteristic velocities

If there are U classes, the Jacobian $\mathbf{J}$ (7.6) is a U by U matrix. In the general case with large number of vehicle classes ($U > 4$) the eigenvalues λ_i of the Jacobian can not be computed analytically. However, we are able to determine whether they are real,

finite and nonnegative. Therefore, we need the following preliminaries, which implies that the characteristic velocities are real, finite and nonnegative. The first one is an application of a generalized Taylor series approximation and was proven by (Hille & Phillips, 1957):

Preliminary 7.1. *Any bounded continuous function has a series approximation that converges to the value of the function itself.*

The other preliminaries are results from basic linear algebra (see e.g., (Strang, 1988)):

Preliminary 7.2. *The matrices* $\mathbf{A}$ *and* $\mathbf{S}\mathbf{A}\mathbf{S}^{-1}$ *have the same eigenvalues for any invertible matrix* $\mathbf{S}$ *of appropriate size.*

Preliminary 7.3. *The eigenvalues of a real and symmetric matrix are real.*

Preliminary 7.4 (Gershgorin's circle theorem)**.** *Suppose* $\mathbf{A}$ *is an* $n \times n$ *matrix. Each eigenvalue of* $\mathbf{A}$ *lies in one of the circles* $C_i, \ldots, C_n$*, where* C_i *has its center at the diagonal entry* $a_{i,i}$ *and its radius* $r_i = \sum_{j \neq i} |a_{i,j}|$ *is equal to the absolute sum of the rest of the row.*

The last preliminary is about Gaussian elimination. Gaussian elimination is the proces in which a matrix A is converted into an upper triangular matrix. This is done by subtracting the first row of the matrix $a_{i,1}/a_{1,1}$ times from all rows i. The first entry of the rows become zero by this process: $a_{2,1} - (a_{2,1}/a_{1,1}) \times a_{1,1} = 0$, $a_{3,1} - (a_{3,1}/a_{1,1}) \times a_{1,1} = 0$, etc. Subsequently, the second row is subtracted from the third to last row $a_{i,2}/a_{2,2}$ times. Again, this leads to zeros, now in the second columns: $a_{3,2} - (a_{3,2}/a_{2,2}) \times a_{2,2} = 0$, $a_{4,2} - (a_{4,2}/a_{2,2}) \times a_{2,2} = 0$, etc. Then the third row is subtracted from the fourth to the last row leading to zeroes in the third column, etc. Once the second last row has been subtracted from the last row, the matrix has been converted into an upper triangular matrix.

Preliminary 7.5. *Suppose* $\mathbf{A}$ *is a symmetric matrix. Pivots are the entries at the main diagonal after applying Gaussian elimination. If all pivots are nonnegative, then all eigenvalues are nonnegative.*

Furthermore, we define two matrices that will be applied later. First, the diagonal matrix $\mathbf{D}$ has zeros everywhere except on the main diagonal. The elements at the main diagonal are defined by:

$$d_i = \sqrt{\frac{1}{s_i} \frac{\partial s}{\partial s_i} \Big/ \frac{\partial v_i}{\partial s}} \tag{7.17}$$

Secondly, the matrix $\mathbf{M}$ is defined by

$$\mathbf{M} = \mathbf{D}\mathbf{J}\mathbf{D}^{-1} \tag{7.18}$$

with $\mathbf{J}$ the Jacobian (7.6).

7.3.3 Weak hyperbolicity

We show that the generalized model is weakly hyperbolic if the velocities are non-increasing, i.e. if (7.12) holds for all classes i and j. In other words: nonincreasing velocity is a sufficient condition for weak hyperbolicity, but it is not a necessary conditions, see Figure 7.1. Therefore, we first show that (7.12) is equivalent to the condition that the Lagrangian fundamental relation does not decrease. Secondly, we show that the eigenvalues of matrix $\mathbf{M}$ (7.18) are real if the Lagrangian fundamental relation does not decrease. Finally, we show that the model is weakly hyperbolic if the matrix $\mathbf{M}$ has real eigenvalues.

Lemma 7.1. *The Eulerian fundamental relation does not increase (i.e. (7.12) holds) if and only if the Lagrangian fundamental relation does not decrease:*

$$\frac{\partial v_i}{\partial s_j} \geq 0 \tag{7.19}$$

Proof. We rewrite the left-hand side of (7.19):

$$\frac{\partial v_i}{\partial s_j} = \frac{\partial v_i}{\partial \rho_j}\frac{\mathrm{d}\rho_j}{\mathrm{d}s_j} = \frac{\partial v_i}{\partial \rho_j}\frac{\mathrm{d}}{\mathrm{d}s_j}\left(\frac{1}{\rho_j}\right) = -\frac{\partial v_i}{\partial \rho_j}\frac{1}{(\rho_j)^2} \tag{7.20}$$

The last term $(1/(\rho_j)^2)$ is positive. Therefore, the signs of $\dfrac{\partial v_i}{\partial s_j}$ and $\dfrac{\partial v_i}{\partial \rho_j}$ are opposite and we conclude that (7.12) and (7.19) are equivalent. □

Lemma 7.2. *If (7.19) holds for all classes i and j, then matrix $\mathbf{M}$ (7.18) has real eigenvalues.*

Proof. We show that matrix $\mathbf{M}$ is real and symmetric. By substituting the elements of the Jacobian $\mathbf{J}$ (7.6) and the diagonal matrix $\mathbf{D}$ (7.17) into matrix $\mathbf{M}$ (7.18) we find its elements:

$$m_{i,j} = \frac{d_i}{d_j}a_{i,j} = \begin{cases} a_{i,i} = \dfrac{s_i}{s_1}\dfrac{\partial v_i}{\partial s_i} + \dfrac{v_1 - v_i}{s_1} & \text{for } i = j \quad \text{(7.21a)} \\ \text{(on the diagonal)} \\ \sqrt{\dfrac{\frac{1}{s_i}\frac{\partial s}{\partial s_i}\Big/\frac{\partial v_i}{\partial s}}{\frac{1}{s_j}\frac{\partial s}{\partial s_j}\Big/\frac{\partial v_j}{\partial s}}}\dfrac{s_i}{s_1}\dfrac{\partial v_i}{\partial s_j} = \dfrac{\sqrt{s_i s_j}}{s_1}\sqrt{\dfrac{\partial v_j}{\partial s_i}\dfrac{\partial v_i}{\partial s_j}} & \text{for } i \neq j \quad \text{(7.21b)} \\ \text{(off the diagonal)} \end{cases}$$

From (7.21a) we conclude that the elements on the main diagonal of $\mathbf{M}$ are real because the Jacobian $\mathbf{J}$ with elements $a_{i,j}$ is real. In the last equality of (7.21b) we use that $(\partial v_j/\partial s)(\partial s/\partial s_i) = \partial v_j/\partial s_i$. If (7.19) holds, then both fractions under the last square root sign of (7.21b) are nonnegative and thus $m_{i,j}$ is real. From (7.21b) we furthermore conclude that $m_{i,j} = m_{j,i}$ and thus matrix $\mathbf{M}$ is symmetric. Now, we have shown that matrix $\mathbf{M}$ is real and symmetric. We apply Preliminary 7.3 to conclude that the eigenvalues of $\mathbf{M}$ are real. □

Theorem 7.2 (Weak hyperbolicity)**.** *The generalized multi-class model with conservation equation (7.4) is weakly hyperbolic if both Condition 7.1 and 7.2 are satisfied.*

Proof. From Theorem 7.1 we conclude that the velocity is nonincreasing and thus (7.12) holds for all classes i and j. Using Lemma 7.1 and 7.2 we conclude that the eigenvalues of $\mathbf{M}$ are real. From Preliminary 7.2 we conclude that by construction the eigenvalues of the Jacobian $\mathbf{J}$ (7.6) are equal to the eigenvalues of matrix $\mathbf{M}$. Consequently, the eigenvalues of the Jacobian $\mathbf{J}$ are real. Using the definition of weak hyperbolicity (Definition 7.2) we conclude that the model is weakly hyperbolic. □

We remark that $\mathbf{M}$ may also have real eigenvalues if (7.12) does not hold for all classes i and j. Therefore, the model may also be weakly hyperbolic if (7.12) does not hold for all classes i and j. We do not provide an assessment procedure for this case, partly because nonincreasing velocity is a reasonable requirement itself.

7.3.4 Finite characteristic velocities

We show that the model has finite characteristic velocities if it is weakly hyperbolic and if furthermore both the fundamental relation and the effective density function are bounded and continuous. (Condition 7.3). In other words, weak hyperbolicity is a necessary but not sufficient condition for finite characteristic velocities, see Figure 7.1.

Theorem 7.3. *The generalized multi-class model with conservation equation (7.4) has finite characteristic velocities if Condition 7.1, 7.2 and 7.3 hold.*

Proof. From Theorem 7.2 and Definition 7.2 we conclude that the model has real eigenvalues and is weakly hyperbolic. What remains is to show that the eigenvalues are furthermore finite. Condition 7.3 states the fundamental relation $v_u = v_u(\rho)$ and the effective density function $\rho = \rho(\rho_1, \ldots, \rho_U)$ are continuously differentiable or bounded and continuous. If they are continuously differentiable, the derivatives $\partial v_i/\partial \rho$ and $\partial \rho/\partial \rho_j$ exist (are finite). Therefore, also the partial derivatives $\partial v_i/\partial \rho_j$ and $\partial v_i/\partial s_j$ exist (are finite). If the fundamental relation and effective density function are not continuously differentiable, but they are bounded and continuous, then we apply Preliminary 7.1. From Preliminary 7.1 we conclude that the fundamental relation and the effective density function can be approximated arbitrarily closely by a continuously differentiable function with finite partial derivatives $\partial v_i/\partial s_j$. Furthermore, spacings are nonzero ($s_u \neq 0$) and thus all entries of matrix $\mathbf{A}$ (7.7) are finite: $|a_{i,j}| < \infty$. We apply Preliminary 7.4 (Gershgorin's circle theorem) to conclude that also the eigenvalues of the Jacobian $\mathbf{J}$ are finite. From Definition 7.3 we conclude that the model has finite characteristic velocities. □

7.3.5 Anisotropy

We show that the generalized model is anisotropic if it is weakly hyperbolic and if furthermore there is a fastest class (Condition 7.4). In fact, we only show that if the model has nonincreasing velocities v_u (is in the upper circle of Figure 7.1) and if furthermore there is a fastest class, the model is anisotropic. As the figure shows, the model may also be anisotropic if the velocity is increasing. However, we do not consider that case because non increasing velocity is a reasonable requirement itself.

In this subsection, we first show that if there is a fastest class, the model may be reformulated such that class 1 is the fastest class. Therefore, in Lagrangian coordinates the coordinate system moves with the velocity of the fastest class. Consequently, the model is anisotropic if the characteristic velocities are nonnegative, i.e. if the eigenvalues of the Jacobian $\mathbf{J}$ are nonnegative.

Lemma 7.3. *The generalized multi-class model that satisfies Condition 7.4 may be rewritten such that in all traffic states class 1 is not slower than any class i:*

$$v_1 \geq v_i \tag{7.22}$$

Proof. Assume that class j is the fastest class, i.e. it is not slower than any other class in any permissible traffic state. The classes can be reordered such that class j becomes class 1. Now, class 1 is the fastest class. Only after this reordering the generalized model (in Eulerian coordinates) is reformulated in Lagrangian coordinates. □

Lemma 7.4. *Matrix* $\mathbf{M}$ *defined by (7.18) has nonnegative eigenvalues if (7.19) holds for all classes i and j and if furthermore (7.22) holds for all classes i.*

Proof. From Lemma 7.2 we conclude that $\mathbf{M}$ is real and symmetric. The rest of this proof consists of applying Gaussian elimination and showing that $\mathbf{M}$ has nonnegative pivots. Next, from Preliminary 7.5 we conclude that $\mathbf{M}$ has nonnegative eigenvalues.

The first step of Gaussian elimination consists of subtracting $m_{i,1}/m_{1,1}$ times row 1 from each row i. This gives zeros on column 1, except for row 1. Applying this subtraction and using the definitions of matrix $\mathbf{A}$ (7.7) and of matrix $\mathbf{M}$ (7.21) gives matrix $\tilde{\mathbf{M}}$ with:
if $i = 1$ (row 1):

$$\tilde{m}_{1,j} \quad = \quad m_{1,j} = \frac{\sqrt{s_1 s_j}}{s_1} \sqrt{\frac{\partial v_j}{\partial s_1} \frac{\partial v_1}{\partial s_j}} = \sqrt{\frac{s_j}{s_1} \frac{\partial v_j}{\partial s_1} \frac{\partial v_1}{\partial s_j}} \tag{7.23a}$$

if $j = 1$, $i \neq 1$ (column 1, except for row 1):

$$\tilde{m}_{i,1} \quad = \quad 0 \tag{7.23b}$$

if $i = j$, $i \neq 1$ (diagonal, except for row 1):

$$\begin{aligned} \tilde{m}_{i,i} &= m_{i,i} - \frac{m_{i,1}m_{1,i}}{m_{1,1}} = a_{i,i} - \frac{\frac{d_i}{d_1}a_{i,1}\frac{d_1}{d_i}a_{1,i}}{a_{1,1}} = \frac{s_i}{s_1}\frac{\partial v_i}{\partial s_i} + \frac{v_1 - v_i}{s_1} - \frac{s_i}{s_1}\frac{\partial v_i}{\partial s_i} \\ &= \frac{v_1 - v_i}{s_1} \end{aligned} \tag{7.23c}$$

if $i \neq 1$, $j \neq 1$, $i \neq j$ (everywhere else, i.e. not row 1, not column 1, not on the diagonal):

$$\tilde{m}_{i,j} = m_{i,j} - \frac{m_{i,1}m_{1,j}}{m_{1,1}} = \frac{d_i}{d_j}a_{i,j} - \frac{\frac{d_i}{d_1}a_{i,1}\frac{d_1}{d_j}a_{1,j}}{a_{1,1}} = a_{i,j} - \frac{a_{i,1}a_{1,j}}{a_{1,1}} = 0 \tag{7.23d}$$

Both in (7.23c) and (7.23d) we use that $i \neq 1$ and $j \neq 1$ and apply (7.7b) to find:

$$\frac{a_{i,1}a_{1,j}}{a_{1,1}} = \frac{\frac{s_i}{s_1}\frac{\partial v_i}{\partial s_1}\frac{s_1}{s_1}\frac{\partial v_1}{\partial s_j}}{\frac{s_1}{s_1}\frac{\partial v_1}{\partial s_1}} = \frac{s_i}{s_1}\frac{\partial v_i}{\partial s_j} \tag{7.24}$$

For clarity, we write the matrix $\tilde{\mathbf{M}}$ as derived in (7.23) in matrix form:

$$\tilde{\mathbf{M}} = \begin{pmatrix} \frac{\partial v_1}{\partial s_1} & \sqrt{\frac{s_2}{s_1}\frac{\partial v_2}{\partial s_1}\frac{\partial v_1}{\partial s_2}} & \cdots & \sqrt{\frac{s_U}{s_1}\frac{\partial v_U}{\partial s_1}\frac{\partial v_1}{\partial s_U}} \\ & \frac{v_1 - v_2}{s_1} & & \emptyset \\ & & \ddots & \\ \emptyset & & & \frac{v_1 - v_U}{s_1} \end{pmatrix} \tag{7.25}$$

In this case, one step of Gaussian elimination is enough to get an upper triangular matrix with zeroes below the main diagonal. The pivots are the elements at the main diagonal of $\tilde{\mathbf{M}}$. The pivots are nonnegative if the Lagrangian fundamental relation does not decrease (i.e. (7.19) holds) for class $i = 1$ and $j = 1$, and if furthermore the class 1 is the fastest class (i.e. (7.22) holds for all classes i). From Preliminary 7.5 we conclude that the eigenvalues of $\mathbf{M}$ are nonnegative. □

Theorem 7.4. *The generalized multi-class model with conservation equation (7.4) is anisotropic if Condition 7.1, 7.2 and 7.4 hold.*

Proof. Lemma 7.3 shows that the model can be rewritten such that class 1 is the fastest class and thus the coordinate system moves with the velocity of the fastest class. It remains to show that the characteristics are not faster than the coordinates. In other words, we need to show that the eigenvalues of the Jacobian $\mathbf{J}$ are nonnegative. In the proof of Theorem 7.2 we show that the eigenvalues are real and that they are equal to the eigenvalues of the matrix $\mathbf{M}$. Using Lemma 7.4 we conclude that the eigenvalues of

M and thus also of the Jacobian **J** are nonnegative. Using the definition of anisotropy (Definition 7.4) we conclude that the model is anisotropic. □

We conclude that the generalized multi-class traffic flow model has nonincreasing velocity (Requirement 7) and is weakly hyperbolic if the fundamental relation is nonincreasing (Condition 7.1) and if the effective density function is nondecreasing (Condition 7.2). The model has finite characteristic velocities (Requirement 8) if furthermore the fundamental relation is continuously differentiable, i.e. if $\partial v_i/\partial \rho_j$ exists for all classes i and j (Condition 7.3). Finally, the model is anisotropic (Requirement 9) if it is weakly hyperbolic and if furthermore there is a fastest class (Condition 7.4). We note that the conditions for hyperbolicity and anisotropy discussed in this section, are only sufficient conditions: they are not necessary. In other words, there may be models which do not satisfy the conditions but are still hyperbolic or anisotropic. However, in the next section, it turns out that the sufficient conditions are useful to assess the multi-class models discussed in Chapter 5 with respect to the requirements on characteristic velocities.

7.4 Assessment of multi-class models

All multi-class models that are discussed in Chapter 5 are assessed. It is verified whether they satisfy Requirement 7, 8 and 9. Therefore, we use the Condition 7.1–7.4 introduced in the previous section. Like in the assessment of the other requirements (Section 7.1) we do not repeat the model equation here but refer to Table 5.2 for an overview of all multi-class models and Figure 5.1 for examples of their fundamental relations. Furthermore, we assume that the parameters have feasible values.

7.4.1 The model by Logghe & Immers

We show that the model by Logghe & Immers satisfies all requirements related to nonincreasing velocity, finite characteristic velocity and anisotropy.

Lemma 7.5. *The fundamental relation of the model by Logghe & Immers defined and reformulated in Section 5.2.1 satisfies Condition 7.1.*

Proof. Condition 7.1 states that the class-specific velocity v_i is a nonincreasing function of the effective density ρ. The derivative of the velocity function is:

$$\frac{\partial v_u}{\partial \rho} = \begin{cases} 0 & \text{(free flow)} \quad (7.26a) \\ -w_1 \dfrac{\rho_{1,\mathrm{jam}}}{(\rho)^2} < 0 & \text{(congestion)} \quad (7.26b) \end{cases}$$

We conclude that the model by Logghe & Immers satisfies Condition 7.1. □

Lemma 7.6. *The effective density function of the model by Logghe & Immers defined in Section 5.2.1 satisfies Condition 7.2.*

Proof. Condition 7.2 states that the effective density ρ is a nondecreasing function of the class-specific densities ρ_i. We determine the derivative of the effective density ρ to the class-specific densities ρ_1 and ρ_2 separately. The derivative of the effective density to ρ_1 is:

$$\frac{\mathrm{d}\rho}{\mathrm{d}\rho_1} = \begin{cases} \text{undefined} & \text{(free flow)} & \text{(7.27a)} \\ \dfrac{\rho_{2,\mathrm{crit}}}{\rho_{2,\mathrm{crit}} - \rho_2} > 0 & \text{(semi congestion)} & \text{(7.27b)} \\ \dfrac{w_1\rho_{1,\mathrm{jam}} + \frac{w_2\rho_{2,\mathrm{jam}}}{\rho_2}}{w_1 + w_2\left(\frac{\rho_{2,\mathrm{jam}}}{\rho_2} - 1\right)} > 0 & \text{(congestion)} & \text{(7.27c)} \end{cases}$$

The inequalities hold because in semi-congestion $\rho_2 \leq \rho_{2,\mathrm{crit}}$ and in congestion $\rho_2 \leq \rho_{2,\mathrm{jam}}$. The derivative of the effective density to ρ_2 is:

$$\frac{\mathrm{d}\rho}{\mathrm{d}\rho_2} = \begin{cases} \text{undefined} & \text{(free flow)} & \text{(7.28a)} \\ \dfrac{\rho_{2,\mathrm{crit}}}{\left(\rho_{2,\mathrm{crit}} - \rho_2\right)^2}\rho_1 > 0 & \text{(semi congestion)} & \text{(7.28b)} \\ \dfrac{w_1\rho_{1,\mathrm{jam}}w_2\rho_{2,\mathrm{jam}}}{\left(w_1\rho_2 + w_2(\rho_{2,\mathrm{jam}} - \rho_2)\right)^2}\rho_1 > 0 & \text{(congestion)} & \text{(7.28c)} \end{cases}$$

The inequalities hold because in semi-congestion $\rho_2 \leq \rho_{2,\mathrm{crit}}$ and in congestion $\rho_2 \leq \rho_{2,\mathrm{jam}}$. We conclude that Condition 7.2 holds. □

Theorem 7.5. *The model by Logghe & Immers defined in Section 5.2.1 has nonincreasing velocity and finite characteristic velocity and is anisotropic.*

Proof. From Lemma 7.5 and 7.6 and Theorem 7.1 we conclude that the velocities are nonincreasing. By furthermore applying Theorem 7.2 we conclude that the model is weakly hyperbolic. Both the fundamental relation $v_u(\rho)$ and the effective density function are bounded continuous function and thus Condition 7.3 holds. We conclude from Theorem 7.3 that the characteristics have finite velocity. Finally, the class with the largest maximum velocity $v_{u,\max}$ is not slower than the other class in any traffic state, i.e. Condition 7.4 holds. From Theorem 7.4 we conclude that the model is anisotropic. □

7.4.2 The model by Ngoduy & Liu

The model by Ngoduy & Liu satisfies all requirements related to nonincreasing velocity, finite characteristic velocity and anisotropy conditionally. We show that the

conditions are satisfied if for all classes i and j the pce-values are constant:

$$\frac{\mathrm{d}\eta_i}{\mathrm{d}\rho_j} = 0 \tag{7.29}$$

and if furthermore for all classes i and j:

$$\eta_i \leq 2\eta_j \tag{7.30}$$

Lemma 7.7. *The fundamental relation of the model by Ngoduy & Liu defined and reformulated in Section 5.2.2 satisfies Condition 7.1.*

Proof. Condition 7.1 states that the class-specific velocity v_i is a nonincreasing function of the effective density ρ. The derivative of the velocity function is:

$$\frac{\partial v_u}{\partial \rho} = \begin{cases} -\dfrac{v_{u,\max} - v_{\mathrm{crit}}}{\rho_{\mathrm{crit}}} < 0 & \text{(free flow)} \quad (7.31a) \\ -w\dfrac{\rho_{\mathrm{jam}}}{(\rho)^2} < 0 & \text{(congestion)} \quad (7.31b) \end{cases}$$

We conclude that the model by Ngoduy & Liu satisfies Condition 7.1. □

Lemma 7.8. *The effective density function of the model by Ngoduy & Liu defined in Section 5.2.2 with constant pce-values (i.e. (7.29) holds) satisfies the nondecreasing effective density Condition 7.2 if and only if (7.30) holds for all classes i and j.*

Proof. Condition 7.2 states that the effective density ρ is a nondecreasing function of the class-specific densities ρ_i. We determine the derivative of the effective density ρ to the class-specific density ρ_i and show that it is only nonnegative if (7.30) holds for all classes i and j. We apply respectively the effective density function $\rho = \bar{\eta}\rho^{\mathrm{tot}}$, the chain rule, the harmonic average pce-value $\bar{\eta} = \frac{\rho^{\mathrm{tot}}}{\sum_u \rho_u/\eta_u}$, the quotient rule and again the harmonic average pce-value and the quotient rule to find the derivative:

$$\begin{aligned} \frac{\mathrm{d}\rho}{\mathrm{d}\rho_i} &= \rho^{\mathrm{tot}}\frac{\mathrm{d}\bar{\eta}}{\mathrm{d}\rho_i} + \bar{\eta}\frac{\mathrm{d}\rho^{\mathrm{tot}}}{\mathrm{d}\rho_i} \\ &= \rho^{\mathrm{tot}}\frac{\mathrm{d}}{\mathrm{d}\rho_i}\left(\frac{\rho^{\mathrm{tot}}}{\sum_u \rho_u/\eta_u}\right) + \bar{\eta}\frac{\mathrm{d}\rho^{\mathrm{tot}}}{\mathrm{d}\rho_i} \\ &= \rho^{\mathrm{tot}}\frac{\left(\sum_u \frac{\rho_u}{\eta_u}\right)\frac{\mathrm{d}\rho^{\mathrm{tot}}}{\mathrm{d}\rho_i} - \rho^{\mathrm{tot}}\frac{\mathrm{d}}{\mathrm{d}\rho_i}\left(\sum_u \frac{\rho_u}{\eta_u}\right)}{\left(\sum_u \frac{\rho_u}{\eta_u}\right)^2} + \bar{\eta}\frac{\mathrm{d}\rho^{\mathrm{tot}}}{\mathrm{d}\rho_i} \\ &= \bar{\eta}\left(2\frac{\mathrm{d}\rho^{\mathrm{tot}}}{\mathrm{d}\rho_i} - \bar{\eta}\frac{\mathrm{d}}{\mathrm{d}\rho_i}\left(\sum_u \frac{\rho_u}{\eta_u}\right)\right) \\ &= \bar{\eta}\left(2\sum_u \frac{\mathrm{d}\rho_u}{\mathrm{d}\rho_i} - \bar{\eta}\sum_u \frac{\eta_u\frac{\mathrm{d}\rho_u}{\mathrm{d}\rho_i} - \rho_u\frac{\mathrm{d}\eta_u}{\mathrm{d}\rho_i}}{(\eta_u)^2}\right) \end{aligned} \tag{7.32}$$

Since the pce-values are constant ($\mathrm{d}\eta_u/\mathrm{d}\rho_i = 0$), the second term in the numerator drops out. Furthermore, $\mathrm{d}\rho_i/\mathrm{d}\rho_i = 1$ and for all $u \neq i$ the derivative is $\mathrm{d}\rho_u/\mathrm{d}\rho_i = 0$. Finally, we find:

$$\frac{\mathrm{d}\rho}{\mathrm{d}\rho_i} = \bar{\eta}\left(2 - \frac{\bar{\eta}}{\eta_i}\right) \tag{7.33}$$

The derivative (7.33) is nonnegative if and only if $\eta_i \leq 2\bar{\eta}$. We conclude that Condition 7.2 is satisfied if and only if (7.30) holds for all classes i and j. □

Lemma 7.8 shows that the difference between pce-values can not be 'too large'. If one of them is more than 2 times larger than any other, the effective density decreases.

Theorem 7.6. *The model by Ngoduy & Liu defined in Section 5.2.2 has nonincreasing velocity, finite characteristic velocities and is furthermore anisotropic if for all classes i and j (7.29) and (7.30) hold.*

Proof. From Lemma 7.7 and 7.8 and Theorem 7.1 we conclude that the velocities are nonincreasing if (7.29) and (7.30) hold for all classes i and j. By furthermore applying Theorem 7.2 we conclude that the model is weakly hyperbolic. Furthermore, both the fundamental relation $v_u(\rho)$ and the effective density function $\rho(\rho_1, \ldots, \rho_U)$ are bounded and continuous functions and Condition 7.3 holds. We conclude from Theorem 7.3 that the characteristics have finite velocity. Finally, the class with the largest maximum velocity $v_{u,\max}$ is not slower than the other classes in any permissible traffic state, i.e. Condition 7.4 holds. From Theorem 7.4 we conclude that the model is anisotropic. □

We note that we can not conclude that the model does not satisfy the requirements if (7.29) or (7.30) does not hold for all classes i and j. For example, even if the pce-values have discontinuities, the model may be anisotropic. However, this would imply infinite characteristic velocities, which is unrealistic. Finally, Ngoduy & Liu show that their model is strictly hyperbolic and anisotropic if there are only two-classes. They claim that it is 'rather complex' to verify analytically strict hyperbolicity if there are more than 2 classes because it is cumbersome or even impossible (for more than 4 classes) to obtain eigenvalues. We have shown that the analysis can be done without exactly knowing the eigenvalues.

7.4.3 Fastlane

We show that Fastlane satisfies all requirements related to nonincreasing velocity, finite characteristic velocity and anisotropy if the parameter conditions introduced in Section 4.4 are satisfied. Let us first recall Lemma 4.1 and 4.2 (Section 4.5) and the

reformulation of the parameter conditions introduced in those Lemma's, for all classes u:

$$a_u \geq 0, \quad b_1^{\mathrm{f}} \leq b_u^{\mathrm{f}} \leq 0, \quad 0 \leq b_u^{\mathrm{c}} \leq b_1^{\mathrm{c}}, \quad a_u^{\mathrm{f}} + 2b_u^{\mathrm{f}}\rho \geq 0 \quad \text{and} \quad a_u^{\mathrm{c}} + b_u^{\mathrm{c}}\rho \geq 0 \tag{7.34}$$

The effective density-velocity fundamental relation of Fastlane is equal to that of the model by Ngoduy & Liu. Therefore, we can apply Lemma 7.7 to show that also in Fastlane the class-specific velocity is a non increasing function of the effective density ($\partial v_u / \partial \rho \leq 1$) and thus satisfies Condition 7.1.

Lemma 7.9. *The effective density function of Fastlane with $b_1 = 0$ satisfies Condition 7.2.*

Proof. Condition 7.2 states that the effective density ρ is a nondecreasing function of the class-specific densities ρ_i. We determine the derivative of the effective density ρ to the class-specific density ρ_i and show that it is nonnegative. Therefore, we substitute the function $f = a_1 - \sum_u b_u \rho_u$ (4.38) into the effective density function ρ (4.51b):

$$\rho = \frac{\sum_u a_u \rho_u}{f} \tag{7.35}$$

The derivative of the effective density is:

$$\frac{\mathrm{d}\rho}{\mathrm{d}\rho_i} = \frac{f \sum_u \frac{\mathrm{d}}{\mathrm{d}\rho_i}(a_u \rho_u) - \frac{\mathrm{d}f}{\mathrm{d}\rho_i} \sum_u a_u \rho_u}{f^2} = \frac{f a_i + b_i \sum_u a_u \rho_u}{f^2} \tag{7.36}$$

We now substitute the other form of the function $f = \frac{\sum_u a_u \rho_u}{\rho} - b_1 \rho$ (4.41) and $b_1 = 0$ to find:

$$\frac{\mathrm{d}\rho}{\mathrm{d}\rho_i} = \frac{\left(\frac{\sum_u a_u \rho_u}{\rho} - b_1 \rho\right) a_i + b_i \sum_u a_u \rho_u}{f^2} = \frac{\sum_u a_u \rho_u (a_i + b_i \rho)}{f^2 \rho} \geq 0 \tag{7.37}$$

In congestion, the inequality holds because all terms are positive, see (7.34). In free flow, we apply the second inequality in (7.34) to find $b_i = 0$. All other terms are nonnegative and thus the inequality also holds in free flow. We conclude that if $b_1 = 0$ then Condition 7.2 holds. □

Lemma 7.10. *The effective density function of Fastlane with $b_1 \neq 0$ satisfies Condition 7.2.*

Proof. Condition 7.2 states that the effective density ρ is a nondecreasing function of the class-specific densities ρ_i. We determine the derivative of the effective density ρ to

the class-specific density ρ_i and show that it is nonnegative. We substitute the function $f = a_1 - \sum_u b_u \rho_u$ (4.38) into the effective density function ρ (4.51a) and reorder:

$$\rho = \frac{f - \sqrt{f^2 + 4b_1 \sum_u a_u \rho_u}}{-2b_1} \tag{7.38}$$

We use $\mathrm{d}f/\mathrm{d}\rho_i = -b_i$ to find the derivative of the effective density is:

$$\begin{aligned} \frac{\mathrm{d}\rho}{\mathrm{d}\rho_i} &= \frac{1}{-2b_1}\left(\frac{\mathrm{d}f}{\mathrm{d}\rho_i} + \frac{2f\frac{\mathrm{d}f}{\mathrm{d}\rho_i} + 4b_1 a_i}{2\sqrt{f^2 + 4b_1 \sum_u a_u \rho_u}}\right) = \frac{1}{-2b_1}\left(-b_i + \frac{2fb_i + 4b_1 a_i}{2\sqrt{f^2 + 4b_1 \sum_u a_u \rho_u}}\right) \\ &= \frac{b_i}{2b_1}\left(1 - \frac{f + 2\frac{a_i}{b_i}b_1}{\sqrt{f^2 + 4b_1 \sum_u a_u \rho_u}}\right) \end{aligned} \tag{7.39}$$

We now substitute the other form of the function $f = (\sum_u a_u \rho_u)/\rho - b_1 \rho$ (4.41) in the f under the square-root sign and observe that the square root term can be written as an absolute term:

$$\begin{aligned} \frac{\mathrm{d}\rho}{\mathrm{d}\rho_i} &= \frac{b_i}{2b_1}\left(1 - \frac{f + 2\frac{a_i}{b_i}b_1}{\sqrt{\left(\frac{\sum_u a_u \rho_u}{\rho} - b_1\rho\right)^2 + 4b_1 \sum_u a_u \rho_u}}\right) \\ &= \frac{b_i}{2b_1}\left(1 - \frac{f + 2\frac{a_i}{b_i}b_1}{\left|\frac{\sum_u a_u \rho_u}{\rho} + b_1\rho\right|}\right) \end{aligned} \tag{7.40}$$

We substitute $(\sum_u a_u \rho_u)/\rho - b_1\rho = f$ (4.41) in the denominator, rewrite and find:

$$\frac{\mathrm{d}\rho}{\mathrm{d}\rho_i} = \frac{b_i}{2b_1}\left(1 - \frac{f + 2\frac{a_i}{b_i}b_1}{|f + 2b_1\rho|}\right) = \frac{b_i}{2b_1}\frac{|f + 2b_1\rho| - f + 2\frac{a_i}{b_i}b_1}{|f + 2b_1\rho|} \tag{7.41}$$

We note that the sign of (7.41) is equal to the sign of the numerator. This is because the signs of all b_u are equal (see (7.34)) and thus the first term is nonnegative ($b_i/(2b_1) \geq 0$). We distinguish between congestion and free flow and analyze these states separately.

In congestion for all classes u, $a_u \geq 0$ and $b_u \geq 0$. Therefore, $f = (\sum_u a_u \rho_u)/\rho + b_1\rho \geq 0$ and $f + 2b_1\rho \geq 0$. Substituting these inequalities in the numerator of the partial derivative of the effective density (7.41) gives:

$$|f + 2b_1\rho| - f + 2\frac{a_i}{b_i}b_1 = 2b_1\rho + 2\frac{a_i}{b_i}b_1 = 2b_1\left(\rho + \frac{a_i}{b_i}\right) \geq 0 \tag{7.42}$$

We conclude that in congestion the partial derivative $\partial\rho/\partial\rho_u$ is nonnegative for all classes u

In free flow the sign of the term between the absolute-signs can be either positive or nonnegative: $f+2b_1\rho \leq 0$ or $f+2b_1\rho > 0$. In the first case $2b_1\rho \leq -f$ and the numerator of (7.41) becomes:

$$\begin{aligned} |f+2b_1\rho| - f + 2\frac{a_i}{b_i}b_1 &= -(f+2b_1\rho) - f + 2\frac{a_1}{b_i}b_1 \\ &= 2\left(\underbrace{-(f+2b_1\rho)}_{\geq 0} + b_1\rho + \frac{a_i}{b_i}b_1\right) \\ &\geq 2b_1\left(\rho + \frac{a_i}{b_i}\right) \end{aligned} \tag{7.43}$$

We now substitute a_i^{f} and b_i^{f} as defined in (4.52a) which gives:

$$|f+2b_1\rho| - f + 2\frac{a_i}{b_i}b_1 \geq 2b_1\left(\rho - \rho_{\mathrm{crit}}\underbrace{\frac{L_i + T_1 v_{i,\max}}{T_i(v_{i,\max} - v_{\mathrm{crit}})}}_{\geq 1}\right) \geq 0 \tag{7.44}$$

The last inequality holds because in free flow $\rho \leq \rho_{\mathrm{crit}}$. In the second case ($f+2b_1\rho > 0$) we have $2b_1\rho > -f$ and the numerator in (7.41) becomes:

$$|f+2b_1\rho| - f + 2\frac{b_1}{b_i}a_i = 2b_1\left(\rho + \frac{a_i}{b_i}\right) \geq 0 \tag{7.45}$$

The inequality holds as we have already shown in (7.44). We conclude that if $b_1 \neq 0$ Condition 7.2 holds both in free flow and in congestion. □

Theorem 7.7. *Fastlane has nonincreasing velocity and finite characteristic velocity and is anisotropic.*

Proof. Fastlane has the same fundamental relation $v(\rho)$ as the model by Ngoduy & Liu. From Lemma 7.7 we conclude that Condition 7.1 is satisfied. From this, combined with Lemma 7.9 and 7.10 and Theorem 7.1 we conclude that the velocities are nonincreasing. By furthermore applying Theorem 7.2 we conclude that the model is weakly hyperbolic. Both $v_u(\rho)$ and $\rho(\rho_1,\ldots,\rho_U)$ are bounded continuous functions and thus Condition 7.3 holds. We conclude from Theorem 7.3 that the characteristics have finite velocity. Finally, the class with the largest maximum velocity $v_{u,\max}$ is not slower than the other classes in any traffic state, i.e. Condition 7.4 holds. From Theorem 7.4 we conclude that the model is anisotropic. □

We note that if the parameters do not satisfy the conditions introduced in Section 4.4 (and repeated in 7.34), the model may not satisfy the requirements related to nonincreasing velocity, hyperbolicity and anisotropy. However, we do not consider that case, partly because the conditions are reasonable.

7.4.4 The model by Nair et al.

We show that the model by Nair et al. has nonincreasing velocity and finite characteristic velocity. We do not draw any conclusion on anisotropy of the model.

Lemma 7.11. *The fundamental relation of the model by Nair et al. defined and reformulated in Section 5.4.1 satisfies condition 7.1.*

Proof. Condition 7.1 states that the class-specific velocity v_i is a nonincreasing function of the effective density ρ. The derivative of the velocity function is:

$$\begin{aligned}\frac{\partial v_u}{\partial \rho} &= \left[\left(1 - c^{\mathrm{rs}} g_u (1-g_u)^{-1}\right)(1-g_u)^{c^{\mathrm{rs}}-c^{\mathrm{ur}}-1} - (1+c^{\mathrm{ur}})\right](1-g_u)^{1+c^{\mathrm{ur}}} \frac{\partial g_u}{\partial \rho} v_{u,\max} \\ &= \Bigg[\underbrace{\frac{1-g_u-c^{\mathrm{rs}} g_u}{1-g_u}}_{\leq 1} \underbrace{(1-g_u)^{c^{\mathrm{rs}}-c^{\mathrm{ur}}-1}}_{\leq 1} - \underbrace{(1+c^{\mathrm{ur}})}_{\geq 1}\Bigg](1-g_u)^{1+c^{\mathrm{ur}}} \frac{\partial g_u}{\partial \rho} v_{u,\max} \geq 0\end{aligned} \tag{7.46}$$

The inequality holds because both $(1-g_u)^{1+c^{\mathrm{ur}}}$ and $v_{u,\max}$ are positive and the term between square brackets and the partial derivative $\partial g_u / \partial \rho$ are nonpositive:

$$\frac{\partial g_u}{\partial \rho} = -p r_{u,\mathrm{crit}} e^{-p r_{u,\mathrm{crit}}} \frac{\partial p}{\partial \rho} = -p r_{u,\mathrm{crit}} e^{-p r_{u,\mathrm{crit}}} (b_{\max} - b_{\min}) \frac{a_1}{d} \leq 0 \tag{7.47}$$

We conclude that the model by Nair et al. satisfies Condition 7.1. □

Lemma 7.12. *The effective density function of the model by Nair et al. defined in Section 5.4.1 satisfies Condition 7.2.*

Proof. Condition 7.2 states that the effective density ρ is a nondecreasing function of the class-specific densities ρ_i. The pce-values are constant and thus:

$$\frac{\mathrm{d}\rho}{\mathrm{d}\rho_i} = \frac{\mathrm{d}}{\mathrm{d}\rho_i} \sum_u \eta_u \rho_u = \eta_i > 0 \tag{7.48}$$

We conclude that Condition 7.2 holds. □

Theorem 7.8. *The model by Nair et al. defined in Section 5.4.1 has nonincreasing velocity, is weakly hyperbolic and has finite characteristic velocities.*

Proof. From Lemma 7.11 and 7.12 and Theorem 7.1 we conclude that the velocities are nonincreasing. By furthermore applying Theorem 7.2 we conclude that the model is weakly hyperbolic. Finally, both the fundamental relation and the effective density function are continuously differentiable functions. We conclude from Theorem 7.3 that the characteristics have finite velocity. □

We can not draw any conclusion on anisotropy because of the following. The model is developed to reproduce disordered traffic flow. In this type of traffic flow one class (e.g., cars) is the fastest class at low densities and another class (e.g., scooters) is the fastest class at high densities. Therefore, there is no fastest class and Condition 7.4 does in general not hold for the model by Nair et al.. To study the anisotropy of the model one would need to consider each case with a different fastest class separately, e.g., the case where cars are fastest needs to be analyzed separately from the case where scooters are fastest.

7.4.5 Other multi-class models

We show that the models by Chanut & Buisson, Benzoni-Gavage & Colombo and Wong & Wong satisfy all requirements related to nonincreasing velocity, finite characteristic velocity and anisotropy.

The model by Chanut & Buisson satisfies the non increasing velocity condition (Condition 7.1) because its fundamental relation is equal to that in the model by Ngoduy & Liu, see Lemma 7.7.

Lemma 7.13. *The fundamental relation of the model by Benzoni-Gavage & Colombo defined and reformulated in Section 5.4.3 with Greenshields' fundamental relation satisfies Condition 7.1.*

Proof. Condition 7.1 states that the class-specific velocity v_i is a nonincreasing function of the effective density ρ. The derivative of the velocity function is:

$$\frac{\partial v_u}{\partial \rho} = -\frac{v_{u,\max}}{\rho_{\text{jam}}} < 0 \tag{7.49}$$

We conclude that the model by Benzoni-Gavage & Colombo with Greenshields' fundamental relation satisfies Condition 7.1. □

Lemma 7.14. *The fundamental relation of the model by Benzoni-Gavage & Colombo defined and reformulated in Section 5.4.3 with Drake's fundamental relation and the model byWong & Wong satisfy Condition 7.1.*

Proof. Condition 7.1 states that the class-specific velocity v_i is a nonincreasing function of the effective density ρ. The derivative of the velocity function is:

$$\frac{\partial v_u}{\partial \rho} = -\frac{\rho}{(\rho_{\text{crit}})^2} v_{u,\max} e^{-\frac{1}{2}\left(\frac{\rho}{\rho_{\text{crit}}}\right)^2} \leq 0 \tag{7.50}$$

We conclude that the model by Benzoni-Gavage & Colombo with Drake's fundamental relation and the model by Wong & Wong satisfy Condition 7.1. □

Theorem 7.9. *The models by Chanut & Buisson, Benzoni-Gavage & Colombo and Wong & Wong defined and reformulated in Section 5.4.2, 5.4.3 and 5.5, respectively, have nonincreasing velocity and finite characteristic velocities and are anisotropic.*

Proof. The model by Chanut & Buisson has the same fundamental relation $v(\rho)$ as the model by Ngoduy & Liu. Furthermore, all models have the same effective density function as the model by Nair et al.. From Lemma 7.7, 7.13, 7.14 and 7.12 and Theorem 7.2 we conclude that the velocities are nonincreasing. By furthermore applying Theorem 7.2 we conclude that the model is weakly hyperbolic. The effective density function and Drake's fundamental relation are continuously differentiable. The other fundamental relations are bounded and continuous. We conclude from Theorem 7.3 that the characteristics have finite velocity. Finally, in all models the class with the largest maximum velocity $v_{u,\max}$ is not slower than the other classes in any traffic state, i.e. Condition 7.4 holds. From Theorem 7.4 we conclude that the models are anisotropic. □

We note that Benzoni-Gavage & Colombo proof that their model is hyperbolic and anisotropic. However, they use a different approach in their proof.

The model by Zhang et al. is the only one that we do not assess based on the criteria for nonincreasing velocity, finite characteristic velocity and anisotropy. This is because they do not specify a fundamental relation. However, the authors claim that their model is strongly hyperbolic. Strong hyperbolicity means that eigenvalues are real and distinct. This is a rather strong requirement for traffic flow models because of the following. Zhang et al. have shown that the interlacing property holds for their multi-class model. The interlacing property means that the characteristic velocities have velocities in between the vehicle velocities. Consequently, in Eulerian coordinates, the eigenvalues have values between the vehicle velocities:

$$\lambda_U \leq v_U \leq \ldots \leq \lambda_1 \leq v_1 \quad \text{or} \quad v_U \leq \lambda_U \leq \ldots \leq v_1 \leq \lambda_1 \tag{7.51}$$

If eigenvalues are distinct, this implies that not all vehicle velocities can be equal. This is in contradiction with Requirement 5 stating that class-specific velocities are equal in congestion. However, as we have already seen, the model by Zhang et al. does not satisfy Requirement 5. Because of the contradiction between Requirement 5 and strong hyperbolicity, we only require weak hyperbolicity.

7.5 Conclusions

We developed and applied a framework to assess multi-class kinematic wave traffic flow models. The models are assessed with respect to the requirements that are proposed in Chapter 3. To assess the models with respect to the requirements related to

nonincreasing velocity, finite characteristic velocity and anisotropy, we use the generalized model formulation (Chapter 5) and the Lagrangian coordinate system (Chapter 6). The Lagrangian coordinate system is useful to analyze the characteristic velocities. This analysis is necessary to assess anisotropy. It is a major advantage of the framework that it is not necessary to know the eigenvalues of the model exactly. In other approaches such as applied by Ngoduy & Liu (2007) the eigenvalues are calculated exactly. However, this is difficult if there are 3 or 4 classes and impossible is there are even more classes.

The results of the assessment of the models are summarized in Table 7.1. The table shows that Fastlane and the model by Chanut & Buisson (2003) are the only ones that satisfy all requirements unconditionally. Three models (Wong & Wong, 2002; Ngoduy & Liu, 2007; Nair et al., 2012), only include flow maximization as a requirement for the numerical method, not for the continuous model itself. The model by Logghe & Immers (2008) does not allow decreasing velocities in free flow. The model by Ngoduy & Liu (2007) only satisfies all requirements under rather strict conditions on the pce-values: they must be constant and not 'too far' apart. In all other models the classes travel at different velocities in congestion. Furthermore, in the models by Nair et al. (2012); Wong & Wong (2002) and the model by Benzoni-Gavage & Colombo (2003) with Drake fundamental relation the velocity is not equal to zero for a certain (finite) jam density. We did not assess anisotropy of the model by Nair et al. (2012). Zhang et al. (2006) do not specify a fundamental relation and therefore we can only assess it with respect to a few requirements. Finally, we found some unexpected results in the models by Logghe & Immers; Nair et al.. In both models the velocity of the 'small' class (cars in the model by Logghe & Immers, scooters in the model by Nair et al.) can increase if some vehicles of the other class (trucks in the model by Logghe & Immers, cars in the model by Nair et al.) are replaced by vehicles of the 'small' class. This may be reasonable in the foreseen application of the disordered model byNair et al.. However, it is not reasonable for motorways with lanes, which is the application Logghe & Immers developed their model for.

The framework to assess multi-class models can be applied to assess any other multi-class kinematic wave traffic flow model. The assessment consists of the following steps:

1. Analyze the model formulation with respect to the following:
    - If the model is formulated such that it is contained in the generalized multi-class model (5.1) or (5.1a), (5.1b) and (5.2) the velocities and flows are uniquely determined by the class-specific densities (Requirement 1)
    - If the model is not formulated in such a way, reformulate the model such that it is contained in the generalized multi-class model. If this is possible the velocities and flows are uniquely determined by the class-specific densities (Requirement 1) and the model can be analyzed further.
    - Check whether the model prescribes which type of flow needs to be maxi-

mized (Requirement 2).

2. Analyze the fundamental relation $v_u(\rho)$ or $v_u(\rho_1, \ldots, \rho_U)$ with respect to the following:
   - In free flow classes may have unequal velocities (Requirement 3).
   - In free flow velocities may decrease (Requirement 4).
   - In congestion the velocities are class independent (Requirement 5).
   - There is a finite jam density at which the velocity of all classes is zero (Requirement 6).
3. Analyze the fundamental relation $v_u(\rho)$ and the effective density function $\rho(\rho_1, \ldots, \rho_U)$ with respect to the following:
   - If $\frac{\partial v_i}{\partial \rho} \leq 0$ and $\frac{\mathrm{d}\rho}{\mathrm{d}\rho_j} \geq 0$ for all classes i and j the model has nonincreasing velocity (Requirement 7).
   - If Requirement 7 is satisfied and if furthermore $v_u(\rho)$ for all classes u and $\rho(\rho_1, \ldots, \rho_U)$ are bounded and continuous functions, or if they are continuously differentiable, the model has finite characteristic velocities (Requirement 8).

   Alternatively, if this is not possible because the fundamental relation and the effective density function can not be separated, analyze the fundamental relation $v_u(\rho_1, \ldots, \rho_U)$ with respect to the following:
   - If $\frac{\partial v_i}{\partial \rho_j} \leq 0$ for all classes i and j the model has nonincreasing velocity (Requirement 7).
   - If Requirement 7 is satisfied and if furthermore $v_u(\rho_1, \ldots, \rho_U)$ is a bounded and continuous function for all classes u, or if it is continuously differentiable, the model has finite characteristic velocities (Requirement 8).
4. Analyze whether there is one class that is not slower than any other class in any permissible traffic state. If Requirement 7 and 8 are satisfied and if furthermore there is such a class, the model is anisotropic (Requirement 9).

We note that the conditions for the last three requirements are sufficient, but not necessary conditions. For example, a model may be anisotropic even if it does not have finite characteristic velocities. Finally, this framework for the assessment of multi-class models, can also be applied in the development of new models.

Table 7.1 *Assessment results of multi-class models.*

	Requirement	Logghe & Immers	Ngoduy & Liu	Fastlane	Nair et al.	Chanut & Buisson	Benzoni-Gavage & Colombo, Greenshields	Benzoni-Gavage & Colombo, Drake	Wong & Wong	Zhang et al.
1	Velocity and flow uniquely defined	✓	✓	✓	✓	✓	✓	✓	✓	✓
2	Flow maximization	✓	m	✓	m	✓	✓	✓	m	✓
3	Unequal velocity in free flow	✓	✓	✓	✓	✓	✓	✓	✓	✓
4	Decreasing velocity in free flow	-	✓	✓	✓	✓	✓	✓	✓	✓
5	Equal velocity in congestion	✓	✓	✓	-	✓	-	-	-	-
6	Zero velocity at jam density	✓	✓	✓	-	✓	✓	-	-	n
7	Nonincreasing velocity	✓	c	✓	✓	✓	✓	✓	✓	n
8	Finite characteristic velocity	✓	c	✓	✓	✓	✓	✓	✓	n
9	Anisotropy	✓	c	✓	n	✓	✓	✓	✓	n

✓ satisfied, - not satisfied, c satisfied conditionally, m only in numerical method, n not assessed.

Chapter 8

Numerical methods for mixed-class models

Numerical methods are used to approximate the solution of the kinematic wave model. This is needed because in most realistic cases it is impossible to solve the problems analytically. When a macroscopic model is applied, usually the space and time domains are divided into intervals: road segments (grid cells) and time steps. For each time step and at grid cell the model equations are solved approximately using numerical methods. The result is the density in each grid cell, at each time step. Alternatively, the Lagrangian model formulation is used and space is not divided into grid cells, but the vehicles are divided into groups. A numerical method is then applied to compute the position of each group at each time step.

The outline of this chapter is as follows. In the first part of this chapter we discuss both approaches based on the Eulerian formulation (Section 8.1) and the Lagrangian formulation (Section 8.2). Time stepping methods are discussed in Section 8.3. Furthermore, we introduce a numerical method based on variational theory in Section 8.4. In the second part of this chapter we assess the accuracy of the numerical methods. Therefore, we introduce two novel accuracy measures in Section 8.5. The measures are especially relevant in traffic flow applications and overcome disadvantages of commonly used accuracy measures. In Section 8.6 we discuss and compare the accuracy of the methods based on the novel accuracy measures. The methods for mixed-class kinematic wave models introduced in this chapter are extended to multi-class models and to networks in the next two chapters.

8.1 The minimum supply demand method

The first numerical methods for the kinematic wave model are based on its Eulerian formulation. Currently, the minimum supply demand method is widely used. In 1994 Daganzo introduces the cell transmission model as a spatially and temporally discrete

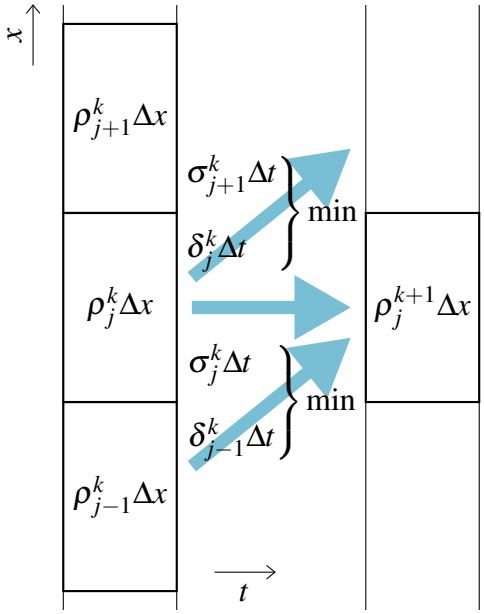

(a) Eulerian formulation: the minimum supply demand method leads to upwind and downwind discretization. The discretization uses the number of vehicles in each cell ($\rho\Delta x$) and the number of vehicles travelling from one cell to the next ($\min(\delta\Delta t, \sigma\Delta t)$).

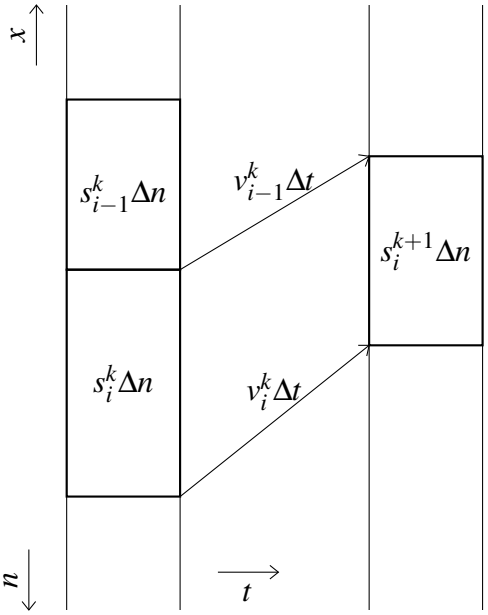

(b) Lagrangian formulation: upwind discretization. The discretization uses the road length taken by each vehicle group ($s\Delta n$) and the distance travelled by each group ($v\Delta t$).

Figure 8.1 *Discretization of the LWR model in Eulerian and Lagrangian formulation.*

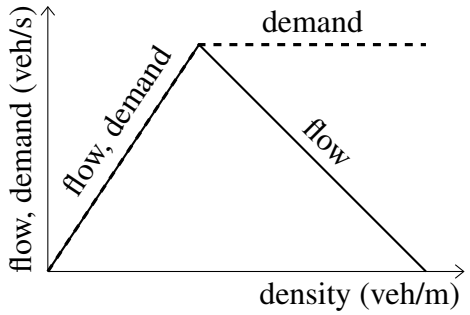

(a) Demand

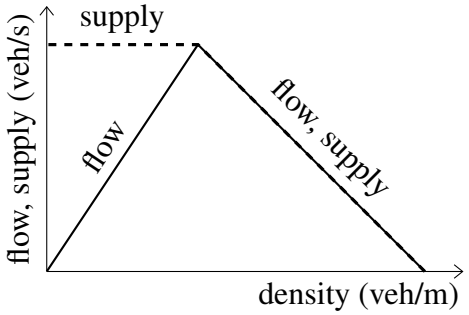

(b) Supply

Figure 8.2 *Example of a fundamental relation (flow, solid line) with demand (broken line) and supply (broken line) as function of density.*

version of the LWR model. Lebacque (1996) describes the cell transmission model as a Godunov method. This results in the minimum supply demand method for the LWR model. The road is partitioned into cells (segments) of length Δx, time is partitioned into time steps of length Δt, see Figure 8.1(a). Within a cell and during a time step the density, flow and velocity are assumed to be constant. Each time step k a fraction of the vehicles in the cell is transmitted to the adjacent downstream cell. The new density $\rho_j^{k+1} = \rho(j\Delta x, (k+1)\Delta t)$ of each cell j is calculated as follows:

$$\rho_j^{k+1} = \rho_j^k + \frac{\Delta t}{\Delta x}\left(q_{j-\frac{1}{2}}^k - q_{j+\frac{1}{2}}^k\right) \tag{8.1a}$$

with $q_{j-\frac{1}{2}}^k$ the inflow into and $q_{j+\frac{1}{2}}^k$ the outflow out of cell j:

$$q_{j-\frac{1}{2}}^k = \min\left(\delta_{j-1}^k, \sigma_j^k\right) \tag{8.1b}$$

δ_j^k the demand:

$$\delta_j^k = \begin{cases} q_j^k & \text{(free flow)} \\ q_{\text{crit}} & \text{(congestion)} \end{cases} \tag{8.1c}$$

σ_j^k the supply:

$$\sigma_j^k = \begin{cases} q_{\text{crit}} & \text{(free flow)} \\ q_j^k & \text{(congestion)} \end{cases} \tag{8.1d}$$

and $q_j^k = q(\rho_j^k)$ the flow derived from the fundamental relation. Demand δ_j^k can be interpreted as the number of vehicles per time unit that want to flow from cell j to cell $j+1$ during the time step k. Supply σ_j^k can be interpreted as the number of vehicles per time unit that can be fitted in the $j+1$-th cell during time step k. Their values are plotted in Figure 8.2 together with the fundamental relation. Figure 8.9 shows simulation results for simple test problems. The test problem and the results are discussed in more detail in Section 8.6.

The minimum supply demand method is widely used in traffic flow simulations based on the LWR model. It is a Godunov method, it is mass (or vehicle) conserving, it finds the entropy (i.e. flow maximizing) solution and it is first order accurate (Lebacque, 1996; LeVeque, 2002). First order methods are often applied to conservation equations. In general they are a good choice if the solution contains discontinuities, such as in traffic flow (LeVeque, 2002). The accuracy of the method is discussed in more detail in Section 8.6. Finally, the method is stable and converges to the analytical solution if the step sizes Δx and Δt satisfy:

$$\mu := \frac{\Delta t}{\Delta x} \max \left| \frac{\mathrm{d}q}{\mathrm{d}\rho} \right| \leq 1 \tag{8.2}$$

In fluid dynamics literature μ is often referred to as the Courant-Friedrichs-Lewy (CFL) number (Courant et al., 1967). The condition (8.2) is called the CFL-condition. Most (realistic) density-flow fundamental relations are steepest at zero density and thus the maximum slope in absolute terms is equal to the maximum velocity: $\max \|\mathrm{d}q/\mathrm{d}\rho\| = v_{\max}$. Consequently, the CFL-condition can be interpreted as follows: within a time step, a vehicle can not cross more than one cell boundary.

8.2 Lagrangian formulation and upwind method

Together with the introduction of the Lagrangian formulation of the LWR model Leclercq et al. (2007) introduces an upwind discretization method for this model. Before discussing the upwind discretization, we first note that the minimum supply demand method switches between an upwind and a downwind spatial discretization (8.1b). I.e. if traffic is in free flow the state in cell j depends on its own state and the state of the upwind (upstream) cell $j-1$:

$$\rho_j^{k+1} = \rho_j^k + \frac{\Delta t}{\Delta x}\left(q_{j-1}^k - q_j^k\right) \tag{8.3}$$

However, in congestion the state in cell j depends on its own state and the state of the downwind (downstream) cell $j+1$:

$$\rho_j^{k+1} = \rho_j^k + \frac{\Delta t}{\Delta x}\left(q_j^k - q_{j+1}^k\right) \tag{8.4}$$

If not all cells $j-1$, j, and $j+1$ are in the same regime (free flow or congestion), then a combination of both upwind and downwind discretization is applied.

The Lagrangian upwind method does not switch between upwind and downwind discretization. In the Eulerian formulation the switching between upwind and downwind is necessary because characteristics move either downstream (in free flow) or upstream (in congestion). In Lagrangian coordinates, however, characteristics always move downwind: in the direction of increasing n. This implies that drivers (or vehicle groups) only react to leading vehicles (or vehicle groups) and not on followers. Therefore, the upwind method is simpler and each time step takes less computing time than the minimum supply demand method. This results in more efficient simulations that are faster and/or more accurate. In Section 8.6 the accuracy of both methods will be compared in more detail.

The Lagrangian upwind method is as follows. In the Lagrangian formulation vehicle number n is an independent variable. Consequently, in the discretization, vehicles are partitioned into groups of Δn vehicles, see Figure 8.1(b). Just as n, Δn is not necessarily integer, it can take any real, positive value. Again, time is partitioned into time steps of size Δt. Each time step k, each vehicle group i is moved downstream. Or, if traffic is in complete stop, the vehicle group remains at its position. Its new position is calculated

with an upwind method:

$$s_i^{k+1} = s_i^k + \frac{\Delta t}{\Delta n}\left(v_{i-1}^k - v_i^k\right) \tag{8.5}$$

with $v_i^k = v(s_i^k)$ the velocity derived from the fundamental relation. We note that this method is much simpler than the equivalent method (minimum supply demand method) in Eulerian coordinates (8.1). Figure 8.9 shows simulation results for simple test problems. The test problem and the results are discussed in more detail in Section 8.6.

The upwind method (8.5) has similar properties as the minimum supply demand method: it is a Godunov method, it is mass (or vehicle) conserving, it finds the entropy (or flow maximizing) solution and it is first order accurate (Leclercq et al., 2007; LeVeque, 2002). The CFL-number is μ^* and the condition for stability and convergence is:

$$\mu^* := \frac{\Delta t}{\Delta n} \max \left| \frac{\mathrm{d}v}{\mathrm{d}s} \right| \leq 1 \tag{8.6}$$

Most (realistic) spacing-velocity fundamental relations are steepest at jam spacing. For example, in the Smulder fundamental relation:

$$\max \left| \frac{\mathrm{d}v}{\mathrm{d}s} \right| = \frac{v_{\mathrm{crit}}}{s_{\mathrm{crit}} - s_{\mathrm{jam}}} = \frac{v_{\mathrm{crit}}}{1/\rho_{\mathrm{crit}} - 1/\rho_{\mathrm{jam}}} = w\rho_{\mathrm{jam}} = \frac{w}{s_{\mathrm{jam}}} \tag{8.7}$$

Consequently, the CFL-condition can be interpreted as follows. It limits the distance a vehicle groups can travel downstream within one time step. In fact, the distance between its new position (x_i^{k+1}) and the old position of the leading vehicle group (x_{i-1}^k) is at least the characteristic velocity in jam times the time step size: $w\Delta t$. To put it precisely: $x_{i-1}^k - x_i^{k+1} \geq w\Delta t$. This implies that even the fastest characteristics in the (t,n) plane, namely the characteristics related to jam, are traced with the upwind method. For readability, in the following the CFL-number for the upwind method μ^* is referred to as μ, whenever it is not necessary to make a distinction between the CFL-number for the minimum supply demand method and the upwind method.

Finally, the discretization method can be simplified. With this simplification one directly computes the position x_i^k of each vehicle group i at each time step k without intermediately calculating its spacing. Therefore, the spacing is discretized with an upwind approximation:

$$s_i = \frac{x_{i-1} - x_i}{\Delta n} \tag{8.8}$$

and the velocity is approximated with an explicit time discretization:

$$v^k = \frac{x^{k+1} - x^k}{\Delta t} \tag{8.9}$$

Substituting (8.8) into (8.5) and subsequently multiplying with Δn gives:

$$x_{i-1}^{k+1} - x_i^{k+1} = x_{i-1}^k - x_i^k + \Delta t \left(v_{i-1}^k - v_i^k \right) \tag{8.10}$$

Furthermore, substituting (8.9) and reordering gives:

$$x_i^{k+1} = x_i^k + \Delta t v_i^k \tag{8.11}$$

The velocity during the k-th time step v_i^k is determined using the fundamental relation and (8.8). This method can be interpreted as follows: the new position of group i is its old position plus the distance it travels during the k-th time step: $\Delta t v_i^k$.

The upwind scheme (8.11) is applied by Leclercq et al. (2007) to show the equivalence between the LWR model and the simplified car-following model by Newell (2002) under the following conditions:

- the fundamental relation $q(\rho)$ is triangular
- the CFL-condition (8.6) is satisfied as an equality
- the vehicle group size $\Delta n = 1$
- time parameter τ (which may be interpreted as reaction time) equals time step size $\tau = \Delta t$

Therefore, the Lagrangian coordinate system does not only lead to more efficient numerical methods, it also makes the coupling between macroscopic and microscopic regions in a hybrid model easier (Leclercq, 2007a).

8.3 Time stepping methods

The minimum supply demand method (8.1) and the upwind method (8.5) apply an explicit time stepping method. This means that the state variables such as density, spacing, velocity and flow at the cell boundaries are assumed to be constant during time step k and equal to their values at its beginning: time $t = k\Delta t$. Their values only change at the end of the time step, at $t = (k+1)\Delta t$. Implicit time stepping methods assume that the values of the state variables may change during the time step. Chronopoulos et al. (1993) propose to apply them to higher-order traffic flow models. They show that larger time steps can be taken and computation time can be reduced. However, this comes at the cost of some accuracy, as we show later.

We apply implicit time stepping methods using the mixed-class model in Eulerian and Lagrangian formulation of the LWR model. It turns out that implicit time stepping methods are best to be applied in combination with the Lagrangian model formulation. Extension of the method to multi-class models and networks are out of the scope of this dissertation. We expect that these extensions are possible, but far from straightforward. It will become computationally more demanding to deal with multiple classes and inhomogeneities. This may outweigh the main advantage of taking larger time steps.

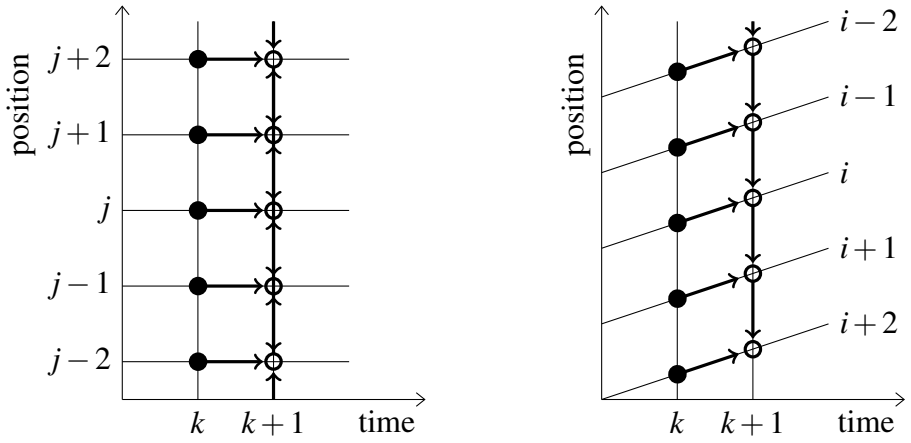

(a) Minimum supply demand method. (b) Upwind method.

Figure 8.3 *Information flow in numerical method with implicit time stepping.*

8.3.1 Implicit time stepping in the minimum supply demand method

We recall the minimum supply demand method in Eulerian coordinates with explicit time stepping (8.1). With implicit time stepping the minimum supply demand method becomes:

$$\rho_j^{k+1} - \frac{\Delta t}{\Delta x}\left(q_{j-\frac{1}{2}}^{k+1} - q_{j+\frac{1}{2}}^{k+1}\right) = \rho_j^k \tag{8.12}$$

with $q_{j-\frac{1}{2}}^{k+1}$ the inflow into and $q_{j+\frac{1}{2}}^{k+1}$ the outflow out of cell j. The inflow and the outflow depend on the actual traffic regimes (free flow or congestion) of the cells $j-1$, j and $j+1$ at time $t = (k+1)\Delta t$. Therefore, there is no straightforward way to solve this equation, unless one knows beforehand the regime in each cell at $t = (k+1)\Delta t$. This is shown schematically in Figure 8.3(a). In (Van Wageningen-Kessels et al., 2009) we discuss this approach under the assumption that either the whole computational domain is in free flow, or it is in congestion. The computations are shown to be more efficient than with explicit time stepping. However, generalization to cases with both congestion and free flow is not straightforward. Therefore, the implicit minimum supply demand method is difficult to apply in practice and we do not show any simulation results.

8.3.2 Implicit time stepping in the upwind method

We recall the upwind method in Lagrangian coordinates with explicit time stepping (8.5). With implicit time stepping the upwind method becomes:

$$s_i^{k+1} - \frac{\Delta t}{\Delta n}\left(v_{i-1}^{k+1} - v_i^{k+1}\right) = s_i^k \tag{8.13}$$

There is a natural order to solve (8.13) for all groups $i = 1, 2, \ldots, I$, namely from the

first vehicle group ($i = 1$) to the last group ($i = I$). The procedure is shown schematically in Figure 8.3(b). The solution procedure is as follows. Once the new spacing of the $i-1$-th vehicle is known, the fundamental relation can be used to compute its velocity. The velocity and the spacing of the i-th group are the remaining unknowns. Substituting the fundamental relation (4.7) and the definition of spacing (6.2) shows that the following equation is to be solved for s_i^{k+1}:

$$s_i^k = \begin{cases} s_i^{k+1} - \dfrac{\Delta t}{\Delta n}\left[v_{i-1}^{k+1} - \left(v_{\max} - \dfrac{v_{\max} - v_{\text{crit}}}{\rho_{\text{crit}}\, s_i^{k+1}}\right)\right] & \text{(free flow)} \quad (8.14a) \\ s_i^{k+1} - \dfrac{\Delta t}{\Delta n}\left[v_{i-1}^{k+1} - w\left(\rho_{\text{jam}} s_i^{k+1} - 1\right)\right] & \text{(congestion)} \quad (8.14b) \end{cases}$$

We note that both s_i^k and v_{i-1}^{k+1} are known. We now discuss how (8.14) can be solved in free flow and in congestion.

Let us first assume that the new traffic is in free flow state, i.e. $s_i^{k+1} \geq s_{\text{crit}}$ Rewriting (8.14a) yields that the following quadratic equation needs to be solved:

$$\left(s_i^{k+1}\right)^2 - \left(s_i^k - \frac{\Delta t}{\Delta n}\left(v_{\max} - v_{i-1}^{k+1}\right)\right) s_i^{k+1} - \frac{\Delta t}{\Delta n}\frac{v_{\max} - v_{\text{crit}}}{\rho_{\text{crit}}} = 0 \tag{8.15}$$

(8.15) has two solutions, only one of which is permissible:

$$s_i^{k+1} = \frac{1}{2}\left[\left(s_i^k - \tfrac{\Delta t}{\Delta n}\left(v_{\max} - v_{i-1}^{k+1}\right)\right) + \sqrt{\left(s_i^k - \tfrac{\Delta t}{\Delta n}\left(v_{\max} - v_{i-1}^{k+1}\right)\right)^2 + 4\tfrac{\Delta t}{\Delta n}\tfrac{v_{\max} - v_{\text{crit}}}{\rho_{\text{crit}}}}\right] \tag{8.16}$$

The other solution of (8.15) is equal to (8.16) but it has a minus sign in front of the square root. Therefore, it is nonpositive and the resulting spacing s_i^{k+1} is not permissible.

Let us now assume that traffic is in congestion state, i.e. $s_{\text{jam}} \leq s_i^{k+1} < s_{\text{crit}}$. Rewriting (8.14b) yields the new spacing:

$$s_i^{k+1} = \frac{s_i^k + \frac{\Delta t}{\Delta n}\left(v_{i-1}^{k+1} + w\right)}{1 + \frac{\Delta t}{\Delta n} w \rho_{\text{jam}}} \tag{8.17}$$

In general, it is not known beforehand whether the new traffic state will be free flow or congestion and thus whether (8.16) or (8.17) should be applied. Therefore, one computes the new spacing using both (8.16) and (8.17). If the solution found with (8.16) is indeed in free flow then this is the correct solution. If the solution found with (8.17) is indeed in congestion then this is the correct solution. Due to numerical errors, it may be that (8.16) gives a free flow solution and (8.17) gives a congestion solution. Or (8.16) does not give a free flow solution and (8.17) does not give a congestion solution. In such cases it is advisable to set the new spacing to critical spacing: $s_i^{k+1} =$

s_{crit}.

Once the new spacing s_i^{k+1} is known, the new velocity v_i^{k+1} can be computed and the procedure starts again to compute the new spacing of the following vehicle group s_{i+1}^{k+1}. Figure 8.9 shows simulation results for simple test problems. The test problem and the results are discussed in more detail in Section 8.6.

8.3.3 Discussion

The implicit methods have the same conservation and entropy properties as the explicit time stepping methods. This is because the spatial discretization did not change. Furthermore, it is still a first order accurate Godunov method. However, the main difference between explicit and implicit time stepping methods relates to their numerical stability. When implicit time stepping is applied, much larger time steps can be taken, without losing numerical stability. In fact, the CFL-condition (8.6) does not need to be satisfied (LeVeque, 2002). Because larger CFL-numbers μ are allowed, larger time steps can be applied. Therefore, less time steps are necessary and thus the computation time decreases. However, this comes at the cost of some accuracy, which will be discussed in more detail in Section 8.6.

There is an important difference between the implicit time stepping methods for the minimum supply demand method and the upwind method. In the minimum supply demand method method, the new traffic state in all grid cells has to be computed at once, see Figure 8.3(a). In contrast, in the upwind method, the new traffic state of the vehicle groups can be computed group by group, see Figure 8.3(a). Therefore, the solution procedure for the upwind method with implicit time stepping is simpler than the procedure for the minimum supply demand method with implicit time stepping. In the simulations (Section 8.6) we only show results for implicit time stepping with the upwind method.

8.4 Variational theory and variational method

In 1993a Newell introduces the cumulative count function $N(x,t)$ in a reformulation of the kinematic wave model. $N(x,t)$ is the number of vehicles that have passed location x at between start time t_0 and time t. This idea is further developed by Daganzo (2005a,b) as he applies variational theory to solve the kinematic wave model. We do not recapitulate their derivation, instead in Appendix B a graphical and more intuitive interpretation of variational theory applied to the kinematic wave model is given.

Leclercq et al. (2008); Leclercq (2009) show that the variational theory leads to exact solutions under certain conditions. For example, the fundamental relation must be piecewise linear, its parameter values must be related in a certain way and the initial traffic state must be piecewise constant. They use variational theory to assess the

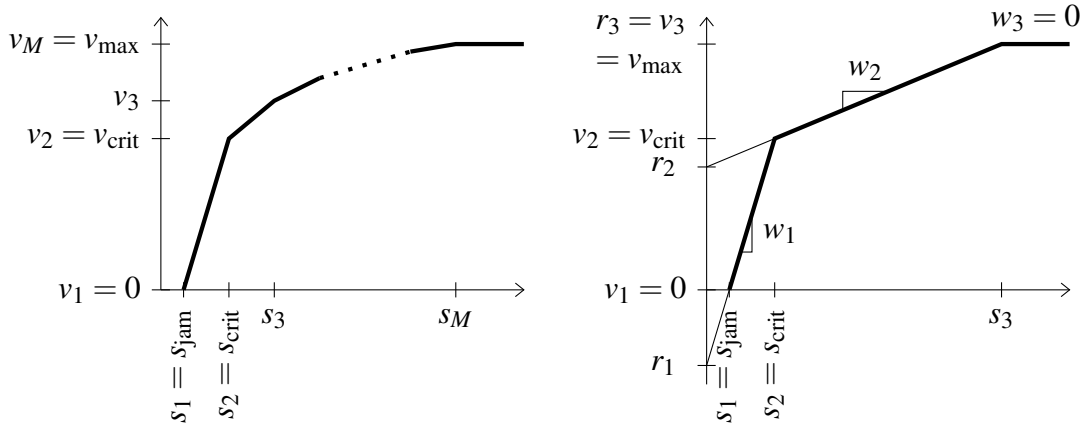

(a) Generic piecewise linear fundamental relation consisting of arbitrary many linear parts.

(b) Piecewise linear fundamental relation consisting of 3 linear parts.

Figure 8.4 *Piecewise linear spacing-velocity fundamental relations.*

accuracy of the minimum supply demand method and the upwind method with triangular fundamental relation. We extend their accuracy analysis to include piecewise linear fundamental relations consisting of three parts in (Van Wageningen-Kessels et al., 2010).

We apply variational theory as an alternative numerical method. We do not require that the continuous model contains a piecewise linear fundamental relation. However, the variational theory method needs a piecewise linear fundamental relation. Therefore, the fundamental relation is approximated by a piecewise linear one. This will inevitably lead to inaccuracies in the solution. Those inaccuracies will be assessed in Section 8.6. We note that both in the minimum supply demand method and the upwind method, the fundamental relation is satisfied exactly in any point in the time space domain. However, with these methods, there are other sources of inaccuracy such as numerical diffusion, which will be discussed in more detail later.

8.4.1 Piecewise linear fundamental relation

Figure 8.4 shows piecewise linear fundamental relations. In Lagrangian formulation the piecewise linear fundamental relation is:

$$v(s) = \min_m \left(v_m + (s - s_m)w_m\right) = \begin{cases} (s - s_{\text{jam}})w_1 & \text{if } s \le s_{\text{crit}} \\ v_{\text{crit}} + (s - s_{\text{crit}})w_2 & \text{if } s_{\text{crit}} < s \le s_3 \\ v_3 + (s - s_3)w_3 & \text{if } s_3 < s \le s_4 \\ \vdots & \\ v_{M-1} + (s - s_{M-1})w_{M-1} & \text{if } s_{M-1} < s \le s_M \\ v_{\max} & \text{if } s > s_M \end{cases} \tag{8.18}$$

with w_m the characteristic velocities in the Lagrangian coordinate system. They correspond to the slope of the m-th linear part of the fundamental relation:

$$w_m = \frac{v_{m+1} - v_m}{s_{m+1} - s_m} \quad \text{if } m \neq M \text{ and } w_M = 0 \tag{8.19}$$

With only three linear parts, the fundamental relation (8.18) reduces to:

$$v(s) = \begin{cases} (s - s_{\text{jam}})w_1 & \text{if } s \leq s_{\text{crit}} \\ v_{\text{crit}} + (s - s_{\text{crit}})w_2 & \text{if } s_{\text{crit}} < s \leq s_3 \\ v_{\text{max}} & \text{if } s > s_3 \end{cases} \tag{8.20}$$

with

$$w_1 = \frac{v_{\text{crit}}}{s_{\text{crit}} - s_{\text{jam}}} \quad \text{and} \quad w_2 = \frac{v_{\text{max}} - v_{\text{crit}}}{s_3 - s_{\text{crit}}} \tag{8.21}$$

Figure 8.7 shows how a Smulders fundamental relation can be approximated with a piecewise linear fundamental relation consisting of three linear parts.

8.4.2 Variational method

Variational theory is applied to solve an initial value kinematic wave problem. First, the fundamental relation is approximated with a piecewise linear fundamental relation. In the following we consider a piecewise linear fundamental relation consisting of three parts. Furthermore, we assume that $w_1 = cw_2$ with c a positive integer. Leclercq (2009) shows that only if the fundamental relation is piecewise linear and $c = 2$, the solution is exact. The results can be generalized to piecewise linear fundamental relations with arbitrary many parts and other wave velocities, though the solution may be less accurate. Secondly, the initial value problem is converted into a minimization problem on a network. The network consists of nodes and waves with velocities w_1, w_2 and w_3, see Figure 8.5. The waves intersect at nodes with $n = i\Delta n$ and $t = k\Delta t$, therefore $w_1 = \Delta n/\Delta t$. At the nodes the position $\tilde{x}_i^k$ of the $n = i\Delta n$-th vehicle at time $t = k\Delta t$ is calculated using:

$$\tilde{x}_i^k = \min\left(\tilde{x}_{i-1}^{k-1} + \Delta t r_1,\ \tilde{x}_{i-1}^{k-c} + c\Delta t r_2,\ \tilde{x}_i^{k-1} + \Delta t r_3 \right) \tag{8.22}$$

with:

$$r_m = v_m - s_m w_m = \begin{cases} r_1 = -s_{\text{jam}} w_1 \\ r_2 = v_{\text{crit}} - s_{\text{crit}} w_2 \\ r_3 = v_{\text{max}} \end{cases} \tag{8.23}$$

We note that the parameters r_m are the velocity values at the intersections of the slope of the fundamental relation and the velocity axis, see Figure 8.4(b). The variational

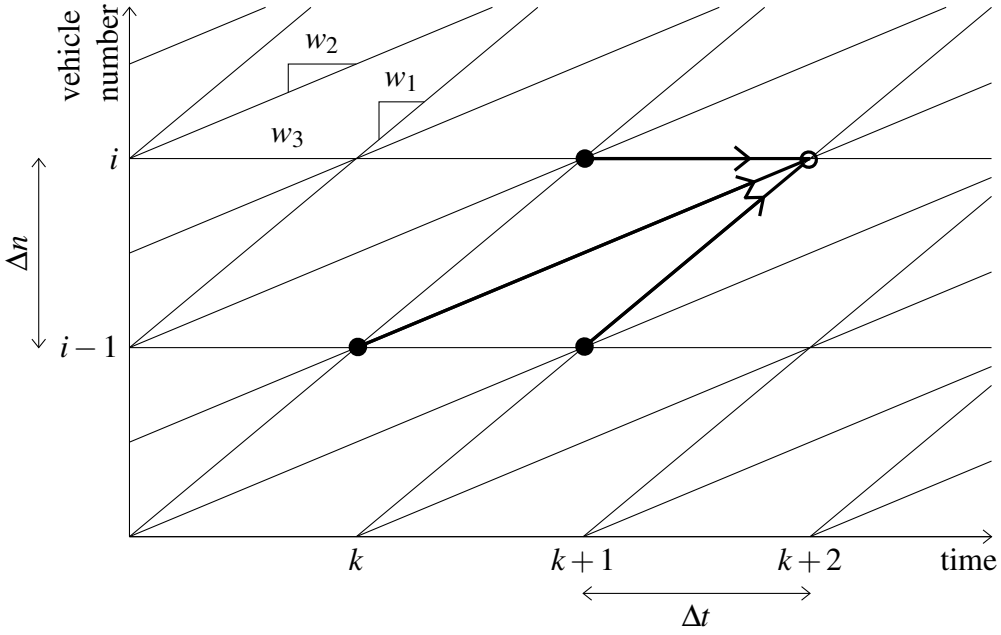

Figure 8.5 *Network to solve the kinematic wave problem using variational theory. It consists of edges with slopes $w_1 = 2w_2$, w_2 and $w_3 = 0$ and nodes. The solution is calculated at the node ∘ using information from three nodes on its left •.*

method (8.22) solves the kinematic wave problem with piecewise linear fundamental relation (8.20) and $c = 2$ exactly, see Appendix B. In the first few time steps of a simulation, information before the initial time ($t = 0$) is needed to calculate $\tilde{x}_{i-1}^{k-c} + c\Delta t r_2$ in (8.22). Therefore, not only the initial traffic state, but also the traffic state at $t = -\Delta t, t = -2\Delta t, \ldots, t = (1-c)\Delta t$ is required. In our simulations, we simply assume that the traffic state at $t < 0$ is equal to the initial traffic state at $t = 0$. However, more advanced and accurate methods may be thought of.

Figure 8.10 shows that the variational theory method does not converge to the exact solution if the resolution increases. This is because the fundamental relation is not piecewise linear. However, the figure also indicates that the variational method does converge to the exact solution of the analogous problem with piecewise linear fundamental relation. This result is discussed in more detail in Section 8.6.

8.5 Test setup and accuracy measures

Traffic flow simulation results are assessed based on their accuracy. Zhang (2001) has pointed out the importance of validating the numerical method before validating the model against observations. Therefore, the numerical solution of a simple test problem should be compared with the analytical solution of the continuous model. We introduce a simple test problem and accuracy measures. They are applied in the next

section to assess the accuracy of the numerical methods introduced in the previous sections.

8.5.1 Test setup

We asses the accuracy of the numerical methods with three simple test cases. They consist of a homogeneous infinitely long road with, initially, a high density region with both downstream and upstream low densities. The initial conditions and the traffic state after some time is shown in Figure 8.6. In the first test case, traffic is in free flow and the following initial conditions hold:

$$\rho(x,0) = \begin{cases} \rho_{\text{crit}} & \text{if } -L \leq x \leq 0 \\ 0 & \text{otherwise} \end{cases} \tag{8.24}$$

with the initial length of the high critical region $L = 10$ km. In the second test case, traffic is in congestion and the following initial conditions hold:

$$\rho(x,0) = \begin{cases} \rho_{\text{jam}} & \text{if } -L \leq x \leq 0 \\ \rho_{\text{crit}} & \text{otherwise} \end{cases} \tag{8.25}$$

with the initial length of the jam density region $L = 2$ km. In the third test case, there is a queue with jam density which dissolves. This test problem represents a traffic light turning green. The following initial conditions hold:

$$\rho(x,0) = \begin{cases} 0 & \text{if } x > 0 \\ \rho_{\text{jam}} & \text{if } -L \leq x \leq 0 \\ \rho_{\text{upstream}} & \text{if } x < -L \end{cases} \tag{8.26}$$

with the initial length of the jam density region $L = 2$ km and the initial upstream density $\rho_{\text{upstream}} = \frac{1}{2}\rho_{\text{crit}}$. In all test cases the Smulders fundamental relation (4.7) is applied. The parameters are as previously used for class 1 in Fastlane, see Chapter 5. All model parameters are given in Table 8.1.

We chose this test setup because it includes the most important aspects of traffic flow on a homogeneous road: free flow and congestion, vehicles driving into a queue and leaving it and spill back of congestion. Furthermore, the Smulders fundamental relation is a realistic generalization of other fundamental relations and is also applied in Fastlane. Still, the setup is rather simple and the location and velocity of shock waves can be computed analytically see Figure 8.6. In the free flow test case there is a shock wave with velocity equal to characteristic velocity at density just below critical density:

$$w_{\text{crit}} = \frac{\mathrm{d}q}{\mathrm{d}\rho}(\rho_{\text{crit}}) = 2v_{\text{crit}} - v_{\max} \tag{8.27}$$

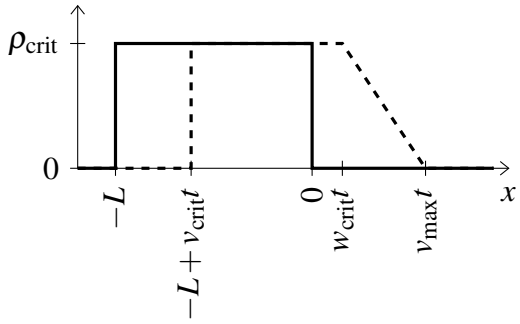

(a) Free flow test case, $0 < t \leq l/(v_{\text{crit}} - w_{\text{crit}})$.

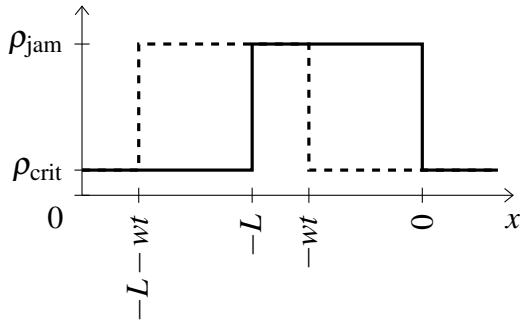

(b) Congestion test case.

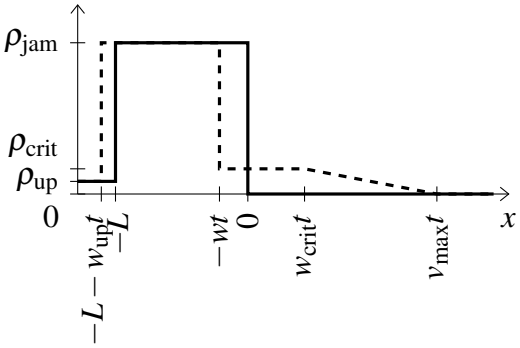

(c) Queue test case, $0 < t \leq L/(w - w_{\text{upstream}})$.

Figure 8.6 *Density profiles in test cases. Solid line: initial density. Dashed line: density at time $t > 0$.*

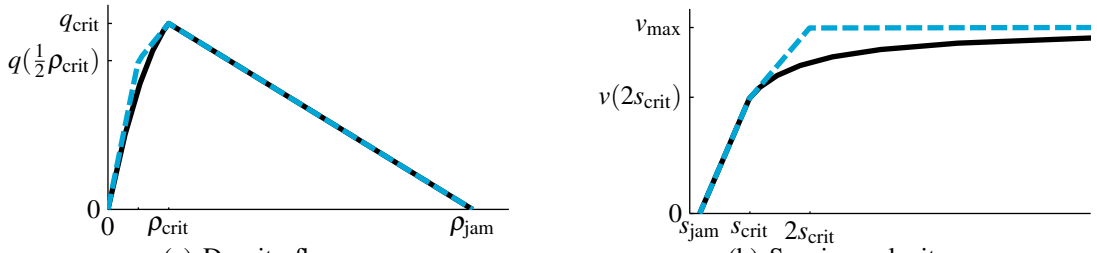

(a) Density-flow. (b) Spacing-velocity.

Figure 8.7 *Smulders fundamental relation (solid line) and its piecewise linear approximation (broken line).*

Table 8.1 *Model parameters.*

maximum velocity	v_{max}	33.3 m/s	=	120 km/h
critical velocity	v_{crit}	20.8 m/s	=	75 km/h
critical density	ρ_{crit}	0.033 veh/m	=	33 veh/km
jam density	ρ_{jam}	0.2 veh/m	=	200 veh/km
(resulting congestion wave parameter	w	4.17 m/s	=	15 km/h)

In the queue test case there is a shock wave with velocity depending on the initial density upstream of the queue:

$$w_{upstream} = \frac{q_{upstream}}{\rho_{jam} - \rho_{upstream}} = \frac{\rho_{crit}}{2\rho_{jam} - \rho_{crit}} \frac{v_{max} + v_{crit}}{2} \tag{8.28}$$

In the base case the numerical parameters are chosen such that the CFL condition (8.2), (8.6) is satisfied as an equality. We apply: time step size $\Delta t = 3$ s, grid cell size $\Delta x = 100$ m and vehicle group size $\Delta n = 2.55$ vehicle. To study the influence of the resolution, the time step size Δt, the grid cell size Δx and vehicle group size Δn are varied such that the CFL-number remains $\mu = 1$. The time step size is varied between $\Delta t = 0.5$ and $\Delta t = 24$ s. To study the influence of the CFL-number, the time step size Δt is varied, but the grid cell size Δx and vehicle group size Δn are not. The CFL-number varies between $\mu = 0.05$ and $\mu = 10$.

8.5.2 Accuracy measures

Zhang (2001) stresses the importance of assessing the accuracy based on criteria that are relevant in traffic flow, such as phase (or regime) transitions and wave velocities. We propose two new accuracy measures that are indeed especially relevant in traffic flow. Furthermore, they can be applied in validating the numerical method against the continuous model and in validation simulation results against observations. Here we focus on validating the numerical method against the continuous model.

Common accuracy criteria use 'average' differences between velocities or densities at

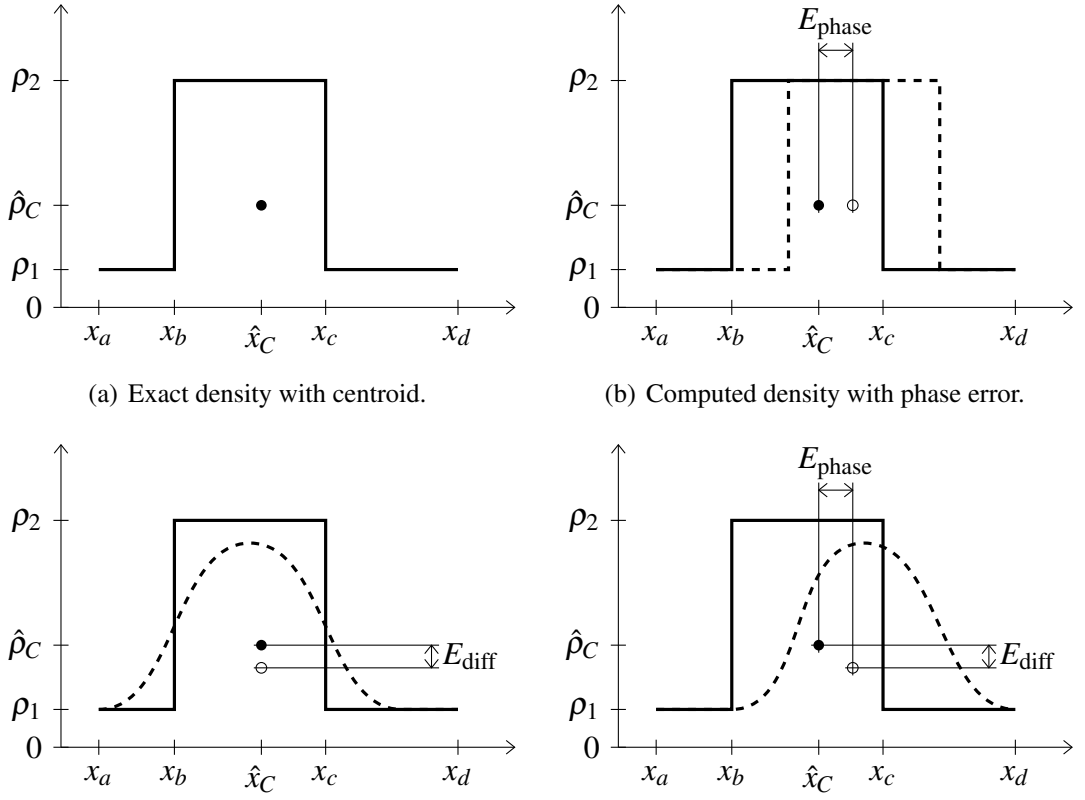

(a) Exact density with centroid.

(b) Computed density with phase error.

(c) Computed density with diffusion error.

(d) Computed density with phase and diffusion error.

Figure 8.8 *Exact and computed densities, with their centroids, phase error and diffusion error. Exact: solid line and solid circle, computed: dashed line and open circle.*

many points in space and time. An example is the root mean square error (RMSE). At a certain time step k the RMSE of the densities ρ_j^k is:

$$E_{\text{rmse}} = \sqrt{\frac{1}{J}\sum_{j=1}^{J}\left(\rho_j^k - \hat{\rho}_j^k\right)^2} \tag{8.29}$$

with $\hat{\rho}_j^k$ the exact density in the j-th grid cell at time step k.

We propose two new accuracy measures based on types of accuracy that are especially relevant in traffic flow applications. It is important to predict correctly the location of a queue or congestion and especially whether it will spill back as far as an on or off ramp or not. Furthermore, large jumps in velocities or densities are common in solutions of the kinematic wave model. Therefore, these discontinuities should be preserved by the numerical method as well. The new accuracy measures are based on the considerations above. The phase error measures whether information travels at the correct velocity, the diffusion error measures how well discontinuities are preserved.

Phase error

The phase error is about the accuracy of information velocity, see Figure 8.8(b). It shows a high density region, its exact location and its computed location at some fixed time. The computed location is downstream of the exact location. The phase error is measured as the distance (in meters) between the centroids of the areas below the exact and the computed density. An example density profile and its centroid are shown in Figure 8.8(a). The x-position centroid can be computed as follows:

$$\hat{x}_C = \frac{\int_{x_a}^{x_b} x\rho(x)\,\mathrm{d}x}{\int_{x_a}^{x_b} \rho(x)\,\mathrm{d}x} = \frac{1}{2}\frac{(x_b-x_a)^2\rho_1 + (x_c-x_b)^2\rho_2 + (x_d-x_c)^2\rho_1}{(x_b-x_a)\rho_1 + (x_c-x_b)\rho_2 + (x_d-x_c)\rho_1} \tag{8.30}$$

Similarly, the x-position of the centroid of the area below the computed density x_C is computed. If the minimum supply demand method is applied the centroid is at:

$$x_C = \frac{\sum_{j=1}^{J} \Delta x \rho_j x_j}{\sum_{j=1}^{J} \Delta x \rho_j} = \frac{\sum_{j=1}^{J} \rho_j x_j}{\sum_{j=1}^{J} \rho_j} \tag{8.31}$$

with $j = 1$ the most upstream cell in the area of interest, i.e. $x_1 > x_a$. $j = J$ is the most downstream cell in the area of interest, i.e. $x_J < x_d$. If the upwind method or the variational method is applied the centroid is at:

$$x_C = \frac{\sum_{i=1}^{I} \Delta n x_i}{\sum_{i=1}^{I} \Delta n} = \frac{\sum_{i=1}^{I} x_i}{I} \tag{8.32}$$

with $i = 1$ the first vehicle in the area of interest, i.e. $x_1 < x_d$. $i = I$ is the last vehicle in the area of interest, i.e. $x_I > x_a$. The difference between the x-positions of the exact and the computed centroid is the phase error:

$$E_{\text{phase}} = x_C - \hat{x}_C \tag{8.33}$$

Diffusion error

The diffusion error relates to discontinuous solutions becoming smooth, see Figure 8.8(c). It shows a high density region, its exact density profile and its computed density profile at some fixed time. The computed profile is smooth, while the exact profile shows discontinuities (shocks). Just as with the phase error we use the position of the centroid to measure the diffusion error. We now compute the distance between the centroids in vehicles per meter, i.e. the vertical instead of the horizontal distance in Figure 8.8(c). The exact centroid density is computed as follows:

$$\hat{\rho}_C = \frac{\int_{x_1}^{x_b} \big(\rho(x)\big)^2\,\mathrm{d}x}{2\int_{x_1}^{x_b} \rho(x)\,\mathrm{d}x} = \frac{1}{2}\frac{(x_b-x_1)(\rho_1)^2 + (x_c-x_b)(\rho_2)^2 + (x_d-x_c)(\rho_1)^2}{(x_b-x_1)\rho_1 + (x_c-x_b)\rho_2 + (x_d-x_c)\rho_1} \tag{8.34}$$

If the minimum supply demand method is applied the centroid density is:

$$\rho_C = \frac{\sum_{j=1}^{J} \Delta x(\rho_j)^2}{2\sum_{j=1}^{J} \Delta x \rho_j} = \frac{\sum_{j=1}^{J} (\rho_j)^2}{2\sum_{j=1}^{J} \rho_j} \tag{8.35}$$

If the upwind method or the variational method is applied the centroid density is:

$$\rho_C = \frac{\sum_{i=1}^{I} \Delta n \rho_i}{2\sum_{i=1}^{I} \Delta n} = \frac{\sum_{i=1}^{I} \rho_i}{2I} \tag{8.36}$$

The difference between the densities of the exact and the computed centroid is the diffusion error:

$$E_{\text{diff}} = \rho_C - \hat{\rho}_C \tag{8.37}$$

Finally, Figure 8.8(d) shows a density profile with both a phase error and a diffusion error. The figure illustrates that the two errors can be measured independently.

In the next section, the phase error and the diffusion error are used to asses the numerical methods from the previous sections.

8.6 Accuracy

Both the minimum supply demand method and the upwind method are first order accurate. That means that the global error is proportional to the grid cell size Δx or the vehicle groups size Δn respectively. However, this does not imply that the accuracy of both methods is similar. We show the differences in accuracy between the minimum supply demand method and upwind method with explicit and implicit time stepping and the variational theory by comparing simulation results of the simple test problem introduced in Section 8.5. We compare the simulation results to each other and to the exact solution. For the comparison we apply the novel accuracy measures. Furthermore, we discuss which factors (such as resolution and CFL-number) influence the accuracy.

8.6.1 Simulation results

The numerical solutions of the test cases are shown in Figure 8.9–8.11. The accuracy of the simulation results is shown in Figure 8.12 and 8.13.

Figure 8.9 shows density plots as a function of time and space. The density is computed with the different numerical methods: minimum supply demand, upwind with explicit time stepping, upwind with implicit time stepping and variational theory. It shows how the exact and numerical density profiles develop over time. The results of the

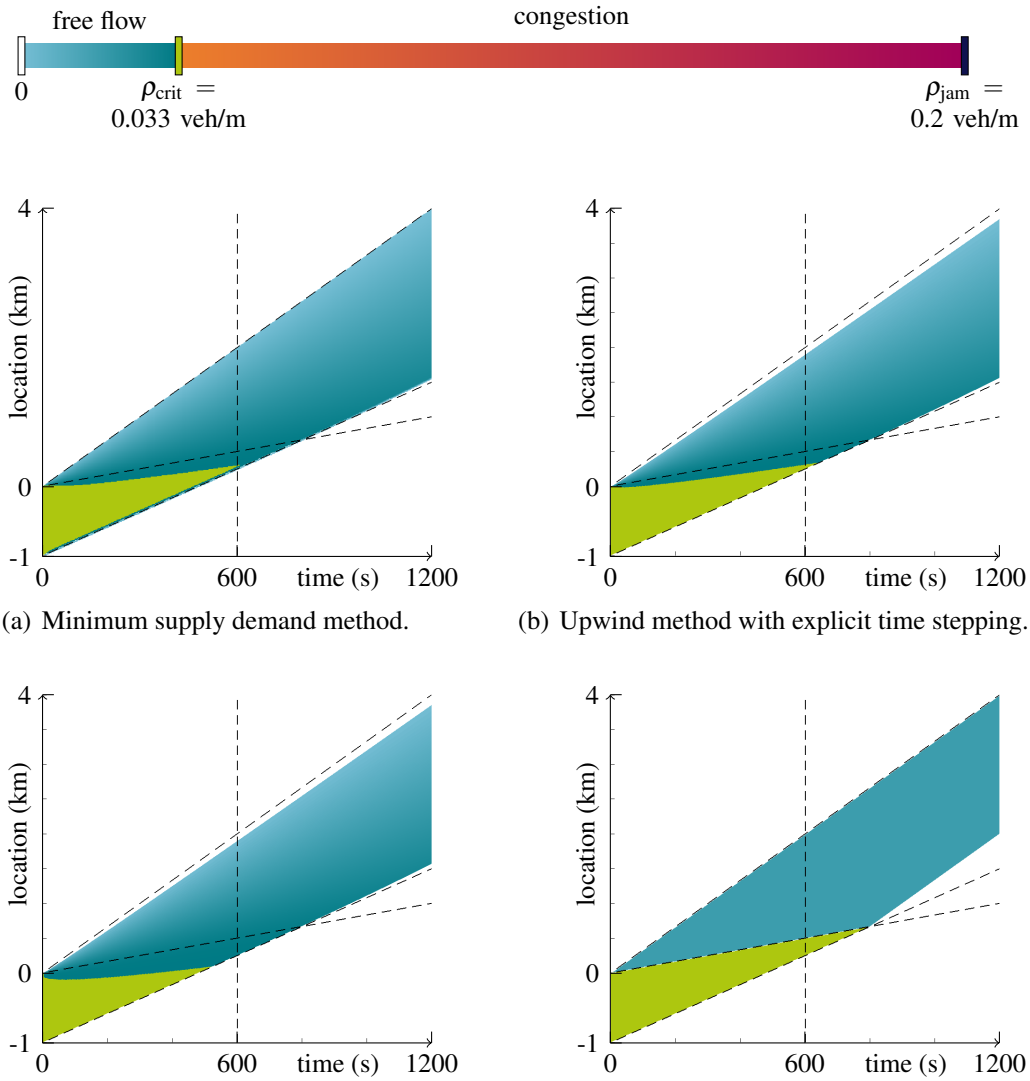

(a) Minimum supply demand method.

(b) Upwind method with explicit time stepping.

(c) Upwind method with implicit time stepping.

(d) Variational method.

Figure 8.9 *Density plots of free flow test case with different numerical methods. The vertical broken line indicates the time for which cross sections are shown in Figure 8.10. The other broken lines indicate sharp boundaries in the analytical solution.*

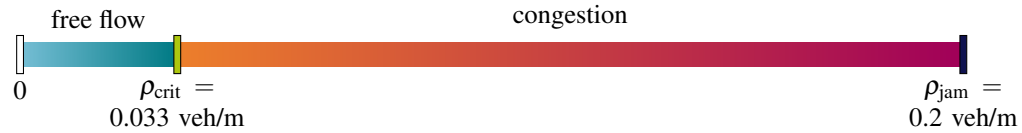

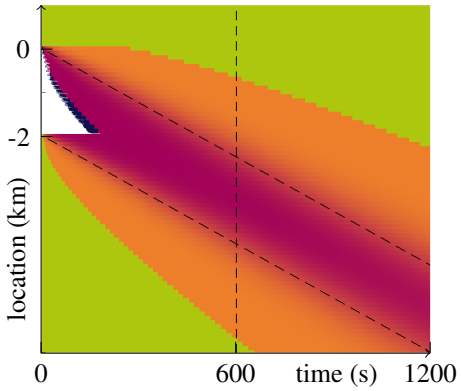

(e) Minimum supply demand method.

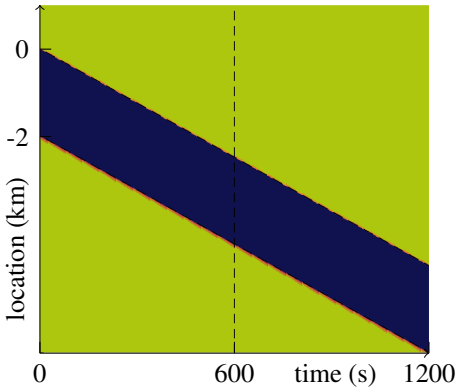

(f) Upwind method with explicit time stepping.

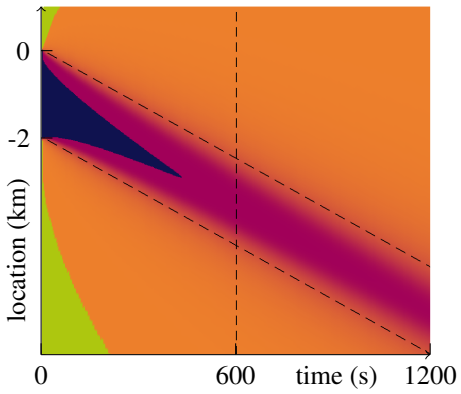

(g) Upwind method with implicit time stepping.

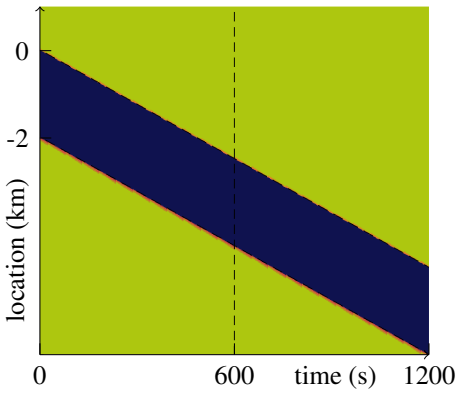

(h) Variational method.

Continued Figure 8.9 *Density plots of congestion test case with different numerical methods. The vertical broken line indicates the time for which cross sections are shown in Figure 8.10. The other broken lines indicate sharp boundaries in the analytical solution.*

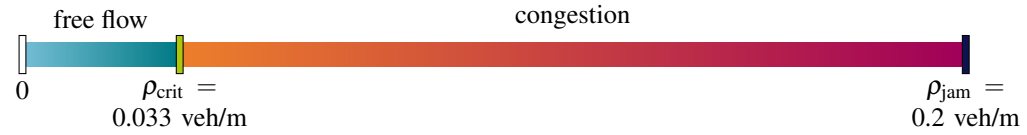

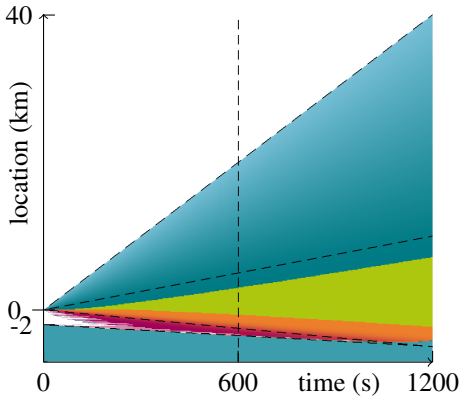

(i) Minimum supply demand method.

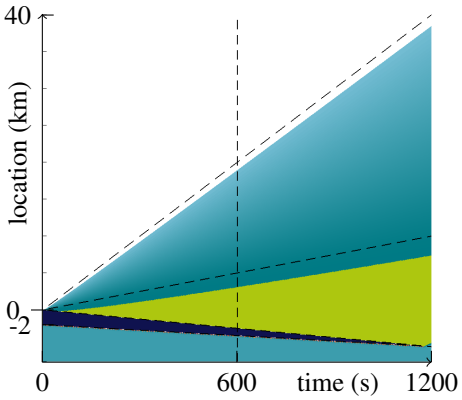

(j) Upwind method with explicit time stepping.

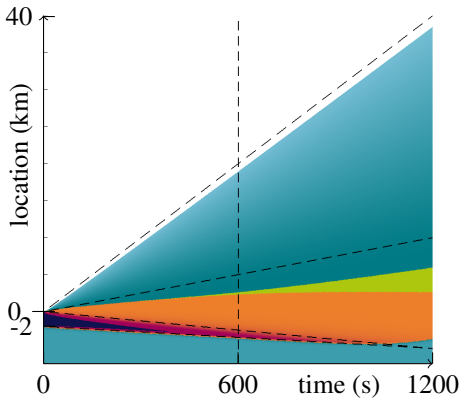

(k) Upwind method with implicit time stepping.

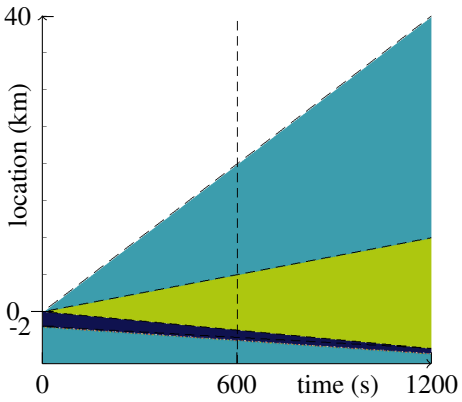

(l) Variational method.

Continued Figure 8.9 *Density plots of queue test case with different numerical methods. The vertical broken line indicates the time for which cross sections are shown in Figure 8.10. The other broken lines indicate sharp boundaries in the analytical solution.*

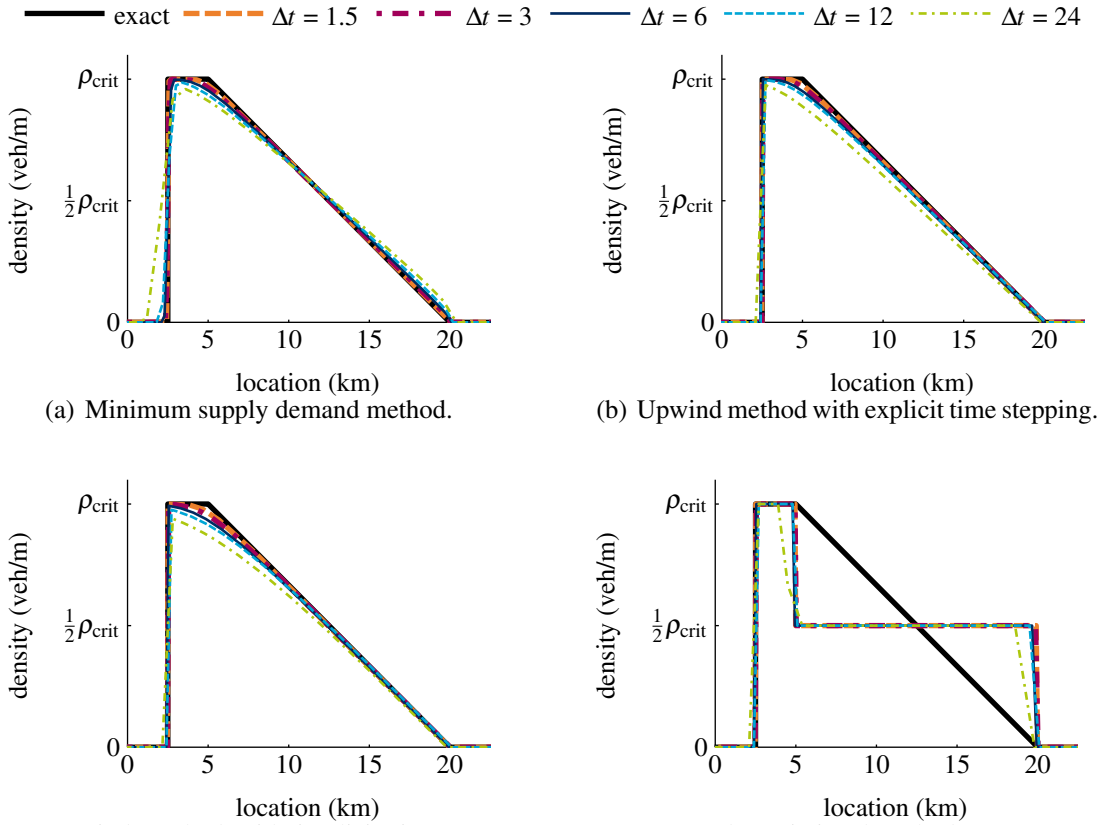

(a) Minimum supply demand method.

(b) Upwind method with explicit time stepping.

(c) Upwind method with implicit time stepping.

(d) Variational method.

Figure 8.10 *Density profiles of free flow test case at* $t = 600$ *s, computed with different numerical methods and different resolutions. (See next pages for congestion and queue test case results.)*

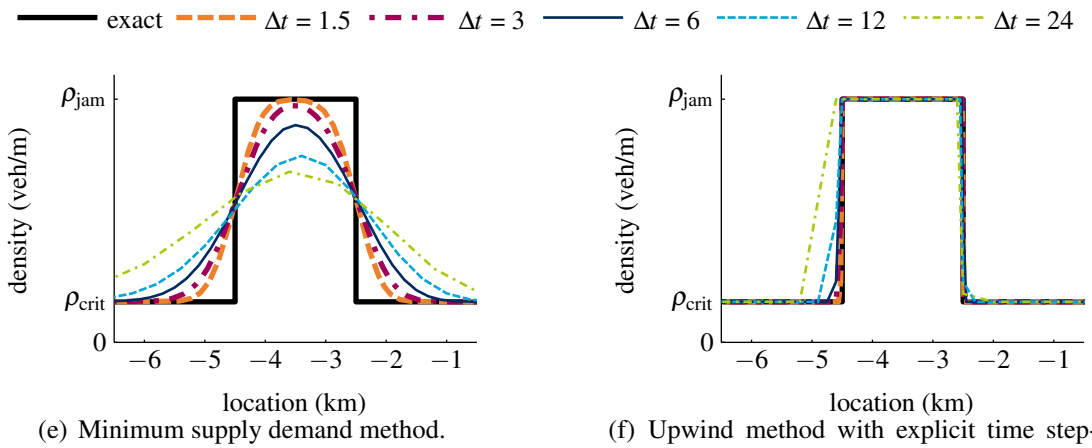

(e) Minimum supply demand method.

(f) Upwind method with explicit time stepping.

(g) Upwind method with implicit time stepping.

(h) Variational method

Continued Figure 8.10 *Density profiles of congestion test case at $t = 600$ s, computed with different numerical methods and different resolutions. (See next page for queue test case results.) We note that in the upwind method with explicit time stepping and with the variational method, the results may seem less accurate with large time steps and vehicle group sizes. However, this is due to the fact that there are no intermediate results to plot for example around -5 km. This effect is also visible in the free flow and queue test case, though less pronounced.*

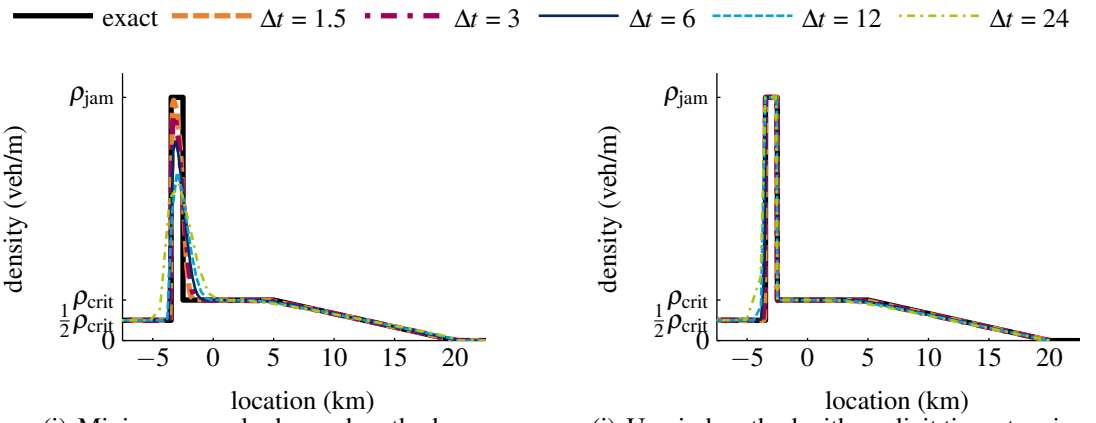

(i) Minimum supply demand method.

(j) Upwind method with explicit time stepping.

(k) Upwind method with implicit time stepping.

(l) Variational method

Continued Figure 8.10 *Density profiles of queue test case at $t = 600$ s, computed with different numerical methods and different resolutions.*

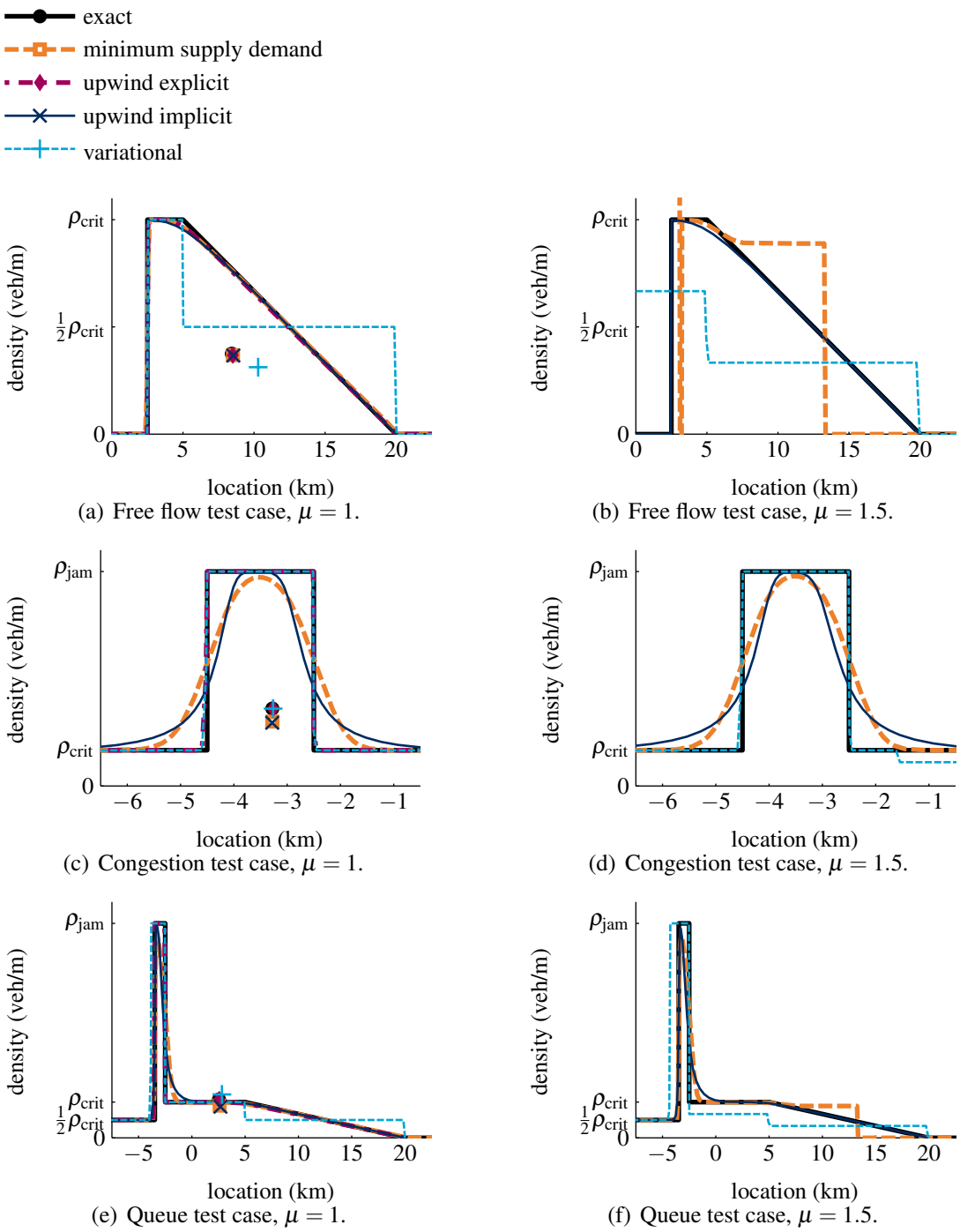

(a) Free flow test case, $\mu = 1$.

(b) Free flow test case, $\mu = 1.5$.

(c) Congestion test case, $\mu = 1$.

(d) Congestion test case, $\mu = 1.5$.

(e) Queue test case, $\mu = 1$.

(f) Queue test case, $\mu = 1.5$.

Figure 8.11 *Density profiles obtained with different numerical methods and CFL-numbers. The upwind explicit method is omitted from the profiles with large CFL-number ($\mu = 1.5$), Figures (b), (d) and (f)) because it is very unstable and would obscure the figures.*

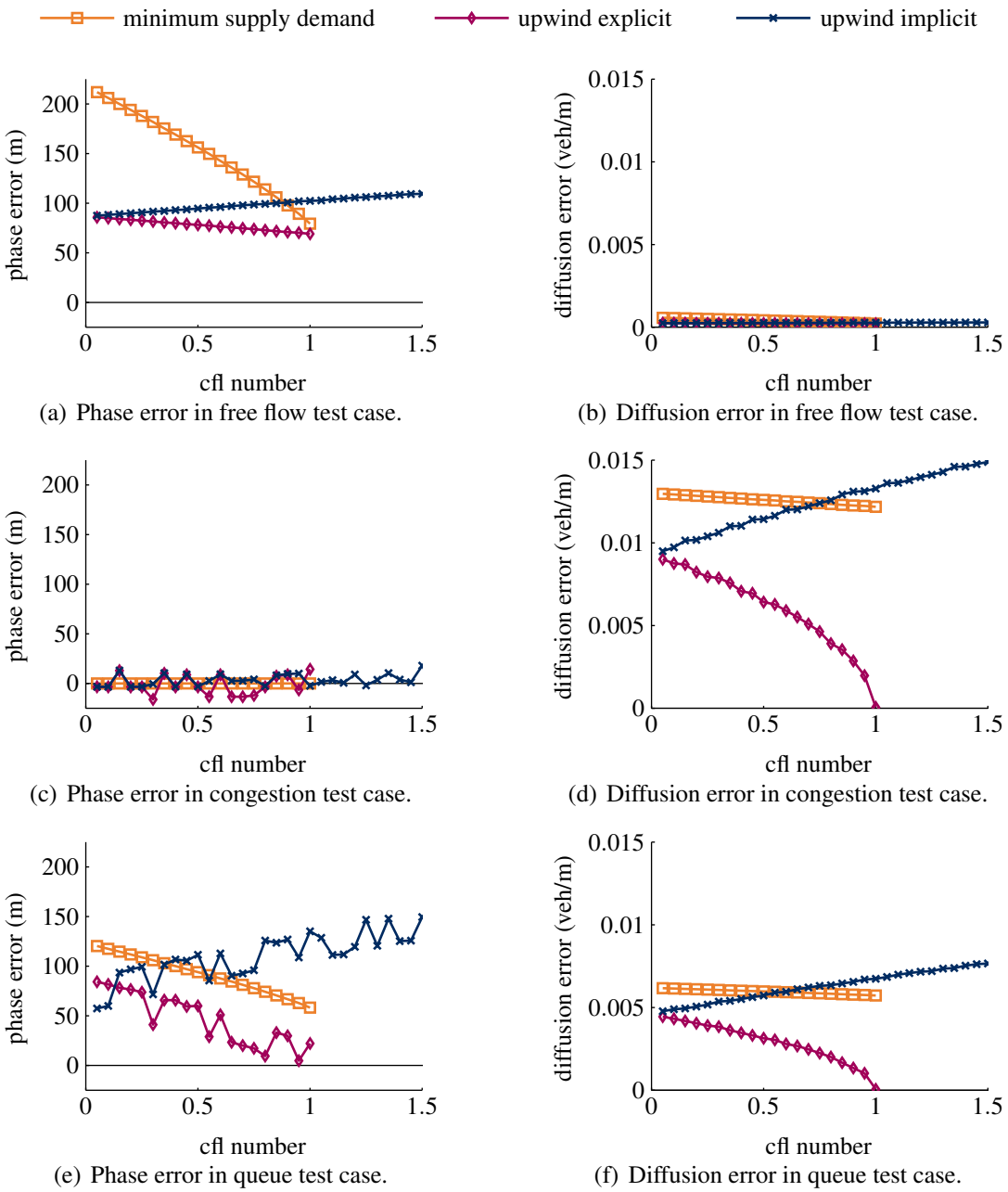

(a) Phase error in free flow test case.

(b) Diffusion error in free flow test case.

(c) Phase error in congestion test case.

(d) Diffusion error in congestion test case.

(e) Phase error in queue test case.

(f) Diffusion error in queue test case.

Figure 8.12 *Accuracy of numerical methods measured with different measures, for varying CFL-number.*

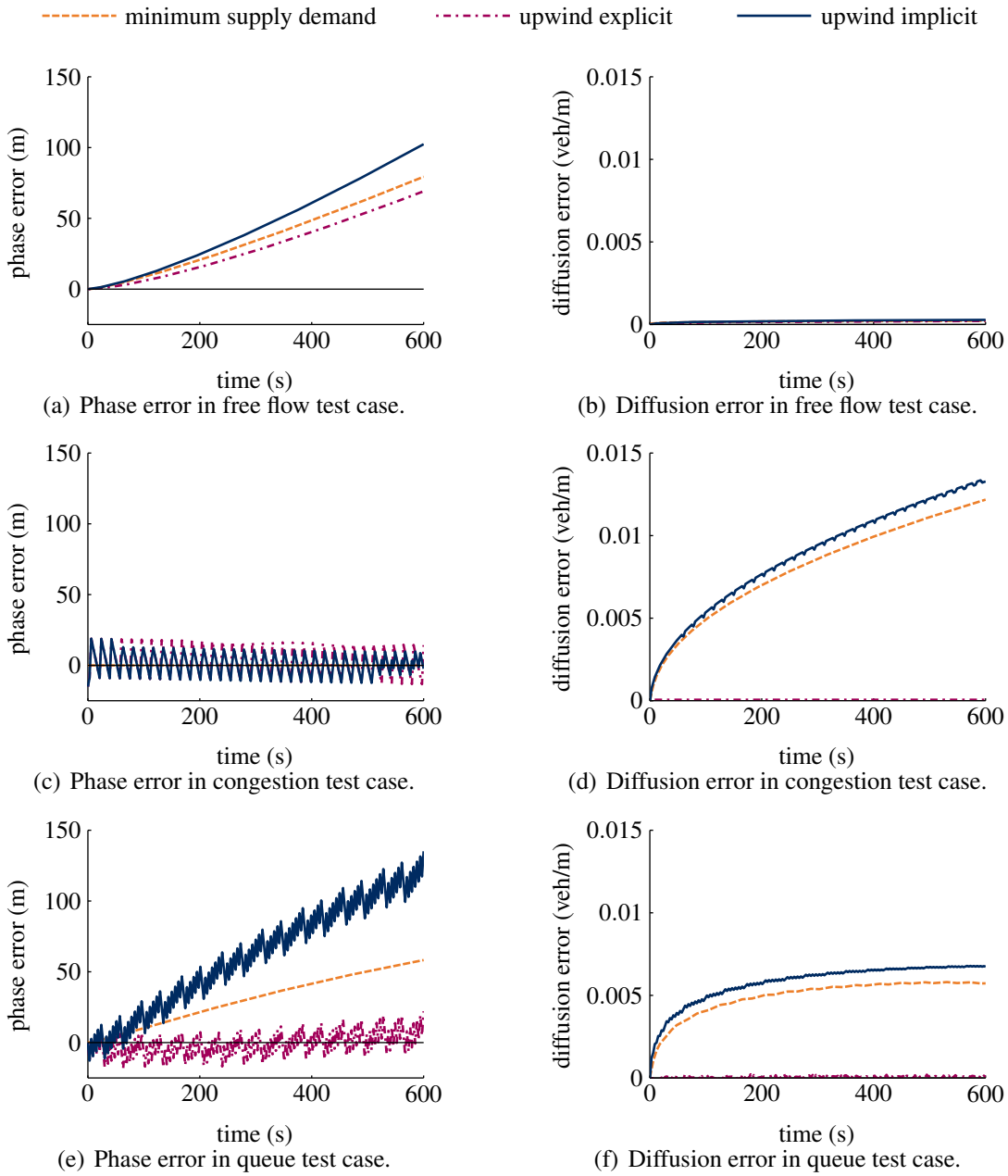

(a) Phase error in free flow test case.
(b) Diffusion error in free flow test case.
(c) Phase error in congestion test case.
(d) Diffusion error in congestion test case.
(e) Phase error in queue test case.
(f) Diffusion error in queue test case.

Figure 8.13 *Accuracy of numerical methods measured with different measures, and their change over time.*

congestion test case show a lot of diffusion if the minimum supply demand method or the upwind method with implicit time stepping is applied: the high density region does not have sharp boundaries as the other methods, but the solution is smooth. The queue test case results show that with these methods the queue dissolves more quickly than in the exact solution. The diffusion and phase error are analyzed in more detail below. Most of the analysis is done for one specific time instant $t = 600$ s, which is also indicated in the figures. At that moment, the exact solution can be computed relatively easily, while errors can already be observed in the numerical solution.

Figure 8.10 shows density profiles of the exact and numerical solution at time $t = 600$ s. The density is computed with different numerical methods and resolutions. The figures show that at a high resolution the solution with the minimum supply demand method and the upwind method converges to the exact solution. The numerical solution obtained with the variational method, does not converge to the exact solution. However, it converges to the exact solution of the same initial value problem with the piecewise linear fundamental relation.

Figure 8.11 shows density profiles of the exact and numerical solution at time $t = 600$ s. The density is computed with different numerical methods and CFL-numbers. The figure shows reasonable solutions if the upwind method with implicit time stepping is applied or if the CFL condition is satisfied exactly ($\mu = 1$). However, if $\mu = 1.5$ the solutions obtained with the upwind method with explicit time stepping show instabilities. This also occurs in the free flow test case with the minimum supply demand method. Other tests (not shown here) show that for the other test cases the minimum supply demand method is also unstable if larger CFL-numbers are applied. The lack of instability with relatively small CFL-numbers (but above one) may be explained by the following. If the CFL condition is satisfied, characteristics can not cross more than one grid cell boundary within one time step. If the CFL-number is not satisfied, characteristics may cross more than one cell boundary, but only if their velocity is 'high enough'. If the CFL-number is relatively small (e.g., $\mu = 1.5$), the characteristics need a relatively high velocity do so, i.e. characteristic velocity $c > (2/3)v_{\max}$. This does not, or not sufficiently, occur in the congestion and the queue test case and the minimum supply demand method does not show instabilities.

Figure 8.11 furthermore shows the centroids of the density profiles of the exact and numerical solution computed with $\mu = 1$. It shows that the phase error (i.e. the distance between the exact centroid and the numerically computed centroid in horizontal direction) is small, except for the variational method applied to the free flow test case. In the free flow test case, the diffusion error (the distance between the centroids in vertical direction) is small for all numerical methods except for the variational method. In both other test cases the diffusion error of the minimum supply demand method and the upwind method with implicit time stepping is relatively large. The phase error and diffusion error of the minimum supply demand method and both upwind methods are studied in more detail in the following. The accuracy measures based on the centroids of the solution, give rather extreme results. This is due to the nature of the solution

with discontinuities instead of smooth transitions in the free flow regime. In turn, these are due to the fact that the variational method uses a piecewise linear fundamental relation that is only an approximation of the fundamental relations in the other methods. Therefore, we will not further study the accuracy of this method.

Figure 8.12 shows the phase error and diffusion error for different numerical methods and their dependence on the CFL-number. For the minimum supply demand method and the upwind method with explicit time stepping only the results with $\mu \leq 1$ are shown because if the CFL condition is not satisfied, the method becomes unstable. Other test results (not shown here) show that the errors of the upwind method with implicit time stepping increase almost linearly as function of the CFL-number for CFL-numbers above $\mu = 1.5$, at least until $\mu = 4$. The phase errors in the congestion test case are negligibly small: less than a quarter of a grid cell ($\Delta x/2 = 50$ m) or the total length of 2 vehicle groups in congestion ($2s_{\text{jam}}\Delta n = 25$ m). The apparent oscillations in the phase error in the congestion test case and the queue test case can also be explained by considering the length of a vehicle group. This length is about the same size as the size of the oscillations. Therefore, we expect that the oscillations are due to the averaging of the position over multiple vehicle in the procedure to find the phase error. In the free flow test case the diffusion is much smaller than in the other two test cases. Those results with very small errors will not be discussed further. All other results (i.e. phase error in free flow and queue test case and diffusion error in free flow and congestion test case) show that the errors of both upwind methods are similar for small CFL-numbers. They increase with the CFL-number for the upwind method with implicit time stepping, they decrease in the methods with explicit time stepping. The diffusion error is even zero in the upwind method with explicit time stepping and $\mu = 1$.

Figure 8.13 shows the phase error and diffusion error for different numerical methods and how they evolve over time, from $t = 0$ to $t = 600$ s. Again the phase error in the congestion test case and the diffusion error in the free flow test case are negligibly small and therefore not discussed further. The upwind method with implicit time stepping has the largest errors, but it is similar to the errors of the minimum supply demand method, except for the phase error in the queue test case. Explicit time stepping has the smallest error. It is much smaller than that of the other methods and it increases only slowly, except for the phase error in the free flow test case. The diffusion error of the other methods increases quickly in the first part of the simulation, but the increase rate decreases over time.

8.6.2 Discussion

The test results confirm that the minimum supply demand method and both upwind methods are converging if the CFL condition is satisfied: $\mu \leq 1$. The variational method with $\mu = 1$ converges to the solution of the same problem with piecewise linear fundamental relation. The upwind method with explicit time stepping and $\mu = 1$

gives the most accurate simulation results, both in terms of phase error as diffusion error. The phase error increases (almost) linearly over time. From this we conclude that the error in characteristic velocity is constant. The accuracy of the minimum supply demand method and the upwind method with explicit time stepping is lower if the CFL-number is lower. This implies that decreasing the time step size Δt without decreasing the grid cell size Δx or the vehicle groups size Δn, leads to a lower accuracy. It depends on the numerical method and on the actual traffic state how large this effect is. However, even for very small CFL-numbers ($\mu = 0.05$), the upwind method with explicit time stepping is more accurate than the other methods. Therefore, we conclude that this method is preferred if the CFL condition is satisfied. Only if, for some reason, the CFL condition can not be satisfied, the upwind method with implicit time stepping is preferred. This method is less accurate if $\mu \leq 1$. However, it remains stable even if $\mu > 1$.

8.7 Conclusions

In this chapter, we introduced the upwind method applied to the mixed-class kinematic wave model in Lagrangian formulation. This method is simpler than the minimum supply demand method commonly applied to the kinematic wave model in Eulerian formulation. This is because switching between upwind and downwind discretization is unnecessary in the Lagrangian formulation. Furthermore, we introduced an alternative time stepping method (implicit time stepping) which allows for larger time steps and a numerical method based on variational theory.

We introduced two novel accuracy measures: diffusion and phase error. The new accuracy measures take into account just that type of accuracy that is important in traffic flow applications. The accuracy measures were applied to assess the accuracy of the numerical methods. They can also be applied to assess the accuracy of a model against empirical data. This allows for a more fair comparison of traffic flow models than the currently usual approach of comparing models against empirical data using, for example, the RMSE. However, for this application it may be necessary to develop the measures further. For example, it would be useful to automatically match a high density region in data with the corresponding high density region in the simulation.

Our test results show that the upwind method with explicit time stepping is the most accurate method. All methods introduce phase errors and diffusion errors. The variational method leads to stepwise changes in the velocity in free flow due to the change in the fundamental relation to a piecewise linear fundamental relation. The accuracy in terms of phase error and diffusion is much worse than of the other methods. Therefore, we do not discuss this method further,

The requirement of small time steps is the main drawback of the upwind method with explicit time stepping and also of the minimum supply demand method. This is because the CFL-condition needs to be satisfied and it results in higher computing times.

If an application demands for very low computing times, the upwind method with implicit time stepping is an alternative. With this method, larger time steps can be taken which results in lower computing times.

Regarding the choice of a numerical method we conclude the following:

1. Inaccuracies consist of phase error and diffusion error, the amount of inaccuracy depends on traffic state, numerical method and CFL-number.
2. The upwind method with explicit time stepping gives the most accurate results.
3. If an explicit time stepping method is used:
   (a) $\mu = 1$ gives the most accurate results. If $\mu = 1$ is impossible (e.g., due to the layout of the road), choose $\mu < 1$ because $\mu > 1$ will lead to instabilities.
   (b) Only decreasing the time step size (i.e. decreasing the CFL-number) will lead to less accurate simulation results.
4. If an implicit time stepping method is used, larger time steps may be taken (even with $\mu > 1$), but the larger the time step, the less accurate the simulation result.
5. Decreasing both time step size and grid cell size or vehicle group size such that the CFL-number does not change, will lead to more accurate simulation results.

We have only compared the accuracy of the methods using simulations. It would be interesting to see whether the computation times are influenced by the methods as we expect (e.g., lower computation times with the upwind method than with the minimum supply demand method). Future research includes an extension of the variational method with piecewise linear fundamental relation consisting of more than three parts. It will increase the number of velocity steps in free flow and therefore increase the accuracy. The accuracy of the other numerical methods can be studied further by applying other, more realistic, test cases. In such cases, it may not be possible to obtain the exact solution. The results show that the solution with the upwind method and explicit time stepping and high resolution is very accurate. Therefore, that solution can be applied as a reference solution. Furthermore, phase error and diffusion error can also be based on velocity and spacing instead of density. This will lead to better accuracy estimates in test cases with a small low-density region that needs to be traced. Finally, the accuracy measures introduced here can also be applied to assess traffic flow models. In that case they are used to compare measurements with model results. That way, models are assessed on criteria that are more relevant in traffic flow modeling than simply the RMSE.

In the next two chapters the upwind method with explicit time stepping is extended to multi-class models (in particular Fastlane) and to networks including nonhomogeneous roads, on ramps, off ramps etc.

Chapter 9

Numerical methods for multi-class models

In the previous chapter we introduced numerical methods for mixed-class kinematic wave models. In this chapter we extend the methods to multi-class kinematic wave models. We limit our scope to explicit time stepping methods, because of two reasons. The explicit methods are easiest to extend to multi-class models. Furthermore, based on the results from the previous chapter we expect accurate simulations can be done with these methods. A multi-class minimum supply demand method was introduced by Chanut & Buisson (2003). However, they do not include dynamic pce-values. Furthermore, Ngoduy (2010) introduces an alternative numerical method which uses eigenvalues. However, it is difficult to approximate the eigenvalues accurately if there are many (more than 3 or 4) vehicle classes.

We introduce and compare a minimum supply demand method and an upwind method for the generalized multi-class kinematic wave model, with dynamic pce-values. The minimum supply demand method is based on the Eulerian formulation of the model, the upwind method on its Lagrangian formulation. We show that the (dis)advantages of both methods are similar to the (dis)advantages of their mixed-class counterparts.

The outline of this chapter is as follows. In Section 9.1 we introduce a minimum supply demand method for the generalized multi-class kinematic wave model. In Section 9.2 the upwind method is introduced. In Section 9.3 we compare both methods using a simple test problem. We conclude this chapter with a short discussion in Section 9.4.

9.1 Multi-class minimum supply demand method

A minimum supply demand method is developed for the generic multi-class model. Each time step k the following steps are taken to calculate the new state in each grid cell j.

Preparation Determine flow over grid cell boundary $q^k_{u,j-\frac{1}{2}}$ by taking minimum of supply and demand.

Actual time step Determine new class-specific densities $\rho^{k+1}_{u,j}$ by adding inflow and subtracting outflow.

New values other variables Apply the effective density function, the fundamental relation and the pce function to determine the new pce-values $\eta^{k+1}_{u,j}$, class-specific flow $q^{k+1}_{u,j}$ and effective flow q^{k+1}_j.

The steps are discussed in more detail in the rest of this section. Figure 9.1 shows simulation results of a simple test problem. The test problem and the results are discussed in more detail in Section 9.3.

9.1.1 Preparation

In the preparation part of the time step the flow over the cell boundaries is determined using the class-specific demand and supply, all in vehicles per time unit. The total demand and supply is calculated equivalently to the mixed-class demand (8.1c) and supply (8.1d):

$$\delta^k_j = \begin{cases} q^k_j & \text{(free flow)} \\ q_{\text{crit}} & \text{(congestion)} \end{cases} \quad \text{and} \quad \sigma^k_j = \begin{cases} q_{\text{crit}} & \text{(free flow)} \\ q^k_j & \text{(congestion)} \end{cases} \tag{9.1}$$

with the q^k_j effective flow in pce vehicles per time unit. Therefore, also the unit of the demand and supply is pce vehicles per time unit. The total supply and demand is divided among the vehicle classes using the class-specific shares λ_u:

$$\lambda^k_{u,j} = \begin{cases} \dfrac{\eta^k_{u,j} v^k_{u,j}}{\sum_u \eta^k_{u,j} v^k_{u,j}} & \text{if } \rho^k_{u,i} = 0 \text{ for all classes } u \qquad (9.2a) \\ \dfrac{\eta^k_{u,j} \rho^k_{u,j}}{\rho^k_j} & \text{if } v^k_{u,i} = 0 \text{ for all classes } u \qquad (9.2b) \\ \dfrac{\eta^k_{u,j} q^k_{u,j}}{q^k_j} & \text{otherwise} \qquad (9.2c) \end{cases}$$

This implies that in most cases (9.2c) the share is simply the fraction of the effective flow taken up by class u. However, if the effective flow is zero (and thus $\rho^k_{u,i} = 0$ for all classes u or $v^k_{u,i} = 0$ for all classes u), all shares λ_u would be zero and $\sum_u \lambda_u \neq 1$. Therefore, if the effective flow is zero, the share is a fraction determined by the velocities (9.2a) or densities (9.2b). Using the shares, the total supply and demand is distributed among the vehicle classes as follows:

$$\delta^k_{u,j} = \lambda^k_{u,j} \delta^k_j \quad \text{and} \quad \sigma^k_{u,j} = \lambda^k_{u,j-1} \sigma^k_j \tag{9.3}$$

The unit of class-specific demand and supply is pce-vehicles per time unit. We note that the share in the previous cell $j-1$ is used to calculate the class-specific supply in cell j. This is because the total supply needs to be distributed over all vehicles that want to cross the cell boundary between cell $j-1$ and cell j, and not over the vehicles that are already in cell j. Finally, for each cell, the class-specific flow from the previous cell $i-1$ to cell i is determined as the minimum of the supply and the demand:

$$q^k_{u,j-\frac{1}{2}} = \frac{1}{\eta^k_{u,j}} \min\left(\sigma^k_{u,j}, \delta^k_{u,j-1}\right) \tag{9.4}$$

9.1.2 Actual time step

The new class-specific density is determined in the actual time step, similar to the new density in the mixed-class minimum supply demand method (8.1b):

$$\rho^{k+1}_{u,j} = \rho^k_{u,j} + \frac{\Delta t}{\Delta x}\left(q^k_{u,j-\frac{1}{2}} - q^k_{u,j+\frac{1}{2}}\right) \tag{9.5}$$

We note that with this approach, the effective flow (in pce equivalent vehicles per time unit) is maximized. Therefore, the numerical method finds the entropy solution of the continuous model.

9.1.3 Computation of variable values

In the last part of the time step, the values of other variables such as the pce-values and the class-specific and effective flow are calculated. For example, for Fastlane, the effective density function (4.51), the fundamental relation (4.49) and the pce function (4.11) are applied. This part of the time step shows the importance of the reformulation of the effective density function as introduced in Section 4.5. It is used to determine the new pce-value $\eta^k_{u,j}$, without using a numerical approximation based on the implicit formulation in Section 4.3.

We note that the method does not guarantee that the new effective density does not exceed jam density. This is because the supply and demand are based on the share, which is in turn based on the old pce-values. However, during the time step, the densities and thus also the pce-values change. With the new pce-values, the effective density may in fact exceed jam density. A simple solution to this problem is to set the effective density to jam density ($\rho = \rho_{\text{jam}}$), whenever it exceeds jam density. The class-specific densities ρ_u are not changed and thus vehicles are conserved.

Finally, in the last part of the time step, the class-specific and the effective flow are determined by:

$$q^k_{u,j} = v^k_{u,j}\rho^k_{u,j} \quad \text{and} \quad q^k_j = \sum_u \eta^k_{u,j} q^k_{u,j} \tag{9.6}$$

9.2 Multi-class upwind method

An upwind method is developed for the generic multi-class model. In each time step k the following steps are taken to calculate the new state for each vehicle group i:

Actual time step Determine new spacing of class 1 $s_{1,i}^{k+1}$ and spacing ratio $(s_1/s_u)_i^{k+1}$ of all other classes u.

New values other variables Determine the new spacing of all classes $u \neq 1$ and the class-specific densities. Apply the effective density function and the fundamental relation to determine the new class-specific velocity $v_{u,i}^{k+1}$.

New positions Calculate the new positions of all vehicle groups.

The steps are discussed in detail in the rest of this section. Figure 9.1 shows simulation results of a simple test problem. The test problem and the results are discussed in more detail in Section 9.3.

9.2.1 Actual time step

We recall from Chapter 6 the conservation equations in the Lagrangian coordinate system (6.28) and (6.34):

$$\frac{\partial s_1}{\partial t} + \frac{\partial v_1}{\partial n} = 0 \tag{9.7a}$$

$$\frac{\partial}{\partial t}\left(\frac{s_1}{s_u}\right) + \frac{\partial}{\partial n}\left(\frac{v_1 - v_u}{s_u}\right) = 0 \quad \text{for all classes } u \neq 1 \tag{9.7b}$$

An upwind method is applied to discretize the equations. Therefore, vehicles of class 1 are grouped into groups of Δn vehicles. The discretization of the conservation equation for class 1 (9.7a) is similar to the discretization of the mixed-class conservation equation (8.5):

$$s_{1,i}^{k+1} = s_{1,i}^{k} + \frac{\Delta t}{\Delta n}\left(v_{1,i-1}^{k} - v_{1,i}^{k}\right) \tag{9.8a}$$

with k the time step index, Δt the time step size, i the vehicle groups index (only referring to vehicles of class 1) and Δn the vehicle group size: the number of vehicles of class 1 per group. We note that the number of vehicles of other classes in one group may vary, i.e. the fraction $\rho_{u,i}^k / \sum_u \rho_{u,i}^k$ depends both on the vehicle group i and the time step k. The discretization of (9.7b) uses the same indices and time step and vehicle group sizes and is as follows:

$$\left(\frac{s_1}{s_u}\right)_i^{k+1} = \left(\frac{s_1}{s_u}\right)_i^{k} + \frac{\Delta t}{\Delta n}\left(\frac{v_{1,i-1}^k - v_{u,i-1}^k}{s_{u,i-1}^k} - \frac{v_{1,i}^k - v_{u,i}^k}{s_{u,i}^k}\right) \tag{9.8b}$$

9.2.2 New value of other variables

Once $s_{1,i}^{k+1}$ and $(s_1/s_u)_i^{k+1}$ are known, the new spacing of the other classes u can be computed:

$$s_{u,i}^{k+1} = \frac{s_{1,i}^{k+1}}{(s_1/s_u)_i^{k+1}} \tag{9.9}$$

The new densities of each class u follows directly:

$$\rho_{u,i}^{k+1} = 1/s_{u,i}^{k+1} \tag{9.10}$$

Subsequently, the effective density function is applied to find the new effective density. Finally, the new class-specific velocities follow from the multi-class fundamental relation.

9.2.3 New positions

Equivalently to the derivation of (8.11), the discretized conservation equation of class 1 (9.8a) can be simplified to:

$$x_{1,i}^{k+1} = x_{1,i}^{k} + \Delta t v_{1,i}^{k} \tag{9.11}$$

This is useful because in most applications the location of each vehicle group is needed, and not only its (class-specific) spacing, density or velocity.

9.2.4 Discussion

Just as in the mixed-class case, the upwind method applied in Lagrangian coordinates is much simpler than the minimum supply demand method applied in Eulerian coordinates. Because of the lack of switching between upwind and downwind discretization the upwind method is computationally less demanding. In the next section we compare the accuracy of the multi-class minimum supply demand and upwind method based on simulation results.

9.3 Accuracy of numerical methods

We compare the accuracy of the multi-class minimum supply demand and upwind method with a simple test case, similar to the queue test case in Chapter 8. The only difference is that we now apply Fastlane with multiple vehicle classes.

Table 9.1 *Model parameters.*

Fundamental relation parameters				
maximum velocity class 1	$v_{1,\max}$	33.3 m/s	=	120 km/h
maximum velocity class 2	$v_{2,\max}$	25 m/s	=	90 km/h
critical velocity	v_{crit}	20.8 m/s	=	75 km/h
critical density	ρ_{crit}	0.033 veh/m	=	33 veh/km
jam density	ρ_{jam}	0.2 veh/m	=	200 veh/km
gross vehicle length class 1	L_1	$1/\rho_{\text{jam}}$		5 m
gross vehicle length class 2	L_2			18 m
minimum time headway class 1	T_1			1 s
minimum time headway class 2	T_2			1.5 s
(resulting congestion wave parameter	w	4.17 m/s	=	15 km/h)

9.3.1 Test setup

The test setup is as follows. There are two-classes with different maximum velocity $v_{u,\max}$, gross vehicle length L_u and minimum time headway T_u. Initially, the fraction of vehicles of class 2 is the same everywhere and equal to $\gamma = \rho_2/(\rho_1+\rho_2) = 0.1$. The test case represents a traffic light turning green. This leads to the following initial conditions:

$$\rho(x,0) = \begin{cases} 0 & \text{if } x > 0 \\ \rho_{\text{jam}} & \text{if } 0 \le x \le L_{\text{queue}} \\ \rho_{\text{upstream}} & \text{if } x < L_{\text{queue}} \end{cases} \tag{9.12a}$$

$$\rho_2(x,0) = \gamma(\rho_1(x,0)+\rho_2(x,0)) \tag{9.12b}$$

with the initial length of the jam density region $L = 2000$ m and the initial upstream effective density $\rho_{\text{upstream}} = \frac{1}{2}\rho_{\text{crit}}$. The multi-class Smulders fundamental relation (4.49) is applied, with the same parameters as previously used in Fastlane, see Chapter 5. All model parameters are given in Table 9.1. The same numerical parameters as in the base case in Chapter 8 are applied. That is, the grid cell size $\Delta x = 100$ m, vehicle group size $\Delta n = 2.5$ vehicles and time step size $\Delta t = 3$ s. Therefore, the CFL-condition is satisfied exactly ($\mu = 1$).

We do not compute the analytical solution of the test problem. However, we use the solution obtained with the upwind method with a high resolution ($\Delta n = 0.42$ vehicles, $\Delta t = 0.5$ s, $\mu = 1$) as a reference solution. We have shown in the previous chapter that with a high resolution the accuracy of this solution is high and therefore it can be applied as a reference solution.

9.3.2 Simulation results

The numerical solutions of the test case are shown in Figure 9.1 and 9.2. Figure 9.1 shows the effective density, but also the class-specific velocities and the fraction of

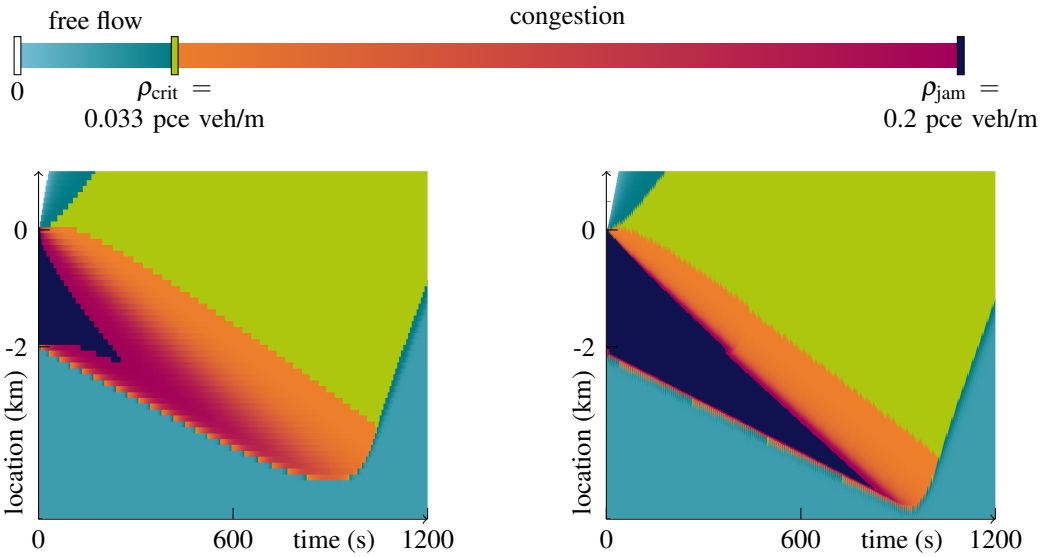

(a) Effective density with minimum supply demand method.

(b) Effective density with upwind method.

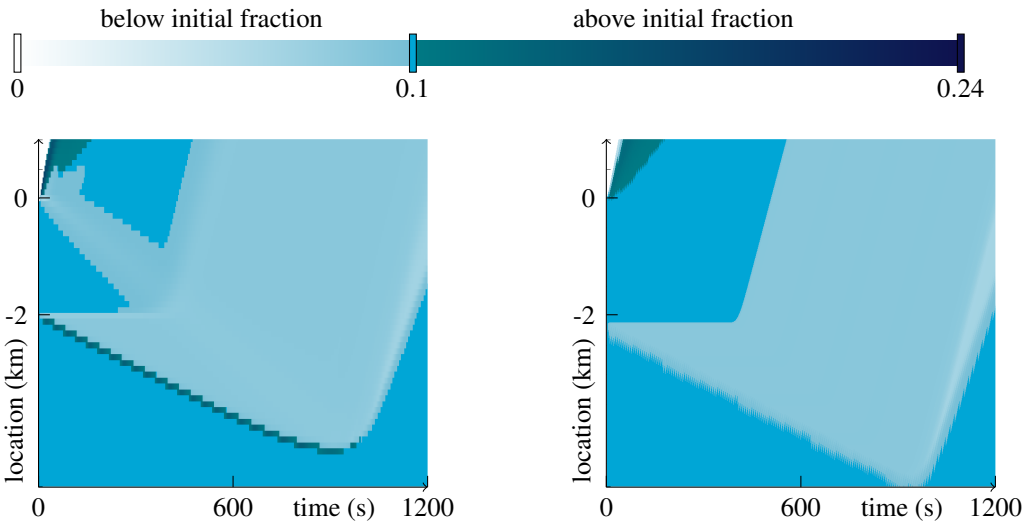

(c) Fraction of class 2 with minimum supply demand method.

(d) Fraction of class 2 with upwind method.

Figure 9.1 *Simulation results with multi-class minimum supply demand method and multi-class upwind method.*

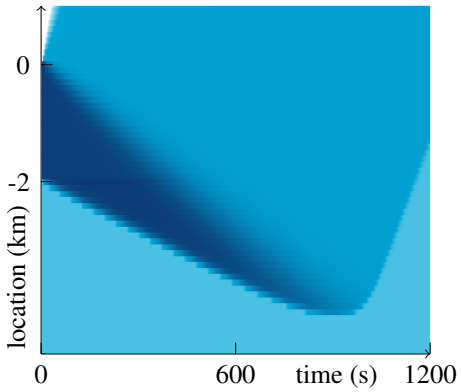

(e) Density of class 1 with minimum supply demand method.

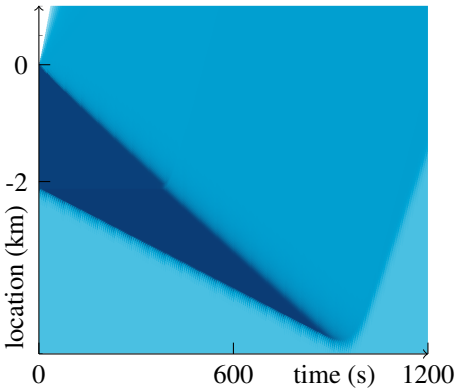

(f) Density of class 1 with upwind method.

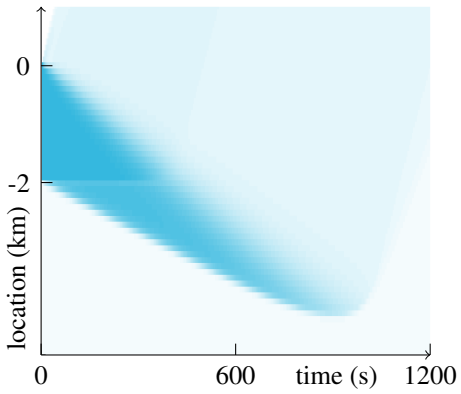

(g) Density of class 2 with minimum supply demand method.

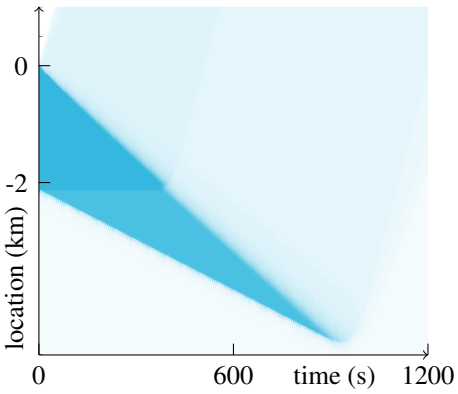

(h) Density of class 2 with upwind method.

Continued Figure 9.1 *Simulation results with multi-class minimum supply demand method and multi-class upwind method.*

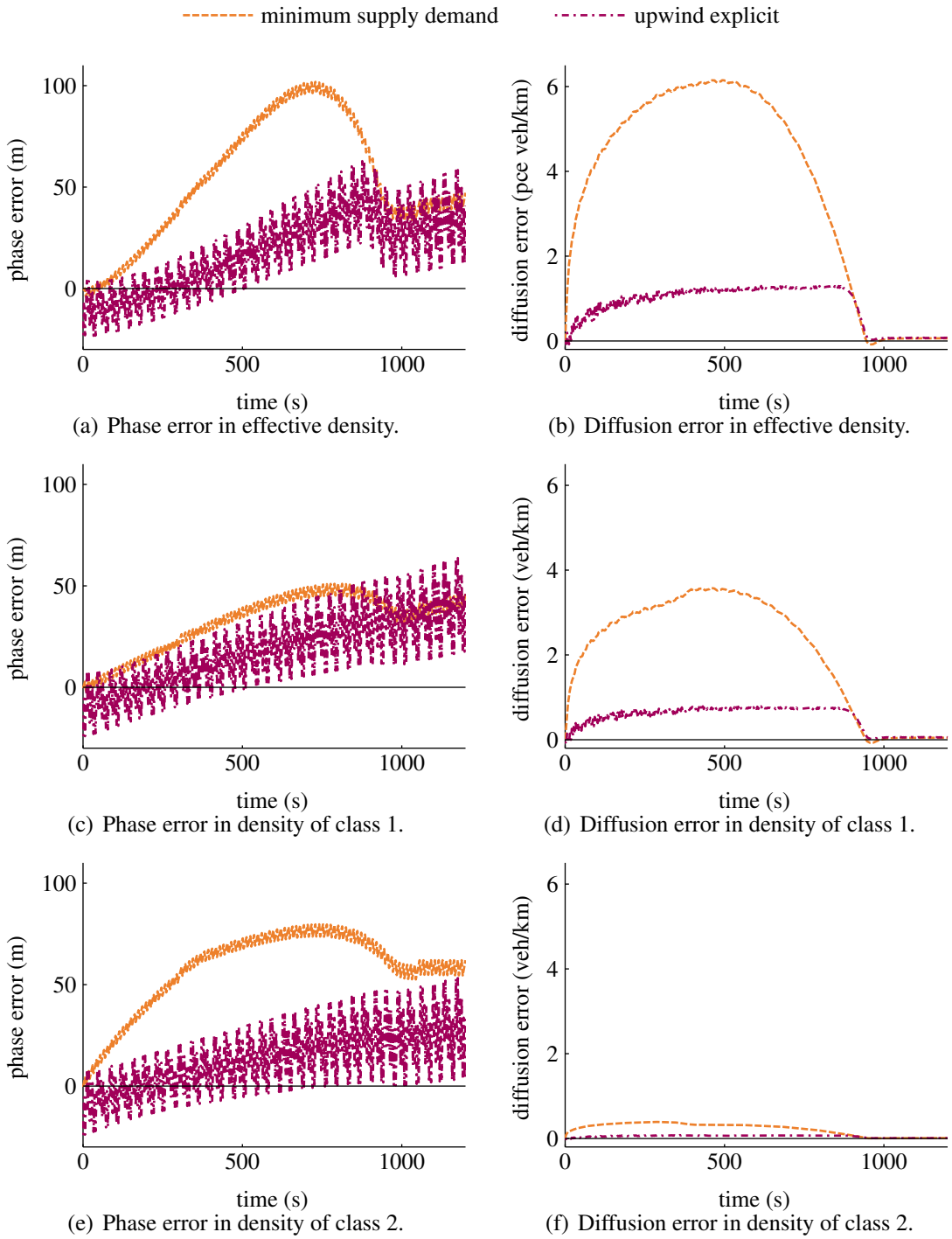

(a) Phase error in effective density.
(b) Diffusion error in effective density.
(c) Phase error in density of class 1.
(d) Diffusion error in density of class 1.
(e) Phase error in density of class 2.
(f) Diffusion error in density of class 2.

Figure 9.2 *Accuracy of multi-class numerical methods with different measures, and their change over time.*

vehicles of class 2. The results with the minimum supply demand method are more diffusive than the results with the upwind method. Just as in the mixed-class case, congestion, and especially the queue, spills back further upstream with the upwind method than with the minimum supply demand method. The phase error and diffusion error and their evolution over time are shown in Figure 9.2. The errors are largest about halfway the simulation. On one hand, the errors have had some time to develop themselves. On the other hand, the queue is still relatively long. The figure shows that both the accuracy of the upwind method is higher than that of the minimum supply demand method. However, after the queue has dissolved (at around $t = 950$ s) the accuracy of both methods is similar. Except for the size, there is not much difference between the error in the effective density and the class-specific densities of class 1 and 2.

9.4 Conclusions

The minimum supply demand method based on the Eulerian formulation of the kinematic wave model and the upwind method based on its Lagrangian formulation are extended to multi-class models. Similar conclusions as for the mixed-class model and numerical methods hold. The upwind method is computationally less demanding because there is no switching between downwind and upwind discretization. The computational results with the upwind method are more accurate: both the phase error and diffusion error are smaller.

Future research includes a more detailed study of the accuracy of the upwind method for the generalized multi-class kinematic wave model. Therefore, more test cases should be studied with a larger variety of characteristic waves, for example by including other traffic compositions. The numerical solution may be compared with the analytical solution, instead of with a reference solution that is also obtained numerically. Furthermore, the accuracy of the method applied to models with more than two-classes can be studied, as well as the accuracy when the method is applied to other models than the Fastlane model. The method may also be applied to compare the simulation results of multi-class kinematic wave models. The computational time of the upwind method can be reduced by combining it with implicit time stepping or the variational method. Finally, an alternative numerical method based on the other formulation of the conservation equation in Lagrangian coordinates (6.29) (Yuan et al., 2011; Yuan, 2013) can be studied further. This method is expected to be more accurate if there are only few vehicles of class 1. The accuracy can be evaluated in more detail using the same methods as presented in this chapter.

We conclude that the upwind method based on the Lagrangian coordinate formulation of the generalized multi-class model leads to more efficient simulations on homogeneous roads than the minimum supply demand method. In the next chapter we extend the upwind method to inhomogeneous roads and networks.

Chapter 10

Networks

The final step in the development of our traffic flow model and accompanying numerical method is the introduction of nodes. Previously, we only considered long homogeneous roads. In this chapter we discuss how to deal with inflow and outflow boundaries and inhomogeneities. Inhomogeneities are, for example, changes in the fundamental relation due to changes in the number of lanes or speed limit, off ramps (diverges) and on ramps (merges). In our model links are homogenous road stretches connected by nodes. Boundaries and inhomogeneities are located at nodes. Therefore, we refer to models for inflow and outflow boundaries, inhomogeneities, merges and diverges as node models.

Most discussions on boundaries and inhomogeneities in traffic flow models assume that the model is formulated in Eulerian coordinates, e.g., (Newell, 1993b; Daganzo, 1995a; Jin & Zhang, 2003; Lebacque, 1996; Helbing & Treiber, 1999; Tampère et al., 2011; Flötteröd & Rohde, 2011). Most articles discuss both a continuous node model and its discretization based on the minimum supply demand method. In fact, also the continuous node models use concepts from the minimum supply demand method. Tampère et al. (2011) propose a generic node model for nodes with multiple incoming and outgoing links, see Figure 10.1(a). Their article includes simple, but consistent and realistic, models for merges with two incoming links (Figure 10.1(d)) and diverges with two outgoing links (Figure 10.1(c)). They discuss how to include realistic rules for overtaking at diverges and priority at merges. Furthermore, they propose a method to include capacity constraints of the node itself. We shortly review the model and built on it for our multi-class node model and node model in Lagrangian formulation. Because the main application of our model is simulation of motorways, we restrict ourselves to nodes that are present on this type of roads. It implies that we only consider nodes with at most three links (one-to-one, one to two and two to one nodes). Furthermore, we do not consider capacity constraints of the node itself. The methods may be extended to intersection models for other nodes with more links or restrictions on the capacity of the node itself.

Ngoduy (2010) proposes a node model for a multi-class kinematic wave model. How-

ever, he assumes that vehicles are always able to overtake, for example to take a different outgoing link. Furthermore, his merge model violates the invariance principle, which implies that traffic flow over the node depends heavily on the flows over the incoming links. Lebacque & Khoshyaran (2005) have shown that this is an unreasonable assumption. As an example, consider the case with low flows (in total below the capacity of the outgoing link) from both incoming links. If the flow from one incoming link is halved, the flow from the other incoming link to the outgoing link is also halved, according to Ngoduy's model.

The main challenge for node modelling in Lagrangian formulation is that nodes move with respect to the coordinate system, which moves with the vehicles. Therefore, one may develop node models similar to the ones that are used in microscopic models. However, the continuous link model describes the 'average' vehicle behaviour. Therefore, also the node model and its discretization should describe the average vehicle behaviour and thus we do not resort to microscopic node models describing the behavior of individual vehicles. We consider macroscopic node models and introduce node models in Lagrangian formulation in analogy to those in Eulerian formulation. We develop such models and show that they are, in most cases as accurate as node models in Eulerian formulation. It even turns out that part of the node model and its discretization is simpler in Lagrangian than in Eulerian formulation.

The outline of this chapter is as follows. In Section 10.1 we discuss mixed-class node models in Eulerian formulation and the minimum supply demand method for these models, based on (Tampère et al., 2011). We extend the method to multi-class models in Section 10.2. In Section 10.3 we discuss mixed-class node models in Lagrangian formulation and in Section 10.4 the discretization of Lagrangian node models. The methods are applied in simulations in Section 10.5. Furthermore, in that section the accuracy of the minimum supply demand method for nodes and the upwind method for nodes are compared. Finally, we conclude with Section 10.6. It includes a few remarks on extensions of the mixed-class upwind method for nodes to multi-class models.

10.1 Node model and minimum supply demand method

Nodes have one or multiple incoming and one or multiple outgoing links, see Figure 10.1 for some examples. Our goal is to describe how, in a mixed-class kinematic wave model, the flux over the node can be computed, given the traffic state at the incoming and outgoing links. We will do this for different types of nodes, with one or two incoming and one or two outgoing links. The results can be generalized to nodes with more links, but this generalization is not in all cases straightforward.

Node models in Eulerian formulation use concepts from the minimum supply demand method. The demand of the incoming links and the supply of the outgoing links is computed. The flux over the node is the minimum of both, possibly corrected for some complicating factors if there are multiple incoming or outgoing links. Therefore, we

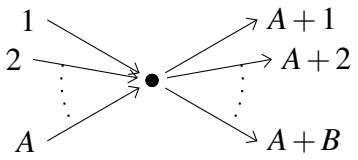

(a) Node with A incoming and B outgoing links.

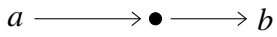

(b) 1 tot 1 node.

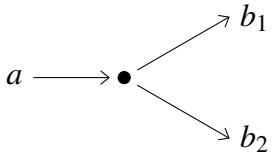

(c) Diverge node with 2 outgoing links.

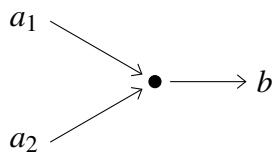

(d) Merge node with 2 incoming links.

Figure 10.1 *Different types of nodes. Only (b), (c) and (d) are discussed in detail in this chapter.*

skip the step of describing the continuous node model and immediately turn to the discretized node model. Our goal is to present a method to calculate the flux from the last cell of the incoming link(s) to the first cell of the outgoing link(s). The last cell of an incoming link is denoted with a, the first cell of an outgoing link is denoted b. Each time step k the demand at last cell of the incoming link δ_a^k and the supply at the first cell of the outgoing link σ^k is calculated. This is done similarly to the minimum supply demand method for homogeneous roads (8.1c) and (8.1d):

$$\delta_a^k = \begin{cases} q_a^k \\ (q_{\text{cap}})_a \end{cases} \quad \text{and} \quad \sigma_b^k = \begin{cases} (q_{\text{cap}})_b & \text{(free flow)} \\ q_b^k & \text{(congestion)} \end{cases} \tag{10.1}$$

with q_a^k the current flow in incoming cell a and q_b^k the current flow in the outgoing cell b. $(q_{\text{cap}})_a$ and $(q_{\text{cap}})_b$ are their respective capacities. In most cases the flux (the flow over the node during one time step) is not simply the minimum of the supply and demand, because some other influences have to be taken into account. In the rest of this section we discuss what influences the flux and how to calculate it.

10.1.1 Boundary conditions

At inflow and outflow nodes, boundary conditions are applied. We assume the flow at the inflow boundary is known, either from measurements or for example from origin-destination matrices. At the outflow boundary, we assume that either the flow is known, or there is free flow downstream.

Imposing a flow boundary condition directly leads to an ill posed problem in some situations (Helbing & Treiber, 1999). In this context ill posed means that there is no solution to the boundary value problem that both satisfies the boundary condition and

solves the conservation of vehicles equations within the computational domain. For example, if the density is very high near the inflow boundary, the problem becomes ill posed if the boundary condition prescribes a flow above the actual flow just downstream of the boundary. Similar problems occur when imposing velocity or density boundary conditions in this way. Furthermore, when prescribing both inflow and outflow, it may not be possible to guarantee conservation of vehicles.

Therefore, the minimum supply demand method is used in order to impose the boundary condition flow whenever possible, but preventing the problem from becoming ill posed. Additional cells (ghost cells) are added just upstream the inflow boundary and just downstream the outflow boundary. The boundary is then treated as a one-to-one node, see Figure 10.1(b). In the upstream ghost cell the demand is set equal to the prescribed boundary flow. If there is a prescribed boundary flow at the downstream boundary, the supply in the downstream ghost cell is set equal to this flow. If it is assumed that there is free flow downstream, the supply in the ghost cell is set to any value equal to or above the capacity of the last link. Finally, the node flux is the minimum of the supply in the cell downstream of the node and the demand in the cell upstream of the node.

10.1.2 Spatio-temporal changes in the fundamental relation

At a node the fundamental relation can change, for example due to a change in road layout such as a reduction of the number of lanes. Furthermore, it can change temporarily, for example due to weather or an accident. This can be included in the model by making the fundamental relation time and space-dependent:

$$q(\rho) = q(\rho, t, x) \tag{10.2}$$

The grid cell boundaries and the time steps are aligned with, respectively, the nodes and the moments at which the fundamental relation changes. The node is then treated as a one-to-one node, see Figure 10.1(b). The flow is not only density-dependent, but also depends on the location (grid cell j) and the time (time step k):

$$q_j^k = q(\rho_j^k, k\Delta t, j\Delta x) \tag{10.3}$$

Subsequently, downstream supply and upstream demand are calculated using (10.1) and the node flux is the minimum of both.

10.1.3 Diverges

Diverges are nodes with one incoming and multiple outgoing links, see Figure 10.1(c). A simple example is an off ramp. At a diverge turn fractions are assumed to be known. The turn fraction α_b to outgoing link b is the fraction of all vehicles arriving at the node

that want to go to link b. Turn fractions are, for example, derived from routes or origin destination matrices, they can be measured directly, or they are based on the capacity of the outgoing links. Turn fractions may be time-dependent but for readability we omit the dependence on time in the equations.

In the diverge node model, the turn fractions are used to distribute the demand over the outgoing links. Here we restrict ourselves to two outgoing links, see Figure 10.1(c). The grid cell boundaries are aligned with the node. The flux from the last cell of the incoming link to the first cell of both outgoing links is calculated. The procedure proposed here is also discussed in e.g., (Tampère et al., 2011). The total demand δ and the supplies of the outgoing cells σ_{b_1} and σ_{b_2} are calculated using (10.1). We assume that vehicles exit in a first in first out (FIFO) sequence and vehicles may be delayed by their leaders irrespective of their destination. Therefore, if the inflow into one outgoing cell is constrained by the available supply, also the inflow into the other outgoing cell is constrained. Consequently, the flux over the node is not only restricted by the demand and supply, it is also restricted by the turn fractions:

$$f_{b_1} = \alpha_{b_1} f \leq \sigma_{b_1}, \quad f_{b_2} = \alpha_{b_2} f \leq \sigma_{b_2}, \quad f = f_{b_1} + f_{b_2} \leq \delta_a \tag{10.4}$$

with f the total flux and f_{b_1} and f_{b_2} the flux to cell b_1 and b_2, respectively. Combining (10.4) into one equation yields the flux to link b_1:

$$f_{b_1} = \alpha_{b_1} f = \alpha_{b_1} \min\left(\frac{\sigma_{b_1}}{\alpha_{b_1}}, \frac{\sigma_{b_2}}{\alpha_{b_2}}, \delta_a\right) \tag{10.5}$$

The flux to link b_2 can be found similarly and both fluxes are rewritten:

$$f_{b_1} = \min\left(\beta_{b_1}, \beta_{b_2}, 1\right) \alpha_{b_1} \delta_a, \quad f_{b_2} = \min\left(\beta_{b_1}, \beta_{b_2}, 1\right) \alpha_{b_2} \delta_a \tag{10.6a}$$

with reduction factors:

$$\beta_{b_1} = \frac{\sigma_{b_1}}{\alpha_{b_1} \delta_a}, \quad \beta_{b_2} = \frac{\sigma_{b_2}}{\alpha_{b_2} \delta_a} \tag{10.6b}$$

To summarize, the diverge node model consists of (10.6) together with the demand and supply as defined in (10.1).

10.1.4 Merges

Merges are nodes with multiple incoming and one outgoing link, see Figure 10.1(d). A simple example is an on ramp. In the case of a merge some extra modeling decisions need to be made. They are related to which of the incoming roads gets priority. Cassidy & Ahn (2005); Bar-Gera & Ahn (2010) show that at a merge, drivers give priority following some fixed merge ratio. The merge ratio might be time-dependent (e.g., high in the morning peak, low in the afternoon peak), but does not depend on the actual flow. The fixed merge ratio can result from specific traffic regulations imposed

(priority rules), which are sometimes enforced by geometrical measures (e.g., lane markings). Unless such local priority rules are explicitly known, there are different methods for estimating priority ratios. They are for example based on the capacity of the incoming links or directly on flow measurements. Since we focus on an appropriate macroscopic representation and not on the underlying microscopic drive behavior, we assume the merge priority ratios to be known and we describe how they can be used in merge modeling. We summarize the discrete model in Eulerian coordinates that was presented before in slightly different versions by several authors such as Daganzo (1995a); Lebacque (1996, 2005); Tampère et al. (2011).

We only discuss how to model a merge with two incoming links, see Figure 10.1(d). Again, grid cell boundaries are aligned with the node. The flux from the last cell of both incoming links to the first cell of the outgoing link is calculated. Demand and supply are calculated using (10.1). The merge priority ratio for link a_1 is $\gamma_{a_1} \in [0,1]$. A high merge priority ratio means that vehicles from incoming link a_1 usually get priority over vehicles from link 2. The merge priority ratio for link a_2 is $\gamma_{a_2} = 1 - \gamma_{a_1}$. The merge priority ratio is used to distribute the available supply of link 3 over the incoming links. This may lead to an underutilization of the outgoing links. This is for example the case if the demand from incoming link a_1 is satisfied but the demand from incoming link a_2 is not, while furthermore the supply is not fully utilized either. In such a case, the remaining supply is assigned to the incoming link of which the demand is not satisfied, a_1 in the example. Tampère et al. (2011) show that this leads to the following fluxes over the merge node:

$$f_{a_1} = \min\left(\beta_{a_1}\sigma_b, \delta_{a_1}\right), \quad f_{a_2} = \min\left(\beta_{a_2}\sigma_b, \delta_{a_2}\right) \tag{10.7a}$$

with reduction factors:

$$\beta_{a_1} = \max\left(\gamma_{a_1}, 1 - \frac{\delta_{a_2}}{\sigma_b}\right), \quad \beta_{a_2} = \max\left(\gamma_{a_2}, \left(1 - \frac{\delta_{a_1}}{\sigma_b}\right)\right) \tag{10.7b}$$

To summarize, the merge node model consists of (10.7) together with the demand and supply as defined in (10.1).

10.2 Multi-class node models

We extend the node models from the previous section to multi-class node models. For application in the minimum supply demand method for nodes, only the last cell of the incoming link(s) and the first cell of the outgoing link(s) are used in this procedure. The methods proposed here can be applied to Fastlane but also to any other multi-class model that is contained in the generalized model in Chapter 5.

10.2.1 One-to-one node

In the case of a one-to-one node (with e.g., a change in the fundamental relation or a boundary node), the effective demand and supply are equal to the mixed-class demand and supply (10.1). Subsequently, the class-specific demands, supplies and fluxes are calculated as in the multi-class minimum supply demand method for homogeneous roads, see Section 9.1.

10.2.2 Diverge node

In the case of a diverge, the turn fractions may be different for each vehicle class. The effective total demand δ_a and effective cell specific supplies σ_{b_1} and σ_{b_2} are calculated as in the multi-class minimum supply demand method for homogeneous roads (9.1). The effective demands and supplies are distributed over classes similar to the distribution for a homogeneous road (9.3):

$$\delta_{u,a} = \lambda_{u,a}\delta_a, \quad \sigma_{u,b_1} = \lambda_{u,a}\sigma_{b_1}, \quad \sigma_{u,b_2} = \lambda_{u,a}\sigma_{b_2} \tag{10.8}$$

with the share as in (9.2). Subsequently, the class-specific demand is distributed over the outgoing cells using turn fractions, similar to the distribution for mixed-class:.

$$\delta_{u,b_1} = \alpha_{u,b_1}\delta_{u,a}, \quad \delta_{u,b_2} = \alpha_{u,b_2}\delta_{u,a} \tag{10.9}$$

with turn fraction α_{u,b_1} the fraction of vehicles of class u that wants to go to link b_1. $\alpha_{u,b_2} = a - \alpha_{u,b_1}$ is the remaining fraction of vehicles of class u, they will go to link b_2. We now calculate the class flux to link b_1 without assuming FIFO:

$$f^*_{u,b_1} = \frac{1}{\eta_{u,a}} \min(\delta_{u,b_1}, \sigma_{u,b_1}) = \frac{\alpha_{u,b_1}}{\eta_{u,a}} \min\left(\delta_u, \frac{\sigma_{u,b_1}}{\alpha_{u,b_1}}\right) \tag{10.10}$$

The next step is to introduce FIFO for the different directions. This implies that vehicles can not overtake a vehicle of the same class in order to go to a different outgoing link (just as in the mixed-class node model). However, vehicles can overtake vehicles of other classes, which is a reasonable assumption if velocities are unequal. The class-specific flux to cell b_1 is similar to the mixed-class flux (10.5):

$$f_{u,b_1} = \frac{\alpha_{u,b_1}}{\eta_{u,a}} \min\left(\delta_u, \frac{\sigma_{u,b_1}}{\alpha_{u,b_1}}, \frac{\sigma_{u,b_2}}{\alpha_{u,b_2}}\right) \tag{10.11}$$

The class-specific flux to cell b_2 can be found similarly and both fluxes are rewritten:

$$f_{u,b_1} = \min\left(\beta_{u,b_1}, \beta_{u,b_2}, 1\right) \frac{\alpha_{u,b_1}}{\eta_{u,a}}\delta_u, \quad f_{u,b_2} = \min\left(\beta_{u,b_1}, \beta_{u,b_2}, 1\right) \frac{\alpha_{u,b_2}}{\eta_{u,a}}\delta_u \tag{10.12}$$

with reduction factors:

$$\beta_{u,b_1} = \frac{\sigma_{u,b_1}}{\alpha_{u,b_1}\delta_u}, \quad \beta_{u,b_2} = \frac{\sigma_{u,b_2}}{\alpha_{u,b_2}\delta_u} \tag{10.13}$$

In some cases it may be an unreasonable assumption the class-specific flows are unconstrained by the class-specific flows of other classes. This is for example the case if velocity differences are negligible and there is little possibility to overtake. In such a case the method may be more accurate if FIFO for the different classes is also included in the node model by introducing more reduction factors.

10.2.3 Merge node

The node model for a multi-class merge is relatively straightforward. First, the effective fluxes f_{a_1} and f_{a_2} from cell a_1 and cell a_2, respectively, to the outgoing cell are calculated just as in the mixed-class case (10.7a), (10.7b). The effective fluxes are then distributed over the classes using the shares as in the multi-class minimum supply demand method for homogeneous roads (9.2):

$$f_{u,a_1} = \lambda_{u,a_1} f_{a_1}, \quad f_{u,a_2} = \lambda_{u,a_2} f_{a_2} \tag{10.14}$$

We note that this model uses the assumption that the merge priority rules are equal for all classes. It could be studied further whether this is a reasonable assumption.

10.3 Nodes in the Lagrangian formulation

We introduce a continuous node model in Lagrangian formulation. It uses sinks and sources. It is found that the continuous model is not suitable to discretize directly. Therefore, in the next section, we propose an alternative discretization of the Lagrangian node model.

10.3.1 Sink and source terms

Sinks and sources form the basis of the Lagrangian node model. We derive a conservation equation with sinks and sources in the Lagrangian coordinate system. Therefore, we first introduce its Eulerian formulation which is easier to understand intuitively. The conservation of vehicles equation in Eulerian formulation is rewritten to include a sink/source term:

$$\frac{\partial \rho}{\partial t} + \frac{\partial q}{\partial x} = g(t,x) \tag{10.15}$$

The term $g(t,x) = g_{\text{source}}(t,x) - g_{\text{sink}}(t,x)$ denotes the net time and space-dependent inflow in vehicles per second and per meter. However, we assume that the source is located at a fixed point in space. That is, the length of the ramp is not taken into account but it is set to zero. This is consistent with the node models in the previous sections. Assuming an infinite long road with a ramp or boundary at x_{node} the source $g(t,x)$ can now be written as:

$$g(t,x) = q_{\text{inflow}}(t,x_{\text{node}})h(x) \tag{10.16}$$

with $q_{\text{inflow}}(t,x_{\text{node}})$ the inflow from the ramp or boundary in vehicles per second. At a merge or inflow boundary, there is a net source and $q_{\text{inflow}} > 0$, at a diverge or outflow boundary, there is a net sink and $q_{\text{inflow}} < 0$. In (10.16), h (with unit m^{-1}) can be any function with $\int_{x=-\infty}^{\infty} h(x)\mathrm{d}x = 1$. For example, in the following we use the delta-Dirac function which can loosely be thought of as:

$$h(x) = \delta(x) = \begin{cases} 0 & \text{for } x \neq 0, \\ \infty & \text{for } x = 0, \end{cases} \quad \text{with} \quad \int_{x=-\infty}^{\infty} \delta(x)\,\mathrm{d}x = 1. \tag{10.17}$$

For a rigorous definition of the delta-Dirac function we refer to any calculus or analysis textbook. Alternatively, if one wants to take into account the physical length of the on-ramp $h(x)$ can for example be defined as a block function.

10.3.2 Sink and source terms in Lagrangian formulation

We derive the Lagrangian conservation equation with source term in a way similar to the derivation of the Lagrangian conservation equation in Section 6.1. An alternative graphical derivation is proposed in the next subsection. The graphical derivation is more intuitive, but mathematically less rigorous. In the derivation we apply the same definitions as in Section 6.1. We recall the definition of spacing:

$$s = \frac{1}{\rho} \tag{10.18}$$

the Lagrangian time derivative:

$$\frac{\mathrm{D}}{\mathrm{D}t} = \frac{\partial}{\partial t} + v\frac{\partial}{\partial x} \tag{10.19}$$

and the spacing expressed as partial derivative:

$$s = -\frac{\partial x}{\partial n} \tag{10.20}$$

Substituting the definition of spacing (10.18) into the Eulerian conservation equation

with source term (10.15) and applying the quotient rule gives:

$$\frac{\partial}{\partial t}\left(\frac{1}{s}\right)+\frac{\partial}{\partial x}\left(\frac{v}{s}\right)=g(t,x) \quad \Rightarrow \quad -\frac{1}{s^2}\frac{\partial s}{\partial t}+\frac{1}{s}\left(s\frac{\partial v}{\partial x}-v\frac{\partial s}{\partial x}\right)=g(t,x) \tag{10.21}$$

Multiplying both sides with s^2 and substituting the Lagrangian time derivative (10.19) gives:

$$\frac{\partial s}{\partial t}-s\frac{\partial v}{\partial x}+v\frac{\partial s}{\partial x}=s^2g(t,x) \quad \Rightarrow \quad \frac{\mathrm{D}s}{\mathrm{D}t}-s\frac{\partial v}{\partial x}=s^2g(t,x) \tag{10.22}$$

Finally, (10.20) is substituted to find the Lagrangian conservation equation with source term:

$$\frac{\mathrm{D}s}{\mathrm{D}t}+\frac{\partial v}{\partial n}=s^2g(t,x) \tag{10.23}$$

10.3.3 Graphical derivation and interpretation of sink and source terms

We derive the Lagrangian conservation equation with source term (10.23) in an alternative, graphical way. The graphical derivation is similar to the graphical derivation of the conservation equation in Lagrangian coordinates in Section 6.2.2.

In Figure 10.2 a (t,x) plane with some vehicle trajectories is shown. The box is a platoon of vehicles followed over time Δt. Initially (at t^{old}), the platoon contains Δn^{old} vehicles. During the time interval $\Delta n_{\mathrm{source}}$ vehicles enter the road, e.g., via an on ramp. Finally (at t^{new}), the platoon contains $\Delta n^{\mathrm{new}}=\Delta n^{\mathrm{old}}+\Delta n_{\mathrm{source}}$ vehicles. The number of vehicles that has entered the platoon is determined by the inflow rate per meter $g(x,t)$, the initial length of the platoon $s^{\mathrm{old}}\Delta n^{\mathrm{old}}$ and the duration Δt:

$$\Delta n_{\mathrm{source}}=g(x(n),t)s^{\mathrm{old}}\Delta n^{\mathrm{old}}\Delta t \tag{10.24}$$

We note that the source term g has the dimension $(m\cdot s)^{-1}$. This implies that the source is not located at one point in space, but it has a certain length. The final length of the platoon $s^{\mathrm{new}}\Delta n^{\mathrm{new}}=\int_{n_{\mathrm{first}}}^{n_{\mathrm{last}}}s(t^{\mathrm{new}},n)\,\mathrm{d}n$ is determined by its initial length $s^{\mathrm{old}}\Delta n^{\mathrm{old}}=\int_{n_{\mathrm{first}}}^{n_{\mathrm{last}}}s(t^{\mathrm{old}},n)\,\mathrm{d}n$ and the distances travelled by the first vehicle in the platoon $v_{\mathrm{first}}\Delta t=\int_{t^{\mathrm{old}}}^{t^{\mathrm{new}}}s(t,n_{\mathrm{first}})\,\mathrm{d}t$ and the last vehicle in the platoon $v_{\mathrm{last}}\Delta t=\int_{t^{\mathrm{old}}}^{t^{\mathrm{new}}}s(t,n_{\mathrm{last}})\,\mathrm{d}t$:

$$s^{\mathrm{new}}\Delta n^{\mathrm{new}}=s^{\mathrm{old}}\Delta n^{\mathrm{old}}+v_{\mathrm{first}}\Delta t-v_{\mathrm{last}}\Delta t \tag{10.25}$$

Substituting $n_{\mathrm{last}}=n_{\mathrm{first}}+\Delta n_{\mathrm{source}}$ and rearrangement gives:

$$\begin{aligned} & s^{\mathrm{new}}(\Delta n^{\mathrm{old}}+\Delta n_{\mathrm{source}})=s^{\mathrm{old}}\Delta n^{\mathrm{old}}+v_{\mathrm{first}}\Delta t-v_{\mathrm{last}}\Delta t \\ \Rightarrow \quad & (s^{\mathrm{new}}-s^{\mathrm{old}})\Delta n^{\mathrm{old}}+(v_{\mathrm{last}}-v_{\mathrm{first}})\Delta t=-s^{\mathrm{new}}\Delta n_{\mathrm{source}} \end{aligned} \tag{10.26}$$

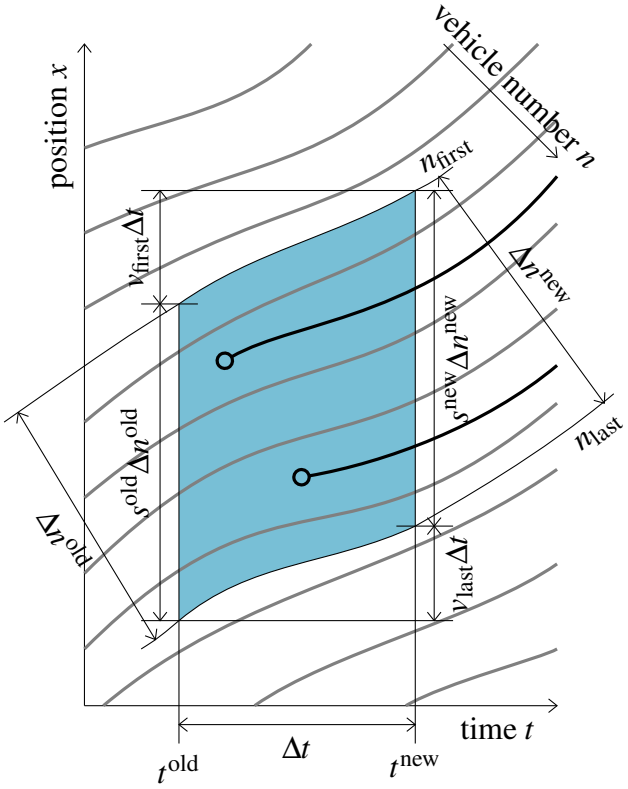

Figure 10.2 *A control volume that follows a platoon of Δn vehicles over a time Δt. The dark trajectories indicate vehicles entering the platoon, for example via an on ramp. This graph is applied to derive the Lagrangian conservation equation with source term.*

Substituting the source term (10.24) and dividing both sides by $\Delta n^{\text{old}}\Delta t$ gives:

$$\begin{aligned}(s^{\text{new}}-s^{\text{old}})\Delta n^{\text{old}}+(v_{\text{last}}-v_{\text{first}})\Delta t &= -s^{\text{new}}g(x(n),t)s^{\text{old}}\Delta n^{\text{old}}\Delta t \\ \Rightarrow \quad \frac{s^{\text{new}}-s^{\text{old}}}{\Delta t}+\frac{v_{\text{last}}-v_{\text{first}}}{\Delta n^{\text{old}}} &= -s^{\text{new}}s^{\text{old}}g(x(n),t) \qquad (10.27)\end{aligned}$$

Finally, we take an infinitesimal control volume, i.e. we let both $\Delta n_1 \to 0$ and $\Delta t \to 0$. Furthermore, we apply the definition of the derivative (6.13) and find the Lagrangian conservation equation with source term (10.23).

10.3.4 Discretization of sinks and sources in upwind method

The Lagrangian conservation equation with source term (10.23) may be discretized using an upwind method similar to the approach for homogeneous roads (8.5) which is introduced hereafter. In the next section we show that this approach has some disadvantages and we propose an alternative approach. Applying the upwind method gives:

$$s_i^{k+1} = s_i^k + \frac{\Delta t}{\Delta n}\left(v_{i-1}^k - v_i^k\right) + \Delta t\,(s_i^k)^2 g_i^k \qquad (10.28)$$

with $(f_{\text{source}})_i^k$ the inflow in $(m \cdot s)^{-1}$ at the position of the i-th vehicle group at time $t = k\Delta t$. Using (10.24) the source term $(f_{\text{source}})_i^k$ can be approximated with:

$$(g_{\text{source}})_i^k \approx \frac{(\Delta n_{\text{source}})^k}{\Delta n^k \Delta t s_i^k} \tag{10.29}$$

Combining (10.28) and (10.29) gives:

$$s_i^{k+1} = (1+\omega^k)s_i^k + \frac{\Delta t}{\Delta n}\left(v_{i-1}^k - v_i^k\right) \tag{10.30}$$

with $\omega^k = (\Delta n_{\text{source}})^k / \Delta n^k$ which can be interpreted as a source fraction. It is the relative growth of the number of vehicles in the vehicle group due to the source. For example, at an on ramp the source fraction may be $\omega = 0.1$ indicating that for each 10 vehicles passing the on ramp on the main road, 1 vehicle enters the road from the on ramp. At an off ramp the source fraction may be $\omega = -0.2$ indicating that for each 5 vehicles arriving at the off ramp, 1 takes the off ramp, the others continue on the main road.

10.4 Discretization of nodes in upwind method

With the proposed discretization (10.30) of the conservation equation with source term, two problems occur: 1) the number of vehicles in the vehicle group changes, and 2) if the fundamental relation changes during a time step, for example because the number of lanes changes as the group passes a ramp, this is not accounted for in the discretization. The first issue is related to the first term on the right hand side of (10.30): if the source fraction $\omega^k = (\Delta n_{\text{source}})^k / \Delta n^k$ is nonzero, the number of vehicles in the group changes. This can be solved with a proper approach for vehicle discretization. The second issue relates to time discretization. Our solution of both issues is discussed below.

10.4.1 Vehicle discretization

With the simple upwind discretization proposed above (10.30), the number of vehicles in one vehicle group changes at nodes. Therefore, the upwind method (8.5) is applied on the homogeneous parts of the road, but we develop another discretization method for the nodes. To keep the number of vehicles in one vehicle group constant there are two options at nodes:

1. Collect all vehicle groups and form new groups. The new groups may include vehicles from multiple vehicle groups on all incoming links. See Figure 10.3(a).
2. Keep the vehicle groups as they are. Only full vehicle groups travel over the node. They may have to wait for other full vehicle groups. See Figure 10.3(b).

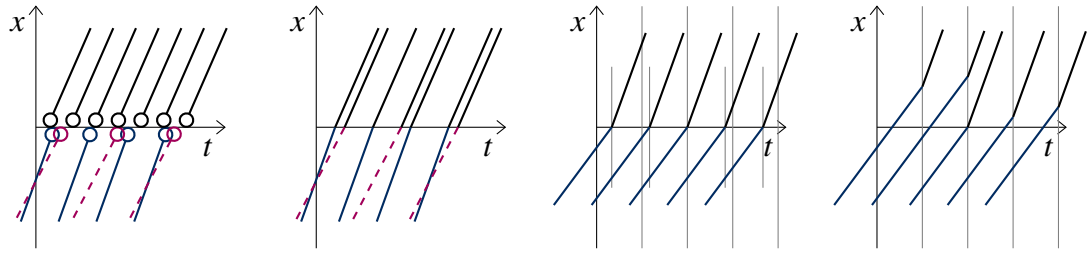

(a) Merge with vehicle discretization with disaggregation and reformation of groups.

(b) Merge with vehicle discretization with only full groups.

(c) Change in fundamental relation and time discretization with intermediate time steps.

(d) Change in fundamental relation and time discretization with change at beginning of time step.

Figure 10.3 *Different types of vehicle and time discretization illustrated with trajectories over a merge node and a node with a change in the fundamental relation. Colors and line styles indicate trajectories on different links (incoming and outgoing).*

The first option is computationally intensive and more difficult to implement. However, the results are expected to be more accurate. The inaccuracies of the second method are expected to be small. In Section 10.5 we analyze the accuracy of this method.

10.4.2 Time discretization

Regarding the time discretization similar approaches can be taken. Here the issue is that when a vehicle group reaches a node, this is usually not exactly at the beginning of a time step. Therefore, it crosses the node during a time step. Which implies that conditions for this vehicle groups and surrounding vehicle groups change during the time step. For example, the fundamental relation changes or a new leading vehicle group enters the road from an on ramp. Again there are two possible approaches:

1. Add an intermediate time step whenever a vehicle group reaches a node during a time step. The conditions change from this intermediate time step onward. See Figure 10.3(c).
2. Wait until the beginning of the new time step to apply new conditions. Old conditions hold until the end of the time step in which the node is reached. See Figure 10.3(d).

Again, the first option is computationally intensive and more difficult to implement. The results are expected to be more accurate but the inaccuracies of the second method are expected to be small. In Section 10.5 we analyze the accuracy of this method.

In the remaining of this section both for the vehicle discretization and the time discretization we apply the second (less accurate but simpler) approach. This implies that only full vehicle groups cross nodes and they are not disaggregated. Any new conditions only apply from the beginning of the time step after the node was crossed. We discuss how to apply this to different types of nodes. Furthermore, in the next section we apply the methods in simulations and show that the results are accurate enough.

10.4.3 One-to-one node

We have already discussed how a node with a change in the fundamental relation can be discretized: after a vehicle group has reached the node, the new conditions only hold from the beginning of the next time step. Similarly, if there is a temporal change in the fundamental relation, it only takes effect from the beginning of the next time step. Therefore, the new position of a vehicle group is computed as follows:

$$x_i^{k+1} = x_i^k + \Delta t v_i^k \tag{10.31}$$

with $v_i^k = v(s_i^k)$ the velocity obtained from the spacing s_i^k and the fundamental relation with parameters that hold at location $x = x_i^k$ at time $t = \Delta t k$.

10.4.4 Inflow node

At an inflow boundary we assume the number of vehicles arriving at the inflow boundary per time unit δ_{inflow} is prescribed. In the discretization, the number of vehicles waiting to enter the network N_{waiting} is counted:

$$N_{\text{waiting}}^{k+1} = N_{\text{waiting}}^k + \int_{t=k\Delta t}^{(k+1)\Delta t} \delta_{\text{inflow}}(t)\mathrm{d}t \tag{10.32}$$

As soon as the cumulative inflow has reached the size of a vehicle group (i.e. if $N_{\text{waiting}}^{k+1} \geq \Delta n$), a vehicle group is formed at the inflow boundary and released at the beginning of the next time step $k+1$. The distance between the position of the previously last group x_{i-1}^k and the location of the inflow node x_{inflow} is used to calculate the spacing: $s_i^k = (x_{i-1}^k - x_{\text{inflow}})/\Delta n$. In turn, the spacing is used to calculate the velocity v_i^k (using the fundamental relation) and the new position (using (10.31)). Furthermore, the number of waiting vehicles is decreased: $N_{\text{waiting}}^{k+1} := N_{\text{waiting}}^{k+1} - \Delta n$.

This discretization implies the following assumption on the inflow demand. In the case of a high inflow demand δ_{inflow} or (heavy) congestion just downstream of the inflow boundary, not all arriving vehicle groups may be able to enter the computational domain. In this approach, those groups are 'stored' and will enter the domain as soon as it is possible. This implies that even after a decrease in the demand, the actual inflow may remain at capacity flow for a while. For example, this happens in one of the test cases in Section 10.5. In our view, this is a realistic inflow model, but other choices may be made as well. For example, the 'stored' groups may be removed after a change in the demand. This will result in an immediate change in the actual inflow.

10.4.5 Outflow node

The outflow is restricted by a given downstream supply (see Section 10.1.1). The supply constraint can be active ($\sigma_{\text{outflow}} \leq q_{\text{cap}}$) or inactive ($\sigma_{\text{outflow}} > q_{\text{cap}}$). The spacing

of the most downstream vehicle group i at the beginning of time step k is computed using the (in)active supply constraint:

$$s_i^k = \begin{cases} \infty & \text{if } \sigma_{\text{outflow}} > q_{\text{cap}} \quad (10.33a) \\ s_{\text{outflow}} \text{ with } \sigma_{\text{outflow}} = \dfrac{v(s_{\text{outflow}})}{s_{\text{outflow}}} & \text{if } \sigma_{\text{outflow}} \leq q_{\text{cap}} \quad (10.33b) \end{cases}$$

In the second case, the outflow is constrained. We assume that the downstream region (since $\sigma_{\text{outflow}} \leq q_{\text{cap}}$) is in congestion and thus (10.33b) has a unique solution. This spacing is in turn used together with the fundamental relation to calculate the velocity v_i^k, which then leads to the new position of vehicle group i using (10.31).

10.4.6 Diverge node

At a diverge (one to two node) the turn fraction α is used to determine to which outgoing link a vehicle group will travel. Therefore, each time step either all vehicles go to one link, or they all go to the other link. As a result, on the time scale of one time step the turn fraction realized by the discrete model is always 0 or 1. However, the goal is to reproduce the turn fraction on a larger time scale of many (say, at least 10 or 20) time steps. Therefore, each time step the actual turn fraction of the last M vehicle groups is calculated:

$$\alpha_1^{M_\alpha} = \frac{\text{number of groups out of the last } M_\alpha \text{ groups that travelled to link } b_1}{M_\alpha} \quad (10.34)$$

If this is below the prescribed turn fraction α_{b_1} the next group i travels to link b_1, otherwise the next group travels to link b_2. Once it is known to which outgoing link a vehicle group will travel, the distance between the position of the last group in the outgoing link at x_{i-1}^k and the current position x_i^k is used to calculate the spacing: $s_i^k = (x_{i-1}^k - x_{i-1}^k)/\Delta n$. In turn, the spacing is used to calculate the velocity v_i^k (using the fundamental relation) and the new position (using (10.31)).

For this method to work properly, the value of M_α has to be chosen appropriately. The appropriate value of M_α depends largely on the value of the turn fraction, on how accurately it needs to be reproduced and on possible changes in the turn fraction and how quickly the simulation should react. For example, if the turn fraction is $1/2$ and does not change, $M_\alpha = 1$ would suffice, just as any other odd valued M_α. However, if the turn fraction can be written as an irreducible fraction with a large denominator, M_α needs to be large. For example, if $\alpha_1 = 23/100$ we need $M_\alpha = 99$ to reach this turn fraction numerically. However, if it would suffice to have a realized turn fraction of $\alpha_1^{M_\alpha} = 1/4$, then $M_\alpha = 3$ would suffice. Furthermore, the value of M_α should not be too large in order to allow for quick adaptation if the turn fraction α_1 changes over time.

We note that it is not necessary to take explicitly into account the FIFO rule and the delay by vehicles going to another (congested) link. Unlike in the minimum supply

demand method, the approach proposed above takes this delay into account naturally. Furthermore, it is relatively straightforward to replace the turn fractions by routes. In that case each vehicle groups that enters the network gets assigned a certain route which describes which link to take at the diverges. This adaptation is much more complicated to apply in the minimum supply demand method. In Section 10.5 we show the influence of the choice of M_α on the realized turn fractions in a simple test problem.

10.4.7 Merge node

In the discretization approach we use the merge priority ratio γ to determine whether or not a vehicle group from one of the two incoming links can continue on the outgoing link. Therefore, first it is determined which of the two most downstream vehicle groups should get priority over the other. Without loss of generality, let us assume that the vehicle group from incoming link a_1 (i_{a_1}) has priority over the vehicle group from the other incoming link (i_{a_2}). We will discuss later how to determine which group has priority. Secondly, the available space upstream and downstream of the node is distributed over the most downstream vehicle groups in the incoming links. The distribution is illustrated in Figure 10.4 and described in more detail hereafter.

The available space d (in meters $\times$ number of lanes) upstream and downstream of the node is computed:

$$d_{a_1} = (x_{\text{node}} - x^k_{i_{a_1}})L_{a_1}, \quad d_{a_2} = (x_{\text{node}} - x^k_{i_{a_2}})L_{a_2}, \quad d_b = (x^k_{i_b} - x_{\text{node}})L_b \tag{10.35}$$

with $x^k_{i_{a_1}}$ the position of the most downstream group at incoming link a_1, $x^k_{i_{a_2}}$ the position of the most downstream group at incoming link a_2, and $x^k_{i_b}$ the position of the most upstream group at the outgoing link, see Figure 10.4(a). The available space (10.35) is now distributed over the incoming vehicle groups i_{a_1} and i_{a_2}. Therefore, the following rationale is applied:

1. Each vehicle group gets at least all the available space at its own link.
2. The vehicle group with priority gets at least critical spacing, if the available space permits.
3. The vehicle group without priority gets all remaining space.

This leads to the following:

$$s^k_{i,a_1} = \frac{\max\left(d_{a_1}, \min\left(\Delta n s_{\text{crit},a_1}, d_{a_1} + d_b\right)\right)}{\Delta n L_{a_1}} \tag{10.36a}$$

$$s^k_{i,a_2} = \frac{(d_{a_1} + d_{a_2} + d_b - \Delta n L_{a_1} s_{i,a_1})}{\Delta n L_{a_2}} \tag{10.36b}$$

with s_{crit,a_1} the critical spacing (per lane) at the incoming link with priority a_1. Thirdly,

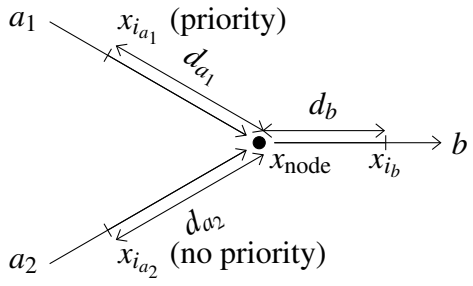

(a) Available space per link: distance between vehicle group and node.

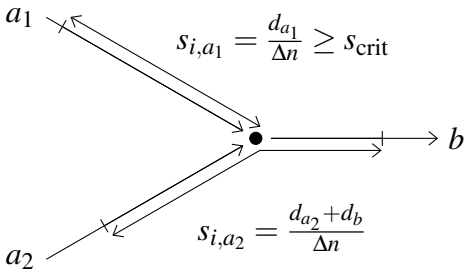

(b) Distribution of available space if group with priority is far from node.

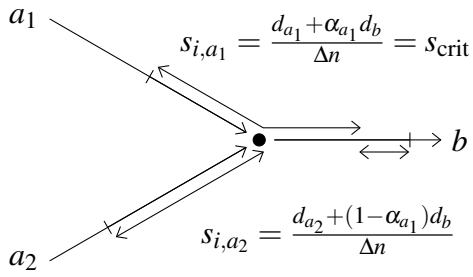

(c) Distribution of available space if group with priority is close node and downstream group is far from node.

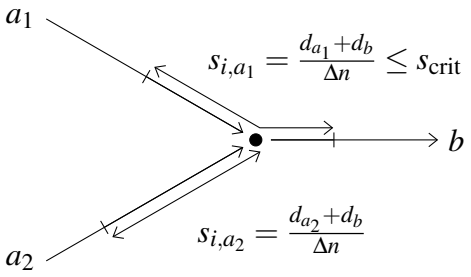

(d) Distribution of available space if group with priority and downstream group are both close to node.

Figure 10.4 *Available space per incoming and outgoing link and its distribution over both incoming vehicle groups during one time step. The distribution depends on the proximity to the node of the most downstream vehicle group at the incoming link with priority (here link a_1) and the most upstream group at the outgoing link. For readability we assume that each link has only one lane and the same fundamental relation.*

the spacings (10.36) are used to calculate the velocities v_{i,a_1}^k and v_{i,a_2}^k (using the fundamental relation) and the new positions x_{i,a_1}^{k+1} and x_{i,a_2}^{k+1} (using (10.31)).

Finally, we discuss how to determine which of the vehicle groups gets priority (group i_a in the example above). This is calculated using the actual merge ratio over the last M_γ groups passing the node:

$$\gamma_1^{M_\gamma} = \frac{\text{number of groups out of the last } M_\gamma \text{ groups that came from link 1}}{M_\gamma} \tag{10.37}$$

If this actual merge ratio is below the prescribed merge ratio ($\gamma_1^{M_\gamma} < \gamma_1$), the group from link a_1 gets priority, otherwise the group from link a_2 gets priority. The value of M_γ can be chosen on similar grounds as the value of M_α: not too small to allow for an accurate approximation of the desired turn fraction, and not too large to allow for quick adaptations. In Section 10.5 we show the influence of the choice of M_γ on the realized merge rates in a simple test problem.

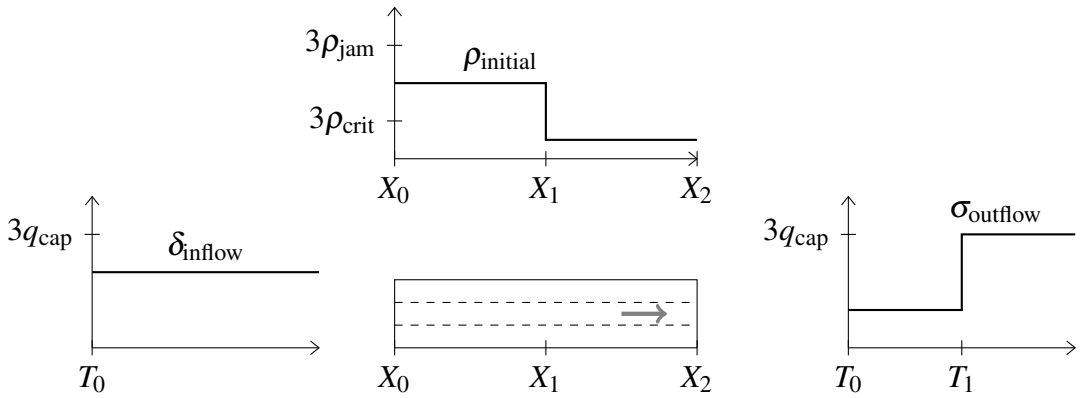

Figure 10.5 *Test layout initial and boundary conditions.*

10.5 Simulations and results

We perform simulations to compare the node discretization methods both in the minimum supply demand method and the upwind method. The simulation results for both methods are compared to each other but also to the analytical solution. Because we compare to the analytical solution we only do simulations of simple test problems for which the analytical solution can be obtained relatively easily using shock wave theory. Therefore, we do not include numerical methods for multi-class nodes in the comparison.

10.5.1 Test setup

We study four different test cases with different road layouts. The tests are designed such that the numerical solution of all types of nodes and initial and boundary conditions can be studied separately. In all tests the model parameters are taken equal to the model parameters in Chapter 8. Table 8.1 shows these parameters of the fundamental relation per lane. At locations where there are multiple lanes the fundamental relation parameters are scaled accordingly. Furthermore, the numerical parameters are the same as in the base case in Chapter 8 and 9: grid cell size $\Delta x = 100$ m and time step size $\Delta t = 3$ s. The vehicle group size depends on the number of lanes. It is chosen such that the CFL-condition is satisfied exactly, which implies $\Delta n = 5$ vehicles in two test cases (initial and boundary conditions and spatio-temporal change in fundamental relation) and $\Delta n = 7.5$ in the other two test cases (diverge and merge). To study the influence of the resolution, we repeat the simulations with higher resolution: time step size $\Delta t = 0.6$ s and vehicle groups size such that the CFL-condition is satisfied exactly ($\mu = 1$). We discuss the setup of each of the test cases below.

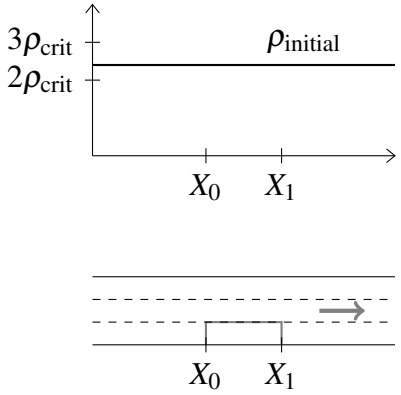

3 lanes, except for 2 lanes if $T_1 < t \leq T_2$

Figure 10.6 *Test layout change in fundamental relation.*

Initial and boundary conditions

The first test is designed to assess the numerical implementation of initial and boundary conditions, see Figure 10.5. It consists of a three lane road with inflow boundary at $x = X_0 = -1000$ m and outflow boundary at $x = X_2 = 1000$ m. There is one jump in the initial conditions at $x = X_1 = 0$ m and one jump in the outflow boundary conditions at $t = T_1 = 500$ s. The inflow boundary conditions are constant. The simulation starts at $t = T_0 = 0$ s. The following values are used:

$$\rho(x, T_0) = \begin{cases} \frac{3}{2}\rho_{\text{crit}} = 0.05\,\text{veh/m} & \text{if } x < X_1 \\ 12\rho_{\text{crit}} = 0.4\,\text{veh/m} & \text{if } x \geq X_1 \end{cases} \tag{10.38a}$$

$$\delta_{\text{inflow}}(X_0, t) = \rho(X_0) v(\rho(X_0)) = 1.35\,\text{veh/s} \tag{10.38b}$$

$$\sigma_{\text{outflow}}(X_2, t) = \begin{cases} \rho(X_2) v(\rho(X_2)) = 0.83\,\text{veh/s} & \text{if } t < T_1 \\ q_{\text{cap}} = 2.08\,\text{veh/s} & \text{if } t \geq T_1 \end{cases} \tag{10.38c}$$

The values of the initial and boundary conditions are chosen such that the downstream part of the domain ($x \geq X_1$) is initially congested and the outflow is restricted during the first part of the simulation (until $t = T_1$). This results in a congested area that travels upstream and reaches the inflow boundary conditions. Furthermore, because of congestion just downstream of the inflow boundary, the actual inflow is lower than the inflow demand. Therefore, even after the congestion has solved, the inflow will remain high (at capacity) for some time. Figure 10.9 shows the analytical solution, together with the numerical solutions, which will be discussed later.

Change in fundamental relation

The second test is designed to assess the numerical implementation of a change in the fundamental relation, see Figure 10.6. It consists of a three lane road. However, part of one lane (between $x = X_0 = 0$ m and $x = X_1 = 1000$ m) is not used during a certain

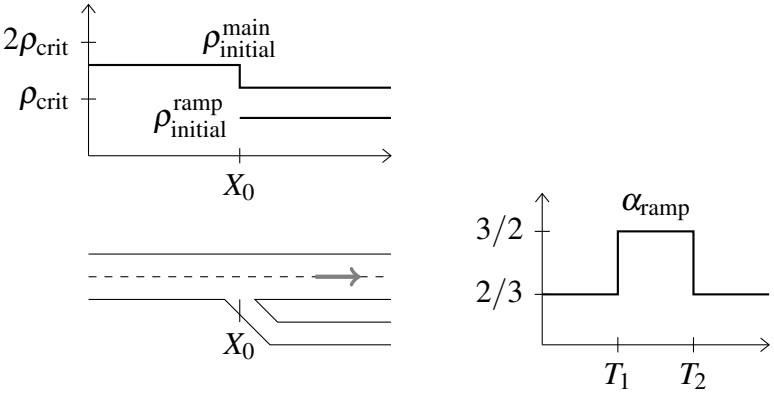

Figure 10.7 *Test layout diverge.*

time period (between $t = T_1 = 100$ and $t = T_2 = 400$ s). The initial density is constant: $\rho(x, T_0) = \frac{9}{4}\rho_{crit} = 0.075$ veh/m. The road length upstream and downstream of the lane drop are high such that the boundary conditions do not influence the solution. The simulation starts at $t = T_0 = 0$ s.

The value of the initial condition is chosen such that the three lanes can accommodate all demand and there is no congestion. However, congestion is created when the number of lanes changes to two. Congestion spills back and dissolves again after all three lanes become available again. Figure 10.10 shows the analytical solution, together with the numerical solutions, which will be discussed later.

Diverge

The third test is designed to assess the numerical implementation of a diverge, see Figure 10.7. It consists of a two lane road with a one lane off ramp that bifurcates from the main road at $x = X_0 = 0$ m. The turn fraction changes during the simulation:

$$\alpha_{ramp}(t) = \begin{cases} 0.7 & \text{if } T_1 < t \leq T_2 \\ 0.3 & \text{otherwise} \end{cases} \tag{10.39}$$

with $T_1 = 60$ s and $T_2 = 300$ s. The initial density is as follows:

$$\rho_{main}(x, T_0) = \begin{cases} \frac{3}{2}\rho_{crit} = 0.05\,\text{veh/m} & \text{if } x < X_1 \\ 0.0285\,\text{veh/m} & \text{if } x > X_1 \end{cases} \tag{10.40}$$

$$\rho_{ramp}(x, T_0) = 0.0143\text{veh/m} \tag{10.41}$$

The road upstream and downstream of the ramp and the ramp itself are long such that the boundary conditions do not influence the solution. The simulation starts at $t = T_0 = 0$ s.

The initial densities are chosen such that the density does not change as long as the turn fraction is constant. Furthermore, during the first simulation period (until $t = T_1 = 200$

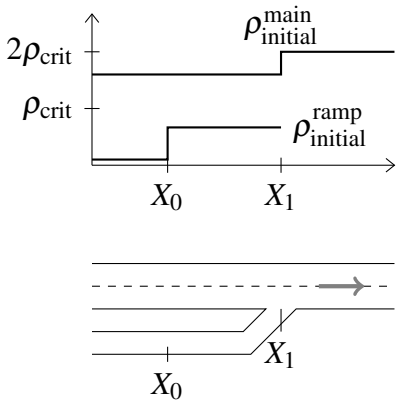

Figure 10.8 *Test layout merge.*

s) the whole computational domain is in free flow. However, after the change in the turn fraction at $t = T_1$, the off ramp can not accommodate the demand anymore and congestion sets in. Congestion spills back on the main road, also blocking vehicles that do not want to take the off ramp. After the turn fraction has returned to its original value at $t = T_2 = 1000$ s, the congestion dissolves again. Figure 10.11 shows the analytical solution, together with the numerical solutions, which will be discussed later.

For the upwind discretization of the node we need to choose a value M_α (see Section 10.4.6). We try four different values: 'very small' $M_\alpha = 2$, 'small' $M_\alpha = 5$, 'normal' $M_\alpha = 10$, 'large' $M_\alpha = 20$.

Merge

The fourth, and last, test is designed to assess the numerical implementation of a merge, see Figure 10.8. It consists of a two lane road with a one lane on ramp that merges at $x = X_1 = 0$ m. Initially, there is a high density region on the ramp just upstream of the merge until $x = X_0 = -6000$ m. Further upstream, the initial density is low. The merge ratio is $\gamma_{\text{main}} = 0.6$. The initial densities are as follows:

$$\rho_{\text{main}}(x, T_0) = \begin{cases} 1.2\rho_{\text{crit}} = 0.04\,\text{veh/m} & \text{if } x < X_1 \\ 2\rho_{\text{crit}} = 0.067\,\text{veh/m} & \text{if } x > X_1 \end{cases} \tag{10.42a}$$

$$\rho_{\text{ramp}}(x, T_0) = \begin{cases} 0.9\rho_{\text{crit}} = 0.03\text{veh/m} & \text{if } x < X_0 \\ 0.1\rho_{\text{crit}} = 0.0033\,\text{veh/m} & \text{if } x > X_0 \end{cases} \tag{10.42b}$$

The main road upstream and downstream of the merge and the ramp itself are long such that the boundary conditions do not influence the solution.

For the upwind discretization of the node we need to choose a value M_γ (see Section 10.4.7). We try four different values: 'very small' $M_\gamma = 2$, 'small' $M_\gamma = 5$, 'normal' $M_\gamma = 10$, 'large' $M_\gamma = 20$.

The initial density is chosen such that the total flow over the upstream main road and the flow over the ramp is larger than the capacity of the downstream main road. Therefore, congestion will set in upstream of the merge. However, the inflow from the ramp is lower than the initial ramp flow. It is chosen such that the congestion will dissolve again. Figure 10.12 shows the analytical solution, together with the numerical solutions, which will be discussed later.

10.5.2 Simulation results

All simulation results are shown in Figure 10.9–10.15. The same patterns can be observed in the results of the tests with normal numerical settings (initial and boundary conditions (Figure 10.9), change in fundamental relation (Figure 10.10), diverge (Figure 10.11) and merge (Figure 10.12 and 10.13). Both the solution with the minimum supply demand method and the upwind method are in general in accordance with the analytical solution. Furthermore, most results with high resolution (not shown) are closer to the analytical solution, which indicates that the numerical solution converges to the analytical solution. However, high resolution does not lead to more accurate results in the merge test case with upwind method. This is discussed in more detail later.

In the solution obtained with the minimum supply demand method there is some numerical diffusion. We have already discussed this type of numerical inaccuracy in Chapter 8 for homogeneous links. We conclude that it is not specific to the numerical methods for nodes.

In the solution obtained with the upwind method some oscillations can be seen: at the boundaries and in some regions within the domain, e.g., region 'A' in Figure 10.9(b), regions 'D' and 'E' in Figure 10.10(b) and most regions in Figure 10.11(b), 10.11(d), 10.12(b), 10.12(d). Closer observation shows that the oscillations emerge at the inflow boundary and at positions where there is a change, such as a change in the fundamental relation or a merge. They travel either upstream or downstream with the characteristics. However, the waves that form the boundaries between 2 regions travel with the correct velocity. For example, the upstream front of congestion is (almost) at the same location in the numerical solution as in the analytical solution. This indicates that 'on average' the flow in the region that exhibits oscillations is equal to the analytical flow. Furthermore, Figure 10.13 shows that increasing the resolution, leads to narrower and less pronounced oscillations. This indicates that the oscillations are a numerical artefact. However, with high resolution the numerical wave velocities do not improve: the slope of the numerically computed boundary between region F and G and, respectively, F and H remains unequal to the slope of the dashed line indicating the analytical boundary. Finally, we note that these oscillations are very similar to the oscillations that can be observed in the simulation of moving bottlenecks in the Eulerian coordinate system, such as in (Laval & Daganzo, 2006).

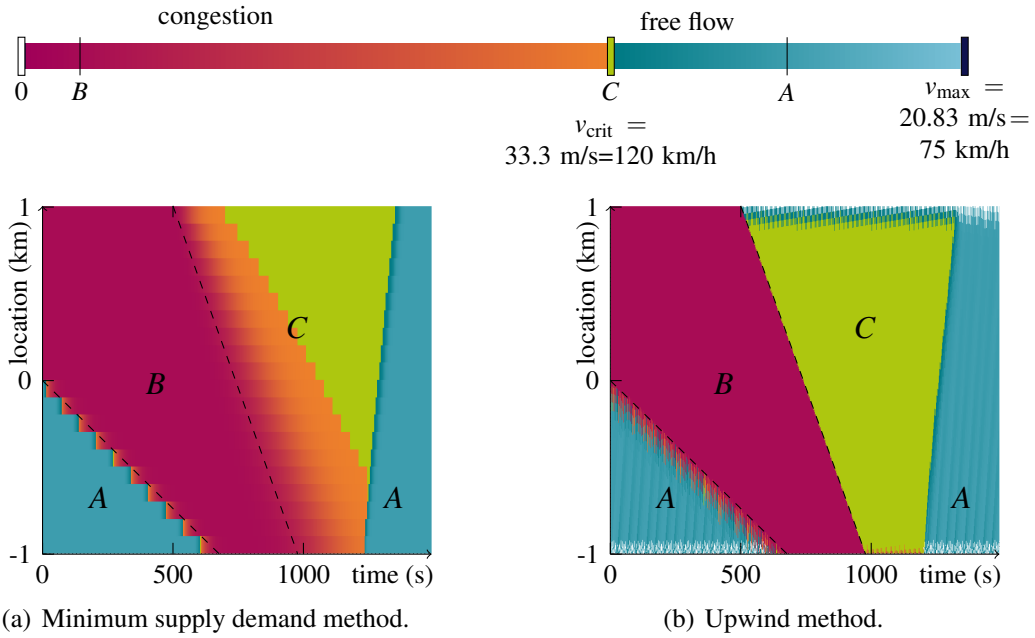

(a) Minimum supply demand method. (b) Upwind method.

Figure 10.9 *Simulation results boundary conditions. Colors indicate vehicle velocity.*

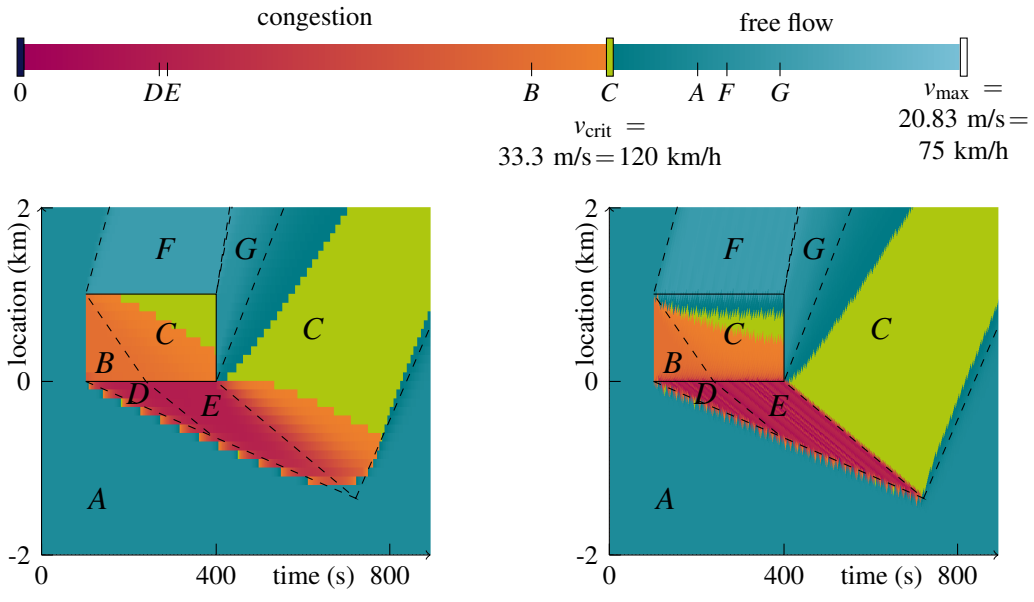

(a) Minimum supply demand method. (b) Upwind method.

Figure 10.10 *Simulation results spatio-temporal change in fundamental relation. Colors indicate vehicle velocity.*

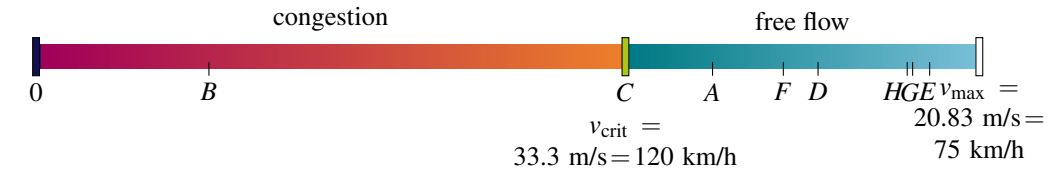

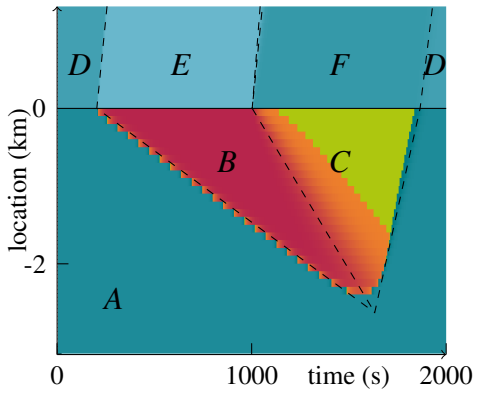

(a) Minimum supply demand method, main road.

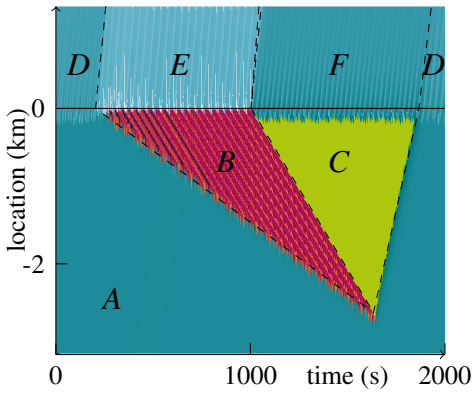

(b) Upwind method with $M_\alpha = 5$, main road.

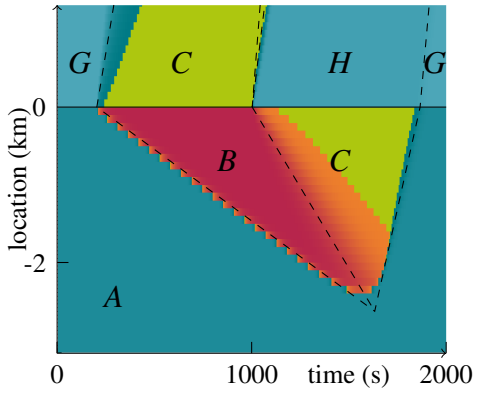

(c) Minimum supply demand method, ramp and upstream part of main road.

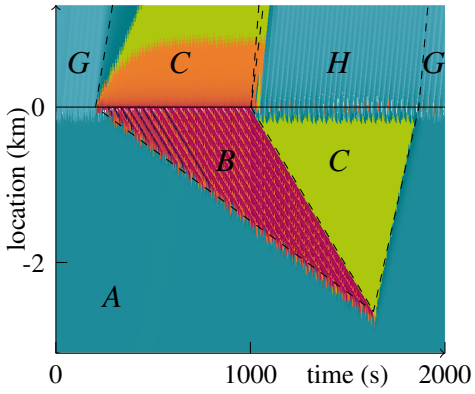

(d) Upwind method with $M_\alpha = 5$, ramp and upstream part of main road

Figure 10.11 *Simulation results diverge. Colors indicate vehicle velocity.*

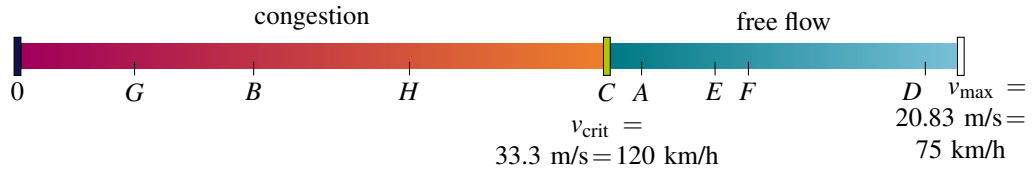

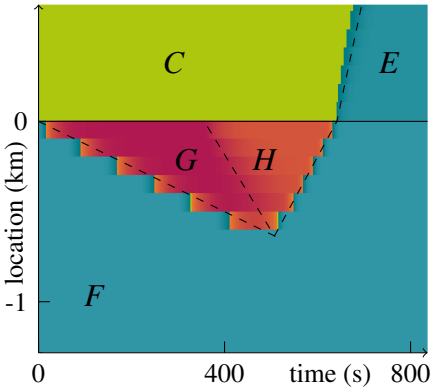

(a) Minimum supply demand method, main road.

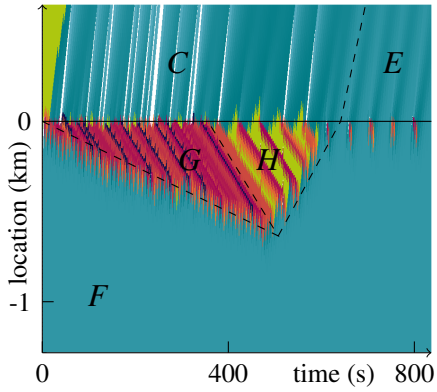

(b) Upwind method with $M_\gamma = 10$, main road.

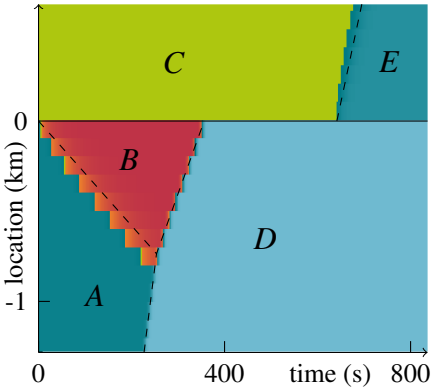

(c) Minimum supply demand method, ramp and downstream part of main road.

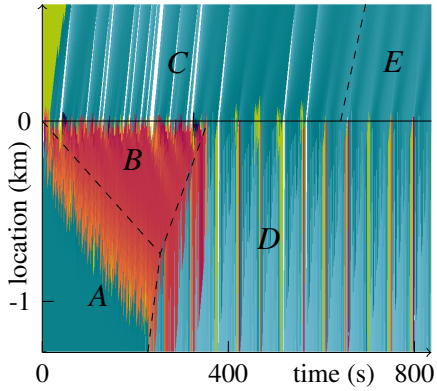

(d) Upwind method with $M_\gamma = 10$, ramp and downstream part of main road

Figure 10.12 *Simulation results merge. Colors indicate vehicle velocity.*

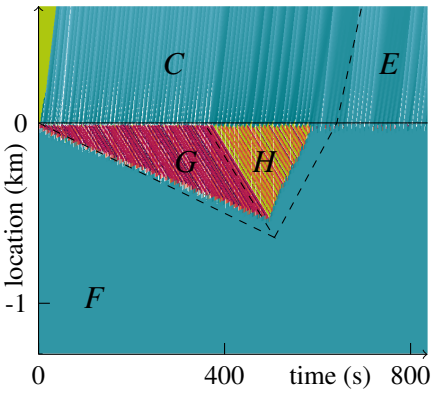

(a) Main road.

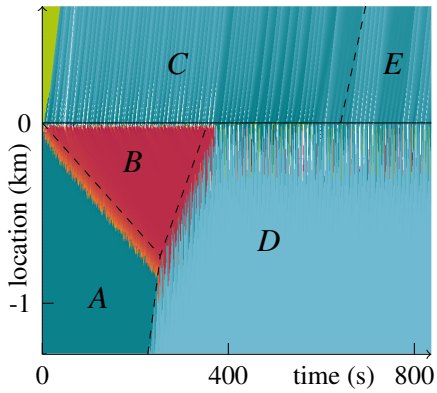

(b) Ramp and downstream part of main road

Figure 10.13 *Simulation results merge, upwind method with $M_\gamma = 10$, high resolution ($\Delta t = 0.6$ s, $\Delta n = 1$ veh). Colors indicate vehicle velocity, see legend of Figure 10.12.*

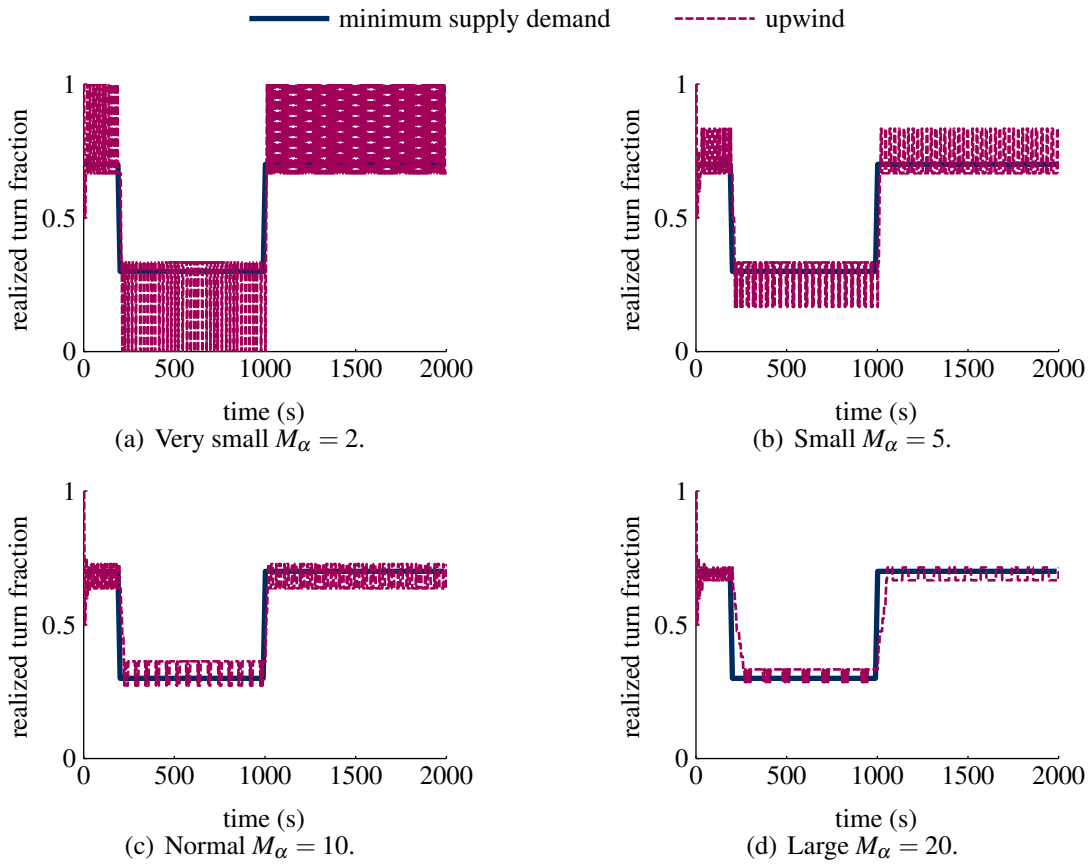

(a) Very small $M_\alpha = 2$.
(b) Small $M_\alpha = 5$.
(c) Normal $M_\alpha = 10$.
(d) Large $M_\alpha = 20$.

Figure 10.14 *Turn fractions realized in the diverge test problem, with different numerical methods and numerical turn fraction parameters M_α.*

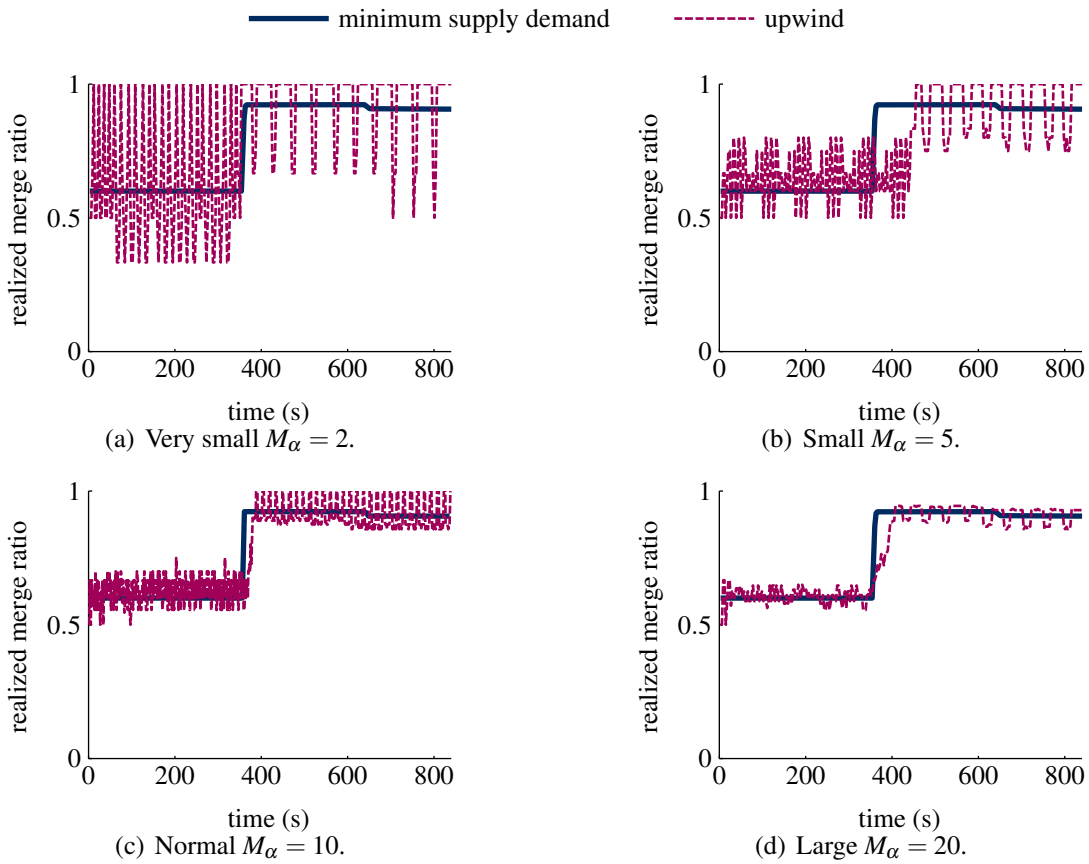

(a) Very small $M_\alpha = 2$.
(b) Small $M_\alpha = 5$.
(c) Normal $M_\alpha = 10$.
(d) Large $M_\alpha = 20$.

Figure 10.15 *Merge ratios realized in the merge test problem, with different numerical methods and numerical merge ratio parameters M_γ.*

In the diverge and the merge test problem we also study the realized turn fraction and merge ratio, respectively. The results are shown in Figure 10.14 and 10.15. The realized turn fraction and merge ratio with the minimum supply demand method are equal to the prescribed values. However, with the upwind method, the realized values depend on the number of previous groups that is taken into account when determining which outgoing link the next group will take (M_α) or determining which incoming link will get priority (M_γ). The figures show that with high values ($M_\alpha = 20$, $M_\gamma = 20$) there is a delayed response. This also influences the time it takes before congestion is dissolved. With low values ($M_\alpha = 2$, $M_\gamma = 2$) the realized turn fractions and merge ratios are not accurate. Intermediate values of $M_\alpha = 5$, $M_\alpha = 10$, $M_\gamma = 5$ and $M_\gamma = 10$ give the most accurate results.

10.6 Discussion and conclusions

In this chapter we have studied node models and their numerical implementations. Node models in Eulerian coordinates for mixed-class kinematic wave models form the basis of our node models in Lagrangian coordinates and multi-class node models. The derivation of the node model in Lagrangian coordinates includes an intuitive interpretation of the sink and source terms. The multi-class node models are discretized based on the minimum supply demand method. The discretization of the node models in Lagrangian coordinates is based on the upwind method. Until now only simple nodes, with at most two incoming and two outgoing links have been studied, including inflow and outflow boundaries. The methods may be extended to more generic nodes.

Simulations show that the discretized node models yield accurate results and largely agree with analytical results. However, oscillations are created in the upwind node discretization. They do not influence wave velocities of the primary waves (e.g., velocity with which congestion spills upstream and with which it dissolves again). However, they may be interpreted wrongly, for example as stop and go waves. Therefore, methods should be developed to smooth out the oscillations or to prevent their creation. The discretization may be improved further by including intermediate time steps and or disaggregating and re-aggregating vehicle groups as described in Section 10.4.1 and 10.4.2. Alternatively, ideas about hybrid models and their micro-macro and macro-micro interfaces may be applied to improve the discretization methods (Bourrel & Lesort, 2003; Burghout et al., 2005; Leclercq, 2007a; Laval & Leclercq, 2008). For example, applying the Green-Riemann formula can be applied in a similar way as in (Leclercq, 2007a) to discretize the nodes differently and find a more accurate solution. Finally, Jin & Zhang (2013) propose a new approach to diverges which lead to more accurate solutions in the Eulerian coordinate system. Their approach may be extend to the Lagrangian coordinate system.

Advantages of the upwind method for nodes include the more natural introduction of rules for turn fractions and priority taking at merges. Furthermore, extensions of

the method to include routes are more straightforward than with the minimum supply demand method. Moreover, upwind methods for nodes are needed for simulation tools which apply the upwind method on links. In Chapter 8 and 9 we have shown that the upwind method for homogeneous roads has many advantages compared to the minimum supply demand method. Therefore, further development of the node models and their upwind discretization proposed in this chapter is valuable.

Other future research includes node models for multi-class kinematic wave models. We have described the discretization of simple multi-class nodes in Eulerian coordinates. Our colleagues are working on similar models for more generic nodes (Smits et al., 2012) and on the discretization of multi-class nodes in Lagrangian coordinates (Yuan et al., 2012, in press). These methods may be tested using similar simulation studies as presented in this chapter.

Chapter 11

Conclusions

The goal of this last chapter is to summarize the main findings of the dissertation and to give an outlook for future research. The context of this dissertation is the development and analysis of a traffic flow model suitable for traffic management of networks with heterogeneous vehicles and drivers. After the literature review we conclude that a multi-class kinematic wave model is suitable for this goal. Furthermore, the application calls for efficient simulation methods, which are developed as well.

The outline of this chapter is as follows. In Section 11.1 we summarize our main findings and conclusions. We discuss applications, including scientific recommendations and practical implications in Section 11.2. Finally, Section 11.3 outlines future research directions.

11.1 Main findings and conclusions

In this section we summarize our main findings and conclusions. We follow the structure of this dissertation by first discussing the findings related to the model tree, secondly, the model development and analysis, thirdly, the Lagrangian coordinate system and finally we discuss the findings related to the numerical methods.

11.1.1 Traffic flow modelling

In Chapter 2 we introduced a model tree, see also Appendix A. The tree shows how traffic flow models have developed into four families since they were first introduced in the 1930's. The family of fundamental relations does not include traffic dynamics, whereas the micro- meso- and macroscopic models describe how traffic states evolve over time.

Furthermore, the model tree shows the state of the art in traffic flow modelling and current trends, including:

- Convergence of certain branches towards a generalized model. The generalized model can be used to analyze qualitative properties of all models within that branch (Wilson, 2008; Hoogendoorn & Bovy, 2001a; Del Castillo, 2012; Van Wageningen-Kessels et al., 2011b).
- Extensions and adaptations of the kinematic wave model to better reproduce key phenomena such as capacity drop, hysteresis and scattered fundamental diagrams (Zhang, 1999; Lebacque, 2002; Wong & Wong, 2002).
- Introduction of multi-class versions of previously developed models (Hoogendoorn, 1999; Bagnerini & Rascle, 2003; Ossen & Hoogendoorn, 2006), and especially multi-class kinematic wave models (Wong & Wong, 2002; Benzoni-Gavage & Colombo, 2003; Chanut & Buisson, 2003; Zhang et al., 2006; Laval & Daganzo, 2006; Ngoduy & Liu, 2007; Logghe & Immers, 2008; Van Lint et al., 2008; Nair et al., 2012).
- Combining microscopic and macroscopic models into hybrid models (Bourrel & Lesort, 2003; Leclercq, 2007a; Moutari & Rascle, 2007).

In this dissertation we add a new model to the tree that combines these trends. Furthermore, we conclude that the development of a multi-class kinematic wave model can yield a model with the required computational efficiency.

11.1.2 Multi-class traffic flow modelling

Chapter 3, 4, 5 and 7 are devoted to multi-class kinematic wave traffic flow modelling. They consist of the development and application of a theoretical framework for multi-class kinematic wave traffic flow modelling. The framework is introduced in Chapter 3 and consists of a set of principles and a set of requirements. We conclude that the principles applied in the LWR model can be adapted in order to be applied to multi-class models. The principles are used in the development of our multi-class kinematic wave traffic flow model Fastlane in Chapter 4. Fastlane uses the concept of passenger class equivalent (pce) values. We show that a simple safe-distance car-following model can be applied to make the pce-values state dependent. We conclude that this leads to a consistent model.

Fastlane is further generalized in Chapter 5. We show that only a few adaptations are necessary to generalize the model such that any single-pipe multi-class kinematic wave traffic flow model known from literature (Wong & Wong, 2002; Benzoni-Gavage & Colombo, 2003; Chanut & Buisson, 2003; Zhang et al., 2006; Ngoduy & Liu, 2007; Logghe & Immers, 2008; Van Lint et al., 2008; Van Wageningen-Kessels et al., under review; Nair et al., 2012) is contained in the generalized model. We conclude that all models (implicitly) contain the following four elements:

- Class specific conservation of vehicles equations.
- Definition of class specific flow.
- Class specific fundamental relations expressing the class specific velocity as a function of the effective density.
- An effective density function.

The effective density function aggregates all class specific densities into one variable. We find that the (implicit) specifications of the effective density functions vary largely amongst the existing models. This is in contrast to the fundamental relations, which mostly follow traditional shapes.

Finally, the requirements are used to assess multi-class kinematic wave traffic flow models in Chapter 7. Therefore, we use the Lagrangian formulation of the generalized model which is introduced in Chapter 6, see Section 11.1.3. The requirements relate to qualitative properties of the models such as nonincreasing density-velocity fundamental relations and anisotropy. We find that there are only two models that satisfy all our requirements unconditionally: the model by Chanut & Buisson (2003) and Fastlane. We conclude that other models do not satisfy the requirements or only satisfy them if certain parameters are chosen appropriately. Finally, a step-by-step-plan is introduced to assess any future multi-class kinematic wave model with respect to the requirements.

11.1.3 Lagrangian coordinates

Chapter 6 is the core chapter of this thesis. It reformulates the generalized multi-class kinematic wave model into the Lagrangian coordinate system. This coordinate system moves with the vehicles, unlike the traditional Eulerian coordinate system which is fixed in space.

We show that the main advantage of the Lagrangian coordinate system relates to the direction of information. In any kinematic wave traffic flow model it is assumed that vehicles and drivers only react on their leaders and not on their followers. Therefore, characteristics carrying information travel either with the vehicles, or from one vehicle to its follower. In the Lagrangian coordinate system this leads to characteristics with nonpositive velocities, while in the Eulerian coordinate system characteristics may have positive velocity (in free flow) or negative velocity (in congestion). We conclude that this advantage of the Lagrangian coordinate system can be exploited in two ways:

- It enables the eigenvalue analysis which is needed to qualitatively assess multi-class kinematic wave models (Chapter 7).
- It leads to more efficient numerical methods (Chapter 8–10).

11.1.4 Numerical methods and accuracy measures

In Chapter 8–10 we develop numerical methods to solve the (continuous) model equations that are introduced in the first part of this dissertation. In Chapter 8 we discuss

four different numerical methods for mixed-class models:

- The minimum supply demand method.
- The upwind method with explicit time stepping.
- The upwind method with implicit time stepping.
- The variational method.

The first method is applied to the model in Eulerian coordinates, the other methods to the model in Lagrangian coordinates.

To measure the accuracy of the numerical methods, we develop two novel measures: diffusion error and phase error. The diffusion error measures how much smoother the numerical solution is when compared to the exact solution. The phase error compares velocities in the numerical solution with velocities in the exact solution. For example, it compares the velocity with which congestion spills back upstream in the numerical solution with its velocity in the exact solution. We find that the solution of the upwind method with explicit time stepping is more accurate than the other solutions. The traditional minimum supply demand method leads to relatively large diffusion and phase errors. The upwind method with implicit time stepping is less accurate but allows for much larger time steps, which may be an advantage if computational time is very important. The variational method can lead to very accurate solutions, but only in certain settings mainly involving a piecewise linear fundamental relation. Therefore, we study the upwind method with explicit time stepping further.

The upwind method with explicit time stepping (or upwind method, for short) and the minimum supply demand method are extended for multi-class models in Chapter 9. Similarly to the numerical methods for mixed-class models, we conclude that the multi-class upwind method is more accurate than the multi-class minimum supply demand method.

The upwind method and the minimum supply demand method are extended for networks in Chapter 10. Therefore, we develop numerical methods for (simple) nodes. From simulation results we conclude that nodes are more accurately discretized using the minimum supply demand method than with the upwind method. However, we also show that certain elements in node models, such as turn fractions and routes, can be included in the upwind method more naturally.

11.2 Applications and practical implications

In this section we make recommendations for the scientific community and discuss practical implications of our results.

The Fastlane model is an advanced multi-class kinematic wave traffic flow model. It allows for a fast and accurate simulation of traffic flow on road networks. Therefore, it should result in much better traffic flow predictions than the ones resulting from most

simulation tools that are currently applied in practice. Fastlane is especially suitable in situations where heterogeneity of vehicles and drivers plays a large role, such as in and around logistics hubs. Furthermore, the model is well suited to be applied in traffic management in such areas (Schreiter, 2013) and the model in combination with its Lagrangian formulation is well suited for efficient traffic state estimation (Yuan, 2013).

If the Fastlane model does not satisfy the criteria of a scientist or practitioner in search for a model, the step-by-step plan for qualitative model assessment provides an efficient tool for model selection. It shows how any single-pipe multi-class kinematic wave model can be analyzed quickly for certain desirable qualitative properties. Only if the model has these properties may it be worthwhile to further study the applicability of the model. This assessment can be performed before the (usually costly) steps of model calibration and validation. Furthermore, the same plan can be applied during the development of any new multi-class kinematic wave model. It shows whether a model (under development) has desirable qualitative properties. Therefore, it can indicate whether the model is worthy of further development or whether it should be changed such that it gains the desirable properties. The plan may also indicate that only under certain conditions (e.g. parameter values) the model has qualitatively desirable properties.

Once it is established that a certain model has qualitatively desirable properties, the next steps are to calibrate and validate the model and numerical methods. In the calibration and validation, our novel accuracy measures are preferred over traditional measures such as the root mean square error. In the novel methods, the estimations or predictions are compared with analytical or high quality numerical solutions (in the validation of the numerical method) or with (high quality) measured traffic states (in the case of model calibration and validation). Moreover, the accuracy measures can be applied to compare estimations and predictions of any type of traffic flow model, yielding better insight in the applicability of the model. Futhermore, the novel accuracy measures also have potential practical implications: they might be applied in the assessment of data quality and traffic state estimation and prediction methods that are used in practice.

Finally, scientist and practitioners who apply traffic flow models can take advantage of the novel numerical methods based on the Lagrangian coordinate system. The efficient numerical methods can be applied in simulation tools for which computation time and accuracy are both important. They can be applied for simulation of motorway networks, both in combination with mixed-class and multi-class methods. The novel numerical methods yield more accurate and faster simulation results, which makes the model better applicable, both in real time and off-line. Moreover, they can be applied within the Fastlane model, but they would also result in superior simulation results if applied in combination with other models such as the ones that are currently applied in practice.

11.3 Future research

In the final section of this dissertation we suggest future research directions. We distinguish the following research themes: 1) identification of research needs and further generalization of traffic flow models using the model tree, 2) model development and analysis, 3) efficient numerical methods and 4) further application and development of models formulated in the Lagrangian coordinate system.

11.3.1 Model tree to identify research needs

The family tree shows trends and current developments, but it also shows branches in which developments are not as fast as in others. In this context we identify three main trends: 1) multi-class models, 2) hybrid models and 3) generalized models. For example, most branches include multi-class models. However, not all models have been extended to include multiple classes. The tree shows that there are little or no multi-class versions of for example cellular-automata models. Moreover, hybrid models have been proposed but can be developed much further. Hybrid models are able to combine advantages of different types of models. Examples of new models include mesoscopic models combined with micro- or macroscopic models. Existing hybrid models can be extended to include multiple vehicle classes. Another type of hybrid models can combine mixed-class and multi-class models. Finally, current generalized models include many models, but not all. Further generalizations may be needed to efficiently compare models. These gaps may be filled by future models.

11.3.2 Model development and analysis

We have outlined a consistent set of requirements. However, one can dispute the list of fundamental relation requirements. For example, it is argued that it is not strictly necessary that a multi-class model allows free flow velocities to be decreasing. A scientific debate on the requirements for multi-class kinematic wave models, and in fact any type of traffic flow model would be useful. Once there is agreement on the minimal requirements for such models, model developers can focus on the type of models with the desirable properties. Furthermore, a (new) set of requirements may be applied in the assessment of a broader range of traffic flow models.

The models are assessed with respect to the requirements using the generalized multi-class kinematic wave model. It also provides a framework for the development of new models. The generalized model allows to focus on either improvements in the fundamental relation or on improvements in the effective density function. Moreover, any model that is developed within the framework can (relatively easily) be assessed qualitatively using the step-by-step plan. Furthermore, a valuable extension of the generalized model is a multi-lane version of the model, which would then also include

the models by Daganzo (2002); Chanut (2005); Laval & Daganzo (2006). Finally, the requirements for node models (Tampère et al., 2011; Flötteröd & Rohde, 2011) can be extended to include multi-class nodes.

Further improvements of the Fastlane model can be studied. Currently, the space occupancy is a linear function of only the velocity. Parameters are gross vehicle length and minimum time headway. Other space occupancy functions can be thought of, for example based on more advanced car-following models instead of Pipes' safe-distance model (1953). Especially in free flow, the safe-distance model, and thus also the space occupancy function, is disputable. Including another space occupancy function may lead to a more realistic model. Other possible extensions of the Fastlane model include a capacity drop and the introduction of multiple lanes.

In the development of Fastlane a logical next step is to calibrate and validate the model using experimental traffic data (Schreiter, 2013). Furthermore, other calibrated (multi-class kinematic wave) traffic flow models may be compared to Fastlane. This would then yield insight into how our assumptions and modelling choices lead to (significantly) different simulation results.

In the calibration and validation of Fastlane, or any other traffic flow model, our novel accuracy measures can be applied. However, currently, they can only be applied in situations where it is relatively easy to identify centroids of the density or velocity profile. Therefore, a 'bump' in the profile needs to be identified in a reference solution and linked to a bump in the approximate solution. This may be difficult in more realistic settings. Developments of techniques which are able to do this or which circumvent the problem may be useful.

11.3.3 Numerical methods

We have developed efficient numerical methods based on the Lagrangian coordinate system. An alternative method could be based on an alternative Lagrangian model formulation Yuan et al. (2011); Yuan (2013). Methods based on this formulation are supposed to be more efficient in cases with only few vehicles of the reference class. The advantages and disadvantages are explored by Yuan et al. but could be studied further using methods that we propose. Futhermore, our results indicate that implicit time stepping and the variational method may lead to very low computation times, at the loss of some accuracy. The applicability of those methods can be studied further (Van Wageningen-Kessels et al., 2010).

Our upwind method for nodes needs some improvements. In Section 10.6 we have outlined a few approaches to improve its accuracy. Furthermore, the upwind method for nodes may be extended in order to be applied to multi-class models. Currently, a lot of research is done in this field and ideas can be taken from e.g., Flötteröd & Rohde (2011); Tampère et al. (2011); Smits et al. (2012); Yuan et al. (in press). Furthermore, the modelling of nodes in the Lagrangian formulation is equivalent to the modelling

of moving bottlenecks in the Eulerian formulation. (And vice versa: the modelling of moving bottlenecks in the Lagrangian formulation is equivalent to the modelling of nodes in the Eulerian formulation.) Therefore, inspiration for efficient node models in the Lagrangian formulation may be found in the literature on bottleneck models in the Eulerian formulation.

11.3.4 Lagrangian coordinate system

We have exploited one advantage of the Lagrangian coordinate system in the model analysis and numerical methods. The same advantages may be exploited in the context of other types of (traffic flow) models. For example, a Lagrangian formulation of higher-order models has been proposed (Aw et al., 2002). However, to our knowledge, no numerical methods have been developed based on this model formulation. Furthermore, the Lagrangian coordinate system may be applied to pedestrian flow models. This is especially challenging because pedestrians usually walk on two-dimensional surfaces, while vehicles are restricted to lanes (one-dimensional). For this application Lagrangian flow models used in fluid flow problems may serve as a source of inspiration (LeVeque, 2002).

Recently, a third coordinate system for the LWR model has been introduced (Leclercq & Bécarie, 2012; Laval & Leclercq, 2013). In their T-model the goal is to calculate the time at which a certain vehicle reaches a certain location. We expect that this coordinate system has similar advantages as the Lagrangian coordinate system. The model introduced by Laval & Leclercq (2013) can be developed further using similar approaches as presented in this dissertation, such as including multiple classes.

An other advantage of the Lagrangian coordinate system is its natural relation with microscopic traffic flow models. In a hybrid model the coupling between the microscopic and the macroscopic region is relatively simple. At the boundaries vehicle groups are aggregated (from micro to macro) or disaggregated (from macro to micro). Leclercq (2009) shows how the capacity drop can be included in the Lagrangian formulation of the LWR model. Both the capacity drop and bounded acceleration are more straightforward to include in the Lagrangian than in the Eulerian formulation because of the direct relation between the vehicle velocity and the coordinate system. These ideas can be further extended to include vehicle and driver heterogeneity.

Appendix A

Family tree of traffic flow models

See next page for the genealogical tree of traffic flow models. Grey lines indicate descent, black dots indicate publications, black lines indicate that the model has (or multiple very similar models have) been published multiple times.

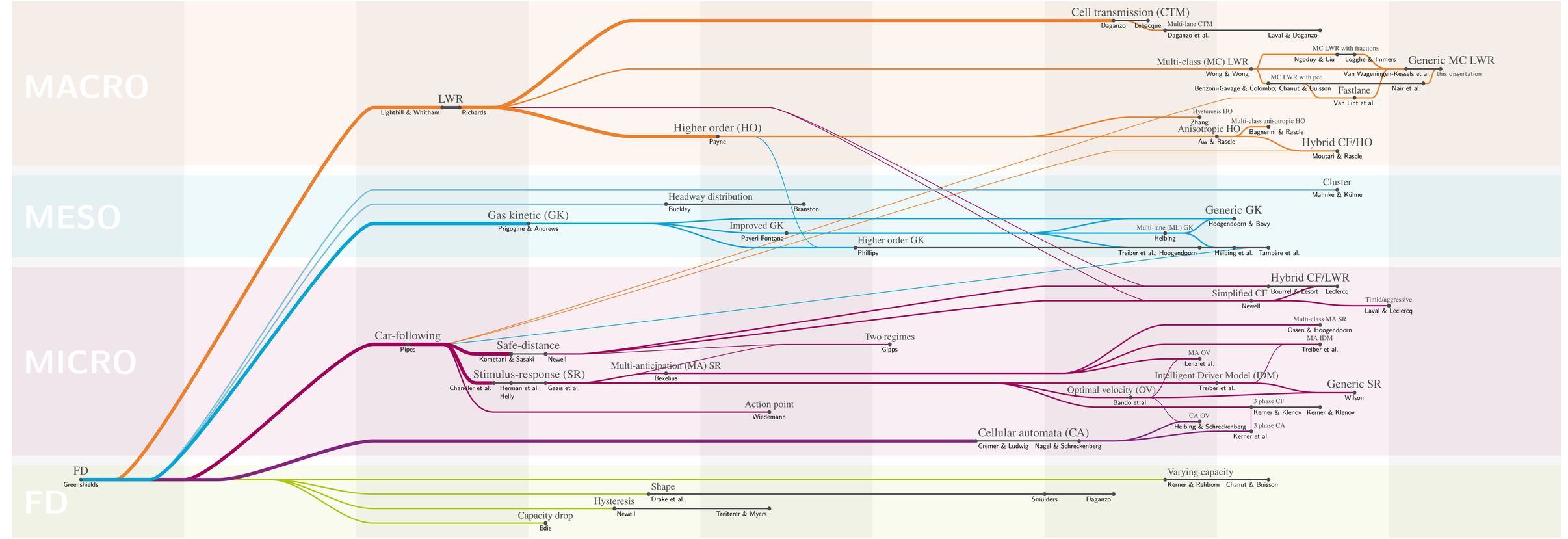
1930
1940
1950
1960
1970
1980
1990
2000
2010
2020
MACRO
MESO
MICRO
FD
FD
Greenshields
LWR
Lighthill & Whitham
Richards
Higher order (HO)
Payne
Cell transmission (CTM)
Daganzo
Lebacque
Multi-lane CTM
Daganzo et al.
Laval & Daganzo
Multi-class (MC) LWR
Wong & Wong
MC LWR with fractions
Ngoduy & Liu
Logghe & Immers
Generic MC LWR
Van Wageningen-Kessels et al.
this dissertation
MC LWR with pce
Benzoni-Gavage & Colombo; Chanut & Buisson
Fastlane
Van Lint et al.
Nair et al.
Hysteresis HO
Zhang
Multi-class anisotropic HO
Anisotropic HO
Aw & Rascle
Bagnerini & Rascle
Hybrid CF/HO
Moutari & Rascle
Cluster
Mahnke & Kühne
Headway distribution
Buckley
Branston
Gas kinetic (GK)
Prigogine & Andrews
Improved GK
Paveri-Fontana
Higher order GK
Phillips
Generic GK
Hoogendoorn & Bovy
Multi-lane (ML) GK
Helbing
Treiber et al.; Hoogendoorn
Helbing et al.
Tampère et al.
Hybrid CF/LWR
Bourrel & Lesort
Leclercq
Simplified CF
Newell
Timid/aggressive
Laval & Leclercq
Car-following
Pipes
Safe-distance
Kometani & Sasaki
Newell
Two regimes
Gipps
Multi-anticipation (MA) SR
Bexelius
Stimulus-response (SR)
Chandler et al.
Herman et al.; Helly
Gazis et al.
Action point
Wiedemann
Multi-class MA SR
Ossen & Hoogendoorn
MA IDM
Treiber et al.
MA OV
Lenz et al.
Intelligent Driver Model (IDM)
Treiber et al.
Optimal velocity (OV)
Bando et al.
Generic SR
Wilson
3 phase CF
Kerner & Klenov
Kerner & Klenov
CA OV
Helbing & Schreckenberg
3 phase CA
Kerner et al.
Cellular automata (CA)
Cremer & Ludwig
Nagel & Schreckenberg
Varying capacity
Kerner & Rehborn
Chanut & Buisson
Shape
Drake et al.
Smulders
Daganzo
Hysteresis
Newell
Treiterer & Myers
Capacity drop
Edie

Appendix B

Variational theory applied to the kinematic wave model

In this appendix we show how variational theory can be applied on the network in Figure 8.5. The network consists of nodes and waves with velocities w_1, $w_2 = w_1/2$ and $w_3 = 0$. The waves intersect at nodes with $n = i\Delta n$ and $t = k\Delta t$, therefore $w_1 = \Delta n/\Delta t$. At the nodes the position $\tilde{x}_i^k$ of the $n = i\Delta n$-th vehicle at time $t = k\Delta t$ is calculated with the minimization problem (8.22), (8.23). We show that the minimization problem indeed solves the kinematic wave problem on an infinitely long homogeneous road with the piecewise linear fundamental relation consisting of three linear parts (8.20), see Figure 8.4(b) and piecewise constant initial conditions. For completeness we repeat the minimization problem:

$$\tilde{x}_i^k = \min\left(\tilde{x}_{i-1}^{k-1} + \Delta t r_1,\, \tilde{x}_{i-1}^{k-2} + 2\Delta t r_2,\, \tilde{x}_i^{k-1} + \Delta t r_3\right) \tag{B.1}$$

with:

$$r_m = v_m - s_m w_m = \begin{cases} r_1 = -s_{\text{jam}} w_1 \\ r_2 = v_{\text{crit}} - s_{\text{crit}} w_2 \\ r_3 = v_{\text{max}} \end{cases} \tag{B.2}$$

The fundamental relation is:

$$v(s) = \min_m (v_m + (s - s_m) w_m) = \begin{cases} (s - s_{\text{jam}}) w_1 & \text{if } s \le s_{\text{crit}} \\ v_{\text{crit}} + (s - s_{\text{crit}}) w_2 & \text{if } s_{\text{crit}} < s \le s_3 \\ v_{\text{max}} & \text{if } s > s_3 \end{cases} \tag{B.3}$$

with

$$w_1 = \frac{v_{\text{crit}}}{s_{\text{crit}} - s_{\text{jam}}} \quad \text{and} \quad w_2 = \frac{v_{\text{max}} - v_{\text{crit}}}{s_{\text{crit}} - s_3} \tag{B.4}$$

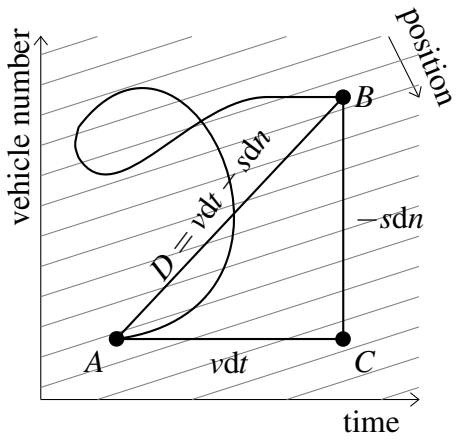

Figure B.1 *The travel distance of a moving observer from point A to point B can be computed exactly using Lemma B.1. The diagonal parallel lines are 'x-trajectories': at these lines, the position x is constant. The lemma states that the distance is independent of the path. In the proof of Lemma B.1 we use that the travel distance from A to B is equal to the distance from A to C plus the distance from C to B.*

and $v_1 = 0$, $s_1 = s_{\text{jam}}$, $v_2 = v_{\text{crit}}$, $s_2 = s_{\text{crit}}$ and $v_M = v_{\max}$.

We first observe that the distance traveled by a moving observer is related to the number of overtakings. Secondly, we relate the number of overtakings to a certain cost. The third step is to show that this can be applied on a homogeneous road with homogeneous traffic conditions to compute the velocity and position of vehicle groups. Finally, we relax the assumption of homogeneous traffic conditions and show that piecewise constant initial conditions are sufficient.

Lemma B.1. *Consider a homogeneous road with homogeneous traffic conditions, i.e. the traffic state (spacing s, velocity v) is the same everywhere in the (t,n) plane. The distance traveled by a moving observer in the (t,n) plane from point $A = (t_0, n_0)$ to point $B = (t_1, n_1) = (t_0 + \mathrm{d}t, n_0 + \mathrm{d}n)$ equals:*

$$D = v\mathrm{d}t - s\mathrm{d}n \tag{B.5}$$

Before we give the proof we refer to Figure B.1 for an illustration of the Lemma. Furthermore, we remark that such a moving observer is not a real traveller or vehicle. It can move in the (t,n) plane without any restrictions.

Proof. We note that the distance traveled by the moving observer is independent of the path. Furthermore, it is equal to the net number of x-trajectories that overtake the moving observer. Let us assume the moving observer first travels from point A to point $C = (t_1, n_0)$ and then to point B. The net number of x-trajectories that overtake the moving observer between point A and point C is $v\mathrm{d}t$. The net number of x-trajectories that overtake the moving observer between point C and point B is $-s\mathrm{d}n$. Consequently,

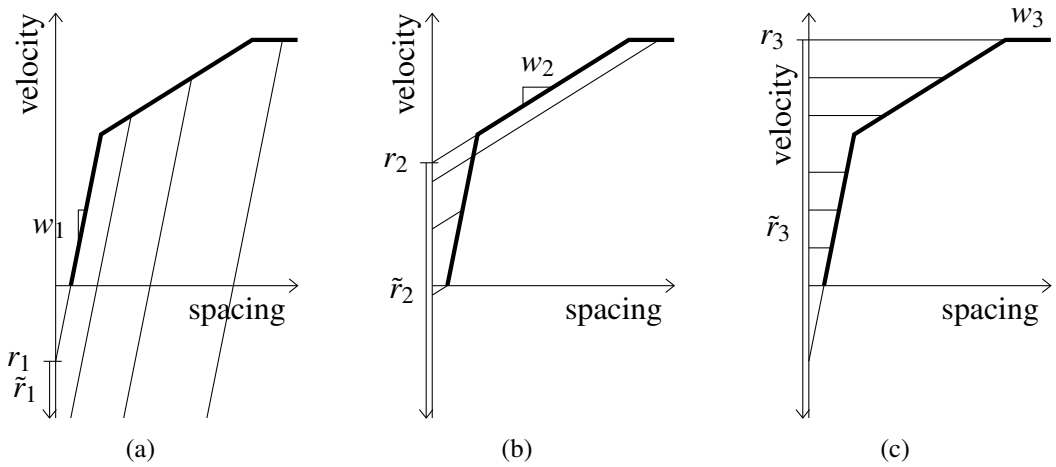

Figure B.2 *Fundamental relation with costs r_m and velocity of moving observer $\tilde{r}_m$.*

the net number of x-trajectories that overtake the moving observer between point A and point B is $v\mathrm{d}t - s\mathrm{d}n$ and thus the distance it travels is $D = v\mathrm{d}t - s\mathrm{d}n$. □

Let us define the average velocity of the moving observer by $\tilde{r}$. Using Lemma B.1 the distance traveled by the moving observer is:

$$\mathrm{d}t\tilde{r} = D = v\mathrm{d}t - s\mathrm{d}n \tag{B.6}$$

Furthermore, we define $\tilde{r}_1$, $\tilde{r}_2$ and $\tilde{r}_3$ as the average velocities of three moving observers travelling over the network in Figure 8.5:

- $\tilde{r}_1$ is the average velocity of moving observer 1, traveling from x_i^{k-1} to x_i^k
- $\tilde{r}_2$ is the average velocity of moving observer 2, traveling from x_{i-1}^{k-2} to x_i^k
- $\tilde{r}_3$ is the average velocity of moving observer 3, traveling from x_{i-1}^{k-1} to x_i^k

Applying (B.6), $w_1 = \Delta n/\Delta t$ and $w_2 = w_1/2$, we find:

$$\tilde{r}_1 = v - s\frac{\Delta n}{\Delta t} = v - sw_1, \quad \tilde{r}_2 = v - s\frac{\Delta n}{2\Delta t} = v - s\frac{w_1}{2} = v - sw_2, \quad \tilde{r}_3 = v \tag{B.7}$$

Lemma B.2. *Consider a homogeneous road with homogeneous traffic conditions. In all permissible traffic states (i.e. with $s \geq s_{jam}$) the velocity of the moving observer is not larger than the associated costs defined by (B.2):*

$$\tilde{r}_1 \leq r_1, \quad \tilde{r}_2 \leq r_2, \quad \tilde{r}_3 \leq r_3 \tag{B.8}$$

Furthermore:

$$\text{if } s_1 \leq s \leq s_2 \text{ then } \tilde{r}_1 = r_1, \text{ if } s_2 \leq s \leq s_3 \text{ then } \tilde{r}_2 = r_2, \text{ if } s \geq s_3 \text{ then } \tilde{r}_3 = r_3 \tag{B.9}$$

Proof. We recall that the cost r_m is the velocity at the intersection with the velocity

axis of the m-th linear part of fundamental relation, see Figure B.2. Furthermore, from (B.7) we conclude that the velocity of moving observer 1 can be obtained similarly, see also Figure B.2(a). This velocity depends on the traffic state (s,v). It is the intersection with the velocity axis of a straight line with slope w_1 that also goes through (s,v). From Figure B.2(a) it can be observed that $\tilde{r}_1 = r_1$ if $s_1 \leq s \leq s_2$ and that $\tilde{r}_1 > r_1$ in all other permissible traffic states. A similar procedure is applied to conclude that the velocities of moving observer 2 and 3 also satisfy (B.8) and (B.9), see Figure B.2(b) and B.2(c) □

Lemma B.3. *Consider a homogeneous road with homogeneous traffic conditions. (B.1) yields the correct vehicle positions at the nodes (k,i) of the network in Figure 8.5.*

Proof. We distinguish between the following traffic states: $s_1 \leq s \leq s_2$, $s_2 < s < s_3$ and $s \geq s_3$. In the first case ($s_1 \leq s \leq s_2$) Lemma B.2 gives:

$$\tilde{x}_i^k = \min \begin{cases} \tilde{x}_{i-1}^{k-1} + \Delta t r_1 & = & \tilde{x}_{i-1}^{k-1} + \Delta t \tilde{r}_1 & = & \tilde{x}_i^k \\ \tilde{x}_{i-1}^{k-2} + 2\Delta t r_2 & \geq & \tilde{x}_{i-1}^{k-2} + 2\Delta t \tilde{r}_2 & = & \tilde{x}_i^k \\ \tilde{x}_i^{k-1} + \Delta t r_3 & \geq & \tilde{x}_i^{k-1} + \Delta t \tilde{r}_3 & = & \tilde{x}_i^k \end{cases} \tag{B.10}$$

Similarly, in the second case ($s_2 < s < s_3$) Lemma B.2 gives:

$$\tilde{x}_i^k = \min \begin{cases} \tilde{x}_{i-1}^{k-1} + \Delta t r_1 & \geq & \tilde{x}_{i-1}^{k-1} + \Delta t \tilde{r}_1 & = & \tilde{x}_i^k \\ \tilde{x}_{i-1}^{k-2} + 2\Delta t r_2 & = & \tilde{x}_{i-1}^{k-2} + 2\Delta t \tilde{r}_2 & = & \tilde{x}_i^k \\ \tilde{x}_i^{k-1} + \Delta t r_3 & \geq & \tilde{x}_i^{k-1} + \Delta t \tilde{r}_3 & = & \tilde{x}_i^k \end{cases} \tag{B.11}$$

And in the third case ($s \geq s_3$) Lemma B.2 gives:

$$\tilde{x}_i^k = \min \begin{cases} \tilde{x}_{i-1}^{k-1} + \Delta t r_1 & \geq & \tilde{x}_{i-1}^{k-1} + \Delta t \tilde{r}_1 & = & \tilde{x}_i^k \\ \tilde{x}_{i-1}^{k-2} + 2\Delta t r_2 & \geq & \tilde{x}_{i-1}^{k-2} + 2\Delta t \tilde{r}_2 & = & \tilde{x}_i^k \\ \tilde{x}_i^{k-1} + \Delta t r_3 & = & \tilde{x}_i^{k-1} + \Delta t \tilde{r}_3 & = & \tilde{x}_i^k \end{cases} \tag{B.12}$$

□

We now relax the assumption of homogeneous traffic conditions.

Theorem B.1. *(B.1) solves the kinematic wave problem with piecewise linear fundamental relation (B.3) and piecewise constant initial condition exactly at the nodes (k,i) of the network in Figure 8.5.*

Proof. The exact solution of the kinematic wave problem (using kinematic wave theory) shows that the spacing is constant between the nodes $(k-1,i-1)$ and (k,i), between $(k-2,i-1)$ and (k,i) and between $(k-1,i)$ and (k,i). This is because characteristics may travel at three different velocities: w_1, w_2 and w_3. The slope of the lines connecting the nodes is equal to these velocities. Therefore, Lemma B.3 can be applied and thus (B.1) solves the kinematic wave problem exactly. □

Bibliography

Ansorge, R. (1990) What does the entropy condition mean in traffic flow theory?, *Transportation Research Part B: Methodological*, 24(2), pp. 133–143. 62, 79

Aw, A., A. Klar, M. Rascle, T. Materne (2002) Derivation of continuum traffic flow models from microscopic follow-the-leader models, *SIAM Journal on Applied Mathematics*, 63(1), pp. 259–278. 66, 118, 238

Aw, A., M. Rascle (2000) Resurrection of "second order models" of traffic flow?, *SIAM Journal on Applied Mathematics*, 60(3), pp. 916–938. 66, 81

Bagnerini, P., M. Rascle (2003) A multiclass homogenized hyperbolic model of traffic flow, *SIAM Journal on Mathematical Analysis*, 35(4), pp. 949–973. 66, 67, 232

Bando, M., K. Hasebe, K. Nakanishi, A. Nakayama (1998) Analysis of optimal velocity model with explicit delay, *Physical Review E: Statistical, nonlinear and soft matter physics*, 58(5), pp. 5429–5435. 57

Bando, M., K. Hasebe, A. Nakayama, A. Shibata, Y. Sugiyama (1995) Dynamical model of traffic congestion and numerical simulation, *Physical Review E: Statistical, nonlinear and soft matter physics*, 51, pp. 1035–1042. 56

Bar-Gera, H., S. Ahn (2010) Empirical macroscopic evaluation of freeway merge-ratios, *Transportation Research Part C: Emerging Technologies*, 18(4), pp. 457–470. 205

Bellomo, N., F. Brezzi (2008) Traffic, crowds and swarms, *Mathematical Models and Methods in Applied Sciences*, 18, pp. 1145–1148. 67

Bellomo, N., C. Dogbe (2011) On the modeling of traffic and crowds: A survey of models, speculations, and perspectives, *SIAM Review*, 53, pp. 409–463. 43, 63, 67, 68, 69, 72

Benzoni-Gavage, S., R. M. Colombo (2003) An n-populations model for traffic flow, *European Journal of Applied Mathematics*, 14(05), pp. 587–612. 35, 63, 64, 65, 67, 101, 103, 104, 110, 112, 113, 114, 116, 133, 154, 155, 156, 158, 232

Bexelius, S. (1968) An extended model for car-following, *Transportation Research*, 2(1), pp. 13–21. 59

Bourrel, E., J.-B. Lesort (2003) Mixing microscopic and macroscopic representations of traffic flow hybrid model based on Lighthill-Whitham-Richards theory, *Transportation Research Record: Journal of the Transportation Research Board*, 1852, pp. 193–200. 56, 67, 228, 232

Brackstone, M., M. McDonald (1999) Car-following: a historical review, *Transportation Research Part F: Traffic Psychology and Behaviour*, 2(4), pp. 181–196. 43, 56, 57, 58, 59, 69, 72

Branston, D. (1976) Models of single lane time headway distributions, *Transportation Science*, 10(2), pp. 125–148. 60

Buckley, D. J. (1968) A semi-Poisson model of traffic flow, *Transportation Science*, 2(2), pp. 107–133. 60

Burghout, W., H. N. Koutsopoulos, I. Andréasson (2005) Hybrid mesoscopic-microscopic traffic simulation, *Transportation Research Record: Journal of the Transportation Research Board*, 1934, pp. 218–225. 228

Cassidy, M. J., S. Ahn (2005) Driver turn-taking behavior in congested freeway merges, *Transportation Research Record: Journal of the Transportation Research Board*, 1934, pp. 140–147. 205

Cassidy, M. J., R. L. Bertini (1999) Some traffic features at freeway bottlenecks, *Transportation Research Part B: Methodological*, 33(1), pp. 25–42. 51

Cassidy, M. J., J. R. Windover (1995) Methodology for assesing dynamics of freeway traffic flow, *Transportation Research Record: Journal of the Transportation Research Board*, 1484, pp. 73–79. 48, 72

Chandler, R., R. Herman, E. Montroll (1958) Traffic dynamics: Studies in car following, *Operations Research*, 6(2), pp. 165–184. 56, 57

Chanut, S. (2005) A first-order macroscopic traffic flow model for mixed traffic including moving bottleneck effects, in: Mahmassani, H., ed., *Transportation and Traffic Theory. Flow, Dynamics and Human Interaction. 16th International Symposium on Transportation and Traffic Theory*, Elsevier, pp. 323–343. 63, 80, 101, 237

Chanut, S., C. Buisson (2003) Macroscopic model and its numerical solution for two-flow mixed traffic with different speeds and lengths, *Transportation Research Record: Journal of the Transportation Research Board*, 1852, pp. 209–219. 53, 63, 64, 65, 67, 70, 71, 101, 103, 104, 110, 112, 113, 114, 116, 132, 133, 154, 155, 156, 158, 191, 232, 233

Chronopoulos, A., A. Lyrintzis, P. Michapoulos, C. Rhee, P. Yi (1993) Traffic flow simulation through high order traffic modelling, *Mathematical and Computer Modelling*, 17(8), pp. 11–22. 164

Coifman, B., S. Kim (2011) Extended bottlenecks, the fundamental relationship, and capacity drop on freeways, *Transportation Research Part A: Policy and Practice*, 45(9), pp. 980–991, papers selected for the 19th International Symposium on Transportation and Traffic Theory. 51

Courant, R., K. Friedrichs, H. Lewy (1967) On the partial difference equations of mathematical physics, *IBM Journal*, pp. 215–234. 162

Cremer, M., J. Ludwig (1986) A fast simulation model for traffic flow on the basis of boolean operations, *Mathematics and Computers in Simulation*, 28(4), pp. 297–303. 59

Daganzo, C. F. (1994) The cell transmission model: A dynamic representation of highway traffic consistent with the hydrodynamic theory, *Transportation Research Part B: Methodological*, 28(4), pp. 269–287. 48, 62, 159

Daganzo, C. F. (1995a) The cell transmission model, part II: Network traffic, *Transportation Research Part B: Methodological*, 29(2), pp. 79–93. 201, 206

Daganzo, C. F. (1995b) Requiem for second-order fluid approximations of traffic flow, *Transportation Research Part B: Methodological*, 29(4), pp. 277–286. 66, 78, 81

Daganzo, C. F. (2002) A behavioral theory of multi-lane traffic flow. Part I: Long homogeneous freeway sections, *Transportation Research Part B: Methodological*, 36(2), pp. 131–158. 63, 101, 237

Daganzo, C. F. (2005a) A variational formulation of kinematic waves: Basic theory and complex boundary conditions, *Transportation Research Part B*, 39, pp. 187–196. 117, 167

Daganzo, C. F. (2005b) A variational formulation of kinematic waves: Solution methods, *Transportation Research Part B*, 39, pp. 934–950. 167

Daganzo, C. F. (2006) In traffic flow, cellular automata = kinematic waves, *Transportation Research Part B: Methodological*, 40(5), pp. 396–403. 55

Daganzo, C. F., W.-H. Lin, J. del Castillo (1997) A simple physical principle for the simulation of freeways with special lanes and priority vehicles, *Transportation Research Part B: Methodological*, 31(2), pp. 103–125. 62

Darbha, S., K. R. Rajagopal, V. Tyagi (2008) A review of mathematical models for the flow of traffic and some recent results, *Nonlinear Analysis: Theory, Methods & Applications*, 69(3), pp. 950–970, trends in Nonlinear Analysis: in Honour of Professor V.Lakshmikantham. 68

del Castillo, J. (2012) Three new models for the flow-density relationship: Derivation and testing for freeway and urban data, *Transportmetrica*, 8(6), pp. 443–465. 50, 51, 53, 66, 68, 78, 80, 81, 232

Drake, J. S., J. L. Schofer, A. D. May (1967) A statistical analysis of speed-density hypotheses, *Highway Research Record*, 154, pp. 53–87. 48, 113

Edie, L. (1961) Car-following and steady-state theory for noncongested traffic, *Operations Research*, 9(1), pp. 66–76. 51

Edie, L. (1965) Discussion on traffic stream measurements and definitions, in: *The 2nd International Symposium on the Theory of Traffic Flow, 1963*, pp. 139–154. 46, 47, 48

Elefteriadou, L., T. D., N. Webster (1997) Development of passenger car equivalents for freeways, two-lane highways, and arterials, *Transportation Research Record: Journal of the Transportation Research Board*, 1572, pp. 51–58. 37, 88

Flötteröd, G., J. Rohde (2011) Operational macroscopic modeling of complex urban road intersections, *Transportation Research Part B: Methodological*, 45(6), pp. 903–922. 201, 237

Gazis, D. C., R. Herman, R. W. Rothery (1961) Nonlinear follow-the-leader models of traffic flow, *Operations Research*, 9(4), pp. 545–567. 56

Gipps, P. G. (1981) A behavioural car-following model for computer simulation, *Transportation Research Part B: Methodological*, 15(2), pp. 105–111. 54, 55, 57

Godunov, S. K. (1959) A difference method for numerical calculation of discontinuous solutions of the equations of hydrodynamics, *Matematicheskii Sbornik*, 47(89), pp. 271–306. 36

Greenberg, J., A. Klar, M. Rascle (2003) Congestion on multilane highways, *SIAM Journal on Applied Mathematics*, 63(3), pp. 818–833. 66

Greenberg, J. M. (2001) Extensions and amplifications of a traffic model of Aw and Rascle, *SIAM Journal on Applied Mathematics*, 62(3), pp. 729–745. 118

Greenshields, B. D. (1934) The photographic method of studying traffic behavior, in: *Proceedings of the 13th Annual Meeting of the Highway Research Board*, pp. 382–399. 35, 45, 46, 48

Greenshields, B. D. (1935) A study of traffic capacity, in: *Proceedings of the 14th Annual Meeting of the Highway Research Board*, pp. 448–477. 48, 113

Grewal, M. S., H. J. Payne (1976) Identification of parameters in a freeway traffic model, *Systems, Man and Cybernetics, IEEE Transactions on*, SMC-6(3), pp. 176–185. 72

Helbing, D. (1997a) Fundamentals of traffic flow, *Physical Review E: Statistical, nonlinear and soft matter physics*, 55, pp. 3735–3738. 80

Helbing, D. (1997b) Modeling multi-lane traffic flow with queuing effects, *Physica A: Statistical and Theoretical Physics*, 242(1-2), pp. 175–194. 61

Helbing, D. (2001) Traffic and related self-driven many-particle systems, *Reviews of Modern Physics*, 73, pp. 1067–1141. 43, 68, 72

Helbing, D., ed. (2008) *Managing Complexity: Insights, Concepts, Applications*, Understanding Complex Systems, Springer, Berlin/Heidelberg. 67

Helbing, D. (2009) Reply to comment on "On the controversy around Daganzo's requiem for and Aw-Rascle's resurrection of second-order traffic flow models" by H.M. Zhang, *The European Physical Journal B: Condensed Matter and Complex Systems*, 69, pp. 569–570. 81

Helbing, D., A. Hennecke, V. Shvetsov, M. Treiber (2001) Master: macroscopic traffic simulation based on a gas-kinetic, non-local traffic model, *Transportation Research Part B: Methodological*, 35(2), pp. 183–211. 61

Helbing, D., A. F. Johansson (2009) On the controversy around Daganzo's requiem for and Aw-Rascle's resurrection of second-order traffic flow models, *The European Physical Journal B: Condensed Matter and Complex Systems*, 69, pp. 549–562. 81

Helbing, D., M. Schreckenberg (1999) Cellular automata simulating experimental properties of traffic flow, *Physical Review E: Statistical, nonlinear and soft matter physics*, 59(3). 59

Helbing, D., M. Treiber (1999) Numerical simulation of macroscopic traffic equations, *Computing in Science and Engineering*, 1(5), pp. 89–99. 201, 203

Helly, W. (1961) Simulation of bottlenecks in single lane traffic flow, in: Herman, R., ed., *Theory of Traffic Flow 1959, proceedings*, Elsevier, Amsterdam, pp. 207–238. 56, 59

Herbin, R., L. Leclercq (2011) a note on the entropy solutions of the hydrodynamic model of traffic flow revisited, *Transportation Science*, 45(1), pp. 138–142. 51

Herman, R., E. W. Montroll, R. B. Potts, R. W. Rothery (1959) Traffic dynamics: Analysis of stability in car following, *Operations Research*, 7(1), pp. 86–106. 56

Hille, E., R. S. Phillips (1957) *Functional analysis and semi-groups*, chap. 10, American Mathematical Society, Providence, Rhode Island, pp. 302–327. 141

Hoogendoorn, S. P. (1999) *Multiclass continuum modelling of multilane traffic flow*, Ph.D. thesis, Delft University of Technology/TRAIL Research school, Delft. 48, 61, 67, 80, 232

Hoogendoorn, S. P., P. H. L. Bovy (2001a) Generic gas-kinetic traffic systems modeling with applications to vehicular traffic flow, *Transportation Research Part B: Methodological*, 35(4), pp. 317–336. 61, 66, 232

Hoogendoorn, S. P., P. H. L. Bovy (2001b) State-of-the-art of vehicular traffic flow modeling, *Proceedings of the Institution of Mechanical Engineers, Part I: Journal of Systems and Control Engineering*, 215, pp. 283–303. 43, 45, 57, 68

Hoogendoorn, S. P., G. J. Martens, O. Tool (2006) Beheersconsequenties groei vrachtverkeer: Rapport analyse individuele voertuiggegevens, Tech. Rep. 010, Adviesdienst Verkeer en Vervoer, Rotterdam, in Dutch. 87

Hoogendoorn, S. P., J. W. C. van Lint, V. L. Knoop (2009) Dynamic first-order modeling of phase-transition probabilities, in: Appert-Rolland, C., F. Chevoir, P. Gondret, S. Lassarre, J.-P. Lebacque, M. Schreckenberg, eds., *Traffic and Granular Flow 07*, Springer, Berlin Heidelberg, pp. 85–92. 62

Jin, W.-L., H. M. Zhang (2003) The inhomogeneous kinematic wave traffic flow model as a resonant nonlinear system, *Transportation Science*, 37(3), pp. 294–311. 201

Jin, W.-L., H. M. Zhang (2013) An instantaneous kinematic wave theory of diverging traffic, *Transportation Research Part B: Methodological*, 48(0), pp. 1 – 16. 228

Kerner, B. S. (2004) Three-phase traffic theory and highway capacity, *Physica A: Statistical and Theoretical Physics*, 333, pp. 379–440. 53

Kerner, B. S. (2009) *Introduction to modern traffic flow theory and control: The long road to three-phase traffic theory*, Springer. 43, 51, 53, 57, 69, 72

Kerner, B. S., S. L. Klenov (2002) A microscopic model for phase transitions in traffic flow, *Journal of Physics A: Mathematical and General*, 35(3). 57

Kerner, B. S., S. L. Klenov (2006) Deterministic microscopic three-phase traffic flow models, *Journal of Physics A: Mathematical and General*, 39(8). 57

Kerner, B. S., S. L. Klenov, D. E. Wolf (2002) Cellular automata approach to three-phase traffic theory, *Journal of Physics A: Mathematical and General*, 35(47). 60

Kerner, B. S., H. Rehborn (1996) Experimental features and characteristics of traffic jams, *Physical Review E: Statistical, nonlinear and soft matter physics*, 53, pp. 1297–1300. 48, 51, 72, 80

Kerner, B. S., H. Rehborn (1997) Experimental properties of phase transitions in traffic flow, *Physical Review Letters*, 79(20), pp. 4030–4033. 53

Knight, F. H. (1924) Some fallacies in the interpretation of social cost, *The Quarterly Journal of Economics*, 38(4), pp. 582–606. 45

Knospe, W., L. Santen, A. Schadschneider, M. Schreckenberg (2004) Empirical test for cellular automaton models of traffic flow, *Physical Review E: Statistical, nonlinear and soft matter physics*, 70(1). 59, 60

Kockelman, K. M. (1998) Changes in the flow-density relation due to environmental, vehicle and driver characteristics, *Transportation Research Record*, 1644, pp. 47–56. 37

Kometani, E., T. Sasaki (1961) Dynamic behaviour of traffic with a nonlinear spacing-speed relationship, in: Herman, R., ed., *Theory of Traffic Flow 1959, proceedings*, Elsevier, Amsterdam, pp. 105–119. 54

Kühne, R., N. Gartner, eds. (2011) *75 Years of the Fundamental Diagram for Traffic Flow Theory: Greenshields Symposium*, vol. E-C149 of *Transportation Research Circular*, Traffic Flow Theory and Characteristics Committee, Transportation Research Board of the National Academies. 46

Kühne, R. D. (2011) Greenshields' legacy: Highway traffic, in: Kühne, R., N. Gartner, eds., *75 Years of the Fundamental Diagram for Traffic Flow Theory: Greenshields Symposium*, vol. E-C149 of *Transportation Research Circular*, Traffic Flow Theory and Characteristics Committee, Transportation Research Board of the National Academies, pp. 3–10. 46

Laval, J. A. (2011) Hysteresis in traffic flow revisited: An improved measurement method, *Transportation Research Part B: Methodological*, 45(2), pp. 385–391. 51

Laval, J. A., C. F. Daganzo (2006) Lane-changing in traffic streams, *Transportation Research Part B: Methodological*, 40(3), pp. 251–264. 62, 67, 222, 232, 237

Laval, J. A., L. Leclercq (2008) Microscopic modeling of the relaxation phenomenon using a macroscopic lane-changing model, *Transportation Research Part B: Methodological*, 42(6), pp. 511–522. 228

Laval, J. A., L. Leclercq (2010) A mechanism to describe the formation and propagation of stop-and-go waves in congested freeway traffic, *Philosophical Transactions of the Royal Society A: Mathematical, Physical and Engineering Sciences*, 368(1928), pp. 4519–4541. 56

Laval, J. A., L. Leclercq (2013) The Hamilton-Jacobi partial differential equation and the three representations of traffic flow, in: *Transportation Research Board 92nd Annual Meeting*, submitted for presentation only. 117, 118, 238

Lebacque, J.-P. (1996) The Godunov scheme and what it means for first order traffic flow models, in: Lesort, J.-B., ed., *Transportation and Traffic Theory: Proceedings of the 13th International Symposium on Transportation and Traffic Theory, 1996*, Pergamon, pp. 647–677. 62, 79, 161, 201, 206

Lebacque, J.-P. (2002) A two phase extension of the LWR model based on the boundedness of traffic acceleration, in: Taylor, M., ed., *Transportation and traffic theory in the 21st century: Proceedings of the 15th International Symposium on Transportation and Traffic Theory, 2002*, pp. 697–718. 62, 67, 129, 232

Lebacque, J.-P. (2005) Intersection modeling, application to macroscopic network traffic flow models and traffic management, in: Hoogendoorn, S. P., S. Luding, P. H. L. Bovy, M. Schreckenberg, D. E. Wolf, eds., *Traffic and Granular Flow '03*, Springer, pp. 261–278. 206

Lebacque, J.-P., M. M. Khoshyaran (2005) First order traffic flow models: intersection modeling, network modeling, in: Mahmassani, H., ed., *Transportation and Traffic Theory. Flow, Dynamics and Human Interaction. 16th International Symposium on Transportation and Traffic Theory*, Elsevier, pp. 365–386. 202

Lebacque, J.-P., S. Mammar, H. Haj Salem (2007) Generic second order traffic flow modelling, in: Allsop, R. E., M. G. H. Bell, B. G. Heydecker, eds., *Transportation and Traffic Theory 2007*, Elsevier, Oxford, pp. 755–776. 66

Leclercq, L. (2007a) Hybrid approaches to the solutions of the "Lighthill-Whitham-Richards" models, *Transportation Research Part B: Methodological*, 41(7), pp. 701–709. 56, 66, 67, 129, 164, 228, 232

Leclercq, L. (2007b) A new numerical scheme for bounding acceleration in the LWR model, in: Heydecker, B. G., ed., *Mathematics in Transport. Selected Proceedings of the 4th IMA International Conference on Mathematics in Transport*, Elsevier, pp. 279–292. 62

Leclercq, L. (2009) Le modèle LWR : théorie, confrontation expérimentale et applications au milieu urbain, Habilitation a diriger des recherches, présentée devant l'Institut National des Sciences Appliquées de Lyon et l'Université Claude Bernard Lyon I, in French. 129, 167, 169, 238

Leclercq, L., C. Bécarie (2012) A meso LWR model designed for network applications, in: *Presented at Transportation Research Board 91th Annual Meeting*. 118, 238

Leclercq, L., S. Chanut, J.-B. Lesort (2004) Moving bottlenecks in Lighthill-Whitham-Richards model: A unified theory, *Transportation Research Record: Journal of the Transportation Research Board*, 1883, pp. 3–13. 129

Leclercq, L., J. Laval, E. Chevallier (2007) The Lagrangian coordinates and what it means for first order traffic flow models, in: Allsop, R. E., M. G. H. Bell, B. G. Heydecker, eds., *Transportation and Traffic Theory 2007*, Elsevier, Oxford, pp. 735–753. 55, 117, 118, 119, 120, 162, 163, 164

Leclercq, L., J. Laval, E. Chevallier (2008) The Lagrangian coordinates applied to the LWR model, in: *Hyperbolic Problems: Theory, Numerics, Applications*, Springer, Berlin Heidelberg, pp. 671–678. 167

Leclercq, L., J. A. Laval (2007) A multiclass car-following rule based on the LWR model, in: Appert-Rolland, C., F. Chevoir, P. Gondret, S. Lassarre, J.-P. Lebacque, M. Schreckenberg, eds., *Traffic and granular flow*, Springer Berlin Heidelberg. 63

Lenz, H., C. K. Wagner, R. Sollacher (1999) Multi-anticipative car-following model, *The European Physical Journal B: Condensed Matter and Complex Systems*, 7, pp. 331–335. 59

Leutzbach, W. (1988) *An introduction to the theory of traffic flow*, Springer-Verlag. 47

LeVeque, R. J. (2002) *Finite volume methods for hyperbolic problems*, Cambridge texts in applied mathematics, Cambridge University Press, Cambridge. 137, 161, 163, 167, 238

Li, M. Z. F. (2008) A generic characterization of equilibrium speed-flow curves, *Transportation Science*, 42(2), pp. 220–235. 48

Lighthill, M. J., G. B. Whitham (1955a) On kinematic waves I: Flood movement in long rivers, *Proceedings of the Royal Society of London. Series A, Mathematical and Physical Sciences*, 229(1178), pp. 281–316. 67

Lighthill, M. J., G. B. Whitham (1955b) On kinematic waves II: A theory of traffic flow on long crowded roads, *Proceedings of the Royal Society of London. Series A, Mathematical and Physical Sciences*, 229(1178), pp. 317–345. 62, 67

Logghe, S., L. H. Immers (2008) Multi-class kinematic wave theory of traffic flow, *Transportation Research Part B: Methodological*, 42(6), pp. 523–541. 64, 67, 77, 101, 103, 104, 105, 107, 114, 116, 132, 133, 146, 147, 156, 158, 232

Mahnke, R., R. Kühne (2007) Probabilistic description of traffic breakdown, in: Schadschneider, A., T. Pöschel, R. Kühne, M. Schreckenberg, D. E. Wolf, eds., *Traffic and Granular Flow '05*, Springer, pp. 527–536. 60

Michaels, R. M. (1965) Perceptual factors in car following, in: *The 2nd International Symposium on the Theory of Traffic Flow, 1963*, pp. 44–59. 58

Moutari, S., M. Rascle (2007) A hybrid Lagrangian model based on the Aw-Rascle traffic flow model, *SIAM journal of applied mathematics*, 68, pp. 413–436. 66, 67, 232

Nagel, K., M. Schreckenberg (1992) A cellular automaton model for freeway traffic, *Journal de physique. I France*, 2(12), pp. 2221–2229. 59

Nair, R., H. S. Mahmassani, E. Miller-Hooks (2011a) A porous flow approach to modeling heterogeneous traffic in disordered systems, *Procedia - Social and Behavioral Sciences*, 17(0), pp. 611 – 627, papers selected for the 19th International Symposium on Transportation and Traffic Theory. 110

Nair, R., H. S. Mahmassani, E. Miller-Hooks (2011b) A porous flow approach to modeling heterogeneous traffic in disordered systems, *Transportation Research Part B: Methodological*, 45(9), pp. 1331 – 1345, selected Papers from the 19th ISTTT. 110

Nair, R., H. S. Mahmassani, E. Miller-Hooks (2012) A porous flow model for disordered heterogeneous traffic streams, in: *Transportation Research Board 89th Annual Meeting Compendium of Papers (DVD)*, Washington D.C. 65, 67, 101, 103, 104, 110, 111, 116, 133, 134, 153, 154, 155, 156, 158, 232

Newell, G. F. (1961) Nonlinear effects in the dynamics of car following, *Operations Research*, 9(2), pp. 209–229. 55, 56

Newell, G. F. (1965) Instability in dense highway traffic, a review, in: *The 2nd International Symposium on the Theory of Traffic Flow, 1963*, pp. 73–83. 51, 77

Newell, G. F. (1993a) A simplified theory of kinematic waves in highway traffic, part I: General theory, *Transportation Research Part B: Methodological*, 27(4), pp. 281–287. 117, 118, 167

Newell, G. F. (1993b) A simplified theory of kinematic waves in highway traffic, part III: Multi-destination flows, *Transportation Research Part B: Methodological*, 27(4), pp. 305–313. 201

Newell, G. F. (2002) A simplified car-following theory: a lower order model, *Transportation Research Part B: Methodological*, 36(3), pp. 195–205. 55, 56, 164

Ngoduy, D. (2010) Multiclass first-order modelling of traffic networks using discontinuous flow-density relationships, *Transportmetrica*, 6(2), pp. 121–141. 64, 101, 191, 201, 202

Ngoduy, D. (2011) Multiclass first-order traffic model using stochastic fundamental diagrams, *Transportmetrica*, 7(2), pp. 111–125. 63, 64, 101, 109

Ngoduy, D., R. Liu (2007) Multiclass first-order simulation model to explain nonlinear traffic phenomena, *Physica A: Statistical Mechanics and its Applications*, 385(2), pp. 667–682. 35, 64, 67, 101, 103, 104, 105, 107, 108, 109, 112, 116, 133, 147, 148, 149, 150, 152, 154, 155, 156, 158, 232

Orosz, G., R. E. Wilson, G. Stépán (2010) Traffic jams: dynamics and control, *Philosophical Transactions of the Royal Society A: Mathematical,Physical and Engineering Sciences*, 368, pp. 4455–4479. 43, 68

Ossen, S., S. P. Hoogendoorn (2006) Multi-anticipation and heterogeneity in car-following empirics and a first exploration of their implications, in: *Intelligent Transportation Systems Conference, 2006. IEEE*, pp. 1615–1620. 59, 67, 232

Papageorgiou, M. (1998) Some remarks on macroscopic traffic flow modelling, *Transportation Research Part A: Policy and Practice*, 32(5), pp. 323–329. 43, 67, 68, 72

Paveri-Fontana, S. L. (1975) On Boltzmann-like treatments for traffic flow: A critical review of the basic model and an alternative proposal for dilute traffic analysis, *Transportation Research*, 9(4), pp. 225–235. 61

Payne, H. J. (1971) Models of freeway traffic and control, in: *Simulation Council Proceedings*, Mathematical models of public systems, pp. 51–61. 65

Phillips, W. F. (1979) A kinetic model for traffic flow with continuum implications, *Transportation Planning and Technology*, 5(3), pp. 131–138. 61

Pipes, L. A. (1953) An operational analysis of traffic dynamics, *Journal of applied physics*, 24(3), pp. 274–281. 11, 54, 55, 87, 237

Prigogine, I. (1961) A Boltzmann-like approach to the statistical theory of traffic flow, in: Herman, R., ed., *Theory of Traffic Flow 1959, proceedings*, Elsevier, Amsterdam, pp. 158–164. 60

Prigogine, I., F. C. Andrews (1960) A Boltzmann-like approach for traffic flow, *Operations Research*, 8(6), pp. 789–797. 60, 61

Richards, P. I. (1956) Shock waves on the highway, *Operations Research*, 4(1), pp. 42–51. 62

Schreiter, T. (2013) *Vehicle-class specific control of freeway traffic*, Ph.D. thesis, Delft University of Technology/TRAIL Research school, Delft. 22, 29, 38, 235, 237

Smits, E., A. J. Pel, B. v. Arem (2012) A multi-class macroscopic intersection model, in: *Proceedings of the 1st European Symposium on Quantitative Methods in Transportation Systems*, Lausanne, pp. 1–7. 229, 237

Smulders, S. (1990) Control of freeway traffic flow by variable speed signs, *Transportation Research Part B: Methodological*, 24(2), pp. 111–132. 48, 85, 108

Stewart, J. (1999) *Calculus: Early Transcedentals*, 4 ed., Brooks/Cole Publishing Company. 121

Strang, G. (1988) *Linear algebra and its applications*, third ed., Harcourt Brace Jovanovich, San Diego. 141

Tampère, C. M. J., R. Corthout, D. Cattrysse, L. H. Immers (2011) A generic class of first order node models for dynamic macroscopic simulation of traffic flows, *Transportation Research Part B: Methodological*, 45(1), pp. 289–309. 201, 202, 205, 206, 237

Tampère, C. M. J., B. van Arem, S. P. Hoogendoorn (2003) Gas-kinetic traffic flow modeling including continuous driver behavior models, *Transportation Research Record: Journal of the Transportation Research Board*, 1852, pp. 231–238. 61

Tilch, B., D. Helbing (2000) Evaluation of single vehicle data in dependence of the vehicle-type, lane, and site, in: Helbing, D., H. J. Herrmann, M. Schreckenberg, eds., *International Workshop on Traffic and Granular Flow 1999: Social, Traffic, and Granular Dynamics*, Springer, Berlin, pp. 333–338. 87

Traffic and Granular Flow (2011) The Ninth International Conference on Traffic and Granular Flow, 2011. abstract book., Moscow, proceedings to be published. 67

Transportation Research Board (2000) *Highway Capacity Manual*, Transportation Research Board of the National Academies, Washington, DC. 64, 108

Treiber, M., D. Helbing (1999) Macroscopic simulation of widely scattered synchronized traffic states, *Journal of Physics A: Mathematical and General*, 32(1). 63

Treiber, M., D. Helbing (2002) Reconstructing the spatio-temporal traffic dynamics from stationary detector data, *Cooper@tive Tr@nsport@tion Dyn@mics*, 1. 48, 72

Treiber, M., A. Hennecke, D. Helbing (1999) Derivation, properties, and simulation of a gas-kinetic-based, nonlocal traffic model, *Physical Review E: Statistical, nonlinear and soft matter physics*, 59(1), pp. 239–253. 61

Treiber, M., A. Hennecke, D. Helbing (2000) Congested traffic states in empirical observations and microscopic simulations, *Physical Review E: Statistical, nonlinear and soft matter physics*, 62(2), pp. 1805–1824. 57, 59

Treiber, M., A. Kesting (2010) *Verkehrsdynamik und -simulationen: Daten, Modelle und Anwendungen der Verkehrsflussdynamik*, Springer, in german. 43, 45, 57

Treiber, M., A. Kesting, D. Helbing (2006a) Delays, inaccuracies and anticipation in microscopic traffic models, *Physica A: Statistical Mechanics and its Applications*, 360(1), pp. 71–88. 59

Treiber, M., A. Kesting, D. Helbing (2006b) Understanding widely scattered traffic flows, the capacity drop, and platoons as effects of variance-driven time gaps, *Physical Review E: Statistical, nonlinear and soft matter physics*, 74(1). 52

Treiber, M., A. Kesting, D. Helbing (2010) Three-phase traffic theory and two-phase models with a fundamental diagram in the light of empirical stylized facts, *Transportation Research Part B: Methodological*, 44(8-9), pp. 983–1000. 43, 45, 53

Treiterer, J., J. A. Myers (1974) The hysteresis phenomenon in traffic flow, in: Buckley, D., ed., *Proceedings of the 6th International Symposium on Transportation and Traffic Theory, 1974*, Elsevier, pp. 13–38. 51, 77

Tyagi, V., S. Darbha, K. R. Rajagopal (2008) A dynamical systems approach based on averaging to model the macroscopic flow of freeway traffic, *Nonlinear Analysis: Hybrid Systems*, 2(2), pp. 590–612, proceedings of the International Conference on Hybrid Systems and Applications, Lafayette, LA, USA, May 2006: Part II. 68

van Lint, J. W. C., S. P. Hoogendoorn, M. Schreuder (2008) Fastlane: A new multi-class first order traffic flow model, *Transportation Research Record: Journal of the Transportation Research Board*, 2088, pp. 177–187. 64, 67, 232

van Wageningen-Kessels, F. L. M., L. Leclercq, C. Vuik, S. P. Hoogendoorn, J. W. C. van Lint (2010) Accuracy analysis of lagrangian godunov scheme using variational theory, in: *5th IMA International Conference on Mathematics in Transport*, London, presented at conference. 168, 237

van Wageningen-Kessels, F. L. M., T. Schreiter, J. W. C. van Lint, S. P. Hoogendoorn (2011a) Modelling traffic flow phenomena, in: *2nd International Conference on Models and Technologies for ITS*, Leuven, extended abstract, available online. 72

van Wageningen-Kessels, F. L. M., J. W. C. van Lint, S. P. Hoogendoorn, C. Vuik (2009) Implicit and explicit numerical methods for macroscopic traffic flow models, in: *Transportation Research Board 88th Annual Meeting Compendium of Papers (DVD)*, Washington D.C. 165

van Wageningen-Kessels, F. L. M., J. W. C. van Lint, C. Vuik, S. P. Hoogendoorn (under review) Generic multi-class kinematic wave traffic flow modelling: model development and analysis of its properties, in: *Transportation and Traffic Theory 2013*. 64, 232

van Wageningen-Kessels, F. L. M., B. van 't Hof, S. P. Hoogendoorn, J. W. C. van Lint, C. Vuik (2011b) Anisotropy in generic multi-class traffic flow models, *Transportmetrica*, in press, available online. 65, 66, 232

Wiedemann, R. (1974) Simulation des Strassenverkehrsflusses, Tech. rep., Institute for Traffic Engineering, University of Karlsruhe. 58

Wilson, R. E. (2008) Mechanisms for spatio-temporal pattern formation in highway traffic models, *Philosophical Transactions of the Royal Society A: Mathematical, Physical and Engineering Sciences*, 366(1872), pp. 2017–2032. 58, 66, 68, 74, 78, 232

Wilson, R. E., J. A. Ward (2011) Car-following models: fifty years of linear stability analysis: a mathematical perspective, *Transportation Planning and Technology*, 34(1), pp. 3–18. 43, 56, 58, 68, 78

Wong, G. C. K., S. C. Wong (2002) A multi-class traffic flow model: an extension of LWR model with heterogeneous drivers, *Transportation Research Part A: Policy and Practice*, 36(9), pp. 827–841. 63, 64, 67, 101, 104, 113, 114, 116, 133, 154, 155, 156, 158, 232

Yuan, Y. (2013) *Lagrangian multi-class traffic state estimation*, Ph.D. thesis, Delft University of Technology/TRAIL Research school, Delft. 22, 29, 38, 125, 200, 235, 237

Yuan, Y., J. W. C. van Lint, F. L. M. van Wageningen-Kessels, S. P. Hoogendoorn (in press) Network discontinuities in Lagrangian traffic state estimation, *Journal of Intelligent Transportation Systems: Technology, Planning, and Operations*. 229, 237

Yuan, Y., J. W. C. van Lint, R. E. Wilson, F. L. M. van Wageningen-Kessels, S. P. Hoogendoorn (2012) Real-time lagrangian traffic state estimator for freeways, *IEEE Transactions on Intelligent Transportation Systems*, 13(1), pp. 59–70. 129, 229

Yuan, Y., F. L. M. van Wageningen-Kessels, J. W. C. van Lint, S. P. Hoogendoorn (2011) Two modeling and discretization choices for Lagrangian multi-class first-order traffic flow model and their related (dis-)advantages, in: *The Ninth International Conference on Traffic and Granular Flow, 2011. Abstract Book.*, Moscow, proceedings to be published. 125, 200, 237

Zhang, H. M. (1999) A mathematical theory of traffic hysteresis, *Transportation Research Part B: Methodological*, 33(1), pp. 1–23. 51, 66, 67, 77, 232

Zhang, H. M. (2001) New perspectives on continuum traffic flow models, *Networks and Spatial Economics*, 1, pp. 9–33. 43, 50, 53, 66, 81, 170, 173

Zhang, H. M. (2003) Anisotropic property revisited–does it hold in multi-lane traffic?, *Transportation Research Part B: Methodological*, 37(6), pp. 561–577. 81

Zhang, H. M. (2009) Comment on "On the controversy around Daganzo's requiem for and Aw-Rascle's resurrection of second-order traffic flow models" by D. Helbing and A.F. johansson, *The European Physical Journal B: Condensed Matter and Complex Systems*, 69, pp. 563–568. 81

Zhang, P., R.-X. Liu, S. C. Wong, S.-Q. Dai (2006) Hyperbolicity and kinematic waves of a class of multi-population partial differential equations, *European Journal of Applied Mathematics*, 17, pp. 171–200. 35, 67, 101, 113, 114, 116, 132, 133, 155, 156, 158, 232

TRAIL Thesis Series

The following list contains the most recent dissertations in the TRAIL Thesis Series. For a complete overview of more than 100 titles see the TRAIL website: www.rsTRAIL.nl.

The TRAIL Thesis Series is a series of the Netherlands TRAIL Research School on transport, infrastructure and logistics.

van Wageningen-Kessels, F.L.M., *Multi-class continuum traffic flow models: Analysis and simulation methods*, T2013/7, March 2013, TRAIL Thesis Series, the Netherlands

Taneja, P., *The Flexible Port*, T2013/6, March 2013, TRAIL Thesis Series, the Netherlands

Yuan, Y., *Lagrangian Multi-Class Traffic State Estimation*, T2013/5, March 2013, TRAIL Thesis Series, the Netherlands

Schreiter, T., *Vehicle-Class Specific Control of Freeway Traffic*, T2013/4, March 2013, TRAIL Thesis Series, the Netherlands

Zaerpour, N., *Efficient Management of Compact Storage Systems*, T2013/3, February 2013, TRAIL Thesis Series, the Netherlands

Huibregtse, O.L., *Robust Model-Based Optimization of Evacuation Guidance*, T2013/2, February 2013, TRAIL Thesis Series, the Netherlands

Fortuijn, L.G.H., *Turborotonde en turboplein: ontwerp, capaciteit en veiligheid*, T2013/1, January 2013, TRAIL Thesis Series, the Netherlands

Gharehgozli, A.H., *Developing New Methods for Efficient Container Stacking Operations*, T2012/7, November 2012, TRAIL Thesis Series, the Netherlands

van Duin, R., *Logistics Concept Development in Multi-Actor Environments: Aligning stakeholders for successful development of public/private logistics systems by increased awareness of multi-actor objectives and perceptions*, T2012/6, October 2012, TRAIL Thesis Series, the Netherlands

Dicke-Ogenia, M., *Psychological Aspects of Travel Information Presentation: A psychological and ergonomic view on travellers response to travel information*, T2012/5, October 2012, TRAIL Thesis Series, the Netherlands

Wismans, L.J.J., *Towards Sustainable Dynamic Traffic Management*, T2012/4, September 2012, TRAIL Thesis Series, the Netherlands

Hoogendoorn, R.G., *Swiftly before the World Collapses: Empirics and Modeling of Longitudinal Driving Behavior under Adverse Conditions*, T2012/3, July 2012, TRAIL Thesis Series, the Netherlands

Carmona Benitez, R., *The Design of a Large Scale Airline Network*, T2012/2, June 2012, TRAIL Thesis Series, the Netherlands

Schaap, T.W., *Driving Behaviour in Unexpected Situations: A study into the effects of drivers compensation behaviour to safety-critical situations and the effects of mental workload, event urgency and task prioritization*, T2012/1, February 2012, TRAIL Thesis Series, the Netherlands

Muizelaar, T.J., *Non-recurrent Traffic Situations and Traffic Information: Determining preferences and effects on route choice*, T2011/16, December 2011, TRAIL Thesis Series, the Netherlands

Cantarelli, C.C., *Cost Overruns in Large-Scale Transportation Infrastructure Projects: A theoretical and empirical exploration for the Netherlands and Worldwide*, T2011/15, November 2011, TRAIL Thesis Series, the Netherlands

van der Vlies, A.V., *Rail Transport Risks and Urban Planning: Solving deadlock situations between urban planning and rail transport of hazardous materials in the Netherlands*, T2011/14, October 2011, TRAIL Thesis Series, the Netherlands

van der Pas, J.W.G.M., *Clearing the Road for ISA Implementation? Applying adaptive policymaking for the implementation of intelligent speed adaptation*, T2011/13, October 2011, TRAIL Thesis Series, the Netherlands

Zegeye, S.K., *Model-Based Traffic Control for Sustainable Mobility*, T2011/12, October 2011, TRAIL Thesis Series, the Netherlands

Máhr, T., *Vehicle Routing under Uncertainty*, T2011/11, September 2011, TRAIL Thesis Series, the Netherlands

Pel, A.J., *Transportation Modelling for Large-scale Evacuations*, T2011/10, July 2011, TRAIL Thesis Series, the Netherlands

Zheng, F., *Modelling Urban Travel Times*, T2011/9, July 2011, TRAIL Thesis Series, the Netherlands

Vlassenroot, S.H.M., *The Acceptability of In-vehicle Intelligent Speed Assistance (ISA) Systems: From trial support to public support*, T2011/8, June 2011, TRAIL Thesis Series, the Netherlands

Kroesen, M., *Human Response to Aircraft Noise*, T2011/7, June 2011, TRAIL Thesis Series, the Netherlands

About the author

Curriculum Vitae

Femke van Wageningen-Kessels was born in Eersel on 18 November 1980. She started her pre-university education ('VWO') in 1992 and received her degree in 1999 from Rythovius College in Eersel. After spending one year at the College of Higher Education Maastricht studying Visual Arts and Design, she decided to move to Delft and started studying at Delft University of Technology (TUDelft). In 2004 she obtained her BSc degree in Industrial Design Engineering. She continued her studies at TUDelft with a master in Applied Mathematics. She obtained her MSc degree in 2007 after finishing her thesis project on 'Numerical methods for the stationary shallow water equations' at VORtech Computing.

In September 2007 Femke started her PhD research on traffic flow modelling and simulation at the department Transport & Planning, Faculty of Civil Engineering and Geosciences at TUDelft. This project was funded by ITS Edulab, the Dutch traffic and transportation laboratory for students, a cooperation between Rijkswaterstaat Centre for Transport and Navigation and TUDelft.

During her time at TUDelft, Femke was involved in many activities. For example, as a BSc student she was secretary of the board of the Delft Student Swimming Association WAVE and she organized events with the Delft's Student Union VSSD and MoTiv. Furthermore, as a MSc student she was team leader of WASUB, TUDelft's student team designing, building and racing with a human powered submarine. As a PhD student, Femke set up and organized bi-weekly literature seminars (DRInX) and masterclasses for MSc students. At TRAIL Research School she developed and taught two intensive PhD-courses and co-organized the bi-annual Congress in 2010. Furthermore, she represented PhD students within the department Transport & Planning.

Femke is interested in the role of women in science and technology and their careers. Therefore, she recently joined the role model database 'Spiegelbeeld', an initiative of VHTO, the Dutch National expert organisation girls/women and science/technology. As such she informs girls at high schools about education and careers in science and technology.

Finally, Femke has recently started a research project on Crowd Management at the department Transport & Planning.

Publications

Journal articles

van Wageningen-Kessels, F. L. M., J. W. C. van Lint, S. P. Hoogendoorn, C. Vuik (2010) Lagrangian formulation of a multi-class kinematic wave model, *Transportation Research Record: Journal of the Transportation Research Board*, 2188, pp. 29–36.

van Wageningen-Kessels, F. L. M., B. van 't Hof, S. P. Hoogendoorn, J. W. C. van Lint, C. Vuik (2011a) Anisotropy in generic multi-class traffic flow models, *Transportmetrica*, in press, available online. 65, 66, 232

van Wageningen-Kessels, F. L. M., Y. Yuan, S. P. Hoogendoorn, J. W. C. van Lint, C. Vuik (2011b) Discontinuities in the Lagrangian formulation of the kinematic wave models2011, *Transportation Research Part C: Emerging Technologies*, in press, available online.

Yuan, Y., J. W. C. van Lint, F. L. M. van Wageningen-Kessels, S. P. Hoogendoorn (in press) Network discontinuities in Lagrangian traffic state estimation, *Journal of Intelligent Transportation Systems: Technology, Planning, and Operations*. 229, 237

Yuan, Y., J. W. C. van Lint, R. E. Wilson, F. L. M. van Wageningen-Kessels, S. P. Hoogendoorn (2012) Real-time lagrangian traffic state estimator for freeways, *IEEE Transactions on Intelligent Transportation Systems*, 13(1), pp. 59–70. 129, 229

Peer reviewed conference contributions

Schreiter, T., F. L. M. van Wageningen-Kessels, Y. Yuan, J. W. C. van Lint, S. P. Hoogendoorn (2012) Fastlane: Traffic flow modeling and multi-class dynamic traffic management, in: *TRAIL Congress*, Rotterdam, available online.

van Wageningen-Kessels, F. L. M., L. Leclercq, C. Vuik, S. P. Hoogendoorn, J. W. C. van Lint (2010a) Accuracy analysis of lagrangian godunov scheme using variational theory, in: *5th IMA International Conference on Mathematics in Transport*, London, presented at conference. 168, 237

van Wageningen-Kessels, F. L. M., T. Schreiter, J. W. C. van Lint, S. P. Hoogendoorn (2011a) Modelling traffic flow phenomena, in: *2nd International Conference on Models and Technologies for ITS*, Leuven, extended abstract, available online. 72

van Wageningen-Kessels, F. L. M., J. W. C. van Lint, S. P. Hoogendoorn, C. Vuik (2008) Numerical time stepping schemes for macroscopic traffic flow models, in: *TRAIL Congress (DVD)*, Rotterdam.

van Wageningen-Kessels, F. L. M., J. W. C. van Lint, S. P. Hoogendoorn, C. Vuik (2009a) Implicit and explicit numerical methods for macroscopic traffic flow models, in: *Transportation Research Board 88th Annual Meeting Compendium of Papers (DVD)*, Washington D.C. 165

van Wageningen-Kessels, F. L. M., J. W. C. van Lint, S. P. Hoogendoorn, C. Vuik (2009b) Implicit time stepping schemes applied to the kinematic wave model in Lagrangian coordinates, in: *Traffic and Granular Flow '09*, Shanghai, presented at conference.

van Wageningen-Kessels, F. L. M., J. W. C. van Lint, S. P. Hoogendoorn, C. Vuik (2009c) Multiple user classes in the kinematic wave model in Lagrangian coordinates, in: *Traffic and Granular Flow '09*, Shanghai, presented at conference.

van Wageningen-Kessels, F. L. M., J. W. C. van Lint, S. P. Hoogendoorn, C. Vuik (2010b) Lagrangian formulation of a multi-class kinematic wave model, in: *Transportation Research Board 89th Annual Meeting Compendium of Papers (DVD)*, Washington D.C.

van Wageningen-Kessels, F. L. M., J. W. C. van Lint, C. Vuik, S. P. Hoogendoorn (2012a) Assessment of multi class kinematic wave models, in: *Latsis Symposium - 1st European Symposium on Quantitative Methods in Transportation Systems*.

van Wageningen-Kessels, F. L. M., J. W. C. van Lint, C. Vuik, S. P. Hoogendoorn (2012b) Genealogy of traffic flow models, in: *Book of abstracts of the Highway Capacity and Quality of Service and Traffic Flow Theory and Characteristics Joint Symposium*.

van Wageningen-Kessels, F. L. M., B. van 't Hof, S. P. Hoogendoorn, J. W. C. van Lint, C. Vuik (2010c) Numerical diffusion in traffic flow simulations: Accuracy analysis based on the modified equation method, in: *TRAIL Congress (DVD)*, Rotterdam.

van Wageningen-Kessels, F. L. M., Y. Yuan, S. P. Hoogendoorn, J. W. C. van Lint, C. Vuik (2010d) Discontinuities in the Lagrangian formulation of the kinematic wave models, in: *Traffic Flow Theory and Characteristics Summer Conference*, Annecy, proceedings available online.

van Wageningen-Kessels, F. L. M., Y. Yuan, S. P. Hoogendoorn, J. W. C. van Lint, C. Vuik (2011b) Sinks and sources in Lagrangian coordinates: derivation, interpretation and simulation results, in: *Transportation Research Board 90th Annual Meeting (DVD)*, Washington D.C.

Yuan, Y., J. W. C. van Lint, F. L. M. van Wageningen-Kessels, S. P. Hoogendoorn (2011a) Lagrangian traffic state estimation for freeway networks, in: *2nd International Conference on Models and Technologies for ITS*, Leuven, extended abstract, available online.

Yuan, Y., F. L. M. van Wageningen-Kessels, J. W. C. van Lint, S. P. Hoogendoorn (2011b) Two modeling and discretization choices for Lagrangian multi-class first-order traffic flow model and their related (dis-)advantages, in: *The Ninth International Conference on Traffic and Granular Flow, 2011. Abstract Book.*, Moscow, proceedings to be published. 125, 200, 237

Yuan, Y., F. L. M. van Wageningen-Kessels, J. W. C. van Lint, S. P. Hoogendoorn, J. L. M. Vrancken (2010) A new Lagrangian traffic state estimator for freeway networks, in: *TRAIL Congress (DVD)*, Rotterdam.

Technical report

van Wageningen-Kessels, F. L. M., Y. Yuan (2008, updated in 2011) Technical documentation Fastlane: Description of model equations and simulation, Tech. rep., TUDelft.

Manuscript under review

van Wageningen-Kessels, F. L. M., J. W. C. van Lint, C. Vuik, S. P. Hoogendoorn (submitted) Genealogy of traffic flow models.

Manuscript in preparation

van Wageningen-Kessels, F. L. M., J. W. C. van Lint, S. P. Hoogendoorn, C. Vuik (in progress) Generic multi-class kinematic wave traffic flow modelling: model development and analysis of its properties.